GEOCHEMISTRY OF GROUND-WATER IN TWO SANDSTONE AQUIFER SYSTEMS IN THE NORTHERN GREAT PLAINS IN PARTS OF MONTANA AND WYOMING

REGIONAL AQUIFER-SYSTEM ANALYSIS

U.S. GEOLOGICAL SURVEY PROFESSIONAL PAPER 1402–C

Geochemistry of Ground-Water in Two Sandstone Aquifer Systems in the Northern Great Plains in Parts of Montana and Wyoming

By THOMAS HENDERSON

REGIONAL AQUIFER-SYSTEM ANALYSIS

U.S. GEOLOGICAL SURVEY PROFESSIONAL PAPER 1402-C

A contribution of the
Regional Aquifer System Analysis Program

UNITED STATES GOVERNMENT PRINTING OFFICE, WASHINGTON: 1985

UNITED STATES DEPARTMENT OF THE INTERIOR

Donald Paul Hodel, *Secretary*

GEOLOGICAL SURVEY

Dallas L. Peck, *Director*

First printing 1985

Second printing 1985

Library of Congress Cataloging in Publication Data

Henderson, Thomas, 1957–
Geochemistry of ground-water in two sandstone aquifer systems in the northern Great Plains in parts of Montana and Wyoming.
(Regional aquifer-system analysis)(U.S. Geological Survey professional paper; 1402–C)
Bibliography; C69–C72.
Supt. of Docs. no.: I 19.16:1402–C
1. Aquifers—Great Plains. 2. Water, Underground—Great Plains. 3. Water chemistry.
I. Title. II. Series: Regional aquifer-system analysis (Series) III. Series: Geological Survey professional paper; 1402–C
GB1199.3.G74H46 1984 551.49'9078 83–600357
Rev.

For sale by the Branch of Distribution
U.S. Geological Survey
604 South Pickett Street
Alexandria, VA 22304

FOREWORD

The Regional Aquifer-System Analysis (RASA) program was started in 1978 after a congressional mandate to develop quantitative appraisals of the major ground-water systems of the United States. The RASA program represents a systematic effort to study a number of the Nation's most important aquifer systems, which, in aggregate, underlie much of the country and which represent important components of the Nation's total water supply. In general, the boundaries of these studies are identified by the hydrologic extent of each system, and accordingly transcend the political subdivisions to which investigations have often arbitrarily been limited in the past. The broad objectives for each study are to assemble geologic, hydrologic, and geochemical information; to analyze and develop an understanding of the system; and to develop predictive capabilities that will contribute to the effective management of the system. Computer simulation is an important element of the RASA studies, both to develop an understanding of the natural, undisturbed hydrologic system, and any changes brought about by human activities, as well as to provide a means of predicting the regional effects of future pumping or other stresses.

The final interpretive results of the RASA program are presented in a series of U.S. Geological Survey Professional Papers that describe the geology, hydrology, and geochemistry of each regional aquifer system. Each study within the RASA Program is assigned a single Professional Paper number, and where the volume of interpretive material warrants, separate topical chapters that consider the principal elements of the investigation may be published. The series of RASA interpretive reports begins with Professional Paper 1400 and thereafter will continue in numerical sequence as the interpretive products of subsequent studies become available.

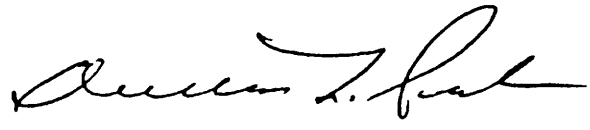

Dallas Peck
Director

CONTENTS

ILLUSTRATIONS

TABLES

SYMBOLS AND DEFINITIONS

α_{i-j}	isotopic fractionation factor between the ith and jth species.
β	reaction progress composite parameter.
β^-	beta particle (electron).
Γ	ratio of carbon input to output rate.
γ_i	activity coefficient of the ith species.
ΔC^0_{pRX}	heat capacity of reaction at constant pressure.
ΔG^0_{fi}	standard free energy of formation of the ith species.
ΔG^0_{RX}	standard free energy of reaction.
ΔH^0_{fi}	standard enthalpy of formation of the ith species.
ΔH^0_{RX}	standard enthalpy of reaction.
δ	isotopic composition expressed as per mil differences in the measured isotopic ratios of sample and standard.
$\delta^{13}C_*$	dissolving carbonate $\delta^{13}C$.
$\delta^{13}C_1$	solution $\delta^{13}C$ at the end of stage 1 evolution.
$\delta^{13}C_2$	solution $\delta^{13}C$ at the end of stage 2 evolution.
ϵps	additive fractionation factor between solution and precipite.
θ	effective porosity.
∂	standard deviation.
A	measured ^{14}C activity, in percent modern carbon.
A_{ND}	^{14}C activity to be expected in the absence of radioactive decay, in percent modern carbon.
a_i	thermodynamic activity of the ith species.
$\mathring{a}_i$	ion size parameter.
(am)	amorphous.
atm	pressure, in atmospheres.
b	saturated thickness of aquifer.
(c)	crystalline.
CEC	cation exchange capacity.
C_T	total inorganic carbon.
D	Deuterium, ^2H.
DO	dissolved oxygen.
DOC	dissolved organic carbon.
dh/dl	hydraulic gradient.
E^0	standard electrode potential.
Eh	oxidation potential, log activity of e^1.
EX	ion exchange substrate.
e^1	electron.
(g)	gaseous.
I	ionic strength.
IAP	ion activity product.
i	denotes ith species.
K_{eq}	thermodynamic equilibrium constant.
K^{ij}_{ex}	thermodynamic constant for the exchange of species i and j on a substrate.
K_{gas}	Henry's Law Constant for the dissolution of a gaseous species.
K_{sp}	thermodynamic solubility constant.
k_D	distribution constant.
m_i	molal concentration of the ith species.
m^L_i	molality of the ith element in the solution phase.
m^X_i	molality of the ith element in the solid phase.
n	neutron.
N	fractional abundance.
n	number of observations.
PDB-1	Peedee belemnite ^{13}C isotopic standard.
P_i	partial pressure of the ith gaseous species.
p	negative log base 10 function.
pH	negative log activity of H^+.
pH_{zpc}	pH of the zero point of charge.
R	gas constant, 8.3147 Joules mole $^{-1}$ °Kelvin^{-1}.
R_i	equilibrium isotopic ratio in the ith phase.
r	correlation coefficient.
SI	saturation index.
SMOW	Standard Mean Ocean Water ^{18}O and ^2H isotopic standard.
SpC	specific conductance.
(s)	solid.
T	transmissivity.
T	temperature.
T_r	reference temperature, 25° Celsius or 298.15° Kelvin.
T_2	temperature of reaction.
t	time, in years.
TU	tritium unit.
$t_{1/2}$	^{14}C half life, in years.
v	ground water flow rate.
x	mole fraction.
Z_i	charge on the ith species.

GEOCHEMISTRY OF GROUND-WATER IN TWO SANDSTONE AQUIFER SYSTEMS IN THE NORTHERN GREAT PLAINS IN PARTS OF MONTANA AND WYOMING

By THOMAS HENDERSON

ABSTRACT

The Kootenai Formation in the Judith Basin, Montana, and the Lance Formation and Fox Hills Sandstone in the Powder River Basin, Wyoming, constitute two important sandstone aquifer systems in the Northern Great Plains region. Ground waters in each of these systems evolve from low dissolved-solids concentration, near-neutral pH, predominantly calcium and magnesium bicarbonate types in their recharge areas, to high dissolved-solids concentration, high pH, predominantly sodium-bicarbonate types in the basins. Oxidation potentials decrease as the waters flow downgradient under confined conditions. Calculation of the saturation states of aquifer minerals suggests several groups of mineral phases that could control ground-water chemistry. Mass transfer modeling indicates, however, that the observed behavior of major and minor dissolved species in both systems can satisfactorily be explained only by equilibration with calcite, dolomite, or calcite and dolomite. The geochemistry of these systems is probably controlled by the incongruent dissolution of dolomite to form calcite. This reaction appears to be driven by cation exchange and the dissolution of carbon dioxide. Plausible carbon dioxide sources include organic carbon oxidation and lignite coalification. Aluminosilicates influence major element chemistry primarily as substrates for cation exchange, which, in combination with carbonate equilibria, buffer ground water pH at values of 8.5 to 8.9. Dissolved-iron concentrations are controlled by equilibration with amorphous ferric oxyhydroxides in oxidizing waters, with amorphous ferric oxyhydroxides and siderite in moderately reducing waters, and with siderite and amorphous ferrous sulfide in strongly reducing waters. Measured variations in dissolved carbonate isotopic composition compare favorably with carbon isotopic evolution, calculated by assuming dedolomitization.

Recharge areas of the two systems are characterized by ground waters with high tritium and carbon-14 activities and relatively low dissolved-solids concentrations, with calcium and magnesium as the predominant cations. Recharge temperatures, calculated from dissolved-argon concentrations and $\delta^{18}O$ and δD isotopic measurements, indicate that recharge is derived primarily from spring snowmelt rather than late spring and summer storms. Ground-water flow directions are generally parallel to trends of increasing dissolved solids concentrations and decreasing divalent to monovalent cation concentration ratios. However, these trends are sometimes obscured in areas of leakage or mixing. Further indication of leakage between aquifers is provided by abrupt changes in major element and isotopic chemistry, which are not characteristic of normally observed geochemical evolution. Ground-water flow rates, calculated by adjusting measured carbon-14 activities for carbonate mass transfer, are comparable to values calculated from aquifer tests and potentiometric data. These carbon-14 flow rates average 1.6 meters per year for the Second Cat Creek sandstone of the Kootenai Formation, and 1.3 meters per year for the Lance–Fox Hills aquifer.

INTRODUCTION

The accurate simulation of aqueous geochemistry through the use of computer models can serve as an invaluable aid in characterizing water quality and availability and in determining mineralogic controls on natural water chemistry. If the controlling influences for a particular aquifer system can be determined, the effects of man-made pertubations to that aquifer system can be evaluated, and plans to minimize deleterious effects can be considered.

This investigation of two confined sandstone aquifer systems of the Northern Great Plains region was initiated in order to: (1) Characterize the geochemical controls on ground-water chemistry; and (2) use ground-water chemistry as a hydrologic tool to locate areas of recharge, discharge, and leakage from adjacent aquifers, and also to determine ground-water ages and rates of flow.

Areas of the Judith Basin, Montana, and the Powder River Basin, Wyoming, were chosen for detailed study because of anticipated population growth in these regions and the need for greater supplies of water in the near future. The Kootenai Formation and Fox Hills Sandstone–Lance Formation were selected as study aquifers on the basis of aquifer geology and hydrology, as well as the availability and distribution of suitable existing water wells.

Available computer models have been used to calculate the status of gas-solution-mineral equilibria involving major- and trace-element species in ground water, and to simulate observed chemical and isotopic variations in the two flow systems, as a means of determining the influence of mineralogic controls on ground-water chemistry. The computer program WATEQ2 (Ball and others, 1979; 1980) was used to calculate aqueous speciation of major and trace elements from detailed analyses of water samples collected during this study from existing domestic, stock, municipal, and industrial wells. WATEQ2 also computes the degree of saturation of a ground water with respect to minerals

present or likely to be present within the aquifer. In addition, a major emphasis was also placed on activity diagrams, which may serve to distinguish between stable and unstable phases that otherwise appear to be in equilibrium with a given ground water.

Simulation of expected changes in the solution chemistry, assuming water quality is controlled by reactions with different mineral phases, was accomplished by the use of the computer program PHREEQE (Parkhurst and others, 1980). Calculation of the resulting isotopic compositions associated with computed mass transfer, particularly in the carbon and sulfur systems, places an additional constraint on a proposed model, in that both chemical and isotopic compositions must be correctly predicted for the model to be considered valid. A U.S. Geological Survey computer program that incorporates the carbon isotopic evolution equations of Wigley and others (1978) was used to calculate the isotopic evolution associated with proposed mass transfer models, as well as to adjust apparent carbon-14 ages for carbonate dilution and precipitation effects. Thus, through the use of geochemical models, many pertinent chemical reactions can be simulated, and their relative effects on solution chemistry can be evaluated and compared to observed ground-water chemistries.

Previous investigations by Plummer (1977) and Thorstenson and others (1979) have used geochemical mass transfer and isotopic evolution models as a means of characterizing chemical reactions responsible for measured changes in dissolved constituents along hydrologic flow paths. Ground-water geochemistry of the limestone Floridan aquifer was determined by Plummer (1977) to be controlled by equilibration with calcite, dolomite, and gypsum, in addition to the oxidation of organic carbon by sulfate reduction. In the Fox Hills–basal Hell Creek aquifer of North Dakota, Thorstenson and others (1979) concluded that equilibration with calcite and dolomite, oxidation of organic carbon by sulfate reduction, and cation exchange by clays control ground-water chemistry. Computed mass transfer between aqueous and solid phases, in combination with measured carbon isotopic data, was then used to calculate ground-water ages and flow rates.

The present investigation uses many of the techniques developed during these previous studies, applying them to two sandstone aquifers in the Judith and Powder River Basins of the Northern Great Plains region. The geochemical data collected are also used for information regarding the hydrologic characteristics of the two flow systems.

A list of chemical reactions pertinent to the discussion of ground-water geochemistry is presented in table 1. In addition, the reader is directed to the supplemental data section for an analysis of the chemical theory used in this report.

The reference surface to which relief features and altitude data of the conterminous United States and Alaska are related is the National Geodetic Vertical Datum of 1929 (NGVD of 1929), formerly called mean sea level. The NGVD of 1929 is referred to as sea level in this report.

ACKNOWLEDGMENTS

The author would like to thank John F. Busby, Donald Langmuir, and Donald C. Thorstenson, for their many helpful suggestions and criticisms. H. W. Dodge, Jr., of the U.S. Geological Survey Uranium and Thorium Resources Branch was instrumental in obtaining core samples of the Fox Hills Sandstone and Donald W. Fisher of the U.S. Geological Survey Water Resources Division was responsible for the determination of dissolved gases. In addition, Jerome B. Krause of the Colorado School of Mines Research Institute was extremely helpful in allowing the use of his mineralogy laboratory facilities and X-ray diffraction data files. This work was supported in part by U.S. Geological Survey contract 14-08-0001-17999.

SAMPLE COLLECTION AND ANALYSIS

SELECTION AND PREPARATION OF WELLS

Knowledge of the depth of a well and the position of screened and cased intervals is critical in determining which aquifer is being sampled. Therefore, wells to be sampled were chosen on the basis of available drillers' logs or other reliable information regarding well construction. This knowledge is especially important in the study of interbedded systems, where numerous sandstone aquifers are isolated by shale aquitards.

Prior to sampling, the selected wells were pumped or allowed to flow for periods of roughly 30 minutes to 1 hour, until temperature, specific conductance, and pH measurements taken at approximately 10 minute intervals, had stabilized. This initial pumping period serves to remove waters influenced by contact with the metal well casing from the well bore and adjacent aquifer and allows for the collection of samples that are representative of waters present in the aquifer.

FIELD PARAMETERS

Several parameters, including temperature, specific conductance, pH, alkalinity, and dissolved oxygen were measured in the field to insure accurate determination.

TABLE 1.—*Pertinent chemical reactions*

Oxidation-reduction	Reaction number
$O_{2(g)} + CH_2O = CO_{2(g)} + H_2O$	(1)
$4NO_3^- + 5CH_2O + 4H^+ = 2N_{2(g)} + 5CO_{2(g)} + 7H_2O$	(2)
$NO_3^- + 2CH_2O + 2H^+ = NH_4^+ + 2CO_{2(g)} + H_2O$	(3)
$4Fe(OH)_{3(am)} + CH_2O + 8H^+ = 4Fe^{+2} + CO_{2(g)} + 11H_2O$	(4)
$2MnO_2 + CH_2O + 4H^+ = 2Mn^{+2} + CO_{2(g)} + 3H_2O$	(5)
$SO_4^{-2} + 2CH_2O + H^+ = HS^- + 2CO_{2(g)} + 2H_2O$	(6)
$CH_3COOH = CH_{4(g)} + CO_{2(g)}$	(7)
$CO_{2(g)} + 4H_{2(g)} = CH_{4(g)} + 2H_2O$	(8)
$FeS_{2(c)} + 7/2O_{2(g)} + H_2O = Fe^{+2} + 2SO_4^{-2} + 2H^+$ (pyrite)	(9)
$FeS_{2(c)} + 14Fe^{+3} + 8H_2O = 15Fe^{+2} + 2SO_4^{-2} + 16H^+$ (pyrite)	(10)
$CH_{4(g)} + 2O_{2(g)} = H_2CO_3^0 + H_2O$	(11)

Eh redox couples		Reaction number
$O_{2(g)} + 4H^+ + 4e^- = 2H_2O$;	$E^0 = 1.229$ volts	(12)
$Fe(OH)_{3(am)} = Fe^{+3} + 3OH^-$;	$pK_{Fe(OH)_{3(am)}} = 37\text{–}39$	(13)
$FeCO_{3(c)} = Fe^{+2} + CO_3^{-2}$;	$pK_{FeCO_3} = 10.22$	(14)
$Fe^{+3} + e^- = Fe^{+2}$;	$E^0 = 0.771$ volts	(15)
$SO_4^{-2} + 10H^+ + 8e^- = H_2S^0 + 4H_2O$;	$E^0 = 0.301$ volts	(16)

Dissolved carbonate equilibria	Reaction number
$CO_{2(g)} + H_2O = H_2CO_3^0$	(17)
$H_2CO_3^0 = HCO_3^- + H^+$	(18)
$HCO_3^- = CO_3^{-2} + H^+$	(19)

Mineral dissolution and weathering	Reaction number
$CaSO_4 \cdot 2H_2O_{(c)} = Ca^{+2} + SO_4^{-2} + 2H_2O$ (gypsum)	(20)
$CaCO_{3(c)} + H^+ = Ca^{+2} + HCO_3^-$ (calcite)	(21)
$CaMg(CO_3)_{2(c)} + 2H^+ = Ca^{+2} + Mg^{+2} + 2HCO_3^-$ (dolomite)	(22)
$CaMg(CO_3)_{2(c)} + 2H^+ = CaCO_{3(c)} + Mg^{+2} + HCO_3^-$ (dolomite) (calcite)	(23)
$K_{0.6}Mg_{0.25}Al_{2.3}Si_{3.5}O_{10}(OH)_{2(c)} + 3.15H_2O + 1.1H^+ =$ (illite) $1.15Al_2Si_2O_5(OH)_{4(c)} + 0.6K^+ + 0.25Mg^{+2} + 1.2H_4SiO_4^0$ (kaolinite)	(24)
$3Na_{0.33}Al_{2.33}Si_{3.67}O_{10}(OH)_{2(c)} + H^+ + 11.5H_2O =$ (Na-montmorillonite) $3.5Al_2Si_2O_5(OH)_{4(c)} + Na^+ + 4H_4SiO_4^0$ (kaolinite)	(25)
$3KAl_2Si_3O_{10}(OH)_{2(c)} + 3H_2O + 2H^+ = 3Al_2Si_2O_5(OH)_{4(c)} + 3K^+$ (muscovite) (kaolinite)	(26)
$NaAlSi_3O_{8(c)} + 6.1H_2O + 1.1H^+ =$ (albite) $1.4[Al(OH)_3]_{0.7}[SiO_2]_{0.3(am)} + Na^+ + 2.6H_4SiO_4^0$ (allophane)	(27)

TABLE 1.—*Pertinent chemical reactions*—Continued

Ion exchange	Reaction number
$Ca^{+2} + Na_2EX = 2Na^+ + CaEX^*$	(28)
$Mg^{+2} + Na_2EX = 2Na^{+2} + MgEX^*$	(29)

Nuclear transmutation	Reaction number
$^{14}N + n = {}^{12}C + {}^3H$	(30)
$^{14}N + n = {}^{14}C + {}^1H$	(31)

Radioactive decay	Reaction number
$^{14}C = {}^{14}N + \beta^-$	(32)

*EX-Ion exchange site

The methods and equipment used to evaluate these parameters are listed in table 2.

MAJOR AND MINOR ELEMENTS

Major and minor element samples were filtered through 124-mm (millimeter) diameter, 0.45-μm (micrometer) membrane filters using a GeoFilter variable speed peristaltic pump and backflush filter plate. Trace element samples were filtered through 124-mm diameter, 0.10-μm membrane filters in order to decrease the amount of suspended matter in the sample (Kennedy and others, 1974; Jones and others, 1974). These samples for major, minor, and trace element analyses were then preserved and stored for later analysis by the U.S. Geological Survey National Water Quality Laboratory in Arvada, Colorado, in accordance with standard U.S. Geological Survey procedures outlined by Brown and others (1970) and Skougstad and others (1978). Precisions for these analyses at the 95 percent confidence level are 1.96 standard deviations (σ) or the detection limit (table 3), whichever is greater.

DISSOLVED GASES

Dissolved-gas samples were collected at selected wells, using evacuated glass flasks of the type described by Hobba and others (1977). The samples were collected at the well discharge point by connecting the sample flask to the well head with plastic tubing and allowing several volumes of water to flow through the sample container to remove adsorbed gases. Stopcocks on the container were then closed to the flowing water and

TABLE 2.—*Field analytical methods (modified from Wood, 1976)*

[All measurements made at the well site in non-flowing water, unless otherwise noted]

Parameter	Analytical method
pH	Orion Research* Model 399A Ionanalyzer with an Orion Model 91-09 combination pH electrode. Apparatus calibrated with NBS primary standard buffers (pH 4.01, 6.86, 7.41, and 9.18 at 25°C, corrected for temperature effects) using two buffers with pH's bracketing measured pH.
Temperature (T), in degrees Celsius (°C)	Mercury thermometer, calibrated from −1° to 51°C in 0.1°C increments. Measured in flowing water at well head.
Specific conductance (SpC), in microsiemens per centimeter (μS/cm at 25°C)	Yellow Springs Instruments Model 33 salinity-conductivity-temperature meter.
Dissolved oxygen (DO), in milligrams per liter (mg/L)	Yellow Springs Instruments Model 57 oxygen meter. Calibrated in air at temperature of sample water and in aliquot of sample water with 5 mL Na_2SO_3 saturated solution. Measurement made with probe submerged in flowing sample water at well discharge point.
Alkalinity (bicarbonate, carbonate), in milligrams per liter (mg/L)	Potentiometric titration with 0.01639N H_2SO_4. Sample filtered through 0.45-micrometer membrane filter. Endpoints determined with inflection points in first derivative of titration curve.

*The use of brand names in this report is for information only and does not constitute endorsement by the U.S. Geological Survey.

TABLE 3.—*Standard or relative deviations and detection limits of analyses performed by the U.S. Geological Survey National Water Quality Laboratory*

[Data from Skougstad and others, 1978; μg/L, micrograms per liter; mg/L, milligrams per liter]

Parameter	Standard deviation[1] (X = parameter concentration)	Relative deviation (percent)	Detection limit	Units
Aluminum	0.073X + 14.97	---	10	μg/L
Ammonium	---	17	0.01	mg/L
Arsenic	---	10	1.0	μg/L
Barium	0.069X + 69.1	---	100	μg/L
Boron	0.079X + 17.1	---	20	μg/L
Bromide	---	3	.1	mg/L
Cadmium	0.192X + 0.09	---	1.0	μg/L
Calcium	0.057X + 0.34	---	.1	mg/L
Chloride	0.057X + 0.25	16	.1	mg/L
Chromium	0.173X + 2.44	---	10	μg/L
Copper	---	23	1.0	μg/L
Fluoride	0.109X + 0.01	---	.1	mg/L
Iodide	---	88	.01	mg/L
Iron	0.056X + 23.90	---	10	μg/L
Lead	0.097X + 1.45	---	1.0	μg/L
Lithium	0.048X + 4.84	---	10	μg/L
Magnesium	0.043X + 0.13	---	.1	mg/L
Manganese	0.049X + 9.59	---	10	μg/L
Molybdenum	0.072X + 0.45	---	10	μg/L
Nitrate	---	22	0.1	mg/L
Nitrite	---	---	.01	mg/L
Nitrate + Nitrite	0.080X + 0.01	---	.01	mg/L
Phosphate	---	12	.01	mg/L
Potassium	0.092X + 0.11	---	.1	mg/L
Selenium	0.275X − 0.13	---	1.0	μg/L
Silica	0.031X + 0.60	---	.1	mg/L
Sodium	0.039X + 0.45	---	.1	mg/L
Strontium	0.104X + 15.4	---	10	μg/L
Sulfate	0.001X + 2.92	---	5	mg/L
Sulfide	---	---	.1	mg/L
Uranium	---	---	---	---
Vanadium	0.069X + 0.422	---	1.0	μg/L
Zinc	0.034X + 16.6	---	10	μg/L

[1]Standard deviations calculated from above expressions and parameter concentration, in units specified.

opened to the evacuated sidearm. Argon, helium, nitrogen, oxygen, carbon dioxide, and methane were later determined, using a gas-chromatographic procedure.

STABLE AND RADIOACTIVE ISOTOPES

Samples were also collected for the determination of the stable isotopic ratios of carbon, oxygen, hydrogen, and sulfur, as well as for the radioactive isotopes, carbon-14 and tritium. The following procedures, outlined by J. F. Busby and others (U.S. Geological Survey, written commun., 1981), were used in collecting these isotope samples:

1. Carbon-13 ($\delta^{13}C$): The reagent used to precipitate dissolved carbonate species from the sample was prepared in the following manner: 454 g of strontium chloride hexahydrate ($SrCl_2 \cdot 6H_2O$) were dissolved in 2 L (liters) of reagent-grade ammonium hydroxide. Dissolved carbon dioxide precipitates and settles out of solution as $SrCO_3$, allowing the supernatant to be decanted and stored for later use at the sampling site.

Samples were collected in 1-L polyethylene sample bottles; these bottles were rinsed twice with raw sample water, then filled to the brim. Approximately 50 mL (milliliters) of the sample was poured out and replaced with the strontium chloride reagent, so that the bottle was again filled to the brim. Caps were tightened twice and sealed with electrical tape at the sampling site. Later the same day, the caps of the bottles were retightened and dipped in melted paraffin to prevent evaporation and exchange of CO_2 with the atmosphere.

2. Oxygen-18 ($\delta^{18}O$), deuterium (δD), and tritium (^3H): Raw-water samples were collected in 120-mL glass bottles for oxygen-18 and deuterium determinations, and in 1000-mL glass bottles for tritium. The bottles were rinsed twice with raw sample water, filled to the brim,

and capped, taking care to exclude any air bubbles. The caps were tightened twice and sealed with electrical tape. Later, the caps were retightened and dipped in melted paraffin to avoid any evaporation or atmospheric exchange.

3. Sulfur-34 ($\delta^{34}S_{SO_4^{-2}}$, $\delta^{34}S_{S^{-2}}$): Samples for determination of sulfur isotopic ratios in dissolved sulfate and sulfide were collected in the Judith Basin, but a lack of appropriate equipment prevented similar sampling in the Powder River Basin. Where samples were collected, a 4- to 6-L raw-water sample was obtained and dissolved sulfide was precipitated by the addition of zinc acetate and sodium hydroxide. The suspension was filtered under nitrogen pressure through 0.10-μm membrane filters, and both filtrate and precipitate were saved for later analysis of sulfate and sulfide isotopic ratios. Unfortunately, insufficient sulfide was present in Judith Basin waters for the determination of isotopic ratios.

4. Carbon-14 (^{14}C): Two reagents were prepared for the collection and preservation of carbon-14 samples: (1) Carbon dioxide-free sodium-hydroxide solution was prepared by dissolving 150 g of sodium hydroxide (NaOH) in 600-mL distilled water. Fifteen milliliters of strontium-chloride solution were added to precipitate any dissolved carbonate. The precipitate was allowed to settle and the supernatant was decanted and stored in 500-mL airtight bottles; (2) carbon dioxide-free strontium-chloride solution was prepared by dissolving 454 g of strontium chloride hexahydrate ($SrCl_2 \cdot 6H_2O$) in 1-L water. One milliliter of sodium hydroxide solution was added to precipitate any dissolved carbonate. After settling, the supernatant was decanted and stored in airtight 500-mL bottles.

The preparation of a carbon-14 (^{14}C) sample consists of precipitating and collecting all dissolved inorganic carbonate species present in a 100-L raw-water sample. This was done by carefully filling a 100-L capacity separatory funnel-like device with raw-sample water delivered through a garden hose, taking care to avoid any splashing that might result in exchange with atmospheric CO_2. During filling, the top of the funnel was capped by a plastic cover to minimize exchange of CO_2 with the atmosphere. When the funnel was nearly full, 500 mL of the CO_2-free NaOH solution was added, followed by the addition of 500-mL of the CO_2-free $SrCl_2$ solution. Several grams of ferrous ammonium sulfate $[Fe(NH_4)_2(SO_4)_2 \cdot 6H_2O]$ were added as a flocculant and the hose removed when the funnel was filled to capacity. A 2-L wide-mouth plastic bottle was rinsed twice and filled with raw-sample water, then screwed onto a closed flap valve on the bottom of the funnel. The flap valve was opened at this point, allowing the precipitate to settle into the jar. Settling of the precipitate was generally complete within one or two hours, although occasionally the first bottle had to be removed and replaced with a second bottle to collect all the precipitate. The sample bottles were removed, capped, tightened several times, and sealed with electrical tape to prevent atmospheric contamination.

MINERALOGIC ANALYSIS

Drill core and outcrop samples of the Fox Hills Sandstone were disaggregated by gently pulverizing in a porcelain mortar and pestle, and sulfide nodules present were removed by hand from the bulk sample. Fractions for clay mineral identification were isolated from the bulk sample by a Stokes Law gravity settling method using water, yielding particles of less than 2 μm in diameter. Bromoform liquid (specific gravity of 2.8) was used for the separation of heavy minerals.

Clay separates were mounted directly on glass slides, while whole rock, heavy mineral, and sulfide fractions were first pulverized in an agate mortar, sieved to remove particles greater than silt size, and then mounted in aluminum sample holders or on glass slides, depending on sample size. These fractions were subsequently examined by X-ray diffraction on a Phillips recording diffractometer employing nickel-filtered copper radiation. Interpretations of diffraction patterns were based on the file card data of the American Society for Testing and Materials (Joint Committee on Powder Diffraction Standards, 1981). Using these procedures, well crystalized minerals occurring in abundances of greater than about five percent were identifiable.

JUDITH BASIN STUDY AREA

PHYSIOGRAPHY

The Judith Basin of central Montana is a topographic depression within an unglaciated section at the western margin of the Northern Great Plains. Locations of major physiographic features in the Judith Basin are presented in figure 1.

TOPOGRAPHY

Rolling, grass-covered plains at elevations of 1,050 to 1,350 m comprise the greater part of the basin, and consist of gently sloping, gravel-covered terraces, dissected by steep-sided stream valleys. Gently dipping sedimentary strata form a belt of foothills separating the basin from the main flanks of the surrounding mountains. The Kootenai Formation outcrops in this belt,

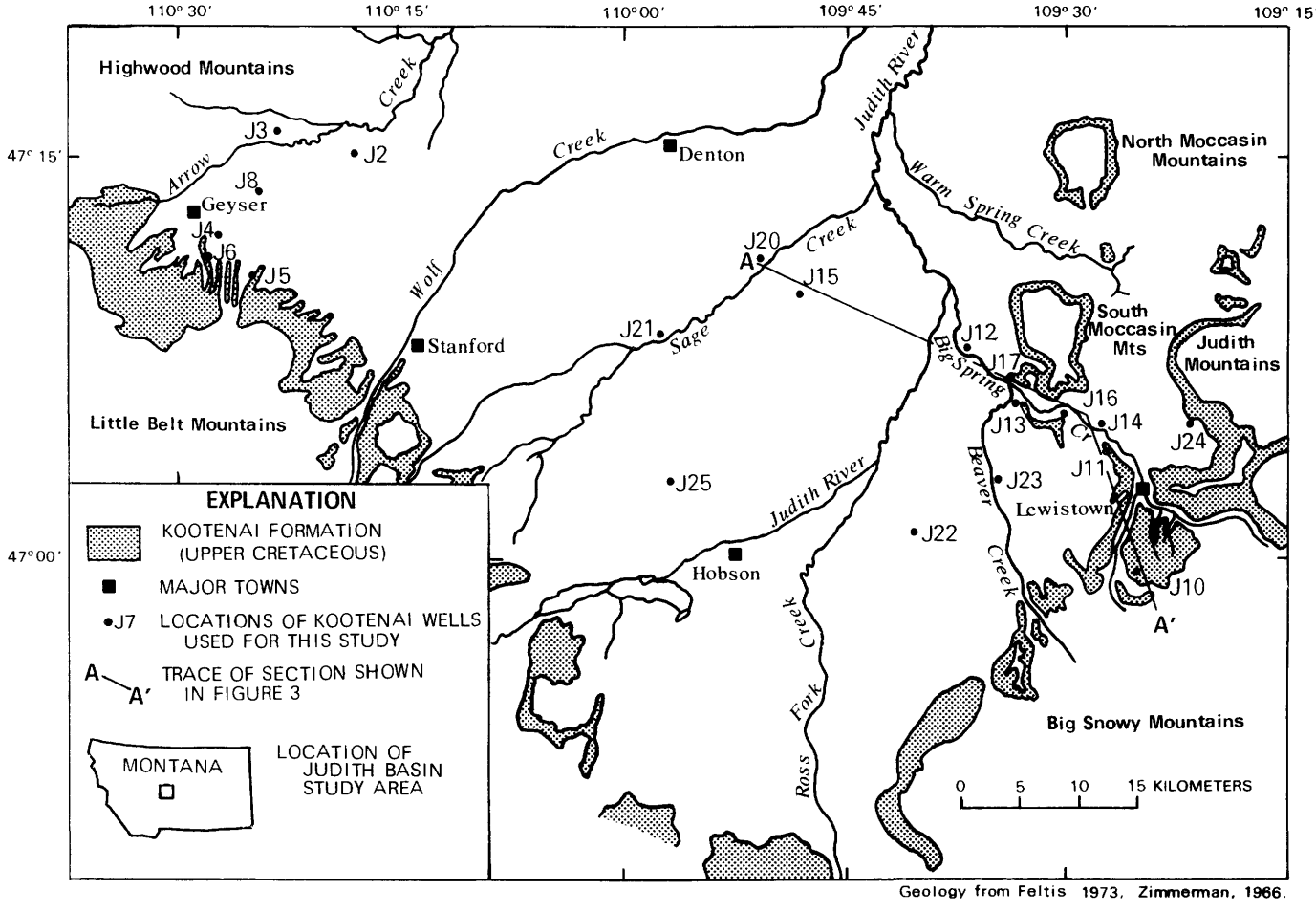

FIGURE 1.—Index map of the Judith Basin area, Montana, showing the outcrop of the Kootenai Formation and the locations of wells sampled.

with a resistant basal sandstone forming the outermost of two persistent, pine-covered strike ridges that encircle the uplifts. The wooded Highwood, Little Belt, Big Snowy, Judith, and North and South Moccasin Mountains rise above the plains to elevations of 1,800 to 2,750 m, effectively surrounding the basin on all sides but the north (Vine, 1956).

DRAINAGE

Runoff in the study area is characterized by high flow periods in the late winter and spring in response to rains and snowmelt from the nearby mountains. The Judith River and Arrow Creek, tributaries of the Missouri River, drain the Judith Basin. The main perennial streams in the eastern Judith Basin, Big Spring and Warm Spring Creeks, exhibit relatively constant flows; Big Spring Creek averaged 5.55 m^3/s (cubic meters per second) and Spring Creek averaged 4.15 m^3/s, during the 1968 water year (Feltis, 1973). Other tributaries contribute considerable seasonal flow, but are commonly dry for extended periods.

CLIMATE

The climate of the Judith Basin is a modified continental or semiarid type. More than half of the seasonal precipitation falls during the months of May, June, and July, with annual averages of 40.8 cm (centimeters) at Lewistown and 39.2 cm at Hobson. Relative humidity is low except in the mountains, which also receive greater precipitation. The average annual temperature at Lewiston is 6°C (degrees Celsius), although extremes above 40°C and below −40°C are not uncommon (Vine, 1956).

GEOLOGY

STRUCTURE

The structural Judith Basin is a large, northward-plunging syncline bordered by anticlinal folds, which form the Big Snowy, Little Belt, Judith, and Moccasin Mountains. The Highwood Mountains, consisting of a

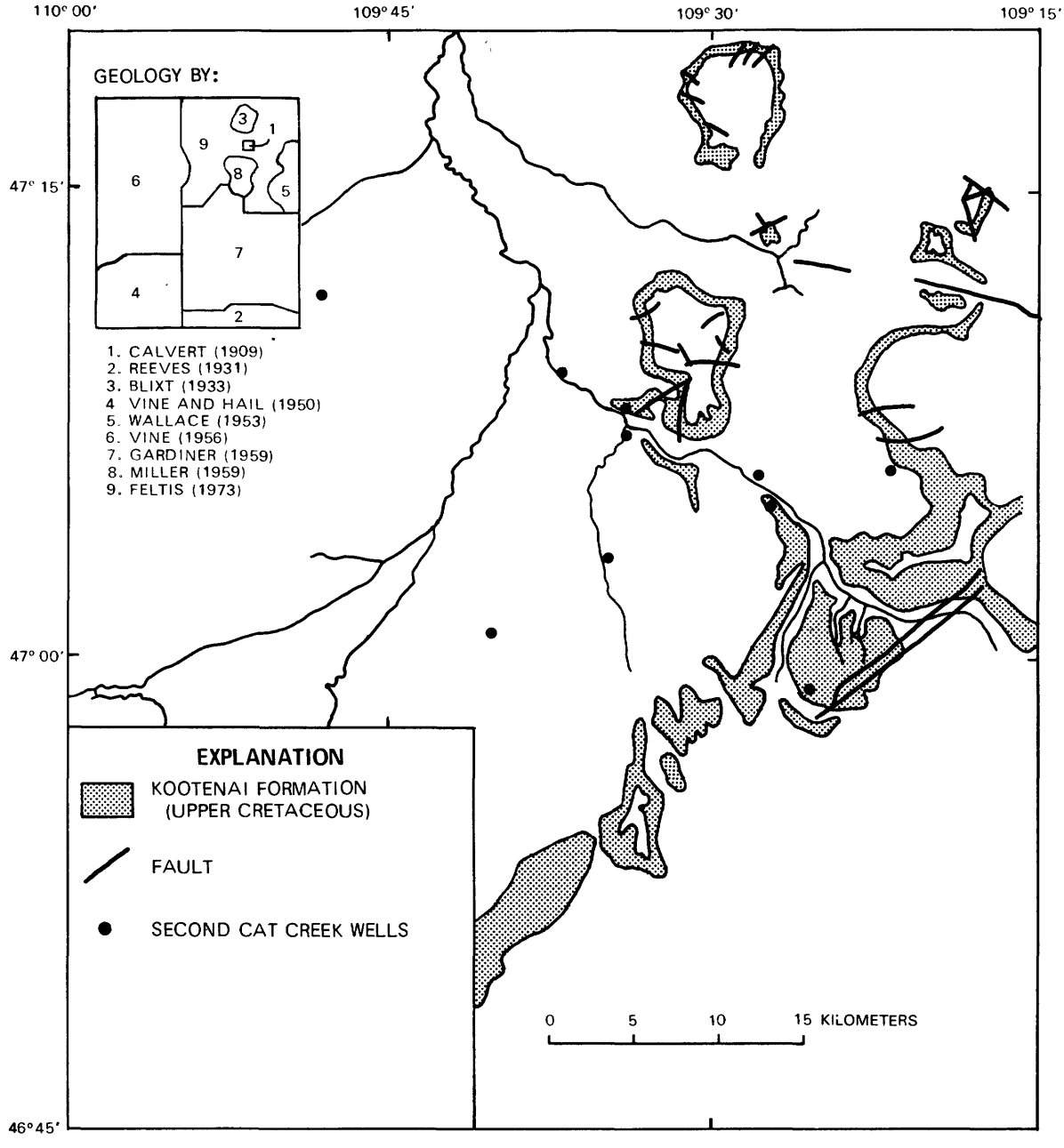

FIGURE 2.—Mapped faults in the eastern Judith Basin, Montana.

highly dissected mass of Tertiary breccia, tuff, lava flows, and related intrusives, border the syncline to the northwest. Emplacement of these rocks did not greatly influence the regional synclinal structure; however, small faults and domes create local structural modifications (Zimmerman, 1966).

Major structural features within the study area are the Big Snowy, Judith, and North and South Moccasin Mountains. The Big Snowy Uplift is an east-west-trending asymmetric anticline, flanked by steeply dipping sedimentary strata to the south and gently inclined beds to the north. Dips in Cretaceous strata on the north flank range from 8 degrees to 10 degrees, becoming horizontal within 10 to 13 km (kilometers) of the mountains. The anticline plunges steeply to the northwest and southeast, disappearing a short distance outside the study area (Reeves, 1931).

The Judith and North and South Moccasin Uplifts consist of a complex series of domes, tilted and faulted sedimentary formations, and masses of intrusive rocks. Figure 2 shows the locations of major faults in the area. Cretaceous strata outcrop along the flanks of the Judith

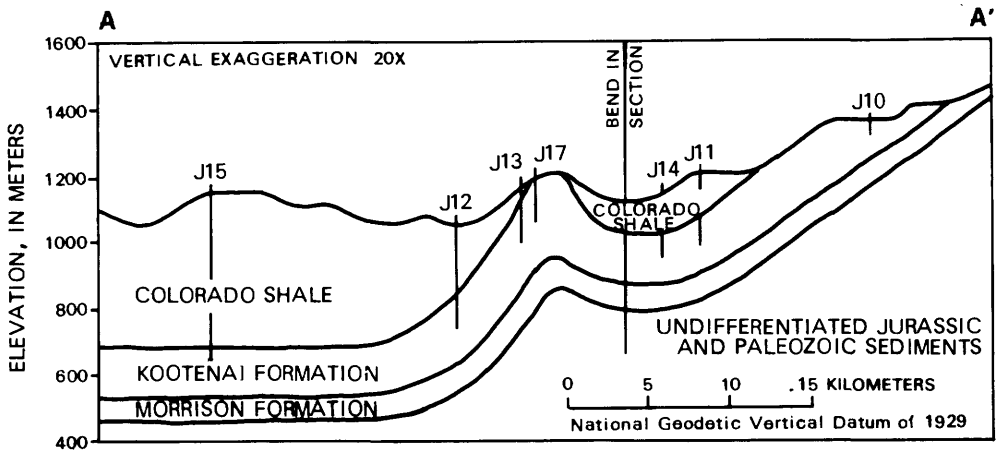

FIGURE 3.—Generalized geologic section of the eastern Judith Basin, Montana, through line A–A′ in figures 1 and 6. Faults in the vicinity of the south Moccasin Mountains have been omitted.

and Moccasin Mountains, generally dipping basinward at angles of 20 degrees to 60 degrees, but are overturned in some areas. A geologic section through the study area demonstrates the relationships between Cretaceous strata and pertinent uplifts (fig. 3).

Structure contours and outcrop patterns in the Lewistown area indicate the presence of a northwest-trending synclinal structure on the north flank of the Big Snowy Uplift, perpendicular to the trend of the anticline (Gardner, 1959). This syncline parallels, and generally underlies, Big Spring Creek in the Lewistown area (fig. 4). Unfortunately, a lack of data near the South Moccasin Mountains prevents following this trend north and west of Lewistown; however, it seems probable that the position of Big Spring Creek is controlled by this structure.

STRATIGRAPHY

The sequence of sedimentary rocks exposed in the Big Snowy Uplift consists of approximately 3,350 m of strata, ranging in age from Precambrian to Holocene. The Upper Jurassic Morrison Formation was deposited in a fluvial or lacustrine environment, and is comprised of 75 to 130 m of variegated siltstones and mudstones interbedded with lenticular yellowish-gray to brown sandstones and minor freshwater limestones (Suttner, 1969). At or near the top of the Morrison is the Great Falls coal bed discussed by Calvert (1909), which was locally exploited at one time. Calvert (1909) reported that the Great Falls coal beds, unlike younger Montana coals, contain up to 5 or 6 percent pyrite. Overlying an erosional unconformity at the top of the Morrison is the Kootenai Formation, a Lower Cretaceous fluvial and lacustrine sequence of crossbedded sandstones, siltstones, shales, and freshwater limestones, totaling 110 to 170 m in thickness (Suttner, 1969). At the base of the Kootenai is a 6- to 30-m-thick bed of crossbedded, gray or orange to white sandstone. Another relatively thick sequence of red to gray lenticular sandstones occur near the middle of the Kootenai. These two persistent sands are commonly referred to as the Third and Second Cat Creek sandstones. The remainder of the Kootenai is composed of red, purple, and gray shales, siltstones, and thinner interbedded sandstones and limestones. Individual sandstone beds vary greatly in thickness, and may thin and disappear over a short distance (Gardner, 1959), making determination of Second and Third Cat Creek sandstones difficult in some instances.

Conformably overlying the red beds of the upper part of the Kootenai Formation are the dark gray to black marine sediments of the Colorado Shale. These shales are Early to Late Cretaceous in age and crop out at or near the surface over much of the basin. Where the entire section is present, the thickness ranges from 450 to 600 m (Feltis, 1973). Several sandstone beds are present among the shales, the most important of which is the First Cat Creek sandstone of the Colorado Shale, which lies directly above the Kootenai Formation. This brown to black sand ranges from 6 to 25 m in thickness, and is interbedded with thin layers of fissile black shale (Gardner, 1959).

MINERALOGY OF THE KOOTENAI FORMATION

Drill cores of the Kootenai Formation from central Montana were unavailable at the time of this study, so no analyses of aquifer or confining bed mineralogy were performed. Instead, stratigraphic descriptions and mineralogic studies in the Judith Basin and southwest Montana were used to determine the mineral phases present within the aquifer system. A listing of these minerals is given in table 4.

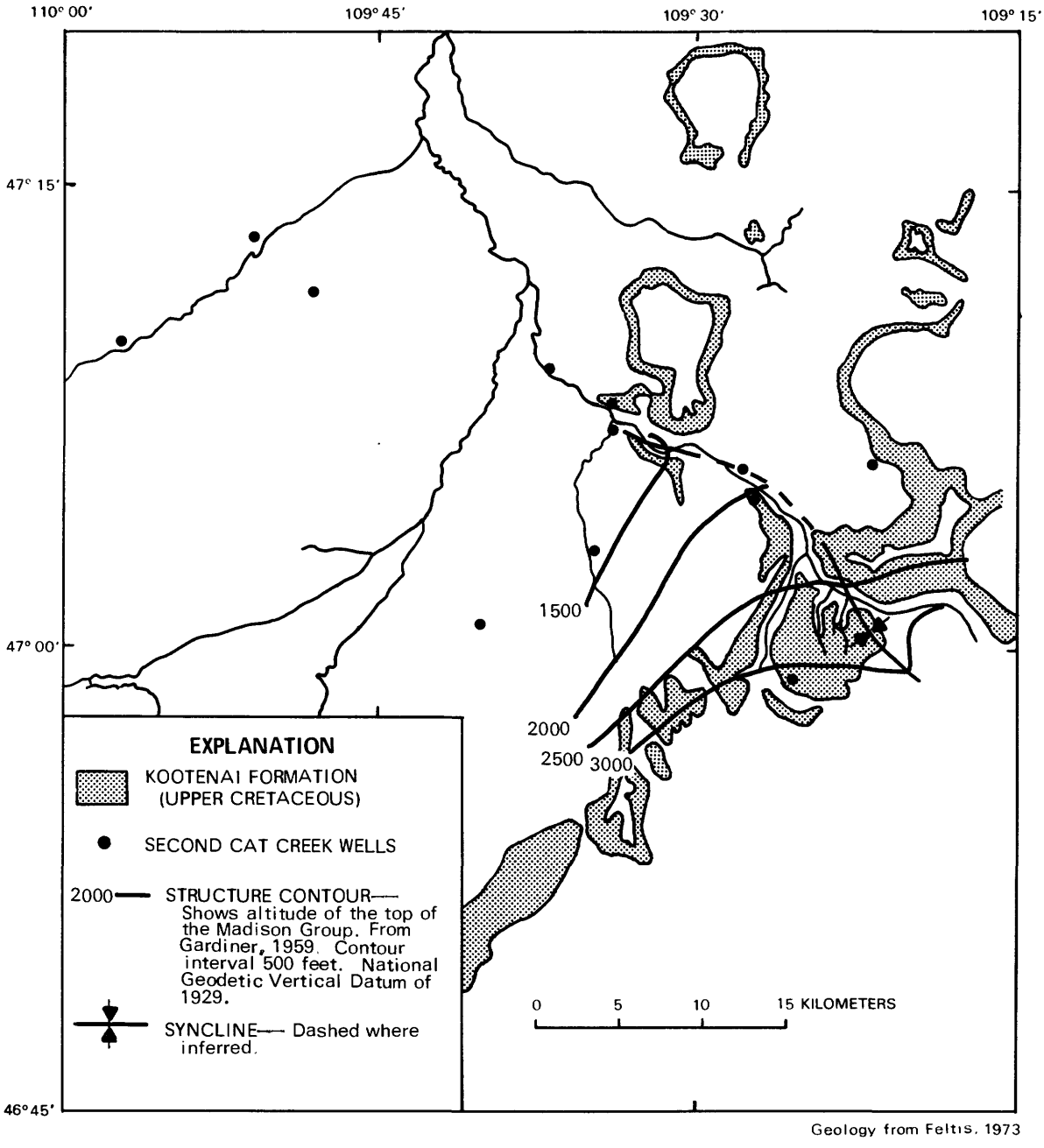

FIGURE 4.—Structure contours on Mississippian Madison Group showing the relationship between Big Spring Creek and an underlying synclinal structure, eastern Judith Basin, Montana [1 foot (in contour interval)=0.305 meter].

A stratigraphic description by Miller (1959) of the Kootenai Formation in the South Moccasin Mountains indicates that the sandstones are composed of light-colored detrital quartz and dark-brown to black chert with minor siderite fragments. Many of the sands are described as calcareous or limonitic, suggesting the presence of calcite and ferric oxyhydroxides, such as amorphous ferric hydroxide, goethite, and hematite. In addition, lacustrine dolomites and dark-gray to black carbonaceous shales were reported as minor occurrences interbedded with the sands and shales. Vine (1956) described a similar mineralogy in a section of Kootenai Formation exposed at Skull Butte Dome near Stanford, but also mentions sandstones and conglomerates containing limestone pebbles.

Ballard (1966) has studied the petrography of basal Kootenai sandstones found at the north flank of the Little Belt Mountains. He classified the Third Cat Creek sandstone in the lower part of the Kootenai as moderate to coarse-grained, moderate to well-sorted, orthoquartzites or quartz arenites. The terrigenous material is almost entirely quartz and chert with quartz cement.

TABLE 4.—*Minerals and other phases present in the Kootenai Formation, central Montana*
[From Ballard, 1966, Miller, 1959, Suttner, 1968, 1969, Vine, 1956]

Mineral	Idealized chemical formula
Quartz	SiO_2
Calcite	$CaCO_3$
Siderite	$FeCO_3$
Dolomite	$CaMg(CO_3)_2$
Hematite	Fe_2O_3
Illite	$K_{0.6}Mg_{0.25}Al_{2.30}Si_{3.5}O_{10}(OH)_2$
Kaolinite	$Al_2Si_2O_5(OH)_4$
Zircon	$ZrSiO_4$
Tourmaline group	---
Garnet group	---
Leucoxene	Secondary Ti oxides
Organic matter	CH_2O

Minor amounts of sandstone fragments and illite, and traces of hematite and organic material are also present. Heavy mineral separations show the presence of trace amounts of tourmaline, zircon, rutile, garnet, and leucoxene (mixed titanium oxides).

In southwest Montana, the mineralogy of the Kootenai and Morrison Formations was investigated by Suttner (1968; 1969) using petrographic and X-ray techniques. For the basal Kootenai sandstones, Suttner observed petrographies similar to those found by Ballard (1966) in the Little Belt Mountains. Calcite cement becomes common in the middle sandstones, and trace quantities of well-preserved sodic plagioclase and potassium feldspar crystals also become evident. The dominant clay minerals observed in Kootenai Formation shales are illite and kaolinite. Minor amounts of montmorillonite, chlorite, and mixed layer clays are also present, but only illite and kaolinite are present in samples taken nearest the Judith Basin.

HYDROLOGY

The surface- and ground-water resources of the Judith Basin have been previously evaluated by Zimmerman (1966) and Feltis (1973, 1977). J. F. Levings (U.S. Geological Survey, written commun., 1981) was investigated ground-water flow in the Kootenai Formation during the present study using hydrologic computer models.

The sandstone beds of the Kootenai Formation constitute the most widely used aquifers south of Big Spring Creek. The Second and Third Cat Creek sandstones constitute the main aquifers, supplying water of good quality and sufficient quantity for domestic and stock use. Isolated sandstone beds also provide water to wells in the area. These bedrock aquifers are recharged by precipitation and infiltration through unconsolidated stream deposits on the outcrop. In the outcrop area the aquifers are unconfined, but the siltstones and shales of the Kootenai and Morrison Formations form confining layers within a short distance downdip. Wells located downdip from the aquifer outcrop commonly flow at the surface.

As indicated by the potentiometric contours plotted in figure 5 (J. F. Levings, U.S. Geological Survey, written commun., 1981), the inferred flow direction is generally northward from recharge areas on the flanks of the Big Snowy and Judith Mountains. Feltis (1973) reported that ground-water discharges from seeps in the Kootenai outcrop along the channel of Big Spring Creek near Hanover, although the magnitude of this discharge is uncertain. The perturbation of the potentiometric surface along Big Spring Creek may be explained by discharge into the creek, drawdown due to extensive utilization of the aquifer in the vicinity of Lewistown, or both. The elongation of the associated cone of depression suggests a zone of high permeability along the stream valley. Such a high permeability zone would be expected if fracturing accompanied the deformation that formed the synclinal structure underlying the valley.

Zimmerman (1966) reported transmissivity values (T) for the Kootenai Formation in the western and southern Judith Basin, ranging from 2.4×10^{-5} to 2.7×10^{-4} m²/s. Feltis (1977) measured an intermediate transmissivity value of 1.2×10^{-4} m²/s for a well (J25) located within the study area (fig. 5) drawing from the Second and Third Cat Creek sandstones and having a saturated thickness (b) of 71 m. Assuming no leakage, constant thickness, and constant effective porosity, Darcy's Law may be used to calculate ground-water flow rates (v) for flow paths perpendicular to the potentiometric contours:

$$v=(-T/b\theta)/(dh/dl),$$

where:

θ=effective porosity (assume 0.20);
dh/dl=hydraulic gradient, determined from potentiometric contours.

Flow rates calculated in this manner using Feltis's intermediate transmissivity value are listed in table 5, and average 2.0 m/yr (meters per year), which is consistent with values given by Freeze and Cherry (1979) for confined sandstone aquifers.

According to Feltis (1973; 1977), wells completed in the sandstones of the Colorado Shale or the Morrison Formation sometimes yield water of suitable quantity

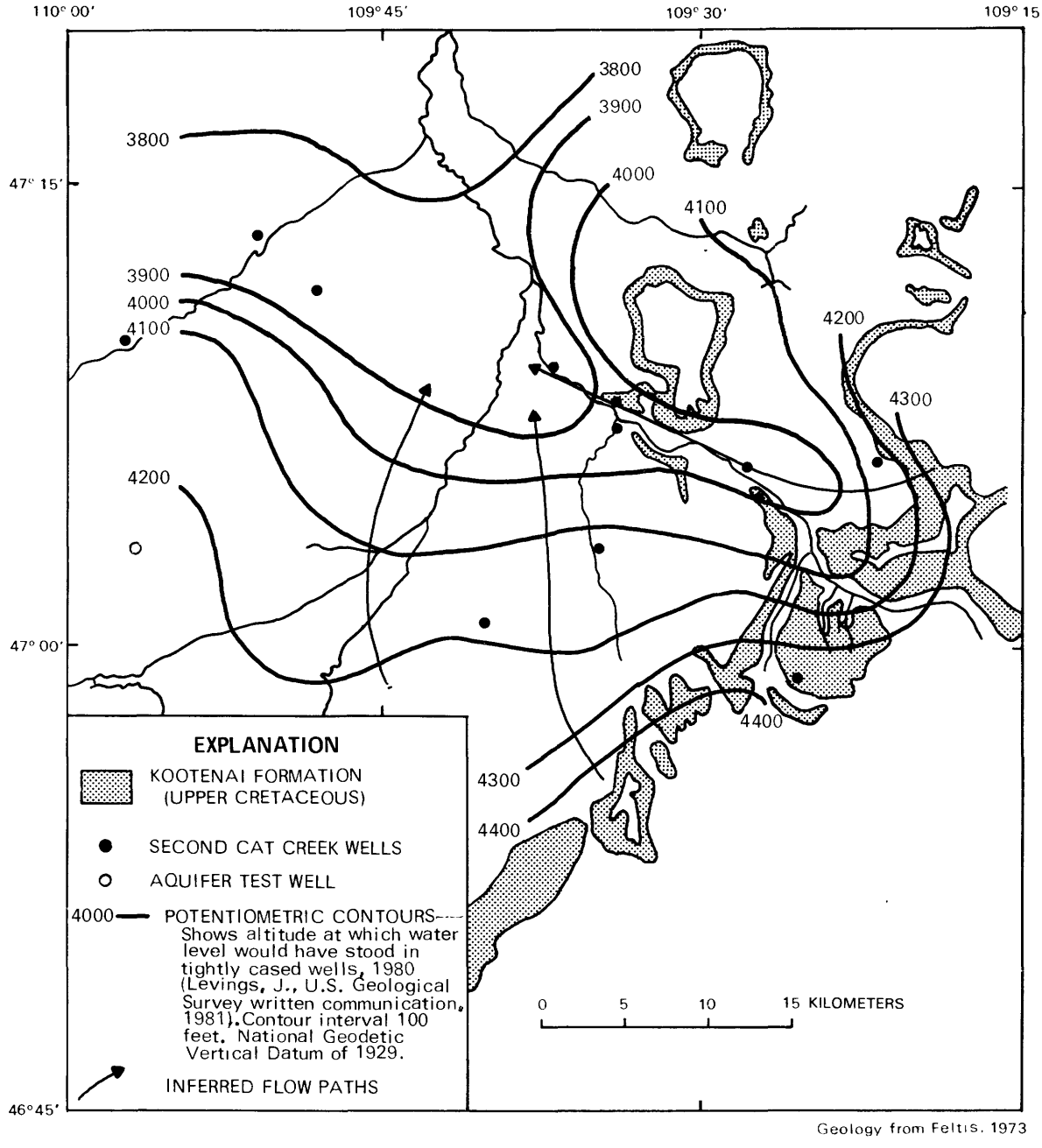

FIGURE 5.—Potentiometric contours and inferred flow paths for the Kootenai Formation, eastern Judith Basin, Montana [1 foot (in contour interval)=0.305 meter].

TABLE 5.—*Flow rates calculated for the Kootenai Formation in the Judith Basin, Montana*

[Data from Feltis (1977) and J. F. Levings (U.S. Geological Survey, written commun., 1981)]

Sample location	*dh* (meters)	*dl* (meters)	Flow rate (meters per year)
J11	-120	11,100	2.6
J13	-140	19,000	1.7
J15	-290	38,900	1.8

and quality for domestic or stock use. The First Cat Creek sandstone of the Colorado Shale often provides moderate amounts of water, as do the isolated sandstone, limestone, or coal beds of the Morrison Formation. Water from the Morrison is commonly high in dissolved sulfate, presumably due to oxidation of the abundant pyrite found in the formation.

Two deeper Mississippian aquifers, the Madison Group and the Kibbey Formation of the Big Snowy

TABLE 6.—*Concentrations of dissolved major elements in waters from the Kootenai Formation, Judith Basin, Montana*

[Concentrations in milligrams per liter (mg/L) unless otherwise specified. °C, degrees Celsius, μS/cm, microsiemens per centimeter, < indicates concentrations below detection limit for that analysis]

Sample	Calcium, Ca	Magnesium, Mg	Sodium, Na	Potassium, K	Na + K	Chloride, Cl	Sulfate, SO_4	Bicarbonate, HCO_3	Carbonate, CO_3	pH	Temperature, *T* (°C)	Specific conductance, SpC (μS/cm at 25°C)
J2 -------	55	15	18	4.1		1.7	24	275	<1	7.59	15.0	454
J3 -------	84	25	22	5.4		3.0	160	241	<1	7.83	12.0	678
J4 -------	120	29	34	2.9		2.2	300	269	<1	7.62	8.3	925
J5 -------	83	24	22	2.1		2.2	150	303	<1	7.68	8.4	715
J6 -------	200	51	20	2.5		2.1	510	268	<1	7.58	8.4	1,250
J8 -------	98	31	29	5.1		2.4	210	248	<1	7.80	12.8	745
J10 ------	39	8.4	2.7	2.5		2.3	9.2	135	<1	6.87	8.2	273
J11 ------	44	15	41	2.7		1.6	62	273	<1	7.70	8.7	498
J12 ------	8.7	3.2	240	2.9		7.4	320	291	4	8.49	16.8	1,130
J13 ------	4.9	2.0	170	2.2		2.9	45	396	2	8.48	11.7	663
J14 ------	51	19	62	3.0		1.4	89	309	<1	7.82	9.4	594
J15 ------	3.1	.9	190	1.9		4.9	64	443	4	8.55	13.4	792
J16 ------	2.4	.5	200	1.7		2.6	4.2	505	5	8.57	9.4	750
J17 ------	43	18	100	7.7		3.8	160	292	<1	7.60	10.9	762
J20[1] -----	.6	.0	230	1.2		5.9	72	420	21	8.8	15	813
J21[1] -----	4.2	.0	160	3.0		.2	76	340	6	8.5	14	748
J22[2] -----	4	0		159		4	51	335	12	---	16	610
J23[2] -----	4.1	2	153	---		.8	46	351	0	8.2	11	630
J24[2] -----	101	39		0		12	60	177	0	---	---	750

[1]Feltis (1977)
[2]Feltis (1973)

Group, exhibit the highest hydrostatic pressures in the basin, and appear to discharge as numerous springs in the study area. Feltis (1973) concluded that faulting and fracturing have contributed to the localization of discharge from these aquifers, resulting in large springs, such as Big Spring, which is the source of the creek of the same name.

DATA PRESENTATION AND INTERPRETATION

MAJOR AND MINOR ELEMENTS

Analyses of the 21 well waters used to chemically characterize the Kootenai aquifer within the Judith Basin are presented in tables 6 and 7. The locations of

TABLE 7.—*Concentrations of dissolved minor and trace elements in*

[Concentrations in micrograms per liter unless otherwise specified, mg/L, milligrams

Sample	Aluminum, Al	Arsenic, As	Barium, Ba	Bromide, Br (mg/L)	Cadmium, Cd	Chromium, Cr	Copper, Cu	Dissolved oxygen, O_2 (mg/L)	Fluoride, F (mg/L)	Iodide, I (mg/L)	Iron, Fe	Lead, Pb
J2 ----------	<10	<1	<2	<0.1	<1	<10	1	<0.1	0.6	<0.01	330	<1
J3 ----------	<10	<1	20	<1	<1	<10	<1	<1	5	.01	1,000	<1
J4 ----------	<10	<1	10	<1	<1	<10	<1	1	5	<.01	880	<1
J5 ----------	<10	1	30	<1	<1	20	<1	<1	4	<.01	460	<1
J6 ----------	<10	<1	10	<1	<1	<10	<1	<1	3	<.01	740	<1
J8 ----------	<10	<1	30	<1	<1	<10	<1	1	5	.01	440	<1
J10 ---------	<10	2	300	<1	<1	<10	4	7	2	<.01	10	<1
J11 ---------	<10	1	40	<1	<1	20	1	<1	4	<.01	520	<1
J12 ---------	<10	<1	20	1	<1	10	1	<1	1.4	.01	60	<1
J13 ---------	<10	1	40	<1	<1	<10	<1	4	2.2	<.01	30	<1
J14 ---------	<10	1	50	<1	<1	<10	<1	<1	3	<.01	900	<1
J15 ---------	<10	1	50	1	<1	20	<1	<1	1.3	.01	30	<1
J16 ---------	<10	1	60	<1	<1	10	<1	<1	2.6	.02	<10	<1
J17 ---------	<10	<1	20	<1	<1	<10	2	---	1.1	.01	140	<1

these sampled wells are plotted in figure 1. Waters from 16 wells (J2–J17) were sampled and analyzed as part of this study; the remaining five (J20–J24) were obtained from previous investigations (Feltis, 1973; 1977). Correlation of ground-water chemistry with available driller's logs and well depths revealed significant vertical variations between samples from the Second and Third Cat Creek sandstones, despite the many similarities in the major element chemistry, mineral saturation indices, Eh and pH of these waters. The variability resulting from considering the whole formation as a uniform aquifer is much greater than if the two sandstones are treated as individual systems, suggesting that although similar geochemical processes are acting to control water chemistries in both aquifers, subtle differences in the stratigraphy, mineralogy, and permeability of the two systems result in the observed variability in the two chemistries. As such, geochemical modeling and detailed discussion of the evolution of ground-water geochemistry with time was restricted to the Second Cat Creek sandstone in the eastern Judith Basin, where the availability of analyses allows such a treatment. Locations of these twelve wells, determined to be perforated in the Second Cat Creek sandstone, are plotted in figure 6. Analyses derived from the literature do not include accurate field pH and alkalinity determinations required for geochemical investigations, and were therefore used primarily as an aid to mapping major element variations.

Maps showing the chemical properties of ground waters in the Second Cat Creek sandstone reveal systematic variations in the concentrations of major elements. The dissolved solids distribution, plotted in figure 7, reveals a gradual increase from recharge areas in the Big Snowy and Judith Mountains north and westward into the basin, as would be expected if mineral dissolution or leakage of highly mineralized waters was occurring along the flow path. The increase in dissolved solids is greater to the north of Big Spring Creek than to the south, suggesting that different mechanisms may control dissolved solids concentrations on either side of the creek. In addition, where the aquifer outcrops on the flanks of the South Moccasin Mountains, recharge would be expected, but low dissolved solids waters of the type sampled in the recharge areas to the south and east are not evident. The absence of low dissolved solids waters suggests that net recharge to the aquifer may be negligible near the South Moccasin Mountains.

Separating the dissolved solids data into its major element components, the relative contributions of major cations and anions to the general increase can be observed. Areal variations in major element concentrations are plotted in figure 8 in the form of Stiff diagrams (Stiff, 1951), which portray cationic and anionic concentrations on three horizontal axes extending to either side of a vertical zero axis. The Stiff diagrams show gradual, uniform increases in sodium plus potassium, chloride, and bicarbonate plus carbonate along the flow path. Calcium and magnesium decrease in concentration basinward. Only sulfate displays significantly different behavior on either side of Big Spring Creek, accounting for the high in dissolved solids near the South Moccasin Mountains. South of the creek, sulfate concentrations increase gradually but remain at low levels, whereas north of the creek, they increase dramatically over a short distance. A trilinear plot of major element concentrations (fig. 9) clearly shows the divergence of compositions between flow paths along the north and south sides of Big Spring Creek.

Uniform increases in sodium with concurrent decreases in calcium and magnesium concentrations are almost certainly indicative of ion-exchange phenomena.

waters from the Kootenai Formation, Judith Basin, Montana

per liter. <indicates concentrations below detection limit for that analysis]

Lithium, Li	Manganese, Mn	Molybdenum, Mo	Nitrite plus nitrate, $NO_2 + NO_3$ (mg/L, as nitrogen)	Organic carbon, C (mg/L)	Phosphate, PO_4 (mg/L as phosphorus)	Selenium, Se	Silica, SiO_2 (mg/L)	Strontium, Sr	Sulfide (mg/L as hydrogen sulfide)	Uranium, U	Vanadium, V	Zinc, Zn
4	<1	<10	<0.01	0.8	0.01	<1	---	<1	0.9	<0.01	<1	<3
70	40	<10	<.01	7	<.01	<1	9.7	1,100	1	16	<1	840
40	80	<10	<.01	2.6	<.01	<1	6.4	1,500	2	13	<1	30
20	80	<10	<.01	2.5	<.01	<1	6.6	1,300	<1	.07	<1	50
50	110	<10	<.01	3.5	<.01	<1	8.8	3,300	<1	1.8	<1	70
70	30	<10	<.01	.2	<.01	<1	8.8	1,300	<1	.09	<1	130
20	<1	<10	3.3	7.4	.04	<1	10	730	2	70	1	70
40	10	<10	<.01	3.3	<.01	<1	7.4	1,400	<1	1.0	<1	130
130	4	<10	<.01	1.1	<.01	<1	8.8	780	<1	1.6	<1	70
120	2	<10	.06	1.0	.02	<1	8.7	870	<1	2.0	<1	30
60	20	<10	<.01	.9	.01	<1	7.8	2,100	<1	---	<1	8
90	4	<10	<.01	.3	.01	<1	9.0	270	<1	1.8	<1	30
50	3	<10	<.01	3.6	.02	<1	7.1	250	3	.11	<1	<3
140	20	<10	.05	.3	<.01	<1	8.1	1,100	4	1.4	<1	40

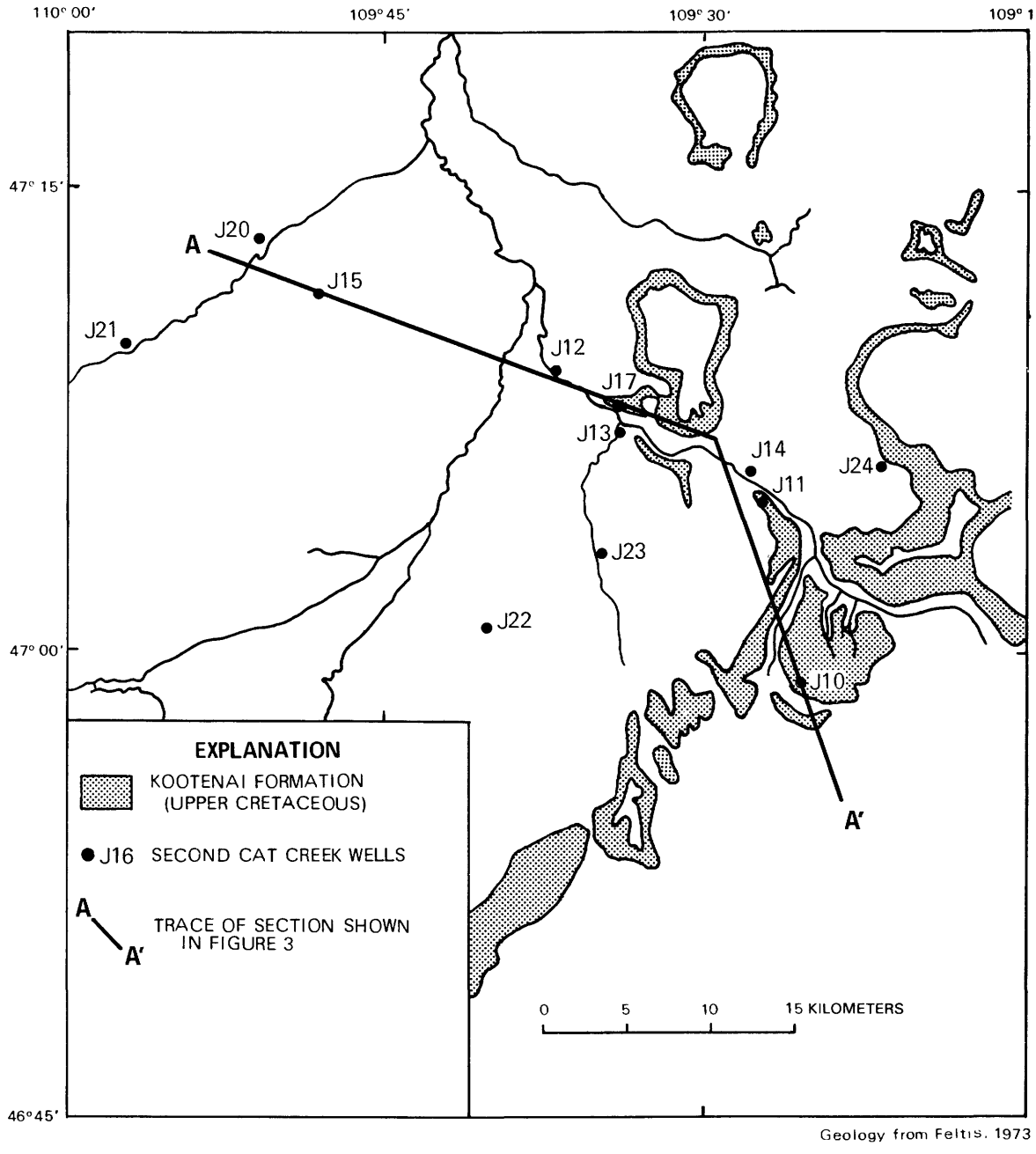

FIGURE 6.—Index map of eastern Judith Basin study area, Montana, showing locations of wells sampled in the Second Cat Creek sandstone of the Kootenai Formation and line A-A′ of geologic section in figure 3.

The log ratio of the molalities of exchangeable divalent and monovalent cations (log/ ([Ca]+[Mg])/[Na]²), an operational parameter plotted in figure 10, demonstrate the progressive nature of the exchange reacions (table 1, reactions 28 and 29) in the aquifer. The progression from positive to negative log ([Ca]+[Mg])/[Na]² values serves to identify areas of recharge and directions of flow in the system.

Either illite or kaolinite may serve as the ion-exchange medium. Because the cation-exchange capacity is several times greater in illite (10–40 meq/100 g (milliequivalents per 100 grams)) than kaolinite (3–15 meq/100 g), illite is probably the dominant exchanger, adsorbing a much greater reservoir of exchangeable sodium than kaolinite. Ferric oxyhydroxides, which are abundant in the Kootenai, have a pH_{zpc} of approximately 6.7 to 8.5, or close to the ground-water pH, indicating that the surfaces of these particles are nearly neutral, and should have minimal exchange capacities.

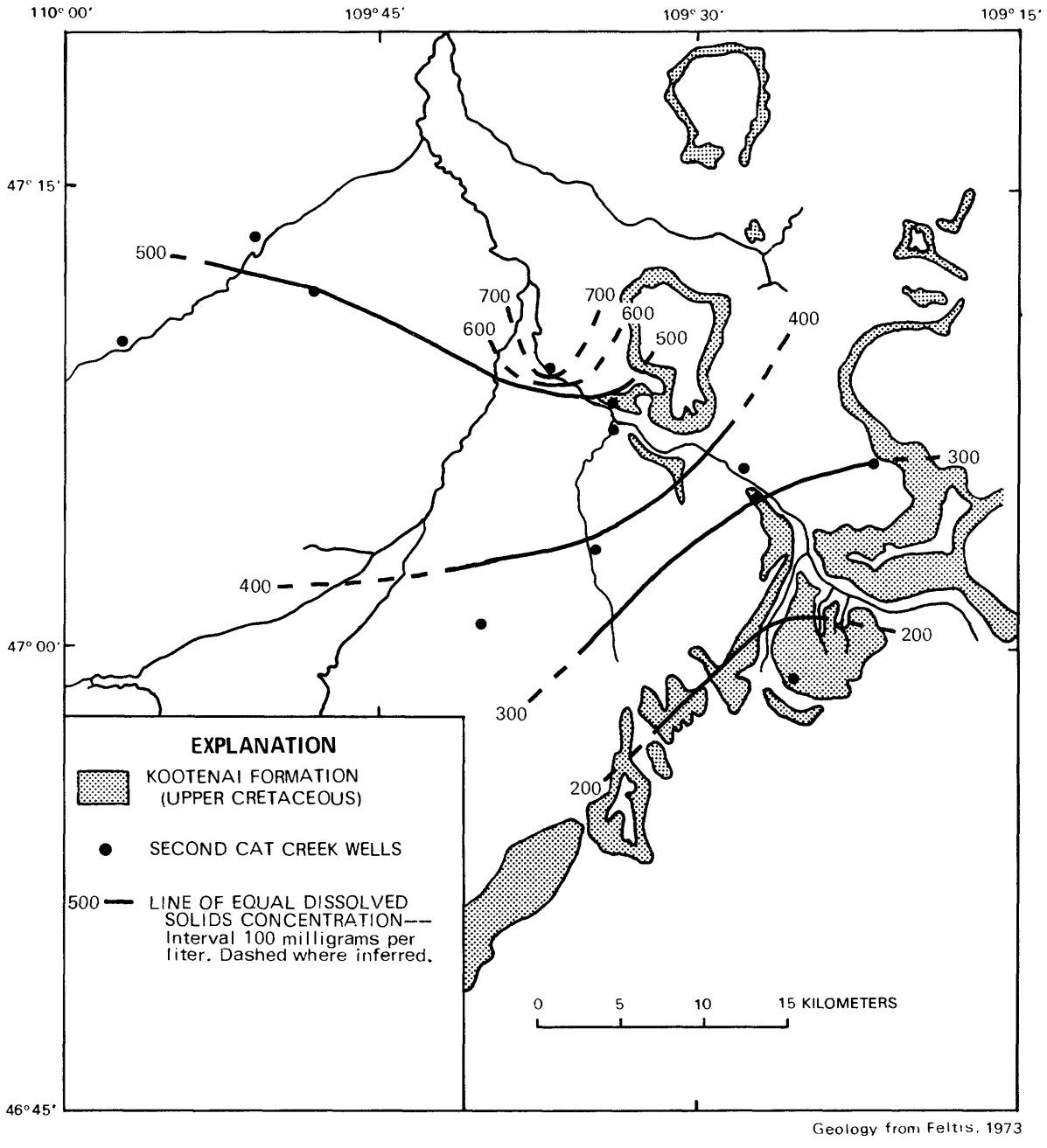

FIGURE 7.—Dissolved solids concentration in waters from the Second Cat Creek sandstone of the Kootenai Formation, eastern Judith Basin, Montana.

Subtle increases in chloride concentration are probably due to leaching of confining layers or leakage from adjacent aquifers. Chloride minerals, such as halite (NaCl) and sylvite (KCl), are commonly associated with sedimentary rocks, but the absence of any marine evaporite sequences in the Kootenai preclude the use of these minerals as a significant chloride source. High chloride waters are commonly associated with shales, and leaching of shale confining beds could readily supply the required amounts of chloride (Johns and Huang, 1967; Billings and Williams, 1967). Similarly, upward leakage of high chloride waters through faults and fractures could transport chloride into the aquifer. Slightly larger increases in chloride concentrations north of Big Spring Creek may reflect differences in controlling mechanisms.

As shown in figure 11, sulfate concentrations also behave differently on either side of Big Spring Creek, suggesting some type of structural controls on groundwater chemistry. The most likely sources of sulfate

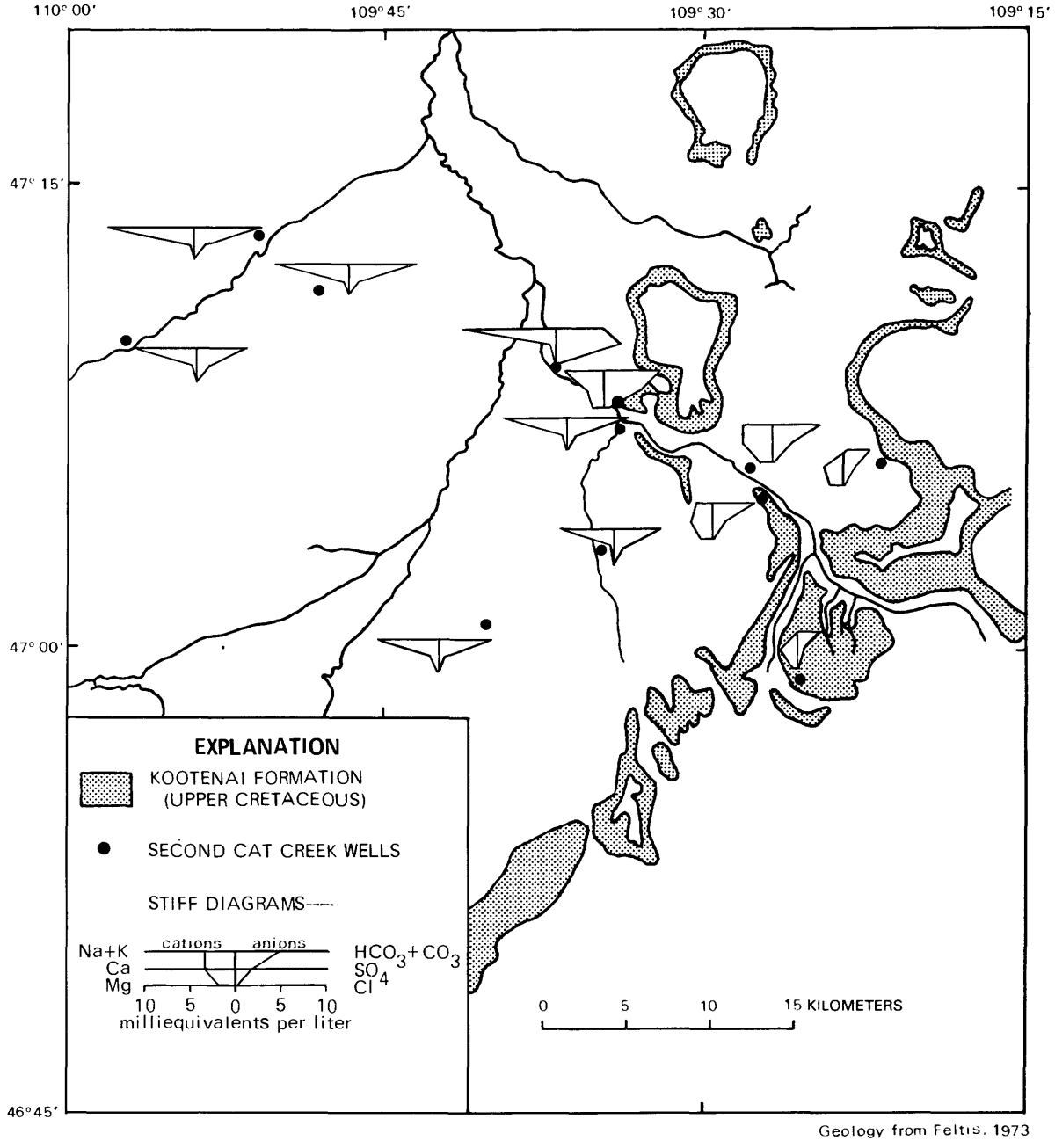

FIGURE 8.—Stiff diagrams for major element concentrations in waters from the Second Cat Creek sandstone of the Kootenai Formation, eastern Judith Basin, Montana.

within the aquifer would be the dissolution of trace amounts of gypsum (reaction 20) or the oxidation of pyrite (reactions 9 and 10), which can proceed in either the presence or absence of molecular oxygen. Either or both of these mechanisms could explain the gradual increases in sulfate observed to the south of Big Spring Creek, as both gypsum and pyrite are commonly found disseminated in shales, but the highly disparate sulfate concentrations on either side of the creek implies the influence of different controls to the north. The occurrence of numerous faults and fractures in the area of the Judith and South Moccasin Mountains (as shown in fig. 2), suggests the possibility of upward migration of high sulfate waters from underlying formations. Analytical data for Morrison and Madison Formation waters typical of the Judith Basin, (presented in table 8) indicate sulfate concentrations several times higher than those measured in waters from the overlying Kootenai Formation. Feltis (1973) commented on the importance of fractures in the Big Snowy, Judith, and North and South

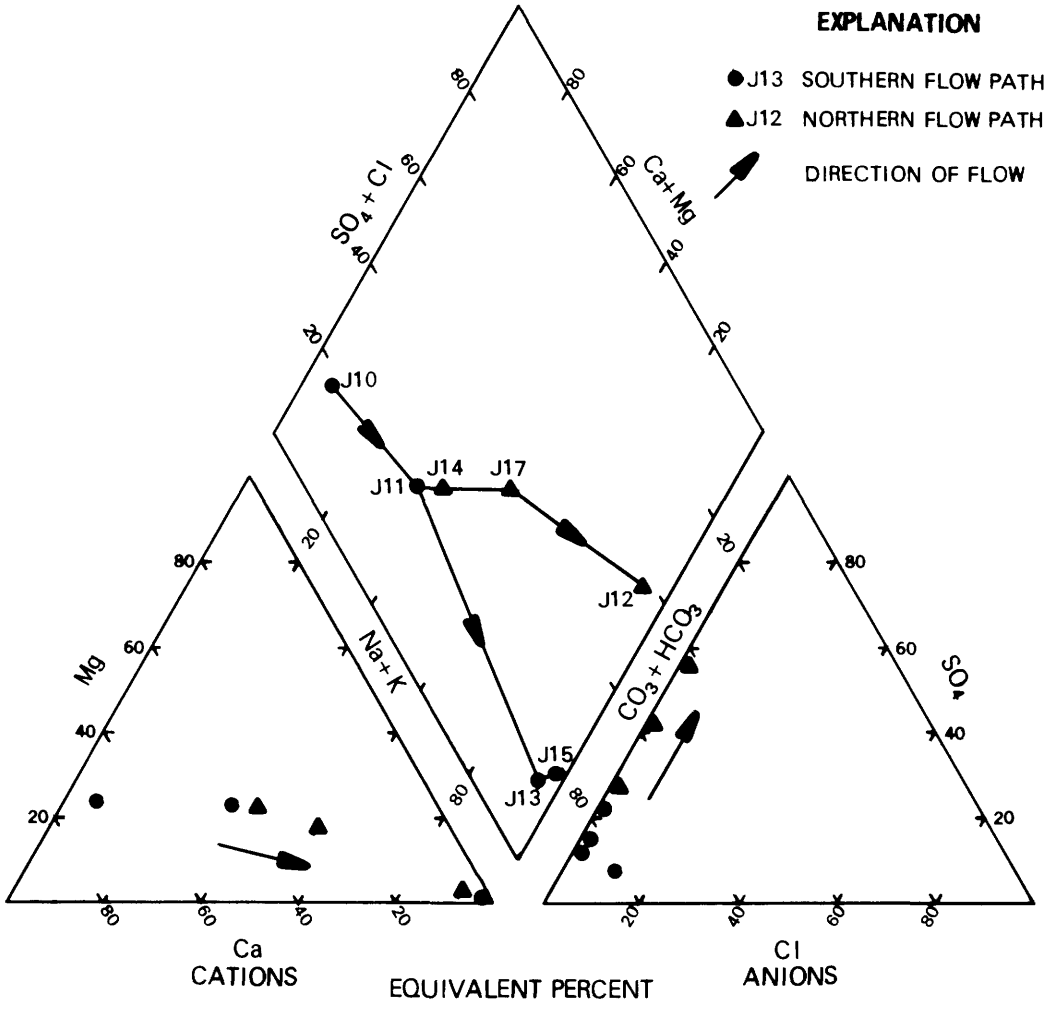

FIGURE 9.—Trilinear diagram showing divergence in composition between water samples taken north and south of Big Spring Creek from the Second Cat Creek sandstone of the Kootenai Formation, eastern Judith Basin, Montana.

Moccasin Mountains region in localizing discharge from these lower formations as springs. This type of fracture-controlled discharge could also serve as hidden recharge to the Kootenai Formation, and would explain the presence of high sulfate waters in the fractured areas. Chloride concentrations are also higher in the underlying aquifers, so leakage would also explain slightly higher chloride concentrations north of the creek. Waters of the Kootenai Formation to the north and south of Big Spring Creek might be isolated from each other by the synclinal structure observed in outcrop and subsurface. Hinge faults and fractures would allow Kootenai Formation ground water to move upward and discharge into the stream bed alluvium, creating distinct flow systems on either side of the creek.

Significant increases in pH are also evident along the flow paths, as shown by the transect along line A–A′ in figure 12. Two reactive mineral groups, carbonates (reactions 21–23) and aluminosilicates (reactions 24–27) could interact with ground waters of the Kootenai and increase the pH. Assuming that the dissolution of these minerals is driven by the dissolution of CO_2 and the subsequent dissociation of $H_2CO_3^0$, the hydrolysis of aluminosilicates will result in an increase in pH but no increase in C_T beyond that contribution supplied by the addition of CO_2. However, when driven by the same mechanism, both congruent and incongruent dissolution of carbonates will result in an increase in pH accompanied by an increase in C_T above and beyond that supplied by the addition of CO_2, thus serving to distinguish between these two groups of dissolution reactions.

Because the relative concentrations of $H_2CO_3^0$, HCO_3^-, and CO_3^{-2} are dependent on the pH of the solution (reactions 17–19) apparent increases in HCO_3^- and CO_3^{-2} may be due to increases in pH accompanied by dissociation of $H_2CO_3^0$, rather than to actual increases in dissolved carbonate species. Calculation of total inorganic carbon (C_T) clarifies this point, in that C_T data reveal whether or not

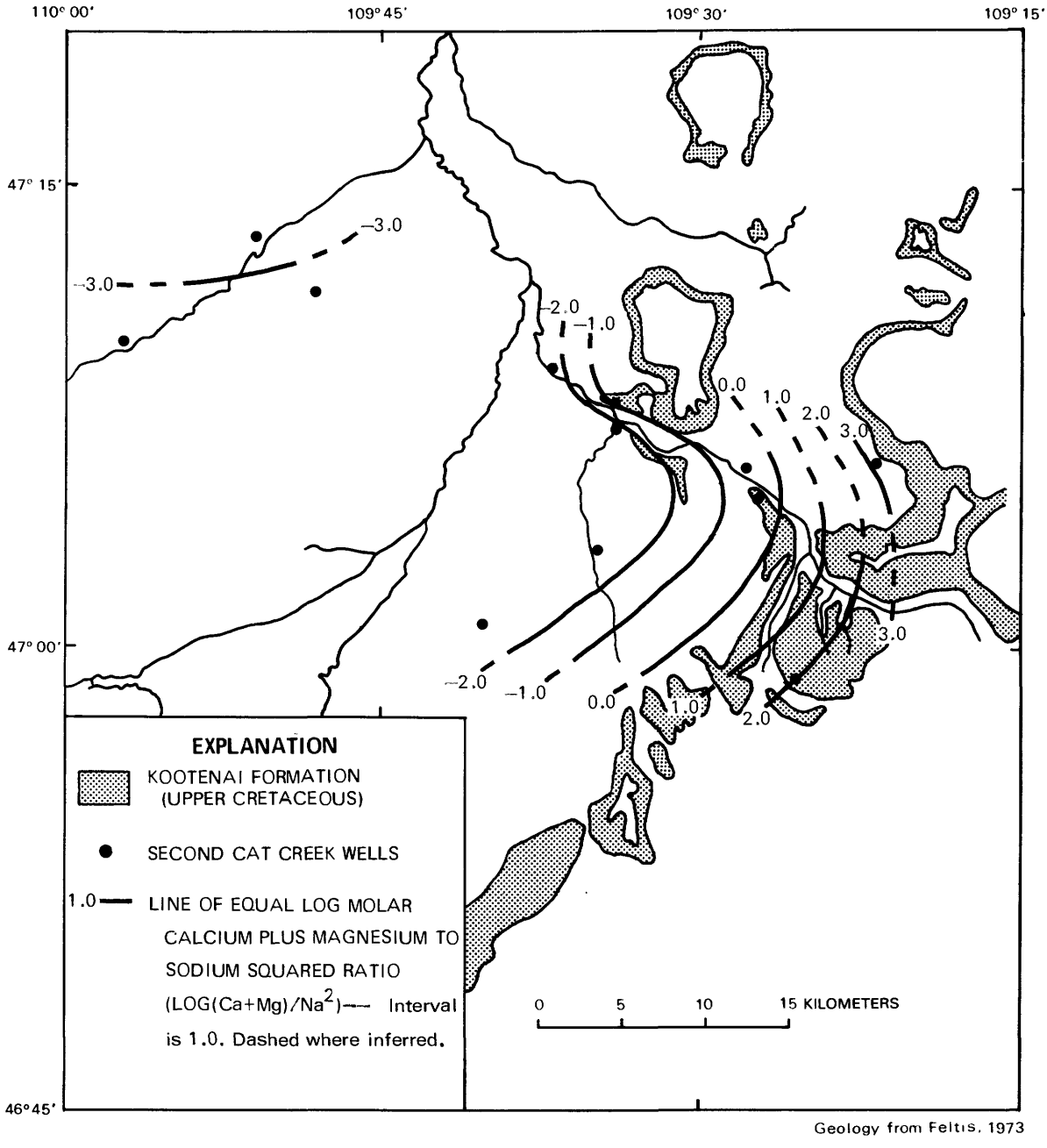

FIGURE 10.—Log molar ratios of calcium plus magnesium to sodium concentrations in waters from the Second Cat Creek sandstone of the Kootenai Formation, eastern Judith Basin, Montana.

an increase in alkalinity is solely the effect of an increase in pH. The aqueous speciation model of WATEQ2 (Ball and others, 1980) was utilized to calculate the distribution of carbonate species from major element, pH, alkalinity, and temperature data. All of the carbonate species were then summed to determine C_T. A transect along line A-A′ in figure 13 demonstrates that C_T generally increases downflow, although a small decrease may be noted north of Big Spring Creek. The observed increases in C_T reflect the presence of carbon sources in the aquifer. Carbon may enter the aqueous system through the oxidation of organic matter during the reduction of oxygen (reaction 1), nitrate (reactions 2 and 3), and (or) sulfate (reaction 6), or during the fermentation of organic matter (reaction 7). Dissolution of carbonate minerals (reactions 21-23) and the migration of gaseous CO_2 (reaction 17) or CH_4 (reaction 11) may also increase C_T.

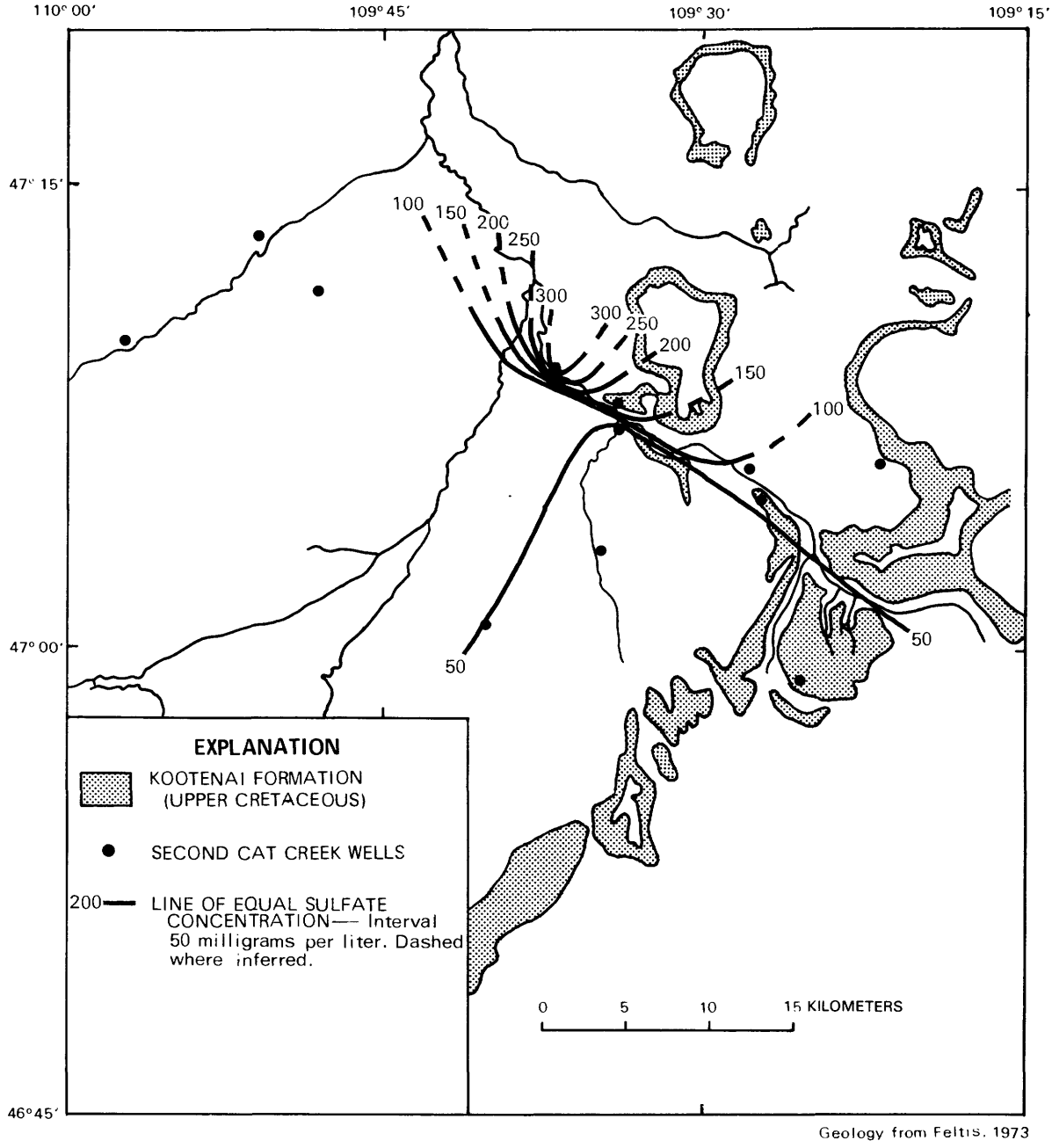

FIGURE 11.—Sulfate concentrations in waters from the Second Cat Creek sandstone of the Kootenai Formation, eastern Judith Basin, Montana.

Acetate fermentation is not a viable mechanism, because the Eh of the system is far too high for this reaction to proceed. The oxidation of organic carbon provides a more feasible carbonate source. Reduction of O_2 and NO_3^- supplies significant quantities of CO_2 ($\geq$0.54 mmol/L) to oxygenated waters, but the rapid consumption of these oxidants and the absence of H_2S in the Second Cat Creek sandstone suggests that the oxidation of organic carbon by O_2, NO_3^-, or SO_4^{-2} does not generate significant quantities of CO_2 far beyond the outcrop area. Sulfate reduction or the coalification of lignite may produce high CO_2 partial pressures (P_{CO_2}) in Morrison or Kootenai strata adjacent to the Second Cat Creek sandstone. The uncharged nature of $CO_{2(aq)}$ and $H_2CO_3^0$ would allow these species to diffuse through microfractures and between clay particles of the shale confining beds into aquifers with lower CO_2 partial pressures, whereas the bulk of any H_2S produced by sulfate reduction would be precipitated in situ as ferrous sulfides. Well J16 appears to be screened in the

TABLE 8.—*Chemical compositions of ground water from aquifers underlying the Kootenai Formation, Judith Basin area, Montana*

[Units in milligrams per liter unless otherwise noted, °C, degrees Celsius]

Formation	Calcium, Ca	Magnesium, Mg	Sodium, Na	Potassium, K	Bicarbonate, HCO_3	Sulfate, SO_4	Chloride, Cl	pH	Temperature, T (°C)	Dissolved solids	Comments
			Na + K								
Morrison	5.9	1.6	380	3.0	448	480	12	8.0	24.5	1,330	Grassrange, Montana [1]
Morrison	6.8	1.8	370	3.0	400	480	11	8.0	15.0	1,275	Grassrange, Montana [1]
Madison	202	52	22		196	549	9	---	---	1,030	Judith Basin composite [2]
Madison	130	40	3.6	1.0	200	330	2.4	7.4	19.6	710	Vanek Warm Spring [3]

[1]Collected by the U.S. Geological Survey from wells located about 45 kilometers due east of Lewistown

[2]Mean composition of eight samples taken within the Judith Basin. Analyses from Zimmerman (1966) and Feltis (1973)

[3]Site 9 from Busby and others (U.S. Geological Survey, written commun., 1981).

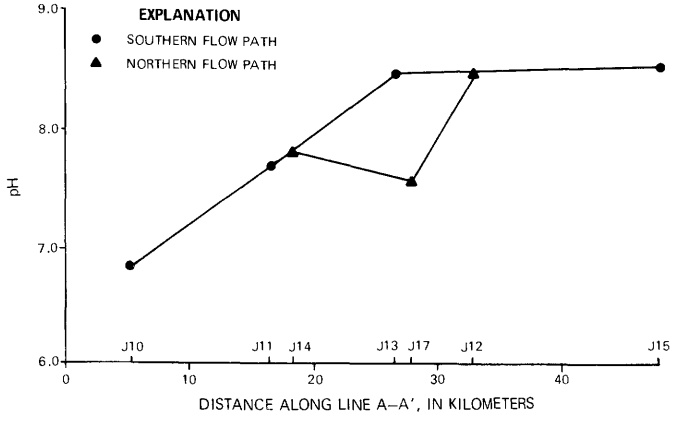

FIGURE 12.—Variations in pH along line A-A' in waters from the Second Cat Creek sandstone of the Kootenai Formation, eastern Judith Basin, Montana.

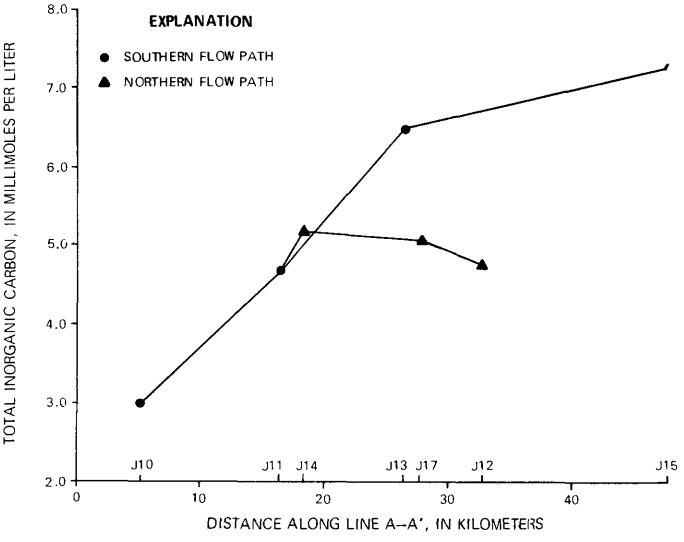

FIGURE 13.—Variations in total inorganic carbon concentrations along line A-A' in waters from the Second Cat Creek sandstone of the Kootenai Formation, eastern Judith Basin, Montana.

Third Cat Creek sandstone and draws water from a zone whereas H_2S is evident. Sulfate is nearly depleted, and C_T and organic carbon are much higher than in wells of the Second Cat Creek sandstone, suggesting the active oxidation of organic matter by sulfate reducing bacteria. Similar CO_2 partial pressures in this and surrounding samples, despite large differences in pH, may indicate that the aquifers in the formation are at a state of equilibrium with respect to dissolved gaseous species, and that CO_2 might indeed be free to migrate from organic-rich to organic-poor zones within the formation.

Migration of CO_2 into the aquifer would increase the acidity of waters present and allow for dissolution of carbonate minerals, which would further increase C_T. The stabilities of calcite, dolomite, and magnesite ($MgCO_3$) in ground waters of the Kootenai Formation may be investigated by calculating the stability fields of these minerals in the system Ca-Mg-CO_2-H_2O. An activity diagram constructed using the data of Ball and others (1980) is presented in figure 14, with compositions of Kootenai Formation ground waters superposed. Calcite is clearly the stable phase, indicating that any dolomite in contact with these waters should dissolve, possibly in an incongruent reaction to form calcite (reaction 23).

Potassium and silica concentrations were nearly constant in waters of the Second Cat Creek sandstone; potassium averaged 3.2 mg/L (milligrams per liter) and silica averaged 8.6 mg/L, while aluminum was below de-

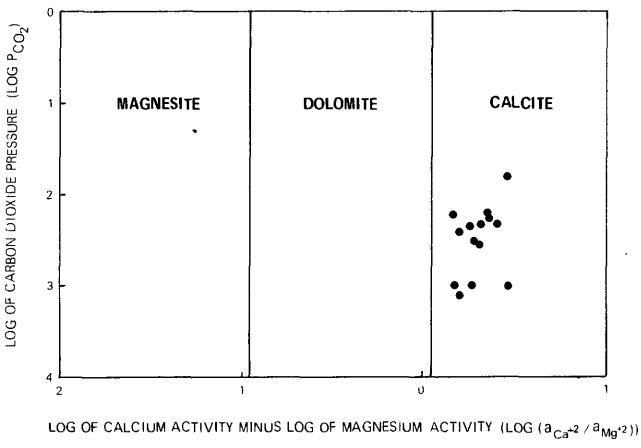

FIGURE 14.—Stability diagram for the system Ca-Mg-CO_2-H_2O at 25°C, with compositions of waters from the Kootenai Formation, Judith Basin, Montana, superposed.

tection (<15 μg/L) in all waters sampled. The silica concentration in sample J2 is anomalously low (0.0 mg/L), probably due to analytical error, and has been discarded. Despite the lack of aluminum data, the stabilities of pertinent aluminosilicates in Kootenai ground waters may be investigated using cation ratio activity diagrams. With thermodynamic data from Helgeson (1969) and an average silica activity of $10^{-3.87}$, the stabilities of illite, kaolinite, montmorillonite, and chloride may be calculated in terms of log $[(a_{Mg^{+2}})/a_{H^+})^2]$ and log $[(a_{K^+})/(a_{H^+})]$. Superposition of Kootenai geochemical data on this stability diagram (fig. 15) shows that kaolinite is the stable phase in all waters sampled. The stability of kaolinite reported by Helgeson (1969) was several kilojoules per mole less than the preferred kaolinite stability value of Bassett and others (1979). Recalculation of the relative stabilities of these aluminosilicates using the reevaluated kaolinite stability results in shifting the illite-kaolinite stability boundary downward into the area of observed compositions, but also creates a stability field for Mg-montmorillonite between that of chlorite and kaolinite (fig. 16). Montmorillonite was not observed in Kootenai shales obtained near the Judith Basin. An increase in illite stability, or further decrease in kaolinite stability (which would still fall within the range of values presented by Bassett and others, 1979) would shift the illite-kaolinite stability boundary downward without enlarging the Mg-montmorillonite field. This final interpretation is consistent with field evidence, although the slight, but highly significant, variability in aluminosilicate stabilities due to variable crystallinity and composition of the pertinent phases renders any conclusions drawn for a particular system highly tentative, and subject to revision as better data for that system become available.

Strontium increases, then decreases in concentration along the Second Cat Creek sandstone flow path (fig. 17). Similar behavior is observed for calcium and magnesium, suggesting similar controls for these alkaline

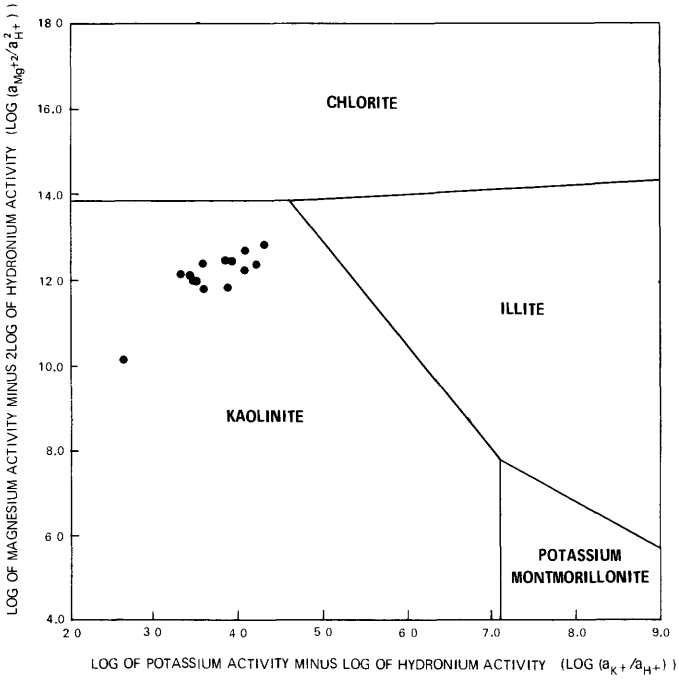

FIGURE 15.—Stability diagram for the system Mg-K-SiO_2-Al_2O_3-H_2O at 25°C, with compositions of waters from the Kootenai Formation, Judith Basin, Montana, superposed. Thermodynamic data from Helgeson (1969). $a_{H_4SiO_4^0}=10^{-3.87}$.

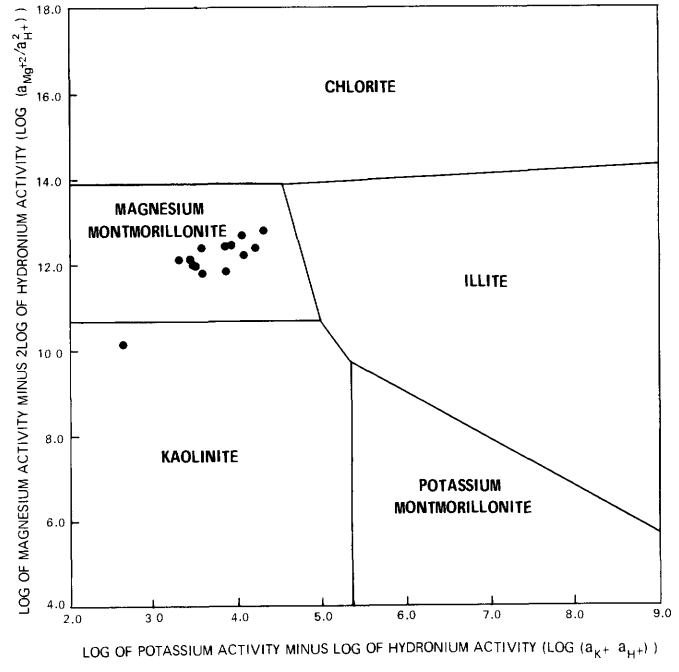

FIGURE 16—Stability diagram for the system Mg-K-SiO_2-Al_2O_3-H_2O at 25°C, with compositions of waters from the Kootenai Formation, Judith Basin, Montana, superposed. Thermodynamic data for kaolinite from Bassett and others (1979). Remaining thermodynamic data from Helgeson (1969). $a_{H_4SiO_4^0}=10^{-3.87}$.

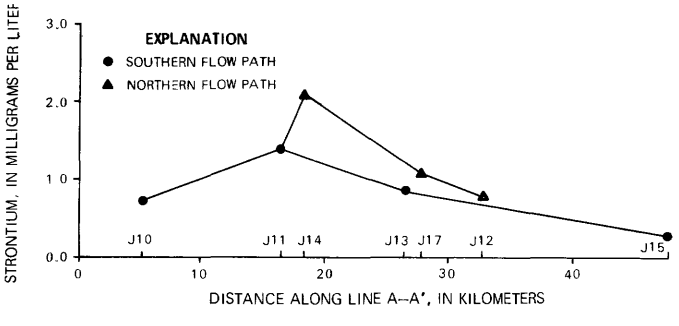

FIGURE 17.—Variations in strontium concentrations along line A-A' in waters from the Second Cat Creek sandstone of the Kootenai Formation, eastern Judith Basin, Montana.

earth elements. The importance of ion exchange in controlling calcium and magnesium levels has already been discussed, and similar controls would be equally effective in producing the observed variations in strontium concentrations (Wahlberg and others, 1965a; 1965b). Strontium might originate from the dissolution of disseminated strontianite ($SrCO_3$) or celestite ($SrSO_4$), which could be present in the aquifer or in confining shale beds, although there is little evidence for the existence of these phases. Strontium may coprecipitate with calcite (Holland and others, 1964), aragonite (Kinsman and Holland, 1969), gypsum or anhydrite (Usdowski, 1973), and would thus be released into the ground-water system upon dissolution of these phases. A positive correlation of greater than 99 percent significance (r=0.716, n=15) was calculated between sulfate and strontium concentrations, so it seems probable that strontium originates from the dissolution of gypsum, which could occur either within the aquifer or in adjacent strata where these phases are present.

Oxidation potential was estimated using the Nernst equation and appropriate redox couples (reactions 12-16); Eh values calculated in this manner are presented in table 9. Eh values in the Second Cat Creek sandstone range from 850 mV in the recharge area to approximately −100 mV for wells farthest from the outcrop (J12, J15) with a minimum of −210 mV (J17) near the South Moccasin Mountains (fig. 18). A general decrease in oxidation potential is indicated, from oxidizing conditions in the recharge area to relatively uniform, moderately reducing conditions a short distance from the outcrop and into the basin. The one highly reducing sulfidic water sampled near the South Moccasin Mountains appears somewhat anomalous. Strongly reducing conditions at J17 may be associated with the presence of faults related to the South Moccasin Uplift. Fluids containing reduced species such as H_2S and CH_4 would be free to migrate upward from lower strata along fracture zones, creating locally reducing conditions where they enter other formations. Alternatively, well J17 may penetrate a zone particularly rich in organic material, which would allow for the biologically mediated reduction of sulfate (Goldhaber and Kaplan, 1974). Failure of the remainder of Second Cat Creek sandstone waters sampled to attain strongly reducing conditions is likely due to a paucity of organic matter suitable as a substrate for sulfate reducing bacteria (Dockins and others, 1980).

Dissolved organic carbon (DOC) concentrations support this conclusion, decreasing rapidly down the flow path and leveling off at an average value of 0.7± 0.4 mg/L (fig. 18). Consumption of DOC during the reduction of O_2 and NO_3^- accounts for the initial DOC decrease. A lack of solid organic matter in the aquifer would prevent further reduction from occurring.

TABLE 9.—*Oxidation potentials calculated for waters from the Kootenai Formation, Judith Basin, Montana, using* O_2-H_2O, $Fe(OH)_{3(am)}$-$FeCO_3$ *or* SO_4^{-2}-H_2S *redox couples*

[O_2, oxygen, H_2O, water, $Fe(OH)_{3(am)}$, ferric hydroxide; $FeCO_3$, siderite, SO_4^{-2}, sulfate; H_2S, hydrogen sulfide; mV, millivolts]

Sample	Calculated Eh (mV)	Redox couple
J2	−230	SO_4^{-2}-H_2S
J3	−214	SO_4^{-2}-H_2S
J4	−207	SO_4^{-2}-H_2S
J5	44	$Fe(OH)_{3(am)}$-$FeCO_3$
J6	51	$Fe(OH)_{3(am)}$-$FeCO_3$
J8	−1	$Fe(OH)_{3(am)}$-$FeCO_3$
J10	848	O_2-H_2O
J11	38	$Fe(OH)_{3(am)}$-$FeCO_3$
J12	−101	$Fe(OH)_{3(am)}$-$FeCO_3$
J13	−62	$Fe(OH)_{3(am)}$-$FeCO_3$
J14	23	$Fe(OH)_{3(am)}$-$FeCO_3$
J15	−77	$Fe(OH)_{3(am)}$-$FeCO_3$
J16	−283	SO_4^{-2}-H_2S
J17	−214	SO_4^{-2}-H_2S

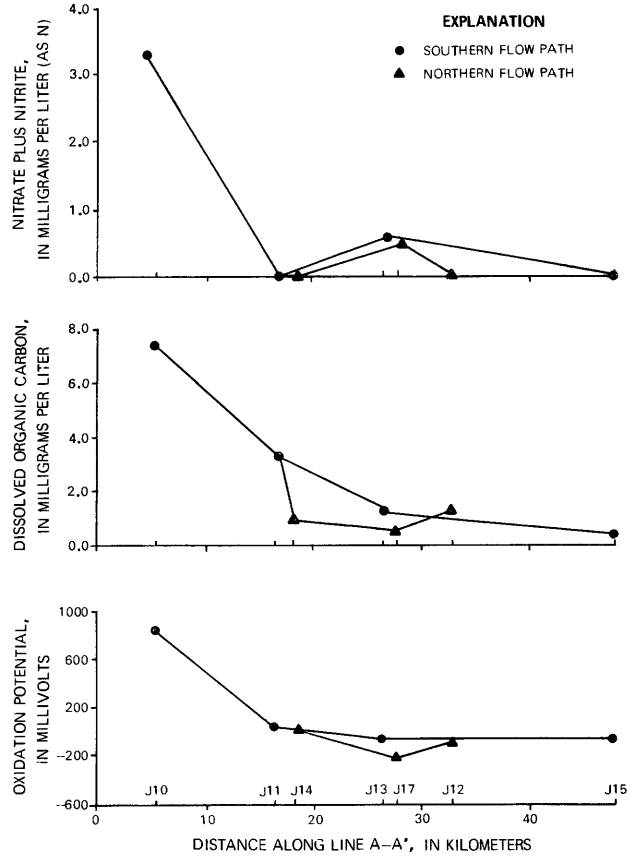

FIGURE 18.—Variations in calculated oxidation potential, nitrate plus nitrite, and dissolved organic carbon concentrations along line A-A' in waters from the Second Cat Creek sandstone of the Kootenai Formation, eastern Judith Basin, Montana.

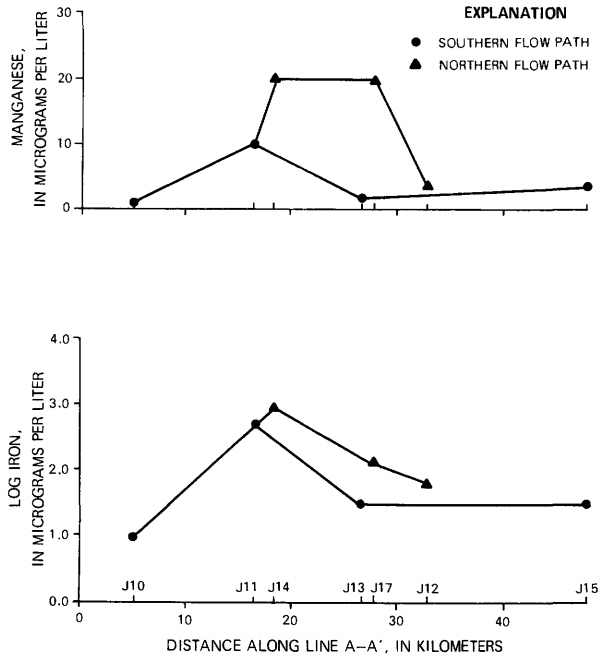

FIGURE 19.—Variations in iron and manganese concentrations along line A–A' in waters from the Second Cat Creek sandstone of the Kootenai Formation, eastern Judith Basin, Montana.

Iron and manganese determinations indicate initially low concentrations of these elements in oxygenated outcrop waters, increasing following the onset of anoxic conditions, then gradually decreasing again (fig. 19). The presence of ferric oxyhydroxides and siderite suggests control of iron concentrations by these phases in oxidizing and moderately reducing waters (Langmuir, 1969; Nordstrom and others, 1979; Champ and others, 1979). Where H_2S is present, ferrous sulfides might similarly control aqueous iron concentrations.

Oxyhydroxide and carbonate solid phases are similarly observed to control manganese concentrations with decreasing Eh (Morgan, 1967). Regulation of manganese by mineral phases similar to those that control iron would explain the covariation in concentration of these two elements as Eh decreases, with oxyhydroxides controlling in oxidizing environments, siderite or rhodochrosite ($MnCO_3$) in moderately reducing environments, and ferrous sulfides in strongly reducing waters (Champ and others, 1979).

DISSOLVED GASES

Interpretation of dissolved gas concentrations was hindered by difficulties encountered during sampling. Many of the waters sampled were highly effervescent as they flowed from the well head, and gas bubbles invariably accumulated on the walls of the sample vessel. Although efforts were made to dislodge as many as possible, many samplers contained some attached bubbles, leading to analytical concentrations greater than the quantity of gas actually dissolved in the sample. Those samples displaying evidence of contamination of this type, such as anomalously high concentrations of N_2(>40 mg/L), Ar(>1 mg/L), and O_2, or field observations of bubbles, were discarded. Because of this difficulty in sampling, the data presented in table 10 are considered only semiquantitative. Discussion of these analyses will be restricted to the observed concentration trends, and to comparisons with the same parameters calculated by other methods. The analyses presented in table 10 are all from the southern flow path of the Second Cat Creek sandstone and are arranged in order of occurrence from outcrop to basin.

Oxygen decreases down the flow path because of decreasing Eh and carbon dioxide decreases down the flow path because of increasing pH. Agreement between these dissolved oxygen values and those measured in the field is relatively good, differing by a maximum of only 7 percent; however, a comparison of analyzed P_{CO_2} and that calculated by WATEQ2 from field-measured pH and alkalinity shows discrepancies of up to 40 percent. Although part of these differences are possibly due to the gas sampling problem, they also reflect errors in pH created by exchange with atmospheric CO_2 during measurement. CO_2 outgassing would tend to make the measured pH higher than the actual in situ value due to the redistribution of HCO_3^- and CO_3^{-2} required to maintain equilibrium among dissolved carbonate species

TABLE 10.—*Concentrations and partial pressures of dissolved gases in water samples from the Second Cat Creek sandstone of the Kootenai Formation, eastern Judith Basin, Montana*

[mg/L, milligrams per liter; atm, atmospheres]

Sample	Oxygen		Carbon dioxide		Nitrogen		Argon		Helium		Methane	
	mg/L	atm	mg/L	atm	mg/L	atm	mg/L	atm	mg/L	atm	mg/L	atm
J10	7.2	0.12	55	0.022	20	0.79	0.80	0.010	0.000	0.000	0.00	0.0000
J13	.5	.009	3.4	.0016	31	1.33	1.09	.015	.002	.001	.02	.0006
J15	.03	.0006	2.7	.0013	31	1.39	1.13	.017	.003	.002	.02	.0006

(reactions 17-19). Using field-measured alkalinities, bicarbonate activity coefficients calculated using WATEQ2, and K_{CO_2} and K_1 [Henry's Law constant for CO_2 dissolution (reaction 17) and the first dissociation constant for $H_2CO_3^0$ (reaction 18), respectively] for the appropriate temperature (Jacobson and Langmuir, 1972), pH values may be calculated from the measured P_{CO_2}:

$$pH = -\log \frac{P_{CO_2} K_1 K_{CO_2}}{(a_{HCO_3^-})}.$$

Such values are given in table 11, and are as much as 0.18 pH units lower than the field-measured pH. These observations are inconsistent with those of Pearson and others (1978), who concluded that field-measured pH's may be as much as 0.2 units higher than pH values in the aquifer, again suggesting that difficulties in sampling have influenced these results.

Concentrations of nitrogen (N_2) indicate initial saturation with atmospheric N_2 in the recharge area (P_{N_2}=0.7 atm); N_2 values increase and then level off at higher concentrations down flow. Bacterially mediated denitrification (reaction 2), which should occur concurrently with O_2 reduction, would explain the decrease in NO_3^- plus NO_2^- and increase in N_2 between J10 and J13, as well as a leveling off of N_2 concentrations after nearly all of the NO_3^- has been consumed. Mass balance calculations indicate that the 0.24 mmol/L NO_3^- present in outcrop area waters is insufficient to account for the observed increase in N_2, however, suggesting that another mechanism may be responsible. Thorstenson and others (1979) postulate that high N_2 concentrations in the Fox Hills-basal Hell Creek aquifer of the Dakotas may be the result of upward leakage or diffusion of N_2 from gas pools at depth, but the presence of N_2 gas pools in the Judith Basin area is uncertain.

Helium, argon, and methane increase in concentration down the flow path. Helium is a product of radioactive decay by alpha emission, and probably accumulates in the ground water as a result of decay of unstable isotopes in the uranium and thorium decay series. Methane is thermodynamically unstable in waters with Eh's above −100 mV, such as samples J13 and J15, and could not have formed in the Second Cat Creek sandstone. Therefore, methane most likely migrated into the aquifer system after being formed in more reducing strata. According to Mazor (1972) argon should remain at concentrations that are representative of atmospheric saturation at the temperature of the recharge waters, but only if the aquifer system is closed to influx and efflux of this gas. The presence of argon in concentrations exceeding its maximum solubility at 0°C ($P_{Ar}=8.12\times10^{-3}$ atm at 1370 m elevation, 4.3×10^{-4} cubic centimeters Ar/cubic centimeter H_2O; Douglas, 1964) by nearly 40 percent suggests either migration of argon into the aquifer or contamination from sampling difficulties. Methane generation at depth might displace noble gases into higher strata where they would be able to accumulate (D. Fisher, U.S. Geological Survey, written commun., 1980); however, the above-mentioned sampling difficulties preclude the drawing of such conclusions.

TABLE 11.—*Comparison of field-measured pH values and pH values calculated from measured P_{CO_2} in water samples from the Second Cat Creek sandstone of the Kootenai Formation, eastern Judith Basin, Montana*

Sample	pH, field measured	pH, calculated	Difference
J10 ---------	6.87	6.69	0.18
J13 ---------	8.48	8.30	.18
J15 ---------	8.55	8.45	.10

ISOTOPIC COMPOSITION

The isotopic compositions of ground waters in the Kootenai Formation are presented in table 12. As shown in figure 20, $\delta^{18}O$ and δD measurements of ground waters from the Kootenai fall slightly below the worldwide meteoric water line of Craig ($\delta D=8\delta^{18}O+10$; 1961b), but roughly correspond to the composition of North American continental precipitation as reported by Gat (1980) ($\delta D=7.95\delta^{18}O+6.03$), indicating the presence of only meteoric water in the aquifer. Gat also reports the data of Yurtsever (1975), who has compiled $\delta^{18}O$ values for continental precipitation and correlated them with mean surface temperatures, allowing a determination of recharge temperature to be made. Kootenai $\delta^{18}O$ measurements range from −20.1 to −17.6, indicating a precipitation temperature near 0°C, which is significantly lower than the mean annual temperature of 6°C for the Judith Basin. This temperature discrepancy suggests that present-day recharge is derived primarily from spring snowmelt, rather than from late spring and early summer rains, and that past recharge events must have occurred under similar conditions. Although significant variability in both $\delta^{18}O$ and δD was observed, it does not seem readily attributable to differences in the aquifers sampled, and so is probably due to variations in the elevations of the Little Belt, Big Snowy, and Judith Mountain recharge areas.

Sulfate $\delta^{34}S$ measurements were obtained for all except two Judith Basin samples, but low concentrations of H_2S precluded the measurement of sulfide $\delta^{34}S$

TABLE 12.—*Isotopic ratios or activities of isotopes in waters from the Kootenai Formation, Judith Basin, Montana*

[pCi/L, picocuries per liter; < indicates concentrations below detection limit for that analysis]

Sample	Oxygen ($\delta^{18}O$)	Hydrogen (δD)	Carbon ($\delta^{13}C$)	Sulfur, SO_4^{-2} ($\delta^{34}S$)	Tritium (pCi/L)	Carbon-14 (percent modern)
J2	-18.8	-143	-16.6	20.6	1.0	<1.3
J3	-18.8	-143	-11.6	22.0	1.9	1.8
J4	-19.1	-148	-9.6	7.6	8.5	11.3
J5	-18.8	-146	-11.6	6.6	6.9	34.1
J6	-19.1	-145	-9.3	10.4	5.1	29.8
J8	-19.0	-147	-14.0	13.2	<2.9	1.3
J10	-18.2	-141	-16.0	.4	410	>98.8
J11	-20.0	-154	-10.2	3.3	5.3	18.4
J12	-18.0	-138	-7.1	11.9	6.5	<.8
J13	-18.2	-138	-7.9	---	<2.1	<.9
J14	-20.1	-154	-10.1	8.6	<4.3	10.0
J15	-17.6	-137	-9.4	2.6	<2.8	<.9
J16	-19.4	-149	-14.4	---	6.0	1.6
J17	-18.2	-139	-9.2	9.0	<2.2	<1.4

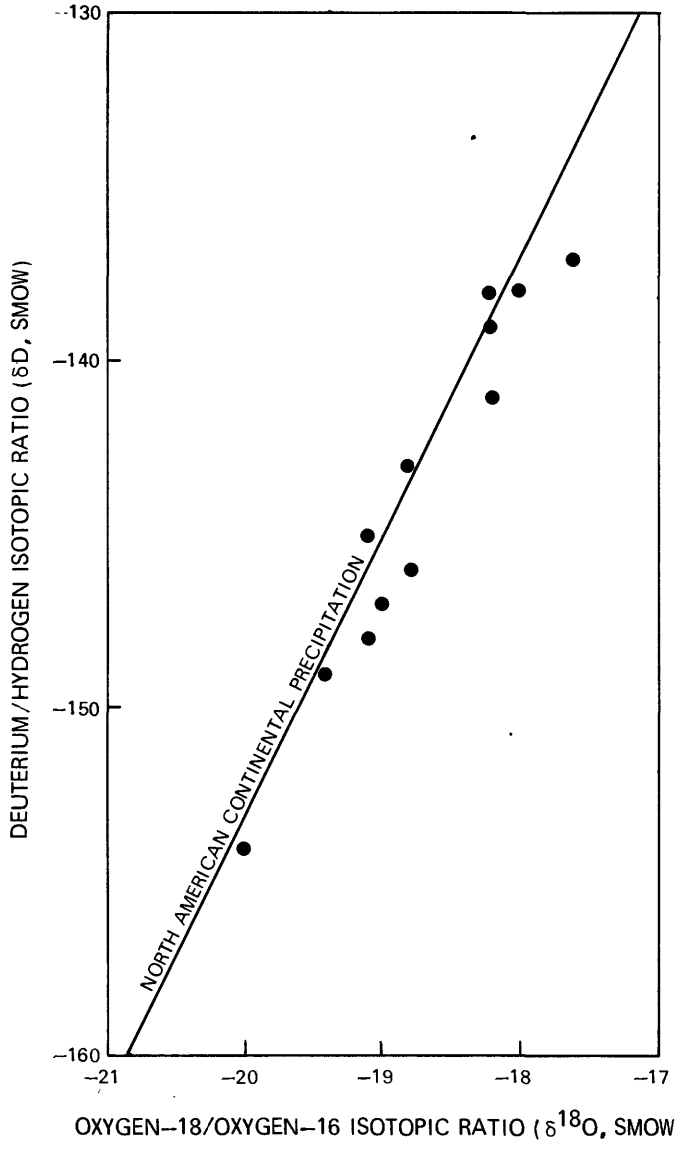

FIGURE 20.—Isotopic composition of North American continental precipitation (Gat. 1980) with isotopic compositions of waters from the Kootenai Formation, Judith Basin, Montana, superposed.

values. Sulfate $\delta^{34}S$ values exhibit considerable variations across Big Spring Creek, despite the close similarity of values for each group on either side of the creek, as shown in figure 21. A two-tailed F-test demonstrates that these two groups were derived from populations with a common variance at the 95 percent significance level, enabling a pooled standard deviation to be calculated. This calculation results in mean $\delta^{34}S$ values at the 95 percent significance level of 2.1 ± 3.2 for the southern population, and 9.8 ± 3.2 for the northern population. The difference in the means of the two populations is much greater than that predicted by a t-test for random variance at the 95 percent significance level, and demonstrates that the null hypothesis of no significant difference in the $\delta^{34}S$ values across Big Spring Creek must be rejected. Because $\delta^{34}S$ is dependent on the source of sulfate (Holser and Kaplan, 1966), it follows that sulfate is derived from significantly different sources on either side of the creek. Bacterial sulfate reduction, which would cause such increases in $\delta^{34}S$, might occur in only one well, J17, where H_2S was present, and so would not account for higher $\delta^{34}S$ values in all three wells near the South Moccasin Mountains. Differences in both the $\delta^{34}S$ values and the sulfate concentrations on either side of the creek support the hypothesis of structurally controlled leakage into the Second Cat Creek sandstone occurring in the fractured region north of Big Spring Creek, but not in the more competent strata to the south.

Waters of the Second Cat Creek sandstone exhibit $\delta^{13}C$ values that increase asymptotically from −16.0 at

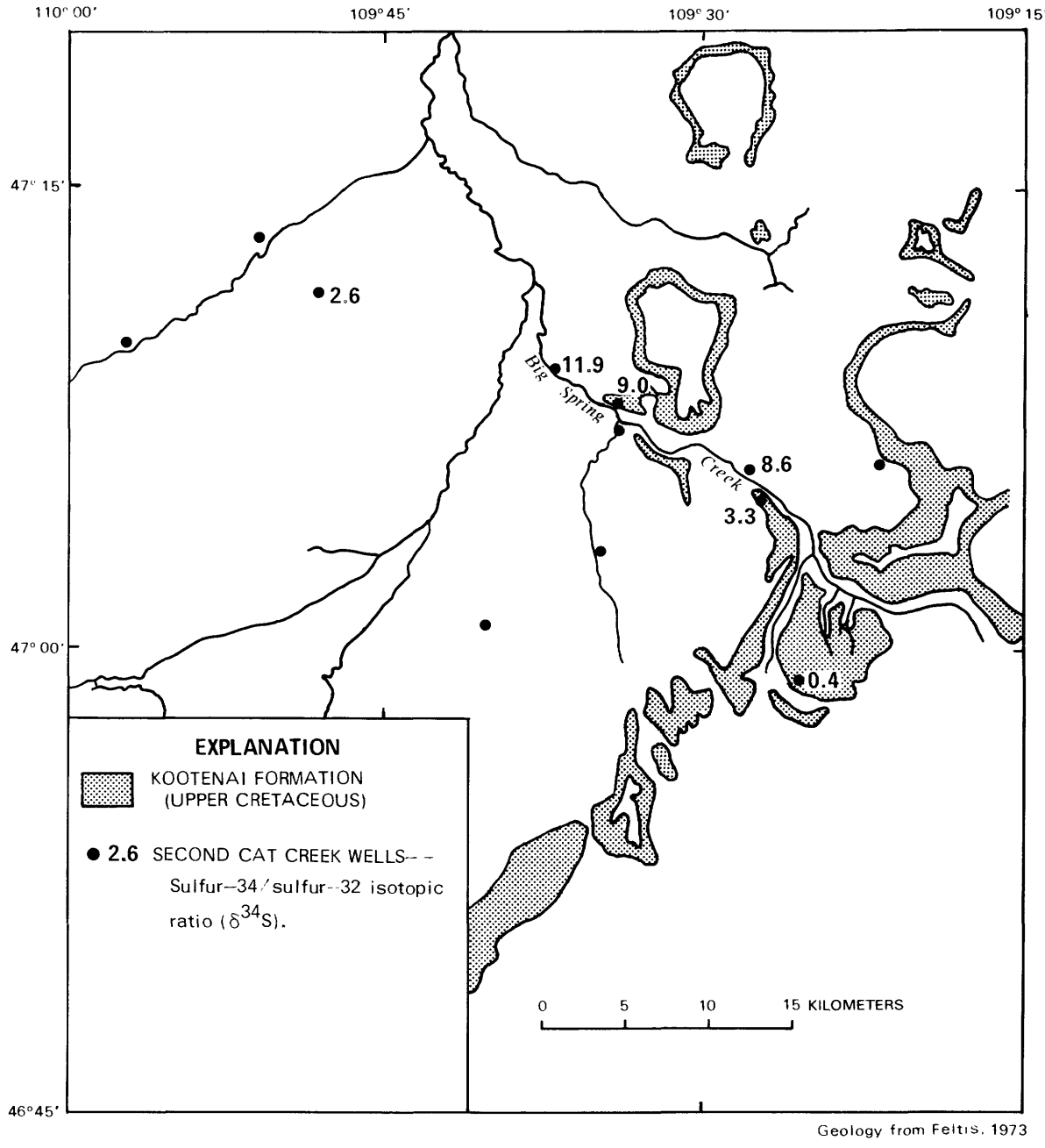

FIGURE 21.—Sulfate $\delta^{34}S$ values in waters from the Second Cat Creek sandstone of the Kootenai Formation, eastern Judith Basin, Montana.

the beginning of closed (to a CO_2 gas reservoir) system conditions (J10), to values ranging from −7.1 to −9.4 in the basin. If CH_4 was migrating into the aquifer and being oxidized by O_2 to form CO_2 (reaction 11), $\delta^{13}C$ values would be expected to decrease basinward from the isotopically light nature of CH_4 (Claypool and Kaplan, 1974). The oxidation of methane as a CO_2 source can therefore be considered negligible.

Wigley and others (1978) conclude from modeling studies that $\delta^{13}C$ should increase asymptotically in systems where aqueous carbonate species are fractionated and removed from the system, as in the incongruent dissolution of dolomite (reaction 23). This $\delta^{13}C$ evolution model corresponds with $\delta^{13}C$ trends in the Second Cat Creek sandstone. As the limiting $\delta^{13}C$ solution value is dependent on input and output $\delta^{13}C$ values, it can be calculated from reaction simulation mass transfers and the isotopic evolution model of Wigley and others (1978) to substantiate the postulated controlling reactions.

Kootenai Formation tritium concentrations are below 10 pCi/L for all samples except J10, which has a value of 410 pCi/L. Low tritium concentrations reflect a lack of recent recharge to the confined system, and support the hypothesis that recharge to the Second Cat Creek sandstone is insignificant in the South Moccasin Mountains. The high tritium value for J10 indicates that recharge occurs primarily in the Big Snowy Mountains (and probably also in the Judith Mountains, where no samples were collected for this study), which is in agreement with conclusions drawn from the dissolved solids distribution and the divalent-monovalent cation ratio data.

GEOCHEMICAL COMPUTER MODELING

SATURATION INDICES

Saturation indices for Kootenai Formation aquifer minerals, calculated using the critically evaluated data and aqueous speciation model of WATEQ2 (Ball and others, 1980), demonstrate that, although the samples originate from at least two distinct aquifers, the equilibrium relationships between aqueous and mineral phases in each aquifer are sufficiently similar to allow a unified discussion of thermodynamic equilibrium in ground waters of the Kootenai Formation. WATEQ2 saturation indices for Judith Basin samples are presented in table 13 for the silicates and aluminosilicates, and in table 14 for the carbonates and sulfates.

Quartz, the major aquifer constituent, appears to have little control on silica concentrations in solution. Highly ordered α-quartz is oversaturated, a condition often observed for crystalline phases that in low-temperature systems do not precipitate directly from solution, but rather form initially as an amorphous or cryptocrystalline polymorph, such as amorphous silica or chalcedony. In most samples, these less crystalline phases are undersaturated, indicating that silica is not in equilibrium with the solution. An exception to this generalization is sample J10, in which chalcedony is at saturation. This well is situated on the Kootenai outcrop where most recharge occurs; judging from the negative SI's for many aquifer minerals, it is probably perforated in sandstones that have been leached of their more reactive carbonate phases, leaving only quartz, ferric oxyhydroxides, and perhaps kaolinite, illite, and montmorillonite to react with infiltrating ground water. As a result, silica concentrations have become high enough to enable chalcedony to reach saturation and possibly precipitate as a grain cement.

Because aluminum was present at concentrations below the detection limit of 0.015 mg/L, this value was entered into WATEQ2 as the aluminum concentration to determine the maximum possible saturation indices of aluminosilicate minerals. Using this upper limit for aluminum concentration, many aluminosilicates are undersaturated, indicating that they do not control aqueous aluminum concentrations.

Albite, a detrital aluminosilicate, is undersaturated in all ground waters of the Kootenai Formation, while allophane, a poorly crystallized, variable-composition aluminosilicate phase, is saturated in all samples. Allophane is commonly encountered as an alteration product on the surfaces of weathered feldspar grains. The presence of this type of alteration is indicative of the final stage of feldspar weathering, which has been characterized in the experiments of Busenberg and Clemency (1976) by the very slow release of cations and silica. Illite and kaolinite are both saturated, as is montmorillonite. Although montmorillonite was not observed in Kootenai shales near the Judith Basin, its presence as an alteration phase cannot be ruled out. It seems probable that one or more of these saturated aluminosilicates controls aqueous aluminum and silica concentrations.

Saturation indices for other detrital silicates reported as trace constituents in Kootenai sandstones were not considered because of the high temperatures required for the formation of minerals such as garnet and tourmaline.

The carbonate minerals, calcite, dolomite, and siderite, which are abundantly represented in the aquifer, are at or near saturation. They appear to play an important role in controlling solution chemistry in most waters sampled except in the ground water from J10, where leaching of the outcrop has apparently eliminated these phases. Calcite is slightly oversaturated in many samples, indicating that determinate errors in field pH measurements, or calcite solid solutions involving manganese, strontium, and iron may be involved. These elements in solid solution would tend to decrease the stability of the solid phase slightly, and also decrease the saturation index of solid solution. For unknown reasons, dolomite saturation indices are rather widely scattered, but the mean dolomite SI shows that the mineral is roughly at saturation in the aquifer. Siderite is near saturation in all but highly oxidizing or strongly reducing samples (J2–4, 10, 16, 17), suggesting that some other iron phase may regulate iron concentrations in these.

Although rhodochrosite ($MnCO_3$) is the thermodynamically stable Mn(II) phase in moderately reducing ground waters (Morgan, 1967), the mineral is undersaturated in many samples. The near equality of all but two of the saturation indices to a value of -1.3, however, is suggestive of a controlling phase of similar composition. Saturation indices for J2 and J10, which

TABLE 13.—*Saturation indices of silicate and aluminosilicate aquifer minerals in waters from the Kootenai Formation, Judith Basin, Montana*

Sample	Silicates			Aluminosilicates				
	Quartz	Chalcedony	Amorphous silica	Albite	Allophane	Kaolinite	Illite	Calcium montmorillonite
J2	---	---	---	---	---	---	---	---
J3	0.42 ± 0.08	− 0.12 ± 0.08	− 0.95 ± 0.08	− 2.57 ± 0.89	− 0.27 ± 0.70	1.32 ± 1.71	1.36 ± 1.98	0.61 ± 2.01
J4	.30 ± .10	− .25 ± .10	− 1.09 ± .10	− 3.26 ± .91	− .28 ± .67	.17 ± .72	.01 ± 2.00	− .39 ± 2.02
J5	.32 ± .10	− .24 ± .10	− 1.08 ± .10	− 3.34 ± .91	− .27 ± .68	.74 ± 1.72	.04 ± 1.99	− .33 ± 2.02
J6	.44 ± .08	− .11 ± .08	− .95 ± .08	− 3.11 ± .89	− .26 ± .67	1.01 ± 1.71	.48 ± 1.98	.16 ± 2.01
J8	.37 ± .08	− .17 ± .08	− 1.00 ± .08	− 2.59 ± .89	− .29 ± .69	1.29 ± 1.71	1.24 ± 1.98	.51 ± 2.01
J10	.50 ± .08	− .05 ± .08	− .90 ± .08	− 4.52 ± .90	− .36 ± .59	1.05 ± 1.71	− .31 ± 1.98	− .04 ± 2.00
J11	.36 ± .10	− .19 ± .10	− 1.03 ± .10	− 2.88 ± .90	− .26 ± .35	.87 ± 1.71	.30 ± 1.99	− .15 ± 2.01
J12	.29 ± .08	− .22 ± .08	− 1.05 ± .08	− 1.43 ± .89	− .74 ± .77	.48 ± 1.71	.67 ± 1.98	− .42 ± 2.01
J13	.37 ± .08	− .16 ± .08	− 1.00 ± .08	− 1.41 ± .89	− .37 ± .77	.77 ± 1.71	.87 ± 1.98	− .00 ± 2.01
J14	.37 ± .09	− .18 ± .09	− 1.02 ± .09	− 2.50 ± .90	− .25 ± .70	.95 ± 1.71	.61 ± 1.98	.02 ± 2.01
J15	.36 ± .08	− .17 ± .08	− 1.01 ± .08	− 1.34 ± .89	− .51 ± .78	.65 ± 1.71	.71 ± 1.98	− .23 ± 2.01
J16	.32 ± .10	− .22 ± .10	− 1.07 ± .10	− 1.55 ± .90	− .29 ± .78	.52 ± 1.72	.34 ± 1.99	− .52 ± 2.02
J17	.36 ± .09	− .18 ± .09	− 1.02 ± .09	− 2.39 ± .89	− .28 ± .67	1.14 ± 1.71	.85 ± 1.98	.18 ± 2.01
Mean and standard deviation	0.37 ± 0.06	− 0.17 ± 0.06	− 1.01 ± 0.06	− 2.53 ± 0.93	− 0.34 ± 0.14	0.88 ± 0.27	0.55 ± 0.48	− 0.05 ± 0.35

TABLE 14.—*Saturation indices of carbonate and sulfate minerals in waters from the Kootenai Formation, Judith Basin, Montana*

Sample	Carbonates					Sulfates	
	Calcite	Dolomite	Siderite	Rhodochrosite	Strontianite	Gypsum	Celestite
J2	0.16 ± 0.06	− 0.08 ± 0.08	− 0.22 ± 0.10	− 2.80 ± 8.20	− 4.09 ± 6.95	− 2.00 ± 0.12	− 5.46 ± 6.95
J3	.41 ± .06	.41 ± .08	.31 ± .07	− 1.13 ± .25	− .95 ± .10	− 1.10 ± .06	− 1.68 ± .10
J4	.29 ± .06	.03 ± .08	− .06 ± .07	− 1.11 ± .14	− 1.06 ± .10	− .75 ± .06	− 1.33 ± .10
J5	.30 ± .06	.13 ± .08	− .16 ± .09	− .94 ± .14	− 1.63 ± .10	− 1.12 ± .06	− .98 ± .10
J6	.41 ± .06	.29 ± .06	− .23 ± .08	− 1.07 ± .12	− .81 ± .10	− .41 ± .06	− .86 ± .10
J8	.44 ± .06	.52 ± .80	− .07 ± .09	− 1.28 ± .31	− .90 ± .10	− .95 ± .06	− 1.52 ± .10
J10	− 1.06 ± .06	− 2.74 ± .08	− 12.13 ± 2.08	− 3.88 ± 8.20	− 2.31 ± .10	− 2.46 ± .27	− 2.94 ± .30
J11	.06 ± .06	− .28 ± .08	− .08 ± .09	− 1.81 ± .86	.93 ± .10	− 1.68 ± .08	− 1.90 ± .10
J12	.15 ± .08	.07 ± .12	− .12 ± .39	− 1.38 ± 2.08	− .32 ± .12	− 1.83 ± .08	− 1.51 ± .10
J13	.07 ± .12	− .14 ± .16	− .31 ± .73	− 1.54 ± 4.12	− 1.12 ± 4.12	− 2.77 ± .12	− 2.22 ± .12
J14	.28 ± .06	.21 ± .08	.33 ± .07	1.36 ± .45	− .59 ± .10	− 1.50 ± .06	− 1.61 ± .10
J15	− .01 ± .14	− .42 ± .24	− .16 ± .73	− 1.11 ± 2.08	− .54 ± .14	− 2.84 ± .14	− 2.59 ± .14
J16	− .08 ± .18	− .77 ± .39	− .66 ± 2.08	− 1.21 ± 2.76	− .55 ± .14	− 4.11 ± .61	− 3.80 ± .61
J17	− .04 ± .06	− .36 ± .08	− .72 ± .19	− 1.60 ± .45	− 1.11 ± .10	− 1.36 ± .06	− 1.65 ± .10
Mean and standard deviation	0.19 ± .18[1]	− 0.03 ± 0.36[1]	− 0.16 ± 0.30[1]	− 1.30 ± 0.25[1,2]	− 0.79 ± 0.40[1,2]	− 1.78 ± 0.99	− 1.89 ± 0.82[2]

[1]Calculated without J10
[2]Calculated without J2

are strongly reducing and oxidizing waters, respectively, are exceptions. It has been determined that calcite is apparently oversaturated with respect to these ground waters, so it is postulated that rhodochrosite occurs as a solid solution in calcite. Bodine and others (1965) reported an experimentally derived distribution constant (k_D) of 17.4 for Mn^{+2} in calcite. The distribution constant relates the molalities of Mn and Ca in solution to mole fractions of these elements in the solid phase:

$$\frac{m^x_{Mn}}{m^x_{Ca}} = k_D \frac{m^L_{Mn}}{m^L_{Ca}},$$

where x and L denote solid and solution phases, respectively. From this relationship and average manganese (0.60 μmol/L) and calcium (1.5 mmol/L) concentrations, it can be determined that calcite in equilibrium with these waters should contain an average of 0.7 mole percent rhodochrosite. The free energy of a calcite containing 0.7 mole percent rhodochrosite was calculated to be −1128.1 kilojoules per mole by assuming ideal mixing between the two components (Berner, 1975), for the reaction:

$$Ca_{(1-x)}Mn_xCO_3 = (1-x)Ca^{+2} + xMn^{+2} + CO_3^{-2},$$

$$\Delta G^0_{\text{ideal mix}} = xRT \ln x + (1-x)RT \ln(1-x),$$

and

$$\Delta G^0_{\text{f Mn calcite}} = \Delta G^0_{\text{ideal mix}} + \Delta G^0_{\text{f calcite}} +$$

$$x(\Delta G^0_{\text{f Mn}^{+2}} - \Delta G^0_{\text{f Ca}^{+2}} - RT \ln k_D),$$

where:

X=mole fraction Mn in solid solution
R=gas constant
T=temperature (degrees kelvin).

Saturation indices computed from this free energy and the enthalpy of pure calcite are presented in table 15.

TABLE 15.—*Saturation indices of a 0.7 mole percent manganese calcite solid solution in waters from the Kootenai Formation, Judith Basin, Montana*

[Free energy for the phase $Mn_{0.007}Ca_{0.993}CO_3$ calculated by assuming an ideal solid solution (Berner, 1975)]

Sample	SI calcite ($CaCO_3$)	SI Mn calcite ($Mn_{0.007}Ca_{0.993}CO_3$)
J3	0.41	0.34
J4	.29	.21
J5	.30	.22
J6	.36	.33
J8	.44	.37
J11	.06	−.02
J12	.15	.09
J13	.07	−.01
J14	.28	.20
J15	−.01	−.08
J16	−.08	−.16
J17	−.04	−.12
Mean and standard deviation	0.19 ± 0.18	0.11 ± 0.19

They demonstrate that apparent oversaturation with respect to pure calcite is largely explained when considering the manganese-calcite solid solution, and they suggest that an impure calcite may also control manganese concentrations in Kootenai ground waters.

Saturation indices for strontianite vary considerably, but are invariably less than zero. Although it is possible that this mineral exists as a solid solution with calcite, the inconsistency of strontianite saturation indices gives little support to the control of strontium concentrations by such a phase in these waters.

Despite the fact that no sulfate minerals were reported in the Kootenai Formation, their ubiquitous nature demands a discussion of sulfate saturation indices. In addition, the use of dissolved sulfate as a conservative tracer in evaluating flow directions and leakage in ground-water systems requires that any sources or sinks for this constituent be considered. Gypsum, the most common of the sulfate minerals, might occur in trace quantities dissiminated throughout the formation, but negative saturation indices indicate that an insufficient amount of this mineral is present to allow solid and aqueous phases to reach equilibrium. Celestite ($SrSO_4$) is similarly undersaturated, and is probably not present in the formation above trace amounts.

In the oxidizing environment, manganese concentrations are probably controlled by the stability of manganese oxyhydroxides. Potter and Rossman (1979) have investigated naturally occurring manganese oxyhydroxides in dendrites, stream deposits, and desert varnishes, and have identified metastable phases, such as romanchite [$(Ba, H_2O)_2Mn_5O_{10}$], hollandite ($BaMn_8O_{16}$), cryptomelene (KMn_8O_{16}), coronadite ($PbMn_8O_{16}$), todorokite [$(Mn, Ca, Mg)Mn_3O_7 \cdot H_2O$], and birnessite [$(Na, Ca, K)Mn_7O_{14} \cdot 3H_2O$]. Unfortunately, thermodynamic stabilities for these phases are unavailable except for birnessite, so equilibrium calculations are impossible in most cases. Using the detection limit of 1 μg/L for the concentration of manganese in sample J10, saturation indices indicate oversaturation with respect to both birnessite, with a value of 4.29, and manganite (γ-MnOOH), with a value of 1.05. Oversaturation with the stable and metastable manganese oxyhydroxide phases in oxidizing environments (Crerar and Barnes, 1974), using the manganese detection limit as the manganese concentration, suggests that either phase may control manganese solubility in oxidizing ground waters of the Kootenai Formation.

Ferric oxyhydroxides are particularly common in the Kootenai, giving rise to the red or purple color seen in exposures of the formation. The saturation indices presented in table 16 show that hematite (Fe_2O_3) is grossly oversaturated in all samples. Goethite (FeOOH) is oversaturated in oxidizing and moderately reducing waters,

TABLE 16.—*Saturation indices of iron oxyhydroxides and sulfides in waters from the Kootenai Formation, Judith Basin, Montana*

[$Fe(OH)_{3(am)}$, amorphous ferric hydroxide; $FeS_{(am)}$, amorphous ferrous sulfide; K_{sp}, solubility product]

Sample	Oxyhydroxides			Sulfides	
	Hematite	Goethite	$Fe(OH)_{3(am)}$ [1]	Pyrite	$FeS_{(am)}$ [2]
Sulfide absent					
J5	12.80 ± 0.34	3.94 ± 0.17	−0.16 ± 0.17	---	---
J6	12.68 ± .32	3.88 ± .16	−.22 ± .16	---	---
J8	12.44 ± .34	3.74 ± .17	−.05 ± .17	---	---
J10	14.12 ± 4.17	4.60 ± 2.09	.49 ± 2.09	---	---
J11	12.99 ± .34	4.01 ± .17	−.07 ± .17	---	---
J12	11.80 ± .82	3.42 ± .41	−.10 ± .41	---	---
J13	11.98 ± 1.48	3.52 ± .74	−.34 ± .74	---	---
J14	13.65 ± .32	4.36 ± .16	.33 ± .16	---	---
J15	12.09 ± 1.48	3.56 ± .74	−.18 ± .74	---	---
Mean and standard deviation	12.73 ± 0.77	3.89 ± 0.39	−0.03 ± 0.27	---	---
Sulfide present					
J2	3.33 ± 0.35	−0.81 ± 0.18	−4.46 ± 0.18	11.01 ± 0.24	1.36 ± 0.15
J3	5.74 ± .32	.40 ± .16	−3.44 ± .16	6.81 ± 1.71	−.81 ± .86
J4	3.91 ± .32	−.51 ± .16	−4.61 ± .16	10.78 ± .86	1.00 ± .43
J16	3.35 ± 4.17	−.79 ± 2.09	−4.82 ± 2.09	8.75 ± 2.16	.41 ± 2.10
J17	2.44 ± .48	−1.25 ± .24	−5.17 ± .24	10.41 ± .48	.55 ± .29
Mean and standard deviation	3.75 ± 1.23	−0.59 ± 0.61	−4.50 ± 0.65	9.55 ± 1.77	0.50 ± 0.82

[1] $K_{sp} = 10^{-38.5}$

[2] $K_{sp} = 10^{-3.0}$

but undersaturated in strongly reducing waters where sulfide is present. Oversaturation is due to the highly ordered, crystalline structures of these minerals, which prevent them from being precipitated directly from solution. Instead, ferric iron precipitates from solution as amorphous ferric hydroxide [$Fe(OH)_{3(am)}$] with crystallization to the more stable goethite or hematite occurring over a period of time (Langmuir and Whittemore, 1971). Using a K_{sp} of $10^{-38.5}$ for the reaction 13, which is characteristic of aged $Fe(OH)_3$ precipitates, saturation indices for ferric hydroxide indicate near saturation in oxidizing and moderately reducing waters, and undersaturation in strongly reducing, sulfidic waters. Whittemore and Langmuir (1975) concluded that log IAP values near −37 are indicative of actively precipitating $Fe(OH)_{3(am)}$, whereas lower values of −39 to −44 imply dissolution of, or equilibrium with, more stable oxyhydroxides. The occurrence of log IAP's near −39, or SI's of zero or slightly less as calculated previously, in oxidizing and moderately reducing Kootenai ground waters, is indicative of equilibration with ferric oxyhydroxides of moderate crystallinity and stability, rather than active precipitation of these phases. Equilibrium with a moderately crystallized phase would be expected in the Kootenai Formation, where previously deposited ferric oxyhydroxides are presently dissolving in modern ground waters.

Undersaturation with respect to $Fe(OH)_{3(am)}$ and goethite in strongly reducing waters is indicative of the control of iron concentrations by some other phase, most commonly iron sulfides. Pyrite was not identified in petrographic or X-ray analyses of the Kootenai Formation nor were any other sulfide minerals. However, because the samples analyzed were collected from the outcrop, pyrite originaly present would have been oxidized to ferric oxyhydroxides. Pyrite is ubiquitous in strongly reducing, aqueous environments (Berner, 1970), and should therefore be present in the Kootenai Formation where these conditions prevail. Saturation indices show gross oversaturation of this mineral in sulfidic waters, whereas amorphous ferrous sulfide ($FeS_{(am)}$) is near saturation. Deviations from zero for $FeS_{(am)}$ saturation indices are most likely the result of determinate errors in the sulfide analyses. Ferrous sulfides have been observed to precipitate from solution in reducing marine (Berner, 1964a; 1964b) and lacustrine (Doyle, 1968b)

sediments, but not in the ground-water environment. Barnes and Clark (1969), however, have reported the presence of mackinawite (FeS), a crystallized ferrous sulfide, as encrustations on steel ground-water well casings. The precipitation of amorphous FeS, followed by aging and crystallization in the presence of S^0 to form pyrite (Berner, 1970) appears to be a feasible mechanism to explain the above saturation indices, which reflect equilibrium with amorphous ferrous sulfide.

REACTION SIMULATION

Consideration of major and trace element geochemistry, Eh and pH variations, and saturation indices in ground waters of the Second Cat Creek sandstone, in association with aquifer mineralogy and petrography, has led to the proposal of several mineral phases and chemical reactions that may control ground-water chemistry. The aluminosilicates illite, kaolinite, montmorillonite, and allophane may be near saturation and may control the chemistry of waters in the unconfined outcrop area. Following the onset of confined conditions, slight oversaturations with respect to calcite, phase relations in the Mg-Ca-H_2O-CO_2 system, and the presence of calcareous cement, suggest precipitation of calcite, whereas saturation with dolomite implies simultaneous equilibration with this carbonate. Carbon isotopic ratios also suggest control of dissolved carbonate concentrations by carbonate minerals.

Oxidation potentials decrease from initially oxidizing values, then level off at moderately reducing values. Consumption of O_2, NO_3^-, and DOC within a short distance from the outcrop, coupled with increasing concentrations of dissolved N_2 and C_T, is indicative of biologically mediated O_2 and NO_3^- reduction reactions. The paucity of organic carbon in the aquifer, as well as the absence of H_2S and the simultaneous saturation with respect to both $Fe(OH)_{3(am)}$ and siderite in most waters of the Second Cat Creek sandstone, indicates that oxidation potentials may be poised by these two iron phases at levels too high to allow for either sulfate reduction or methanogenesis. One sample taken from the fractured South Moccasin Uplift shows the presence of H_2S, which may indicate that reduced gases are free to migrate upward from lower aquifers along these fractures. Sulfur isotopic ratios give no evidence of sulfate reduction occurring at this sampling location.

Sulfate and chloride concentrations are significantly higher in the fractured region to the north of Big Spring Creek than to the south, and sulfur isotopic ratios indicate a significantly different source of sulfate on either side of the creek. The occurrence of high sulfate and high chloride concentrations in aquifers underlying the Kootenai Formation suggests that the composition of waters in the Second Cat Creek sandstone north of Big Spring Creek may be influenced by upward leakage along faults and fractures.

Finally, uniformly decreasing log molar divalent-monovalent cation ratios are indicative of cation exchange. The exchange of monovalent sodium ions adsorbed on clay surfaces for divalent calcium and magnesium ions in solution influences solution-mineral equilibria, and therefore must be considered during reaction simulations.

The effects of the above mechanisms in controlling solution chemistry, both alone and in combination, have been investigated through reaction simulations using the computer program PHREEQE (Parkhurst and others, 1980). Attempts have been made to duplicate measured variations in chemistry from well to well along the flow path by equilibrating an initial solution with desired mineral phases. The varying degrees of success obtained using different controlling phases is interpreted as a measure of the likelihood that a particular reaction or mineral phase controls solution chemistry. Comparisons of pH and C_T between measured and modeled chemistries are particlarly useful in the determination of controlling phases because both parameters vary over a wide range, depending on the choice of controlling reactions. However, final evaluation of controlling phases is based on agreement of all constituents considered in the computer equilibrium model with analyzed concentrations.

To consider the effects of mineral equilibrium in ground waters of the Second Cat Creek sandstone, ion-exchange reactions must first be simulated. This was accomplished by fixing $(a_{Na^+})^2/(a_{Ca^{+2}})$ and $(a_{Na^+})^2/(a_{Mg^{+2}})$ molar activity ratios in the modeled solutions to their calculated values for each sample along the flow path. In effect, this fixes the activities of monovalent and divalent cations on the exchange surface to a particular value for each sample, and implies an infinite reservoir of exchanger as can be seen from the exchange equilibrium expressions (reactions 28 and 29). Such a treatment eliminates the need to consider activities of ions on a solid surface, information that is currently unavailable.

As there is considerable evidence of leakage into the Second Cat Creek sandstone north of Big Spring Creek, areas north and south of the creek were treated as distinct flow systems. The southern flow path is discussed first, being the simpler of the two systems.

The initial modeling solution is similar in major element composition to Montana rainwater (Junge and Werby, 1958), and has been equilibrated, using PHREEQE, with atmospheric partial pressures of O_2 and CO_2 to approximate actual Eh and pH. Sulfate,

chloride, and nitrate were added to the solution as equivalent amounts of gypsum, halite, and calcium nitrate, in order to match measured concentrations, simulating the dissolution of trace amounts of these or similar compounds in the unsaturated zone. The resulting solutions were then equilibrated with different minerals to investigate the influence of these phases in controlling solution chemistry. The minerals chosen as plausible controlling phases are: (1) calcite; (2) dolomite; (3) calcite and dolomite; (4) allophane; (5) kaolinite and illite; (6) kaolinite, illite, and Mg-montmorillonite; and (7) kaolinite, illite, and Ca-montmorillonite. In addition to these phases, the model solutions were also equilibrated with $Fe(OH)_{3(am)}$ in the unconfined aquifer, and with $Fe(OH)_{3(am)}$ and siderite in the confined aquifer system, to allow simulation of iron concentration and Eh poising. A K_{sp} of $10^{-38.5}$, which is characteristic of an aged precipitate, was chosen for $Fe(OH)_{3(am)}$.

Initial PHREEQE simulations demonstrate the effects of equilibrating the rainwater solution with these groups of mineral phases. Carbon dioxide was added to the solution prior to equilibrating with the minerals, simulating the dissolution of CO_2 in the soil zone. To match the calculated C_T concentration in sample J10, CO_2 was added in concentrations of approximately 1.5 millimoles per liter for the carbonate simulations and 3.0 millimoles per liter for the aluminosilicate simulations. Dissolution of these amounts of CO_2 would require equilibration of infiltrating waters with CO_2 partial pressures of $10^{-1.57}$ to $10^{-1.28}$ atm in the unsaturated zone. Garrels and MacKenzie (1971, p. 141) report soil zone P_{CO_2} values on the average of $10^{-2.0}$ and as high as $10^{-0.5}$ atm, which is consistent with the model results.

Following equilibration with mineral phases and the appropriate ion-exchange constants for J10, 0.537 mmol/L carbon with an oxidation state of zero was added to the solution to allow for the reduction of O_2 and NO_3^- present in the outcrop area but absent in samples taken downdip. The simulations then equilibrated the solution with the minerals and the appropriate ion-exchange constants for the downdip samples. As shown in figure 22, these simulations clearly demonstrate that insufficient dissolved carbonate is produced by the dissolution of soil zone CO_2, the reduction of O_2 and NO_3^- by organic carbon, and the equilibration with minerals and ion exchange to account for the observed increases in C_T.

Subsequent simulations required an additional carbon source, if modeled and observed C_T concentrations were to agree. Although the exact mechanism of this CO_2 production remains uncertain, it seems likely that the CO_2 is an oxidation product of organic carbon generated via sulfate reduction processes, or by the coalification of lignite, in strata adjacent to the aquifer.

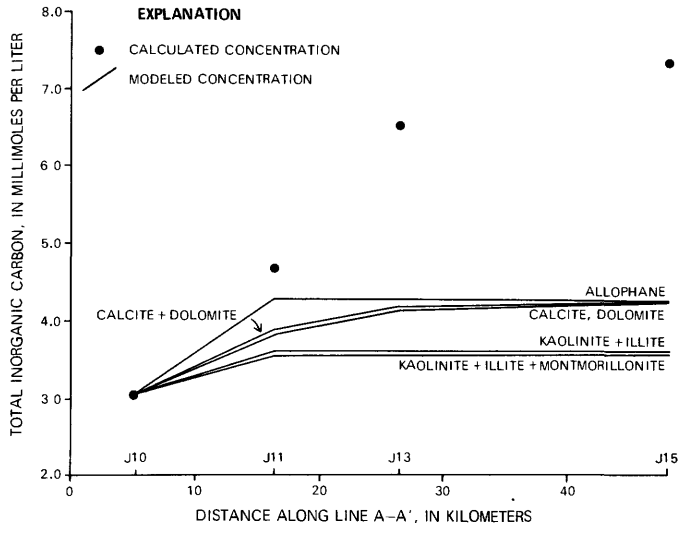

FIGURE 22.—Comparison of calculated total inorganic carbon concentrations with modeled concentrations for mineral equilibration with no CO_2 dissolution, following the reduction of O_2 and NO_3^-, southern flow path of the Second Cat Creek sandstone, eastern Judith Basin, Montana. All simulations include equilibration with calcium-sodium exchange, magnesium-sodium exchange and amorphous ferric hydroxide, as well as siderite in J11, J13, and J15.

Quantities of CO_2 were dissolved along the simulated flow path to match observed C_T concentrations.

The model results, presented in figure 23, indicate that pH values for the confined system are successfully approximated only for the carbonate-ion exchange simulations. Although the kaolinite-illite-ion exchange simulation results in a pH value close to that measured in the sample taken from the unconfined aquifer, the aluminosilicates do not appear to control solution chemistry in the confined portions of the aquifer. Deviations between measured and modeled pH's for sample J10 using the kaolinite-illite-ion exchange model may be the result of the variable compositions and stabilities of these aluminosilicates. Refined geochemical simulations of the unconfined portion of the Second Cat Creek sandstone await an improved characterization of the compositions and stabilities of aluminosilicates present.

Both the calcite-ion exchange and the calcite-dolomite-ion exchange models approximate pH to within 0.1 units of the field-measured value. The presence of dolomite in the aquifer and its instability with respect to calcite in the ground waters sampled (fig. 14) suggests that the calcite-dolomite-ion exchange simulations, which requires mass transfer characteristic of dedolomitization (reaction 23), is the more probable of these two models. In this calcite-dolomite-ion exchange model, dolomite dissolves in response to CO_2 production and Na/Mg exchange, simultaneously precipitating calcite:

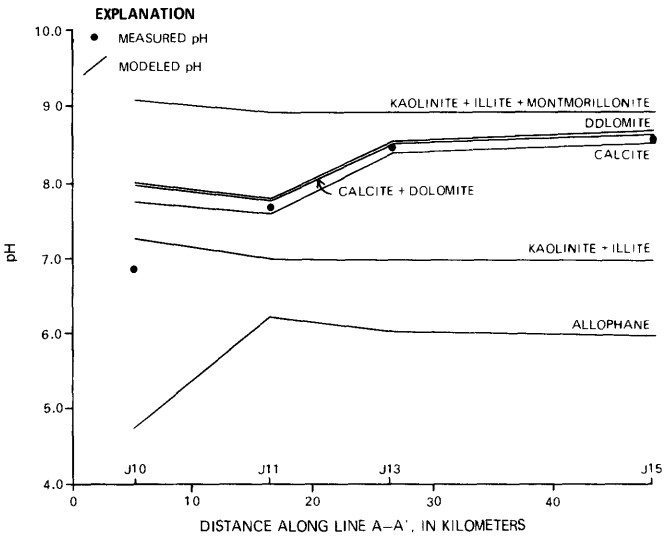

FIGURE 23.—Comparison of field-measured pH values with modeled pH values for mineral equilibration with CO_2 dissolution, southern flow path of the Second Cat Creek sandstone, eastern Judith Basin, Montana. All simulations include equilibration with calcium-sodium exchange, magnesium-sodium exchange and amorphous ferric hydroxide, as well as siderite in J11, J13, and J15.

$$CaMg(CO_3)_2 + H_2CO_3^0 + Na_2EX$$

$$= CaCO_3 + 2HCO_3^- + 2Na^+ + MgEX.$$

In addition, a net excess of calcium in solution is exchanged for sodium on the exchanger surface (reaction 28). The addition of illite and kaolinite to this model results in only minimal changes in mass transfer and final solution composition, suggesting that the importance of these aluminosilicates as ion exchangers far overshadows the influences of their solubilities on major element chemistry. Direct comparisons of simulated and analyzed concentrations for the Second Cat Creek sandstone, as well as the computed mass transfers required to attain these variations, are presented in figure 24.

At this point, it is important to emphasize that the mathematical solution to the set of simultaneous equations required to characterize mass transfer is nonunique. Other reaction schemes may be proposed that would adequately describe the geochemical evolution of ground waters in the Second Cat Creek sandstone. The mass transfer model proposed here is therefore only a reasonable hypothesis—not a unique mathematical solution.

The northern flow path, which includes all samples taken from wells located north of Big Spring Creek, was modeled to simulate upward leakage from the underlying Morrison Formation through numerous faults and fractures in the area. Suitable samples of ground water from the Morrison within the Judith Basin study area were unavailable; therefore, analyses of waters from two wells in the Morrison Formation located in Grassrange, Montana, 45 km east of Lewistown on the northern flank of the Big Snowy Uplift, were used. Although it is unlikely that these waters are identical to those in the area modeled, they are of sufficiently similar hydrogeochemical origin, prevalent chemical character, and dissolved solids content to approximate the composition of Morrison Formation waters within the study area. In addition, the pH and anionic composition of these Morrison waters is similar to that of springs and wells that discharge from the Madison Group (table 8). Therefore, simulated leakage of these Morrison Formation waters into the Second Cat Creek sandstone would also approximate the effects of similar amounts of leakage from the deeper Madison aquifer, although calculated mass transfers would differ because of dissimilar cationic concentrations in the waters of the Madison and Morrison Formations.

Sample J11 was chosen as the starting composition for the northern flow path simulations because of its similarity to the northern flow path outcrop sample J24, which was unsuitable for geochemical modeling. Using PHREEQE in the mixing mode, sufficient Morrison water was added to the simulated J11 water to match analyzed sulfate concentrations along the northern flow path. Sulfate was considered a conservative constituent in these simulations, based on evidence suggesting that sulfate was neither precipitating as a mineral phase nor being reduced to sulfide in the Second Cat Creek sandstone.

The mixed solution was then equilibrated with the same phases that adequately described southern flow path geochemistry, calcite and dolomite, as well as ion exchange, $Fe(OH)_{3(am)}$, and siderite. In addition, the solution was equilibrated with $FeS_{(am)}$, rather than siderite and $Fe(OH)_{3(am)}$, to simulate the chemistry at well J17. It was discovered that although 0.20 millimoles of CO_2 per liter had to be dissolved to adequately describe the geochemistry at well J14, 0.26 and 0.65 millimoles of CO_2 per liter had to be exsolved from the solution to approximate the chemistry at well J17, and 0.65 millimoles of CO_2 per liter had to be exsolved from the solution to approximate the chemistry at well J12. Because the Morrison water composition is only approximate, interpretation of the apparent degassing is uncertain. It is entirely possible that the waters leaking into the Kootenai are higher in sulfate and lower C_T than in the model; however, most of the analyses from lower aquifers suggest a predominance of pH values and bicarbonate and sulfate concentrations equal to or lower than those used in the model (table 8). The presence of waters with compositions that would both increase

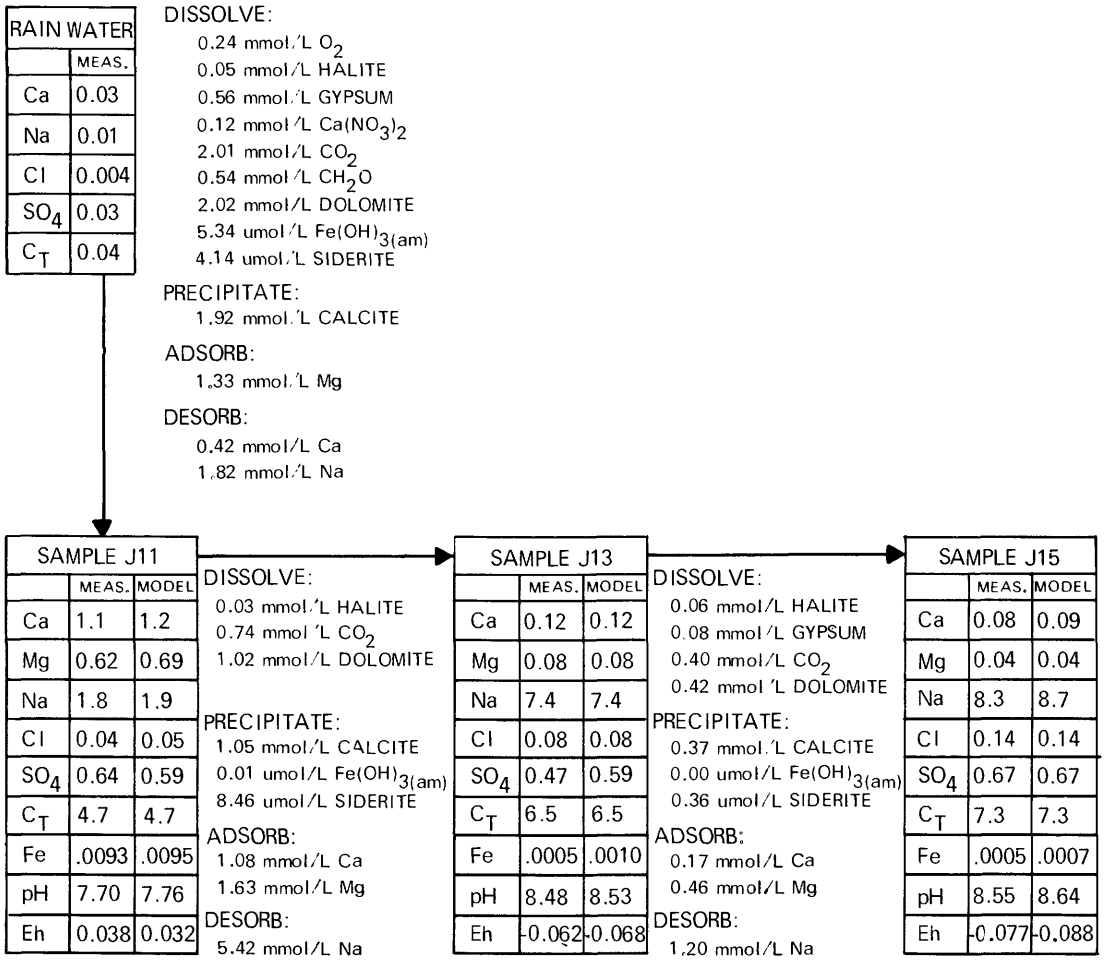

FIGURE 24.—Calculated mass transfer for the calcite-dolomite-cation exchange-CO_2 dissolution model of groundwater evolution along the southern flow path of the Second Cat Creek sandstone, eastern Judith Basin, Montana. Concentrations in millimoles per liter (mmol/L) and micromoles per liter (μmol/L); Eh in volts.

sulfate and decrease C_T, with respect to the composition of water from well J14, appears unlikely. At the same time, correspondence of the aquifer outcrop with the area of CO_2 exsolution (fig. 3) is an indication that such outgassing may indeed occur. In addition, recharge to the Second Cat Creek sandstone in the South Moccasin Mountains is negligible, which would allow for an upward rather than downward mass flux in the unsaturated zone. For the required degassing to occur, the P_{CO_2} of the unsaturated zone would have to be approximately $10^{-2.8}$ atm, as compared to the atmospheric P_{CO_2} of $10^{-3.5}$ atm. Although the unsaturated zone P_{CO_2} required for degassing is somewhat low, it does not appear to be prohibitively so, and may allow CO_2 outgassing to occur at the South Moccasin Mountains.

Further support for upward leakage of water similar to the composition modeled is given by the close agreement of another conservative constituent, chloride. Modeled and observed chloride concentrations differ by a maximum of only 0.03 millimoles per liter in the three waters simulated in this manner, and indicate that the leaking waters have a m_{SO_4}/m_{Cl} ratio identical to that of the Morrison waters.

Mass transfer calculated for the mixing simulations also shows the influence of dedolomitization (fig. 25), but instead of prevalent Na/Mg exchange, Ca/Mg exchange removes from solution the magnesium derived from the dissolution of dolomite, and supplies the calcium required for the precipitation of excess calcite due to CO_2 outgassing:

$$CaMg(CO_3)_2 + Na_2EX + H_2CO_3^0 = CaCO_3 + 2Na^+ + MgEX + 2HCO_3^-,$$

$$2HCO_3^- + 2Na^+ + CaEX = CO_{2(g)}\uparrow + CaCO_3 + H_2O + Na_2EX.$$

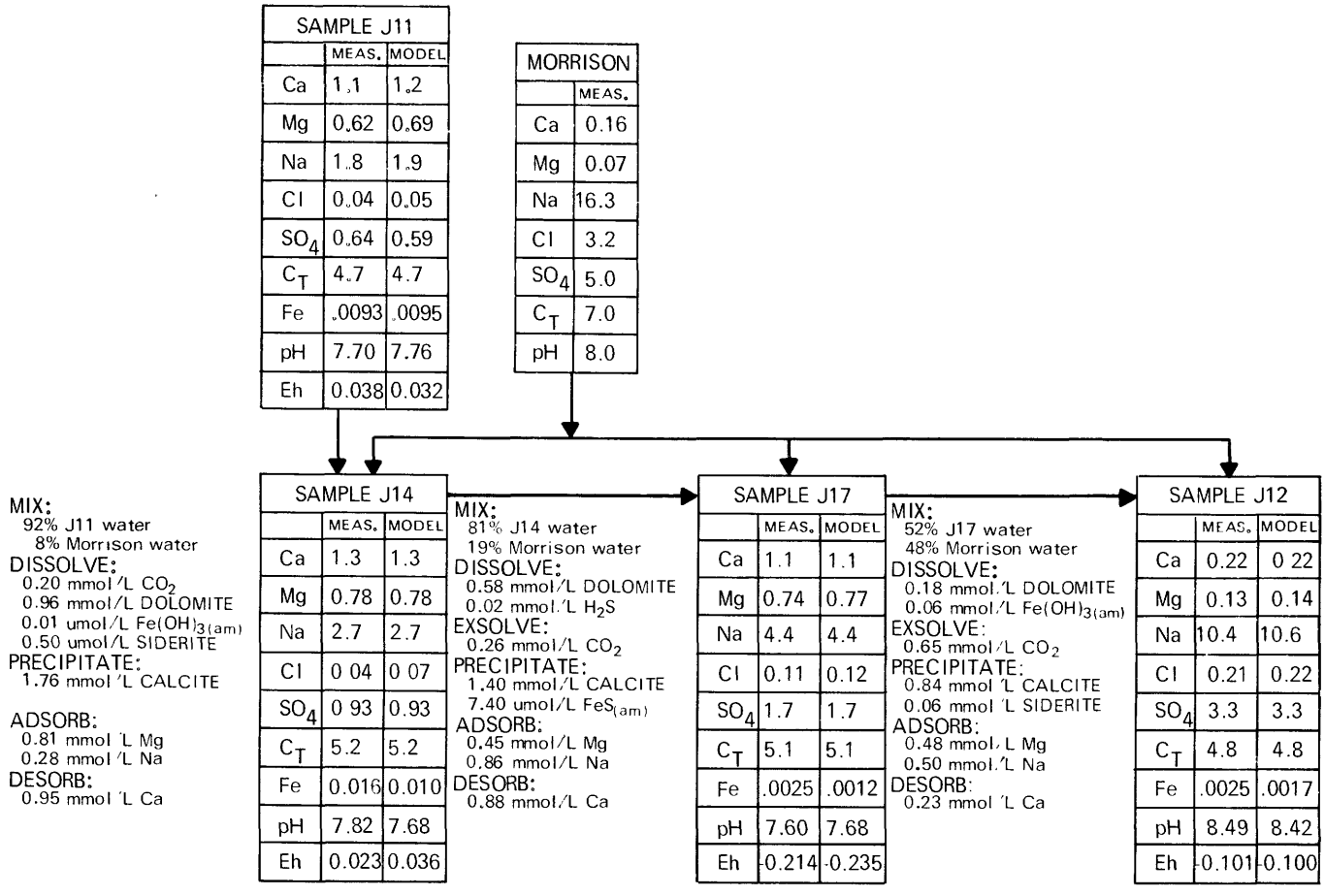

FIGURE 25.—Calculated mass transfer for the calcite-dolomite-cation exchange-Morrison leakage model of ground-water evolution along the northern flow path of the Second Cat Creek sandstone, eastern Judith Basin, Montana. Concentrations in millimoles per liter (mmol/L) and micromoles per liter (μmol/L); Eh in volts.

Increases in calcium and magnesium concentrations of the upward leaking water would require increased desorption of sodium in combination with increased adsorption of magnesium and calcium to maintain equilibrium with ion exchange.

The quality of fit obtained using the dedolomitization model is shown in figure 26. In these plots, precisions of the analytical measurements at the 95 percent significance level (table 3) are superposed on the modeled concentrations, allowing comparisons to be made between analyzed and modeled values. The comparison is generally very good, although several deviations are evident for which no explanations can be offered. Once again, this mass transfer model is a nonunique solution to a set of simultaneous equations. The geochemical evolution of ground-water composition along the northern flow path may be adequately described without invoking upward leakage, but since leakage appears to be occurring, the mixing model is considered most plausible.

CARBON ISOTOPIC EVOLUTION

The evolution of carbon isotopic composition in ground waters of the Second Cat Creek sandstone was simulated through the use of a FORTRAN computer code of the model presented by Wigley and others (1978). This carbon isotopic evolution model considers the effects of mass transfer from an arbitrary number of carbonate sources and sinks in combination with equilibrium fractionation between the solid, gas, and aqueous phases in contact with the aquifer to calculate changes in the $\delta^{13}C$ value of ground-water carbonate. The same model may also be used to calculate the effects of mass transfer on the activity of ^{14}C in ground waters, which then allows for adjustment of raw ^{14}C ages, based on the dilution and precipitation of the radioactive isotope.

Other models of ^{14}C evolution in natural systems, including those of Vogel (1970), Tamers (1975), Mook

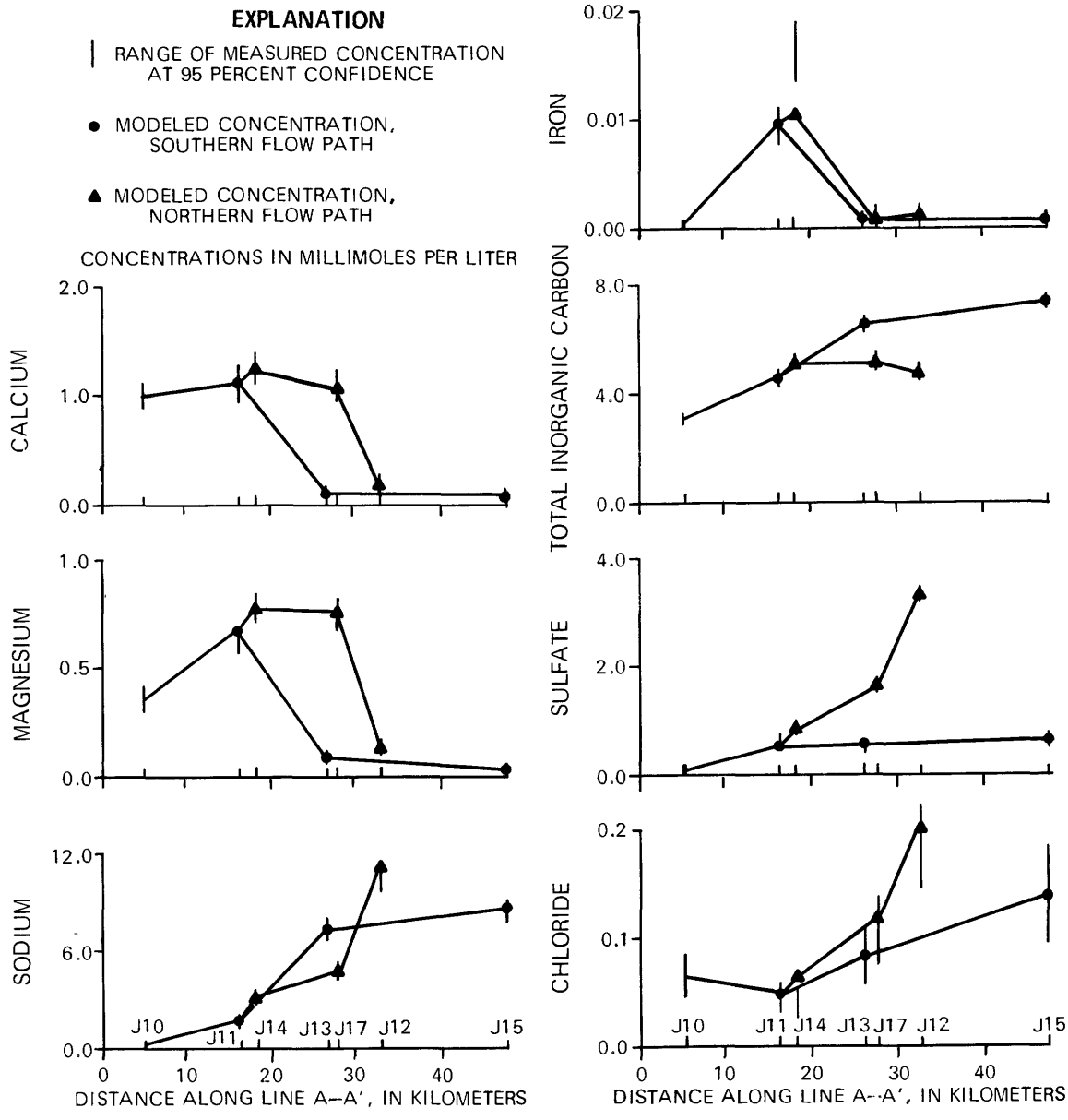

FIGURE 26.—Comparison of measured and modeled concentrations of selected constituents in waters from the Second Cat Creek sandstone of the Kootenai Formation, eastern Judith Basin, Montana.

(1976), and Fontes and Garnier (1979), neglect the effects of ^{14}C precipitation in carbonate minerals, and thereby lead to adjusted ^{14}C ages that are too old when applied to aqueous systems where incongruent dissolution of carbonates is an important mass transfer mechanism.

Unfortunately, samples collected from the northern flow path are unsuitable for isotopic modeling in that they appear to represent a mixture of waters with different evolutionary histories. These samples could be modeled with confidence only if the carbon isotopic composition of the upward leaking waters were known. However, a comparison of observed and calculated $\delta^{13}C$ values for the southern flow path allows a check on the agreement of isotopic and mass transfer models. In addition, adjusted ^{14}C ages for the southern flow path may be used to calculate flow rates and residence times in the unfractured aquifer.

The $\delta^{13}C$ values for carbonate sources were estimated from measurements reported in the literature for comparable materials. A $\delta^{14}C$ value of -28 ± 4 (Craig, 1954) was chosen for sedimentary organic carbon and the CO_2 derived from it, and a freshwater carbonate $\delta^{13}C$ of -4.8 ± 5.1 was used for Kootenai dolomite and calcite (Keith and Weber, 1964). Keith and Weber (1964) also reported $\delta^{13}C$ values with a mean of -2.50 for fresh-

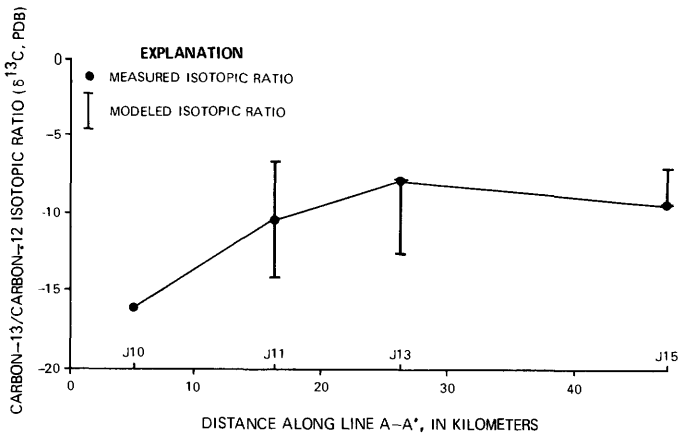

FIGURE 27.—Comparison of measured $\delta^{13}C$ values and the range of modeled $\delta^{13}C$ values for water from the southern flow path of the Second Cat Creek sandstone, eastern Judith Basin, Montana. The range of modeled $\delta^{13}C$ values reflects the uncertainty in the actual $\delta^{13}C$ compositions of aquifer carbon sources.

water Kootenai limestones and dolomites from several areas in Montana, which are consistent with the range of values used. Employing the temperature-dependent fractionation factors of Deines and others (1974), the equations of Wigley and others (1978) were applied to the $\delta^{13}C$ carbonate source values estimated above, the computed mass transfer between samples (fig. 24), and the initial observed $\delta^{13}C$ of the ground water (table 12), to compute the $\delta^{13}C$ values of three successive samples on the southern flow path, assuming the incongruent dolomite dissolution model. Agreement between predicted and observed $\delta^{13}C$ values is excellent within the uncertainty of the isotopic composition of the carbonate sources (fig. 27), and therefore supports the validity of the CO_2 dissolution and dedolomitization model for the Second Cat Creek sandstone.

The equations of Wigley and others (1978) were applied to the measured carbon isotopic compositions (table 12) and the computed mass transfer (fig. 24) in an attempt to adjust raw ^{14}C ages for the effects of dilution and precipitation that occur during ground water-aquifer interactions. Using this approach, an age of 4,800 years was calculated for sample water J11, and >20,000 years for sample water J13. The ^{14}C concentration in sample water J15 was too low to allow for a reliable determination of the raw age. Radiometric flow rates for the Second Cat Creek sandstone, calculated for a flow distance from the outcrop to the well measured perpendicular to the potentiometric contours, compare favorably to the previously derived hydrologic flow rates for the Kootenai Formation (table 17).

TABLE 17.—*Comparison of radiometric and hydrologic flow rates for ground waters of the Kootenai Formation, eastern Judith Basin, Montana*

Sample	Hydrologic flow rate, Kootenai Formation (meters per year)	Radiometric flow rate, Second Cat Creek sandstone (meters per year)
J11	2.6	2.3
J13	1.7	<.9
J15	1.8	---

POWDER RIVER BASIN STUDY AREA

PHYSIOGRAPHY

The physical characteristics of the Powder River Basin are the result of several factors, the most important of which is the regional geologic structure. Dominant features of the topographic basin are the rugged Big Horn Mountains to the west, the elevated but more subdued Black Hills on the east, and the sprawling basin between them (fig. 28).

TOPOGRAPHY

The terrain of the basin floor is composed of hilly to rugged uplands, wide rolling valleys, and isolated badlands. In the study area, the basin floor lies at elevations roughly between 1,200 to 1,300 meters; the Black Hills Uplift reaches moderate elevations of approximately 1,400 to 1,800 meters above sea level. The uplift is characterized by tree and grass-covered peaks and dissected plateaus, the elevated areas giving way to lower sage-covered hills and the basin floor to the west (Wyoming Water Planning Program, 1972).

DRAINAGE

The study area (shown in detail in fig. 29) lies within the Missouri River drainage basin and is drained by tributaries of the Yellowstone, Cheyenne, and Little Missouri Rivers. In the three tributaries in the study area, the Little Powder, Belle Fourche, and Little Missouri Rivers, flow is extremely variable, ranging from virtually nonexistent at times during the winter to occasional floods of greater than 100 m^3/s during the early summer. Keyhole Dam, located approximately 20 km northeast of Moorcroft, impounds runoff in the upper Belle Fourche River for controlled release to farms and ranches downstream later in the season (Whitcomb and Morris, 1964).

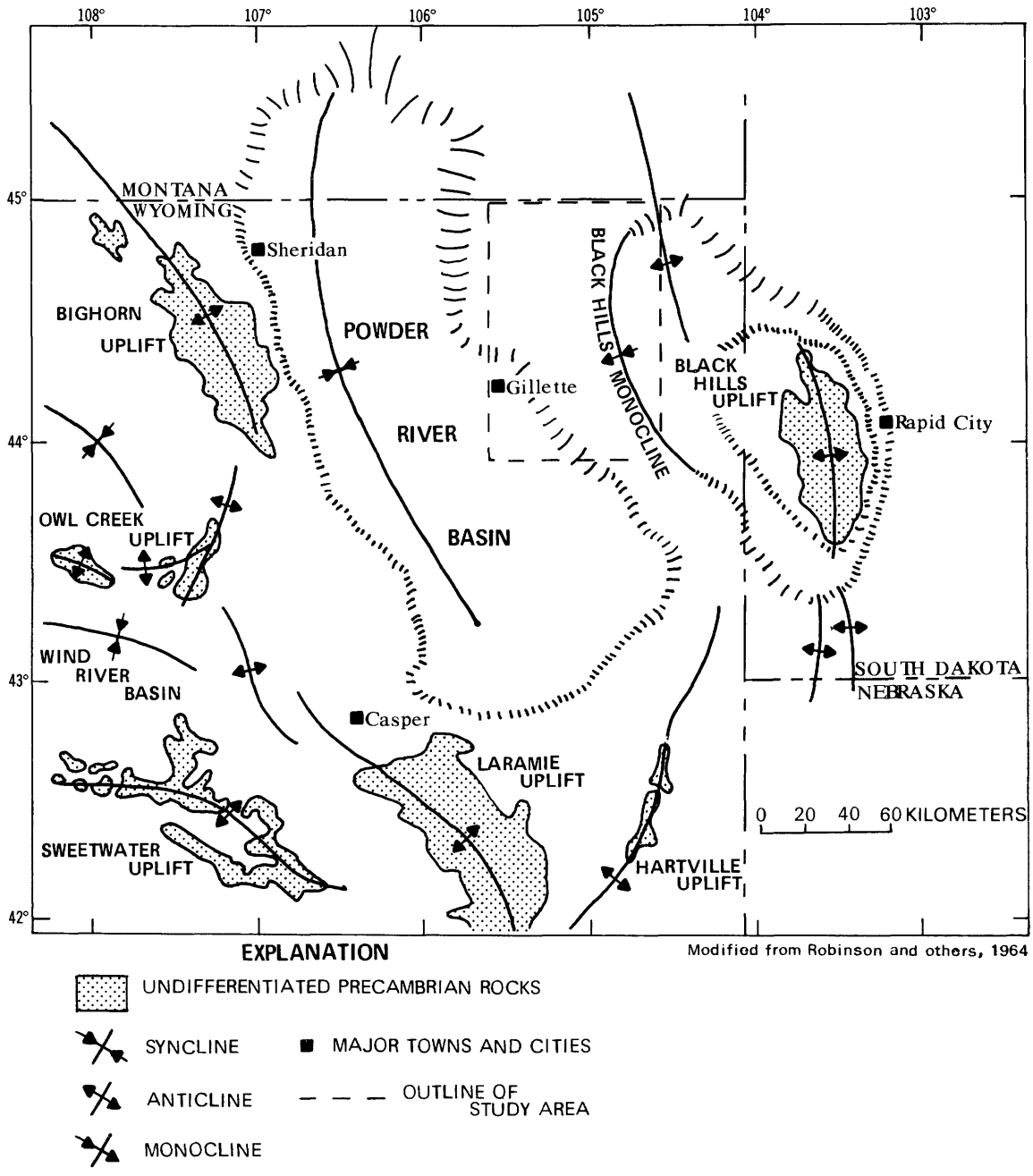

FIGURE 28.—Structural and physiographic features of the Powder River Basin, Wyoming and Montana.

CLIMATE

The study area has a semiarid climate with annual average precipitation at Moorcroft of 35 cm, at Devils Tower of 41 cm (Whitcomb and Morris, 1964), and at Gillette of 40 cm (Wyoming Water Planning Program, 1972). Greater than 50 percent of this precipitation occurs between April and July. Rainfall in the spring and early summer occurs as brief but rather heavy showers, and light snowfalls and occasional heavy snows are common throughout the winter (Whitcomb and Morris, 1964).

Mean annual temperature at Moorcroft is 6.9°C and at Devils Tower is 7.9°C (Whitcomb and Morris, 1964); at Gillette it is 7.3°C (Wyoming Water Planning Program, 1972), with the average monthly temperature during July being roughly 13°C higher than that for January (Whitcomb and Morris, 1964).

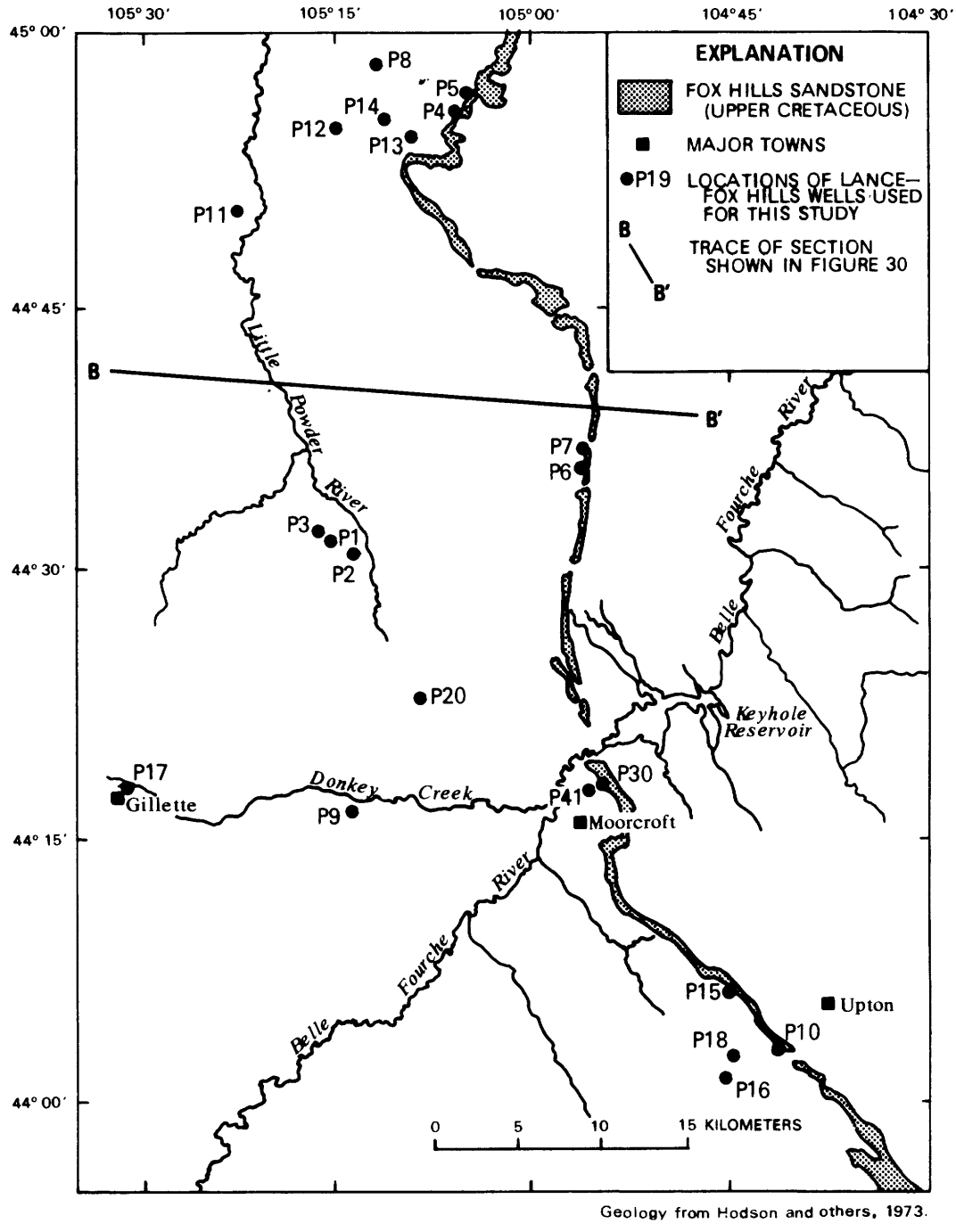

FIGURE 29.—Index map of the Powder River Basin study area showing major towns and perennial streams, outcrop of the Fox Hills Sandstone and the locations of wells sampled.

GEOLOGY

STRUCTURE

The Powder River Basin is a northward-trending structural basin that has evolved as a result of the complex development of the Rocky Mountain region. A trough lying roughly parallel to the Big Horn Uplift (fig. 28) identifies the axis of the basin, where roughly 5,000 m of Phanerozoic sediments have accumulated. The study area occupies the northeastern portion of the basin adjacent to the Black Hills Uplift, a broad northward-trending anticline. The northwest-trending Black Hills monocline divides the basin to the west

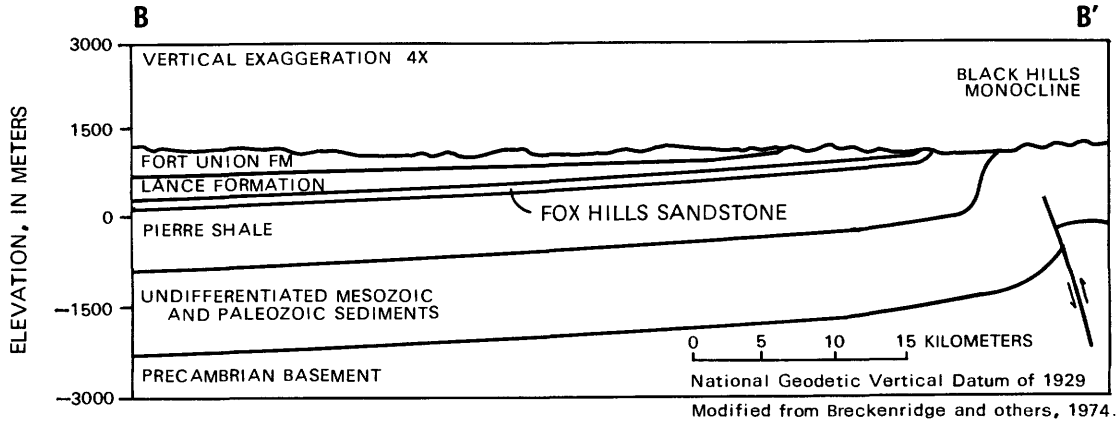

FIGURE 30.—Generalized geologic section of the Powder River Basin study area, Wyoming, through line B–B′ in figure 29.

from the Black Hills Uplift to the east. The monocline consists of a belt of steeply dipping sedimentary strata, 2.5 to 9.5 km wide, across which the structural relief is about 1,800 m. Dips are to the west or southwest along the monocline, ranging from 20 degrees to nearly vertical. The outcrop of the Fox Hills Sandstone lies parallel to the monocline, and delineates the western extent of steeply dipping strata. To the west, the dips of the Lance Formation and younger strata flatten abruptly, ranging from 2 to 5 degrees toward the axis of the basin (fig. 30) (Robinson and others, 1964).

The Belle Fourche Arch, a subtle northeast-trending paleo-arch, extends across the southern part of the study area. According to Slack (1981), the arch is the result of differential vertical uplift along numerous northeast-trending structural lineaments (fig. 31). Underlying zones of weakness in the Precambrian basement, thought to be shear zones of Precambrian age, allow for periodic movement along the lineaments, resulting in structural offsets in the Black Hills monocline, welldefined topographic escarpments, and linear drainage courses. Stratigraphic evidence suggests that these structural lineaments have been rejuvenated periodically throughout the Phanerozoic and that the subtle movements involved have affected depositional environments and, therefore, affected porosities and permeabilities along the crest of the arch (Slack, 1981).

STRATIGRAPHY

Sedimentary rocks exposed on the western flank of the Black Hills Uplift have a combined thickness of about 3,400 m and range in age from Mississippian to Quaternary.

The Upper Cretaceous Pierre Shale is a 625- to 825-m-thick sequence of dark gray marine shales and bentonites with minor interbedded sandstone units. Conformably overlying the Pierre Shale is the Fox Hills Sandstone, and Upper Cretaceous sequence of sandstones and shales that were deposited in an environment ranging from marginal marine to estuarine or tidal flat environment (Dodge and Spencer, 1977). The Fox Hills ranges from 38 to 60 m in thickness, with crossbedded sandstones at the top of the formation grading downward into sandy shales and culminating at the underlying Pierre Shale. The Fox Hills is poorly exposed in outcrop, generally appearing as low grassy ridges. Where exposed, the sandstones are gray to light brown, fine to medium grained, and soft and thin bedded. The rock has a slabby appearance, and locally contains numerous calcareous or ferruginous concretions (Whitcomb and Morris, 1964).

Conformably overlying the Fox Hills Sandstone are the freshwater, fluvial deltaic strata of the Upper Cretaceous Lance Formation (Dodge and Spencer, 1977). The Lance is comprised of 150 to 500 m of yellowish gray, fine- to medium-grained lenticular crossbedded sandstones interbedded with darker gray shaley siltstones and sandy claystones. Black carbonaceous shales are common at the gradational contact with the Fox Hills Sandstone.

The nonmarine sandstones, shales, coals, and tuffs of the Tertiary Fort Union and Wasatch Formations overlie the Lance Formation and crop out at the surface over much of the basin. A geologic map of the study area showing the outcrop areas of stratigraphic units pertinent to this study is presented in figure 32.

MINERALOGY OF THE LANCE-FOX HILLS AQUIFER

Mineralogy of the Fox Hills Sandstone (tables 18 and 19) was determined by X-ray diffraction analysis of four drill-core and two outcrop samples obtained from the

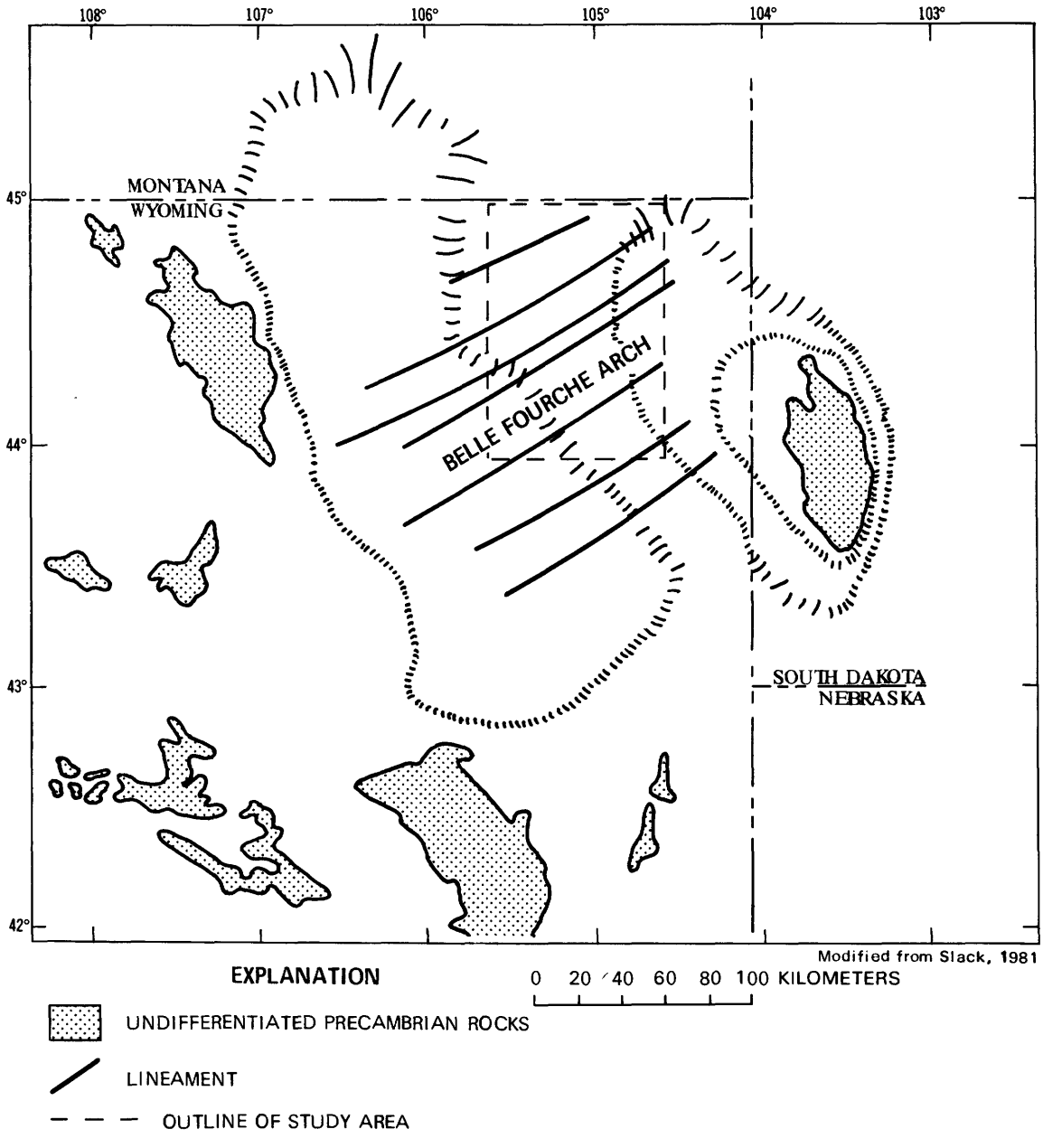

FIGURE 31.—Structural lineaments outlining the Belle Fourche Arch, Powder River Basin, Wyoming and Montana.

study area and from a review of the geologic literature. Sandstone samples from the upper Fox Hills Sandstone were obtained from drill cores taken in the uranium district west of Oshoto and from outcrop samples collected during this study from exposures between Moorcroft and Upton (sec. 9, T. 47 N., R. 67 W.).

The mineral phases identified by X-ray diffraction are listed in table 18. The absence of pyrite in the outcrop was the only difference observed between core and outcrop mineralogies.

Dobbin and Reeside (1930) provided a petrographic analysis by C. S. Ross of the Colgate Sandstone Member of the Fox Hills Sandstone from north of the Powder River Basin near the Fort Peck Reservoir in Montana (T. 21 N., R. 32 E.). The Colgate Sandstone Member is the stratigraphic equivalent of the upper part of the Fox Hills Sandstone in Montana. This petrographic analysis agrees with the results of the analyses by X-ray diffraction and also demonstrates the presence of minor amounts of biotite, tourmaline, garnet, zircon, and apatite. Ross also identified beidellite, a sodium smectite, in the clay matrix.

Stratigraphic descriptions of the Fox Hills Sandstone by Robinson and others (1964) pointed out the presence

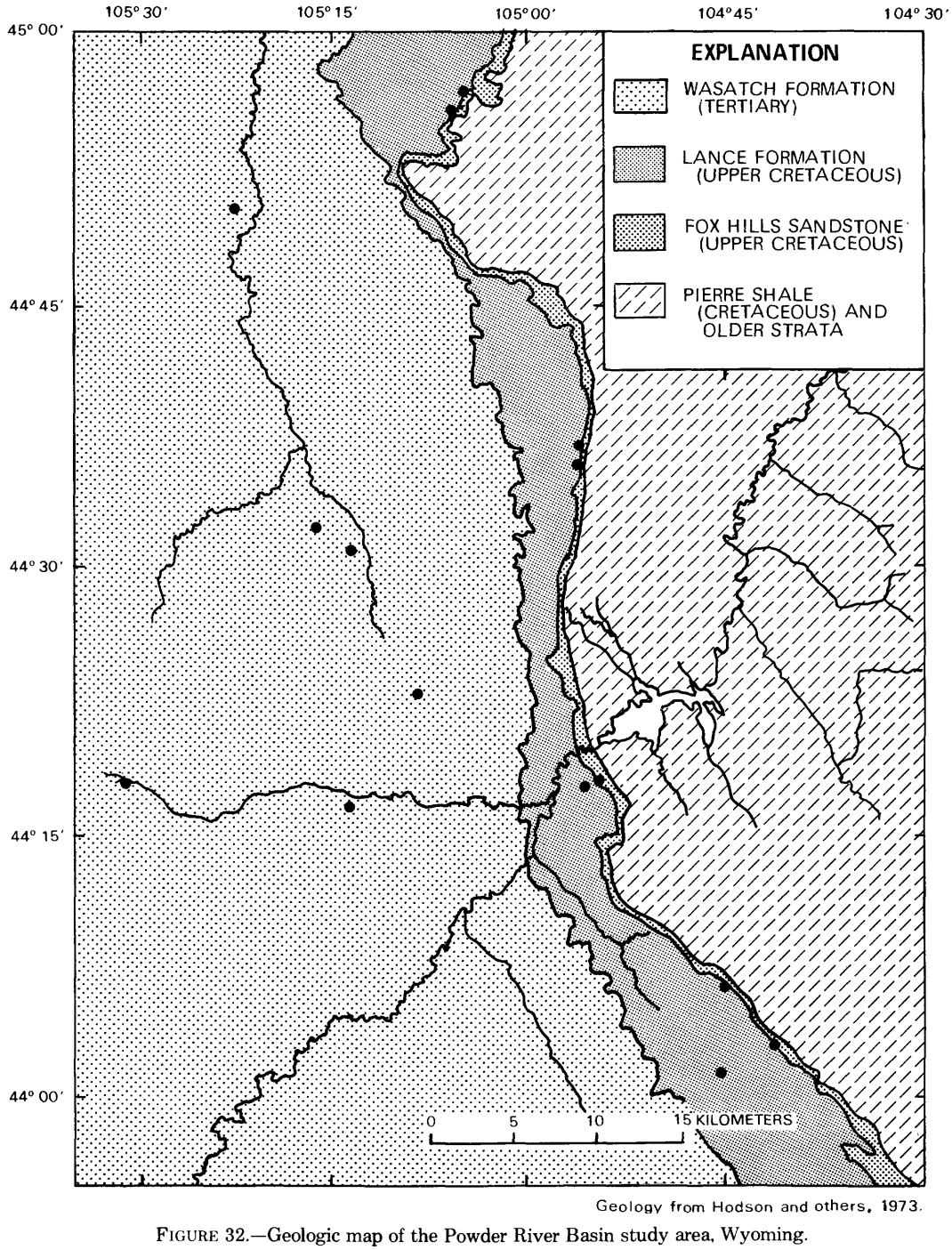

FIGURE 32.—Geologic map of the Powder River Basin study area, Wyoming.

of ferric oxyhydroxides as disseminated grains and ferruginous sandstone nodules, numerous calcareous beds and concretions, and siderite concretions. They concluded that although the lower part of the Lance contains an abundance of thin coal seams and carbonaceous shales, the sandstones of the Lance do not differ appreciably from those of the Fox Hills. Robinson and others (1964) also described selenite in the shales of the upper part of the Lance Formation.

HYDROLOGY

Based on substantial head differences between potentiometric surface maps constructed from data on wells screened in different geologic units, Anna and Croft (1977) concluded that three hydrologically distinct aquifer systems are present in the sediments overlying the Pierre Shale. The lowermost aquifer system, consisting of the upper part of the Fox Hills Sandstone and

TABLE 18.—*Minerals identified by X-ray diffraction in samples of Fox Hills Sandstone from the Powder River Basin, Wyoming*

Fraction	Mineral	Idealized chemical formula
Whole rock	Quartz	SiO_2
	Albite	$NaAlSi_3O_8$
	Microcline	$KAlSi_3O_8$
	Muscovite	$KAl_3Si_3O_{10}(OH)_2$
	Calcite	$CaCO_3$
	Dolomite	$CaMg(CO_3)_2$
Clay (<2 micrometers)	Kaolinite	$Al_2Si_2O_5(OH)_4$
	Smectite	---
	Chlorite	$Mg_5Si_4O_{10}(OH)_8$
Sulfide	Pyrite	FeS_2
Heavy	Rutile	TiO_2

TABLE 19.—*Minerals of the Fox Hills Sandstone identified in previous studies (Dobbin and Reeside, 1930; Robinson and others, 1964), but not detected in X-ray diffraction analyses*

Mineral	Idealized chemical formula
Ferric oxyhydroxides	$Fe(OH)_3$, FeOOH, Fe_2O_3
Siderite	$FeCO_3$
Beidellite	$Na_{0.3}Al_2(Si_{3.7}Al_{0.3})O_{10}(OH)_2$
Biotite	$K(Mg,Fe)_3AlSi_3O_{10}(OH)_2$
Tourmaline	---
Garnet	---
Zircon	$ZrSiO_4$
Apatite	$Ca_5(PO_4)_3$ (F,Cl,OH)

the lower part of the Lance Formation, is confined from below by the Pierre Shale and from above by the siltstones and claystones of the upper part of the Lance Formation. The two overlying Tertiary aquifers of the Fort Union and Wasatch Formations are therefore effectively isolated from the Lance–Fox Hills aquifer. The presence of interbedded siltstones and claystones in the lower part of the Lance decreases the vertical permeability in the aquifer, impeding vertical mixing between the Lance Formation and Fox Hills Sandstone.

A regional potentiometric surface map (D. H. Lobmeyer, U.S. Geological Survey, written commun., 1981), presented in figure 33, indicates the inferred directions of regional ground-water movement. Northward thinning of the aquifer sandstones in the southern part of the study area, in combination with enhanced vertical permeabilities along the Belle Fourche Arch (Slack, 1981), suggests upward ground-water movement and subsequent discharge into the Belle Fourche River. An undetermined fraction of this flow probably continues northwest of the Belle Fourche River and out of the study area.

Recharge to the Lance–Fox Hills aquifer enters the outcrop area of these formations in the central and northern sections of the study area. Recharged water flows west toward the axis of the basin, then north into Montana, as shown by the northern flow line in figure 33. Pump tests on the NGP-RASA (Northern Great Plains Regional Aquifer-System Analyses) test well in the northeastern Powder River Basin (sec. 11, T. 55 N., R. 77 W.) yield hydraulic conductivities of 3.5×10^{-7} m/s for the Fox Hills Sandstone and 1.6×10^{-6} m/s for the Lance Formation, (D. H. Lobmeyer, U.S. Geological Survey, written commun., 1981). Assuming a constant effective porosity of 0.10 to 0.15, and an average hydraulic gradient of 2.2×10^{-3}, Darcy's Law may be used to calculate average flow rates of 0.16 to 1.08 m/yr for the ground water in the Lance–Fox Hills aquifer in the study area.

DATA PRESENTATION AND INTERPRETATION

MAJOR AND MINOR ELEMENTS

Chemical and isotopic analyses of 21 ground-water samples were performed to characterize the Lance–Fox Hills aquifer system in the northeastern Powder River Basin. Major element determinations are presented in table 20; minor and trace element determinations are presented in table 21. The locations of the 18 wells sampled during this study, P1 through P18, are presented in figure 29, with three additional wells, P20, P30, and P41, sampled by Hodson (1971) and Chatham and others (1981). Drillers' logs and well depths were used to locate wells open to the upper part of the Fox Hills Sandstone to minimize the effects of vertical variations in the lithology of this lenticular system. Samples P1, P8, and P12 represent confined ground waters of the lower part of the Lance Formation, and P13, P14, and P18 were sampled from wells located on the Lance outcrop. Samples from the lower part of the Lance were collected to characterize the part of the aquifer that lies above the Lance–Fox Hills contact and to evaluate the possibility of recharge to the Fox Hills occurring as downward leakage through the Lance in the area of the Lance outcrop. Additional information on the composition and geochemical behavior of ground waters from the lower part of the Lance Formation was derived from Chatham and others (1981). Discussion of ground-water chemistry is generally restricted to the upper part of the Fox Hills Sandstone because vertical variations in the chemistry of the Lance–Fox Hills aquifer system prevent consideration of this unit as a whole (Chatham and

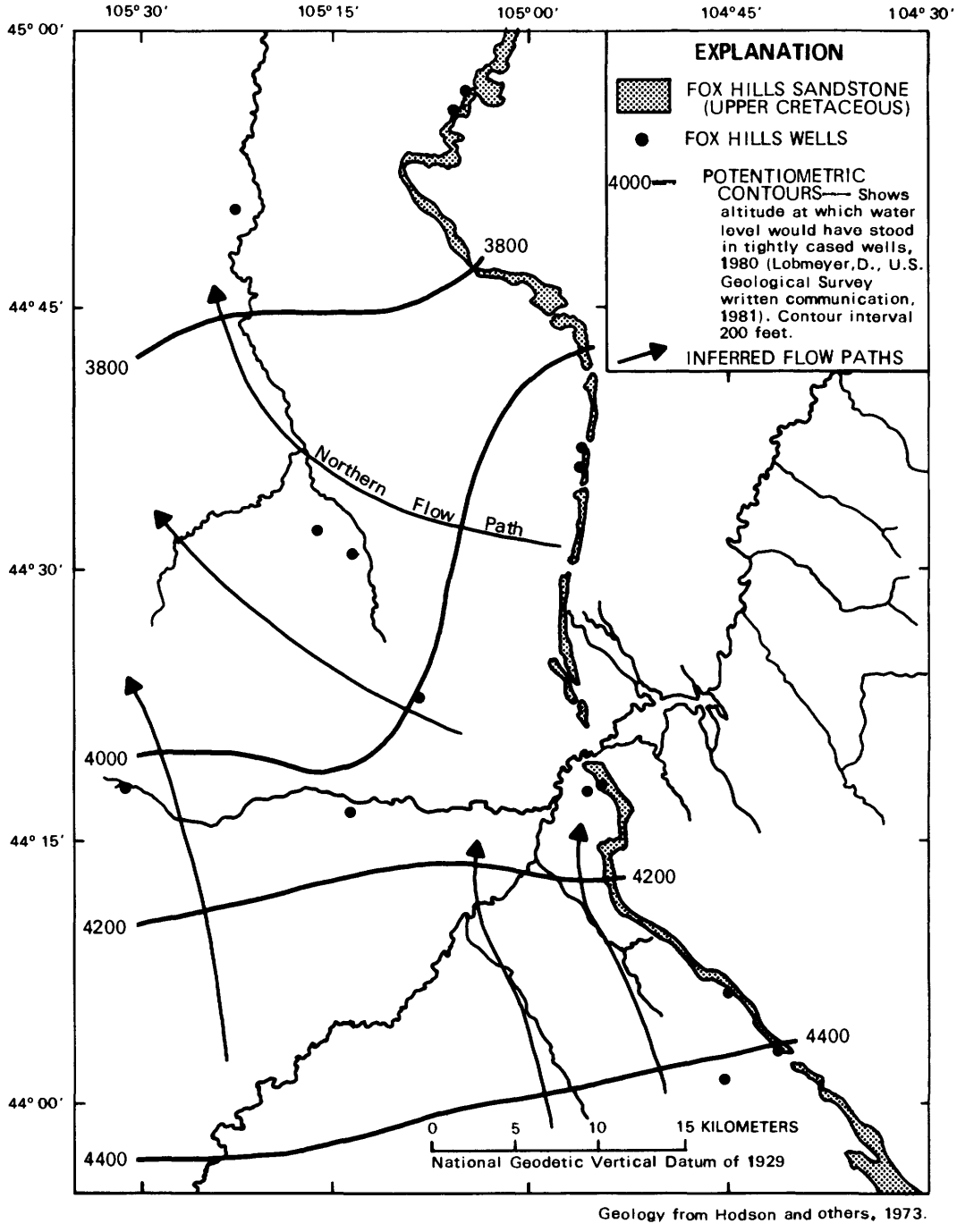

FIGURE 33.—Potentiometric contours and inferred flow paths for the Lance-Fox Hills aquifer, Powder River Basin study area, Wyoming [1 foot (in contour interval)=0.305 meter].

others, 1981). Locations of wells sampled in the upper part of the Fox Hills are shown in figure 34.

The dissolved solids distribution of waters in the upper Fox Hills (fig. 35) reflects the hydrology of the aquifer system. As expected, dissolved solids concentrations increase downflow from initially low values in the northern recharge area. A plume of intermediate dissolved solids content can be attributed to the mixing of recharge waters with older, northwest-flowing waters; waters high in dissolved solids identify the southern discharge area.

Two samples, P9 and P17, are representative of deeper basin waters and have intermediate dissolved solids concentrations. Similarities between waters recharging this area (Hodson and others, 1973) and recharge waters within the study area indicate that the

TABLE 20.—*Concentrations of dissolved major elements in waters from the Lance–Fox Hills aquifer, Powder River Basin, Wyoming*

[Concentrations in milligrams per liter unless otherwise specified. C, degrees Celsius; µS/cm, microsiemens per centimeter; < indicates concentrations below detection limit for that analysis]

Sample	Calcium, Ca	Magnesium, Mg	Sodium, Na	Potassium, K	Chloride, Cl	Sulfate, SO_4	Bicarbonate, HCO_3	Carbonate, CO_3	pH	Temperature, *T* (C)	Specific conductance, SpC (µS/cm at 25 C)
				Na + K							
P1 ----------	1.8	0.6	270	1.4	6.7	120	532	9	8.92	15.8	810
P2 ----------	1.9	4	300	1.3	18	150	583	8	8.91	19.6	1,010
P3 ----------	1.4	<1	330	1.4	23	150	626	12	8.77	18.0	1,150
P4 ----------	92	38	16	7.2	1.3	75	453	<1	7.15	11.0	530
P5 ----------	46	18	64	7.7	4.8	48	377	<1	7.46	11.0	460
P6 ----------	29	16	140	14	2.4	66	483	<1	7.71	9.0	580
P7 ----------	54	42	24	13	5.4	56	386	<1	7.50	9.6	440
P8 ----------	3.8	3	230	1.8	1.9	260	298	3	8.98	11.6	720
P9 ----------	1.7	<1	360	2.0	21	97	790	13	8.64	27.0	1,460
P10 ----------	93	45	490	5.8	1.1	1,000	464	<1	7.71	9.2	1,690
P11 ----------	1.2	<1	820	1.2	24	140	611	18	8.92	23.0	1,200
P12 ----------	2.1	4	240	1.1	2.3	260	268	13	9.21	14.1	780
P13 ----------	25	9.5	220	3.5	2.5	260	403	<1	7.59	10.6	730
P14 ----------	51	24	17	3.2	1.9	13	299	<1	7.63	10.2	388
P15 ----------	29	9.9	600	3.3	9.0	650	912	<1	8.03	9.8	1,620
P16 ----------	150	130	200	7.4	14	740	560	<1	7.42	9.5	1,480
P17 ----------	2.7	4	370	4.0	30	1.6	982	2	8.18	38.9	1,810
P18 ----------	94	43	70	5.0	2.7	150	524	<1	7.25	10.4	690
P20[1] --------	18	12	300	3.8	3.5	384	557	20	8.7	10.0	1,660
P30[2] --------	100	67	170	6	9	610	391	0	6.85	11.6	1,410
P11[2] --------	100	54	130	7	12	490	389	0	7.20	11.1	1,050

[1]Hodson (1971)

[2]Chatham and others (1981)

deep basin samples should be qualitatively similar to waters that eventually evolve from northern study area waters.

Stiff diagrams, plotted in figure 36, show that recharge waters contain variable amounts of sodium, calcium, and magnesium with bicarbonate, changing in cationic concentrations to dominantly sodium types within a short distance of the outcrop. Samples collected downflow from the recharge area also contain increasing concentrations of bicarbonate, sulfate, and chloride. The deep basin samples, P9 and P17, are also predominantly sodium bicarbonate, but contain slightly more bicarbonate and chloride, as well as less sulfate, than samples collected to the north. The high dissolved solids concentrations in waters from the discharge area are apparently caused by additions of sulfate balanced by sodium, with waters there containing sodium, bicarbonate, and sulfate as their major components. In the area where recharge waters are thought to be mixing with more mature waters, an intermediate composition, predominantly sulfate water, is found. This composition has intermediate bicarbonate and low chloride with sodium as the predominant cation, followed by slightly lesser amounts of calcium and magnesium.

Ion-exchange reactions appear to play an important role in the evolution of ground waters in the Fox Hills, as shown by the uniform variation in log molar $([Ca]+[Mg])/[Na]^2$ ratios, an operational parameter, plotted in figure 37. Only samples taken from the outcrop area have more than several milligrams per liter calcium and magnesium, indicating that the divalent cations are exchanged for monovalent sodium ions present on clay surfaces (table 1, reactions 28 and 29) soon after recharge water enters the aquifer. Mixed layer smectite clays, such as the beidellite found in the Fox Hills Sandstone, are known for their high cation exchange capacities. Grim (1968) reported CEC values for smectites on the order of 80 to 150 meq/100 g, which are several times greater than the CEC's for illite (10–40 meq/100 g) and kaolinite (3–15 meq/100 g). The higher CEC of smectite, compared to that of illite and kaolinite, may explain the relatively rapid decrease in calcium and magnesium concentrations in the Fox Hills Sandstone, in contrast to the more gradual decreases observed in the Judith Basin where the latter two clays predominate.

The plot of log molar divalent/monovalent cation ratios (fig. 37) accurately describes the pattern of recharge and ground-water movement along the flow path in the northern half of the study area, but interpretation of the ratios is somewhat more difficult in the southern part. Ambiguity in the contour pattern is most likely the result of conflicting effects, because of the mixing in the outcrop area of older, northeastward moving waters having low log $([Ca]+[Mg])/[Na]^2$ ratios with younger recharge waters having high log $([Ca]+[Mg])/[Na]^2$ ratios. In any event, the log molar divalent to monovalent ratios attain significantly larger values north of the Belle Fourche River than to the south and indicate the greater significance of recharge in influencing the

TABLE 21.—*Concentrations of dissolved minor and trace elements in*

[Concentrations in micrograms per liter unless otherwise specified, mg/L, milligrams per liter;

Sample	Aluminum, Al	Ammonium, NH_4 (mg/L)	Arsenic, As	Barium, Ba	Boron, B	Bromide, Br (mg/L)	Cadmium, Cd	Chromium, Cr	Copper, Cu	Dissolved oxygen, O_2 (mg/L)	Fluoride, F (mg/L)	Iodide, I (mg/L)	Iron, Fe	Lead, Pb
P1 --------	20	0.10	1	70	130	0.1	2	<10	<1	<0.1	2.8	<0.01	40	<1
P2 --------	20	13	<1	50	250	3	<1	<10	<1	<1	2.1	0.3	30	<1
P3 --------	140	08	<1	60	320	4	<1	<10	<1	<1	2.8	0.3	380	1
P4 --------	10	50	<1	60	20	<1	<1	<10	1	5	2	<01	1,100	<1
P5 --------	<1	48	<1	70	20	<1	<1	<10	<1	1.4	1	<01	240	2
P6 --------	10	36	1	80	100	<1	1	<10	4	1	2	<01	1,000	4
P7 --------	10	10	<1	50	20	1	<1	<10	1	2.0	1	<01	30	<1
P8 --------	10	08	1	30	20	<1	<1	<10	<1	<1	1	<01	<10	<1
P9 --------	30	17	<1	100	230	3	<1	<10	<1	<1	3.9	06	60	2
P10 --------	10	2.7	<1	<1	590	3	1	<10	<1	2	3	02	1,300	4
P11 --------	60	17	<1	50	420	4	<1	<10	<1	<1	2.0	09	10	1
P12 --------	10	15	<1	30	60	<1	<1	<10	<1	1	3	<01	<10	1
P13 --------	<1	1.4	<1	10	90	<1	<1	<10	<1	2.4	<1	<01	320	2
P14 --------	30	28	<1	80	30	<1	<1	<10	9	1	<01	20	1	2
P15 --------	50	53	1	<1	1,300	1	<1	<10	1.4	4	0.5	60	<1	3
P16 --------	<1	70	<1	<1	140	1	1	<10	3.0	1	<01	450	1	3
P17 --------	40	7.3	1	200	230	4	<1	<10	<1	<1	3.2	04	20	1
P18 --------	<1	79	<1	50	80	<1	<1	<10	2	<1	2	<01	1,600	2
P20[1] ------	---	---	---	---	120	---	---	---	---	---	1.8	---	100	---
P30[2] ------	---	---	2	---	---	---	---	---	---	8	5	---	500	---
P41[2] ------	---	---	2	---	---	---	---	---	---	<1	1	---	10	---

chemistry and hydrology of the northern area.

Chloride concentrations, plotted in figure 38, increase along the flow path from the recharge area westward and are even higher in the deep basin samples. As in the Kootenai, increases in chloride concentration are thought to result from minor amounts of leakage through shale confining beds. A water sample taken from the underlying Parkman Sandstone Member of the Mesaverde Formation approximately 45 km southwest of Gillette shows the presence of 3,400 mg/L chloride (Wyoming Water Planning Program, 1972). To account for observed increases in chloride of roughly 25 mg/L, an upward leakage of less than 1 percent of this type water from the Pierre Shale would be required. Chloride may also be leached from shale layers within the aquifer, leading to similar changes in chemistry and making a determination of the exact source impossible with the data available.

In the discharge area, where chloride concentrations should be similar to those measured in the deep basin samples because of the similar origins of these two waters, the values are relatively low. Low to intermediate chloride concentrations in this area are another indication that, although water is being discharged to the Belle Fourche River, recharge may be entering the aquifer outcrop and diluting the northward moving water.

Sulfate concentrations, plotted in figure 39, behave differently in the northern and southern portions of the study area. Along the northern flow path, sulfate concentrations increase, then decrease slightly. Comparison with deeper basin samples suggests that sulfate will continue to decrease in concentration as the water matures. In the recharge area, sulfate is probably derived from the dissolution of gypsum (reaction 20) or the oxidation of pyrite (reactions 9 and 10). Gypsum is commonly present in alkali soils from evaporation of soil water in arid climates, but, based on mineralogic and stratigraphic descriptions, appears to be absent in the consolidated sediments of the Fox Hills Sandstone. Pyrite may be oxidized only in the presence of O_2 (reaction 9) or ferric iron (reaction 10), but these oxidants are essentially absent after the appearance of H_2S in the aquifer. Therefore, neither gypsum dissolution nor pyrite oxidation can adequately explain increases in sulfate concentration after the appearance of H_2S. However, high sulfate waters, derived from gypsum dissolution or pyrite oxidation, are present in the overlying Lance Formation (up to 710 mg/L, Chatham and others, 1981). It seems likely, then, that increases in sulfate concentration in the Fox Hills Sandstone probably result from downward movement of high sulfate waters from the overlying, hydrologically continuous Lance Formation.

Subsequent decreases in sulfate concentration appear to be the result of bacterially mediated sulfate reduction (reaction 6). Sulfate-reducing bacteria (*Desulfovibrio* sp.) are ubiquitous in ground waters of the northern Powder River Basin in Montana (R. W. Lee, U.S. Geological Survey, oral commun., 1981) and should be expected in the Lance–Fox Hills aquifer of Wyoming. In the absence of sulfur isotopic compositions, however,

waters from the Lance–Fox Hills aquifer, Powder River Basin, Wyoming

[H_2S, hydrogen sulfide; < indicates concentrations below detection limit for that analysis]

Lithium, Li	Manganese, Mn	Molybdenum, Mo	Nitrate, NO_3 (mg/L)	Nitrite, NO_2 (mg/L)	Organic carbon, organic C (mg/L)	Phosphate, PO_4 (mg/L)	Selenium, Se	Silica, SiO_2 (mg/L)	Strontium, Sr	Sulfide, S (mg/L as H_2S)	Uranium, U	Vanadium, V	Zinc, Zn
10	6	<10	0.13	<0.01	7.1	0.18	<1	9.2	70	0.2	0.37	4	3
20	5	<10	13	<.01	1.9	15	<1	10	70	5	.21	2	3
20	6	<10	.04	<.01	10	15	<1	11	70	2	12	2	3
60	440	<10	13	<.01	14	.06	<1	18	2,400	1	17	2	270
60	120	<10	58	<.01	3.7	.03	<1	15	1,500	2	.02	1	130
40	110	<10	.09	<.01	5.1	<.01	<1	9.7	1,100	3	1.6	2	20
40	3	<10	3.5	<.01	18	<.01	6	11	2,100	1	9.3	1	110
50	20	<10	13	<.01	8.4	<.01	<1	11	130	4	.03	2	3
20	3	<10	.09	<.01	14	.06	<1	12	110	2	16	3	3
280	110	<10	13	<.01	6.9	<.01	<1	9.5	2,100	2	27	2	120
20	4	<10	.09	<.01	15	.31	<1	12	60	2	.07	3	3
10	8	<10	.09	<.01	2.0	18	<1	10	70	4	.04	2	8
110	490	<10	35	<.01	2.8	.03	<1	16	770	3	.01	2	300
30	210	<10	7.0	.03	1.1	.03	<1	13	900	<1	4.2	1	170
90	10	<10	2.1	.07	7.1	.06	<1	8.9	630	1	2.5	3	160
40	240	<10	39	16	6.0	<.01	19	10	5,400	1	7.9	2	150
20	6	<10	18	13	8.6	.06	<1	17	190	2	12	1	<3
30	530	<10	13	<.01	9.4	.00	<1	15	3,100	1	70	1	9
---	---	---	4.9	---	---	---	---	8.0	---	---	---	---	---
---	240	2	6	---	---	0	2	---	---	<1.0	9	1	--
---	170	2	2.4	---	---	0	8	---	---	<1.0	2.0	1	---

the small decrease in sulfate (10 mg/L) along the northern flow path cannot be unequivocally attributed to sulfate reduction. Similarly, mass transfer in the aqueous phase is not sufficiently well defined along the deep basin flow path to infer sulfate reduction. Therefore, the process of sulfate reduction must be considered as likely to occur only in the Lance–Fox Hills aquifer; it cannot be considered as an incontrovertible source of CO_2 in the system.

The highest sulfate concentrations in the study area are found along the Belle Fourche River, where recharge waters are thought to be mixing with older, more mature waters in the aquifer outcrop. The introduction of variable amounts of oxygenated recharge water into a reduced ground-water flow system will undoubtedly result in fluctuations of the redox interface (Eh=OmV), and the oxidation of sulfide minerals, generating sulfate. Additional sulfate may be derived from the dissolution of gypsum in the soil zone, although this source would not readily explain high sulfate concentrations present only in the southern portions of the study area.

Large increases in pH are evident along the northern flow path from the recharge area basinward as shown in figure 40. As previously discussed, increases in pH are commonly observed in ground-water flow systems as a result of dissolution or hydrolysis of aquifer mineral phases. Comparison with the deep basin samples indicates that slight decreases in pH may occur as geochemical evolution continues in the aquifer. In the discharge area, pH's are at low to intermediate values, similar to those measured in waters from the northern recharge area. Low to intermediate pH's in well-buffered, high-bicarbonate waters might support the hypothesis that high sulfate concentrations in these waters are due to pyrite oxidation, although such a conclusion is tenuous.

Total inorganic carbon concentrations were calculated by summing the molalities of all carbonate species computed by WATEQ2. Calculated C_T values, plotted in figure 41, indicate that increases in bicarbonate and carbonate concentrations are representative of increases in C_T along the flow path. Comparison with the deep basin samples indicates that this trend should continue with further ground-water evolution. Concentrations of C_T are highly variable in the discharge area, ranging from 7.9 mg/L at P10 to 15.2 mg/L at P15, suggesting large-scale local variations in ground-water chemistry.

Increases in the concentration of total inorganic carbon along the flow path in the Fox Hills Sandstone reflect an influx of carbon to the aqueous system. As in the Judith Basin, increases in C_T concentration may be the result of oxidation of organic carbon by O_2, NO_3^-, or SO_4^{-2} reduction processes, coalification of lignite, methanogenesis, migration of CO_2 or CH_4 into the aquifer, or the dissolution of carbonate minerals. Although O_2 and NO_3^- reduction processes undoubtedly produce CO_2 in the outcrop area, these compounds are rapidly consumed and unavailable for reaction downdip. The presence of H_2S in all but several outcrop wells suggests that sulfate reduction may be an active process, but a lack of appropriate data and the existence of open

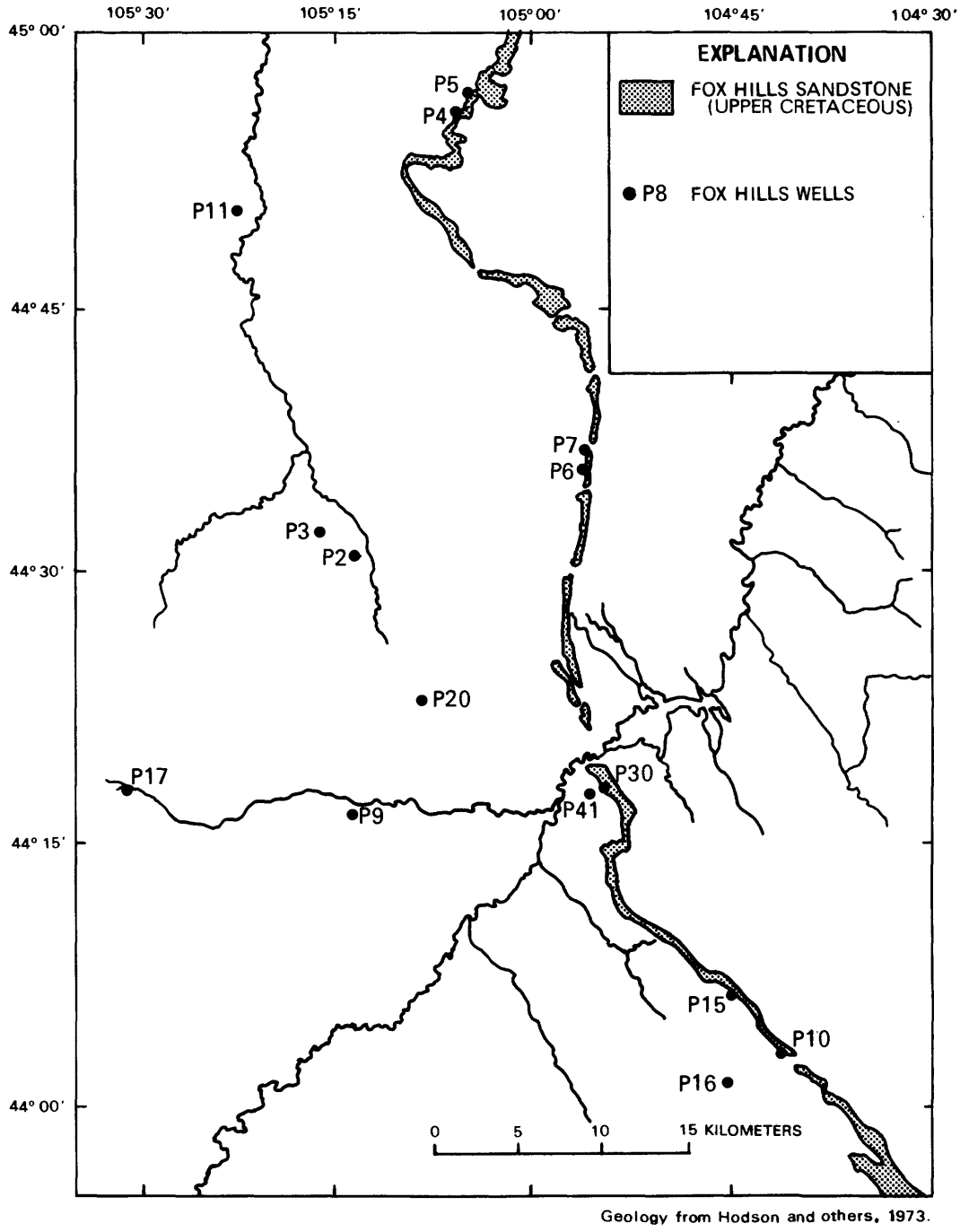

FIGURE 34.—Index map of Powder River Basin study area, Wyoming, showing the locations of wells sampled in the Fox Hills Sandstone.

system conditions with respect to SO_4^{-2} make sulfate reduction impossible to substantiate. Considering the occurrence of lignite beds at the Lance–Fox Hills contact, coalification may provide significant influxes of CO_2. Migration of CO_2 into the aquifer is also possible, although oxidation of migrating CH_4 as a CO_2 source is unlikely because CH_4 would be expected to be relatively stable in anoxic waters of the Fox Hills Sandstone. Acetate fermentation (reaction 7) may also be an active process and would be evident by a 70 per mil carbon isotope fractionation accompanying this reaction (Bottinga, 1969).

Acidity produced by the generation of CO_2 would allow for the dissolution of saturated mineral phases.

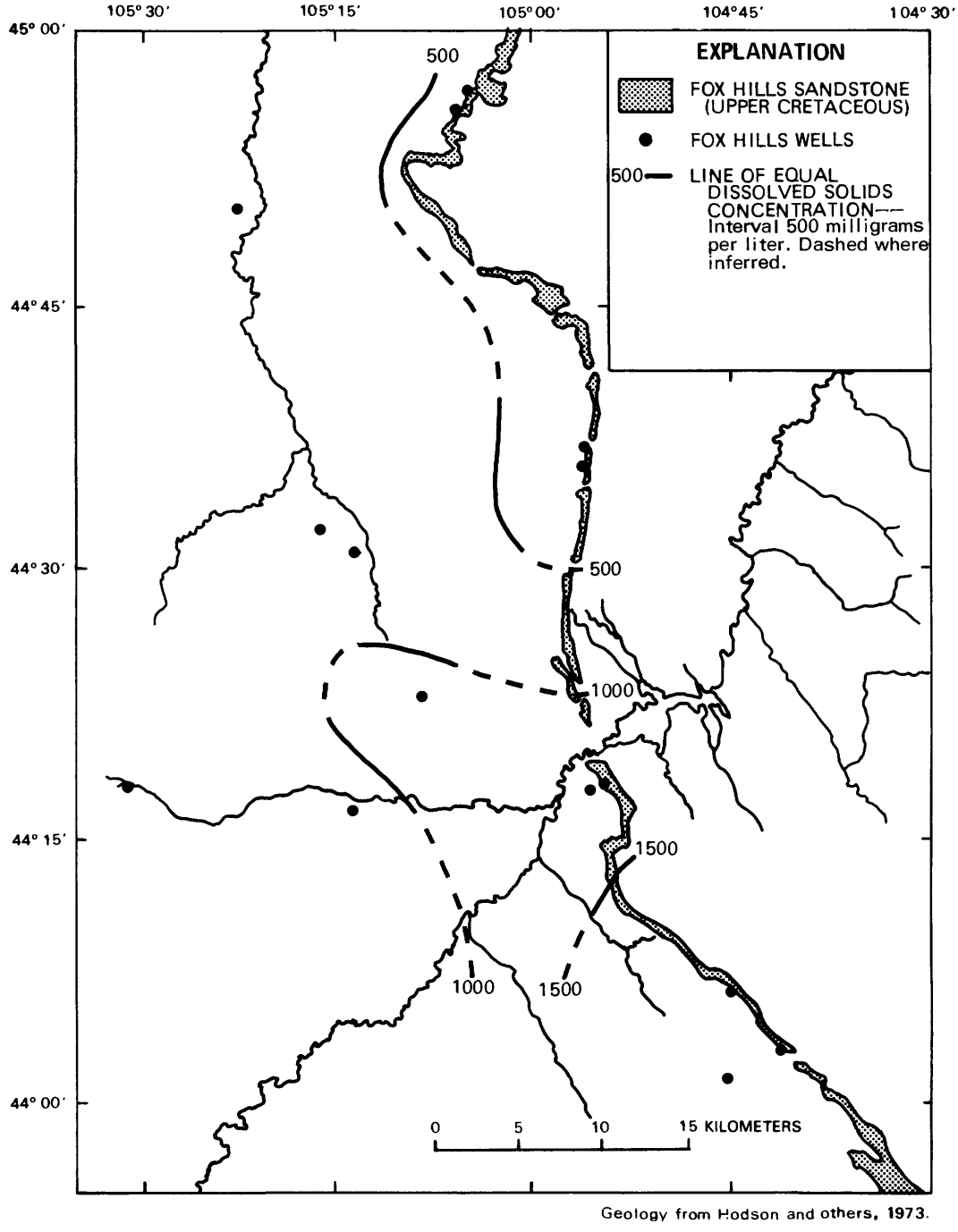

FIGURE 35.—Dissolved solids concentration in waters from the Fox Hills Sandstone, Powder River Basin, Wyoming.

Dissolution of carbonates would lead to further increases in C_T (reactions 21-23); hydrolysis of aluminosilicates (reactions 24-27) would not. A phase diagram for the system Ca-Mg-CO_2-H_2O is presented in figure 42. The compositions of waters from the Fox Hills Sandstone having magnesium concentrations significantly greater than the detection limit plot primarily in the calcite stability field, near the calcite-dolomite stability boundary. Therefore, dolomite should be unstable in these waters, possibly dissolving incongruently to form calcite.

It is interesting to note that the compositions of two Fox Hills Sandstone waters reported by Chatham and others (1981) clearly fall in the dolomite stability field.

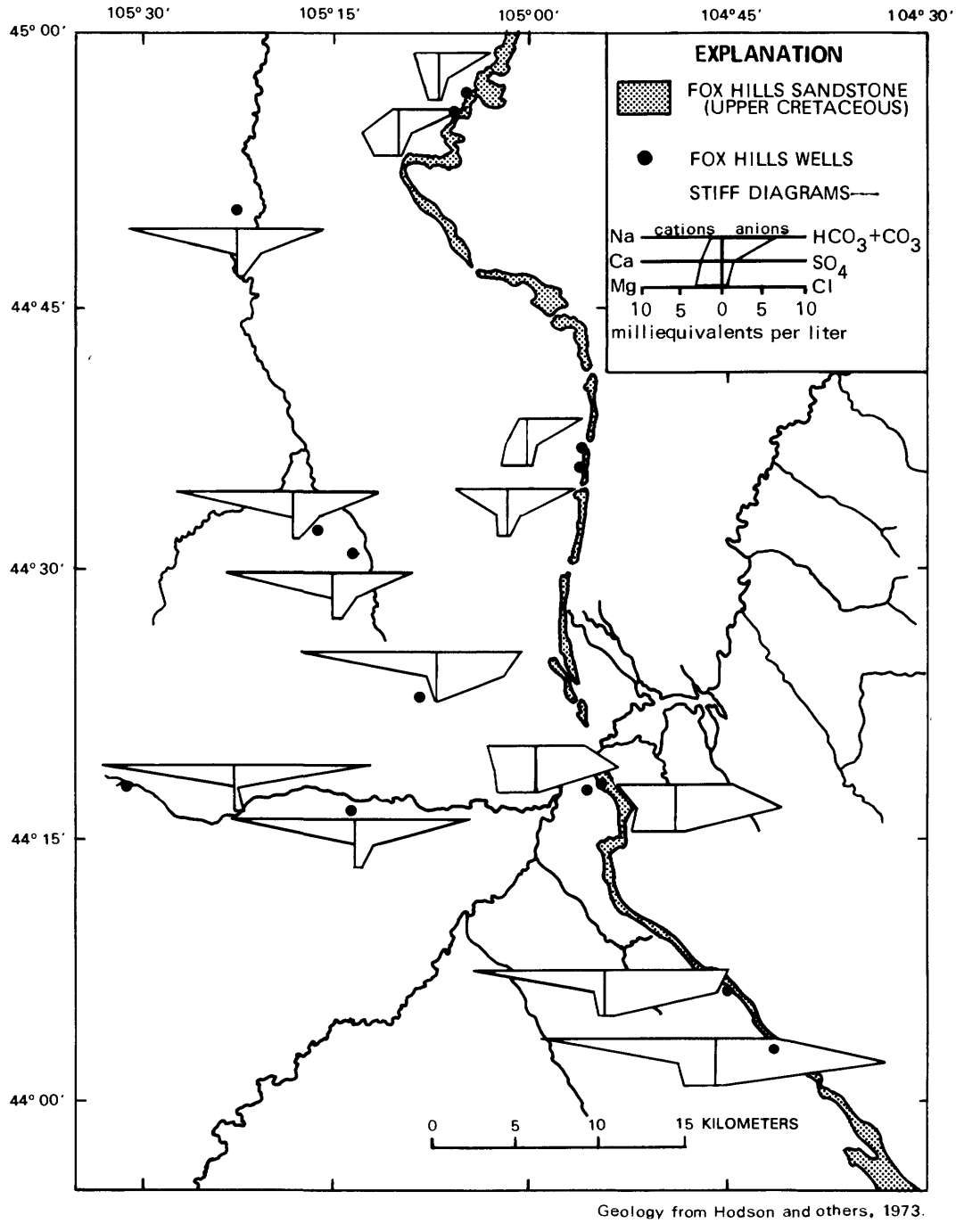

FIGURE 36.—Stiff diagrams of major element concentrations in waters from the Fox Hills Sandstone, Powder River Basin, Wyoming.

These waters are thought to represent mixing between recent recharge and older, high sulfate, high-bicarbonate waters. The resulting mixture has a $(a_{Mg^{+2}})/(a_{Ca^{+2}})$ ratio significantly greater than unity, implying that dolomitization of calcite may be occurring in these waters on a limited scale (Hanshaw and others, 1971; Folk and Land, 1975).

Silica concentrations remain relatively constant along the flow path, averaging 10.7 mg/L, while aluminum concentrations vary irregularly from 0.010 to 0.140 mg/L. Reasons for these fluctuations in aluminum concentration are uncertain, although contamination by wind-blown dust, which was a problem at the well with the highest aluminum concentrations, may explain anomalously high concentrations of aluminum, iron, manganese, and silica in such samples.

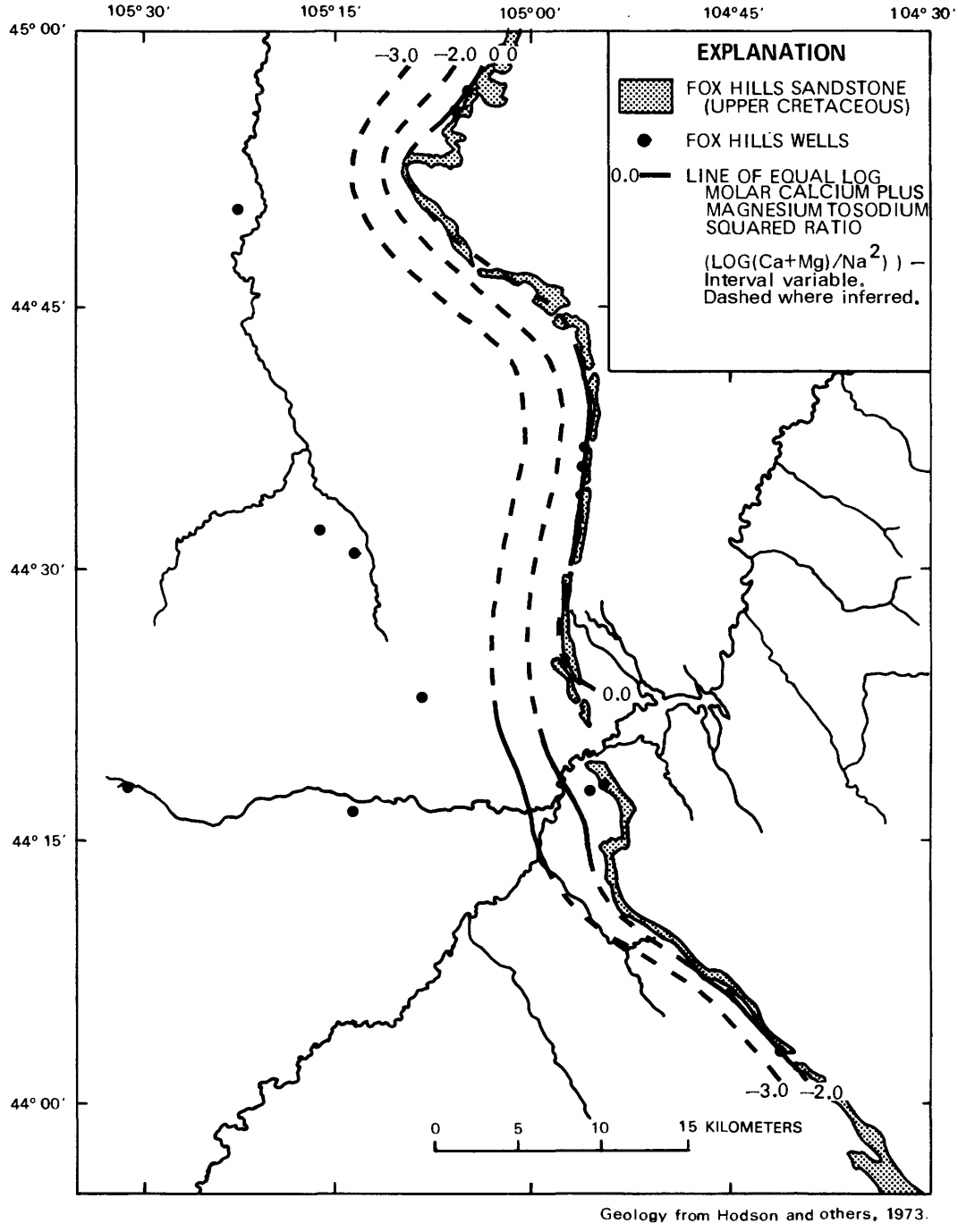

FIGURE 37.—Log molar ratios of calcium plus magnesium to sodium concentrations in waters from the Fox Hills Sandstone, Powder River Basin, Wyoming.

Phase diagrams were calculated using the thermodynamic data of Helgeson (1969) and the kaolinite stability of Bassett and others (1979), to determine which alumino-silicates are stable in the waters sampled. A log $(a_{H_4SiO_4})$–log $(a_{Na^+})/(a_{H^+})$ activity diagram with compositions of waters from the Lance-Fox Hills aquifer superposed (fig. 43) best demonstrates water-mineral relationships in this system. Kaolinite is stable in low pH, low sodium outcrop waters, whereas Na-montmorillonite, a pure end member, is stable in all other waters. Chlorite, which does not plot on this diagram, is unstable in all waters sampled, implying that aluminum and silica concentrations are controlled by kaolinite and a smectite similar in stability and composition to a Na-montmorillonite.

Strontium decreases in concentration basinward

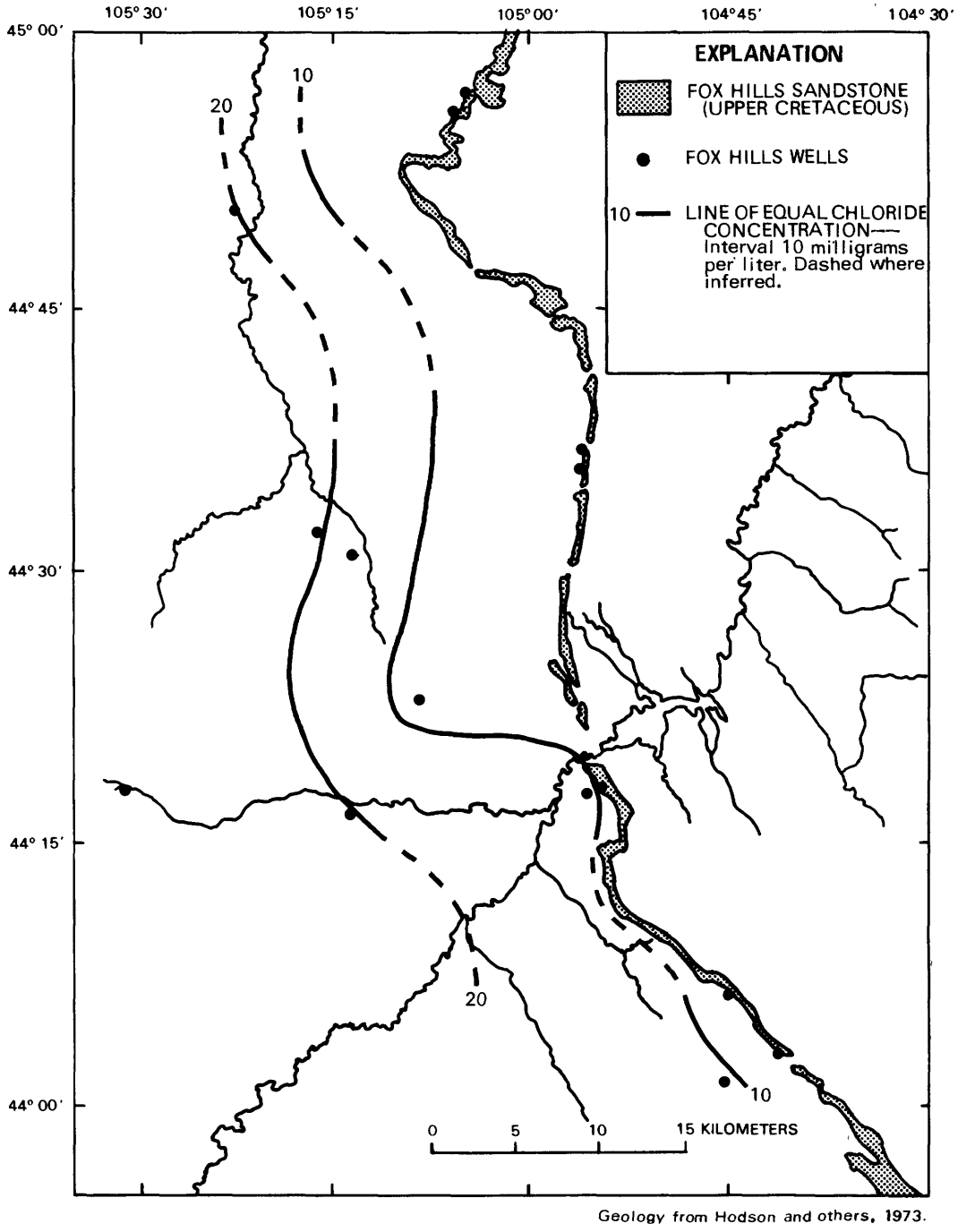

FIGURE 38.—Chloride concentrations in waters from the Fox Hills Sandstone, Powder River Basin, Wyoming.

along the flow path (fig. 44). Variations in strontium concentration are probably related to adsorption on clay surfaces in a manner similar to the other alkaline earths (Wahlberg and others, 1965a; 1965b), but may also reflect equilibrium with respect to carbonates or sulfates present in the system. Celestite, strontianite, or a strontium calcite therefore seem to be the most likely mineral phases to control strontium concentrations.

Oxidation potentials in waters of the Fox Hills Sandstone were calculated using the Nernst equation and the O_2-H_2O (reaction 12) or SO_4^{-2}-H_2S (reaction 16) redox couples, as appropriate. The Eh values calculated from these couples are listed in table 22 and plotted in figure 45. Oxidation potentials vary from positive values in the recharge area to increasingly negative values along the flow path and in the deeper basin samples. Along

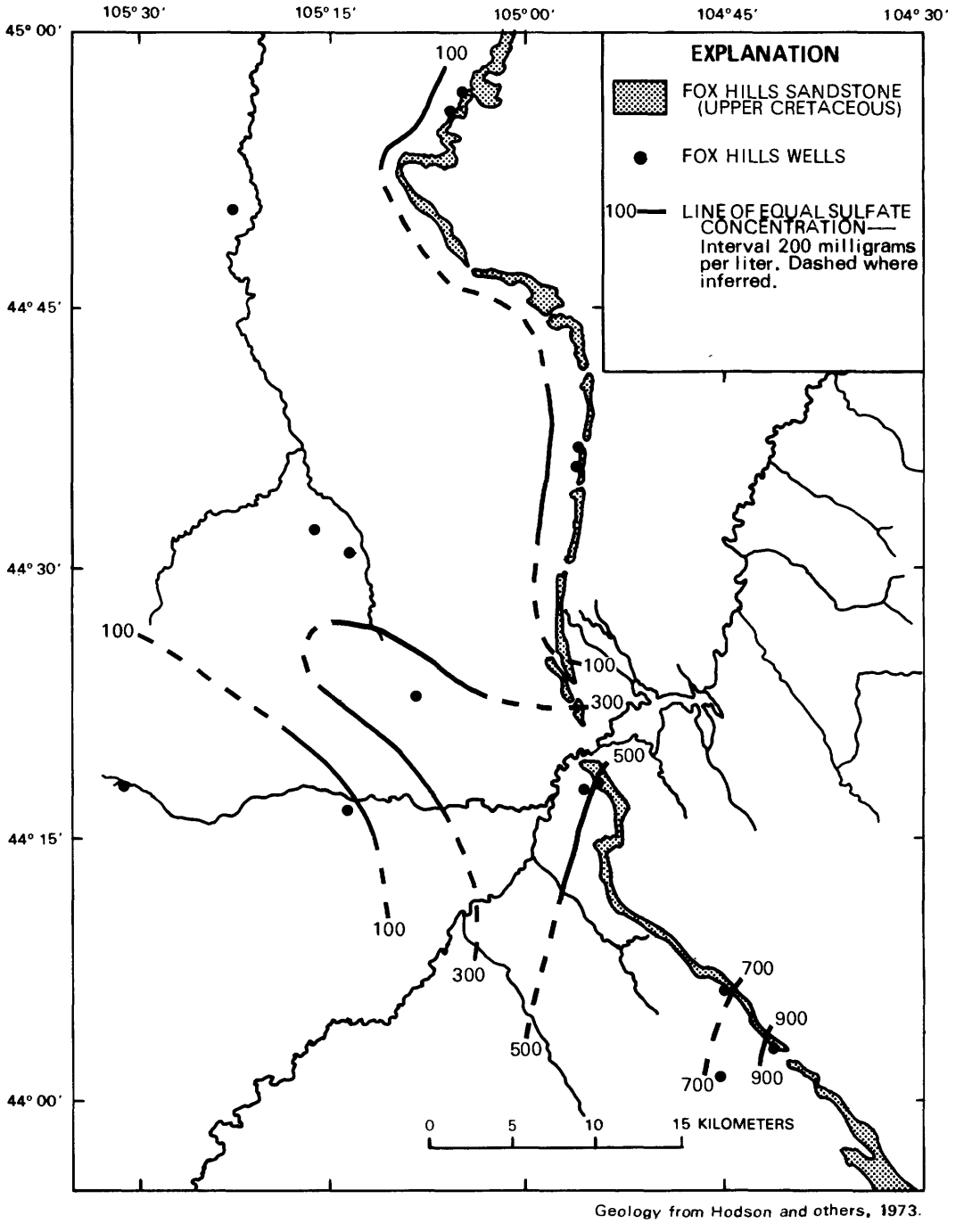

FIGURE 39.—Sulfate concentrations in waters from the Fox Hills Sandstone, Powder River Basin, Wyoming.

the flow path, O_2 and NO_3^- are consumed (fig. 45) followed by the appearance of H_2S immediately downgradient from the aquifer outcrop, suggesting an abundance of reduced phases such as pyrite or organic carbon in the aquifer sandstones. Dissolved organic carbon determinations (fig. 45) indicate much higher concentrations in the Lance-Fox Hills aquifer than in the Kootenai Formation, ranging in a random fashion from 1.1 to 18 mg/L, with a mean of 7.8 mg/L. Waters sampled in the discharge area exhibit highly variable Eh, ranging from positive to negative values, supporting the suspected influx of oxygenated recharge water in this area.

Chatham and others (1981) have observed similar trends in major element concentrations, Eh and pH in their study of the Lance Formation. This similarity

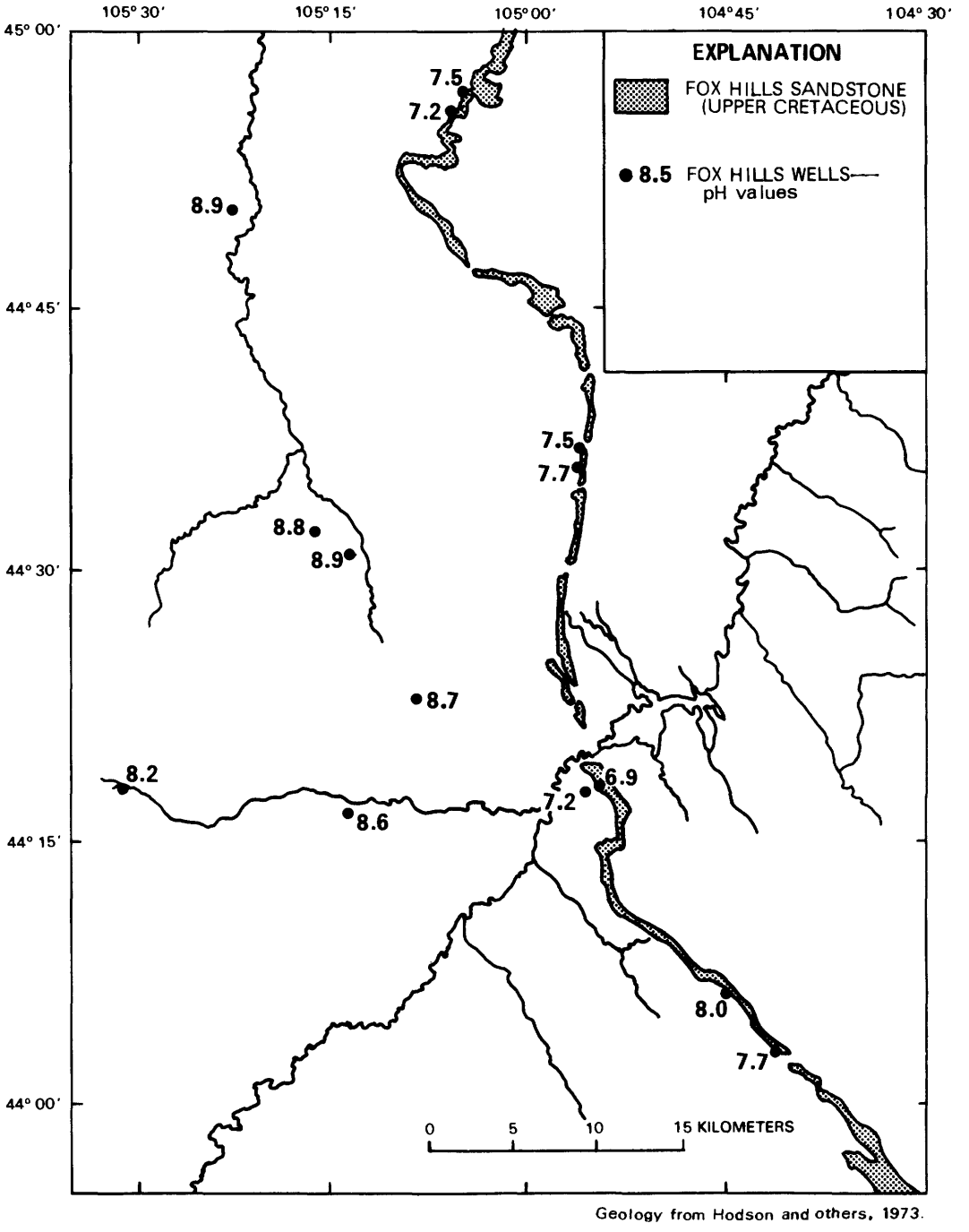

FIGURE 40.—pH values of waters from the Fox Hills Sandstone, Powder River Basin, Wyoming.

suggests that similar geochemical mechanisms control ground water in both the upper part of the Fox Hills and lower part of the Lance Formations, as would be expected from their similar mineralogy and hydrogeology.

Iron and manganese are present in low concentrations in both oxidized and reduced waters (fig. 46), with maxima occurring near the redox interface as for several flow systems described by Champ and others (1979) and Langmuir and Whittemore (1971). Such behavior suggests controls on the aqueous concentrations of these metals similar to those observed in the Judith Basin, or control by oxyhydroxides in oxidized waters and by carbonates or sulfides in reduced waters.

DISSOLVED GASES

As in the Judith Basin, considerable difficulty was encountered in attempting to collect uncontaminated gas samples. Bubbles adhering to the walls of the sampling

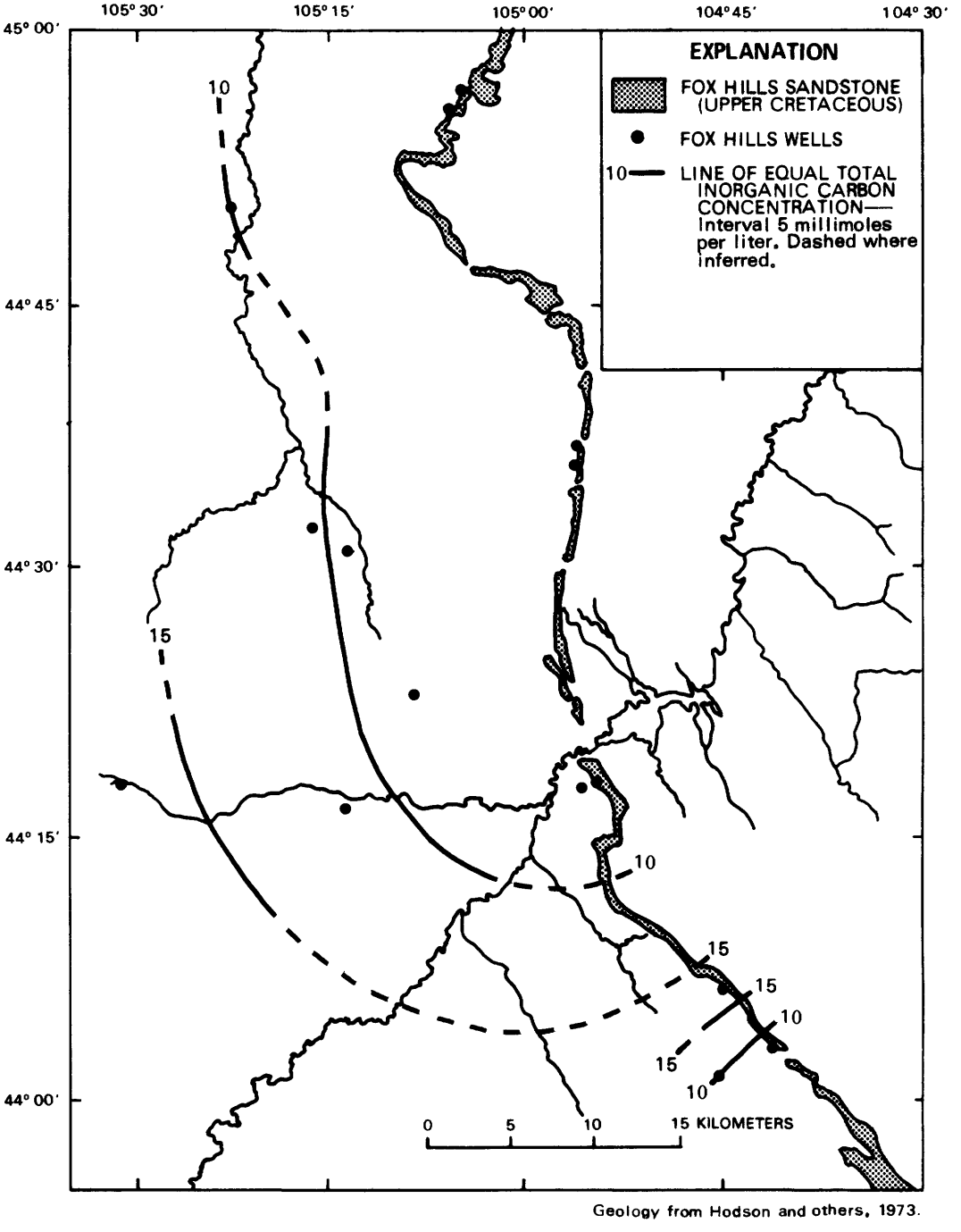

FIGURE 41.—Total inorganic carbon concentrations in waters from the Fox Hills Sandstone, Powder River Basin, Wyoming.

flask were a constant problem when sampling effervescent waters, and some samples were contaminated by the leaking of air into the evacuated sidearm. Analyses with anomalous N_2, Ar, and O_2 concentrations were therefore discarded, leaving those listed in table 23.

Dissolved-oxygen concentrations agree with those measured in the field to within 0.3 mg/L or less for three of the wells sampled, but the analyses for sample P13 differ by 2.0 mg/L, and the analyses for sample P15 differ by 0.6 mg/L. Field notes indicate that the pumps mounted on these two wells were at times drawing air into the sample water, which would account for the widely disparate analyses. Other dissolved gases measured at these wells do not seem anomalous in comparison with remaining samples from the Lance-Fox Hills aquifer, suggesting that the oxygen concentration

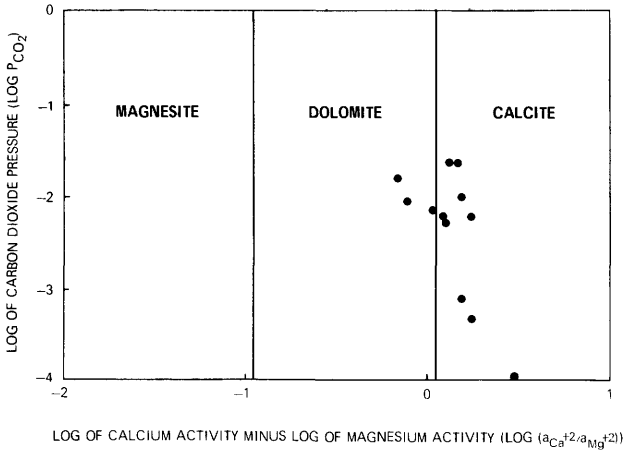

FIGURE 42.—Stability diagram for the system Ca-Mg-CO_2-H_2O at 25°C, with compositions of waters from the Lance-Fox Hills aquifer, Powder River Basin, Wyoming, superposed.

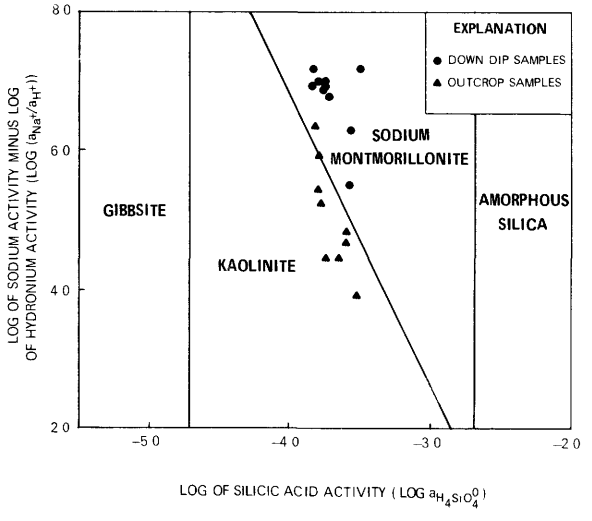

FIGURE 43.—Stability diagram for the system Na-SiO_2-Al_2O_3-H_2O at 25°C, with compositions of waters from the Lance-Fox Hills aquifer, Powder River Basin, Wyoming, superposed. Thermodynamic data for kaolinite from Bassett and others (1979). Remaining thermodynamic data from Helgeson (1969).

measured using the gas sampler may reflect aquifer conditions more accurately than that measured using the dissolved-oxygen probe and meter (table 2).

Comparison of measured CO_2 partial pressures with P_{CO_2} values computed from field-measured pH and alkalinity values using WATEQ2 show relatively good agreement, as shown in table 24. Differences between measured and calculated values lie within 0.1 pH units, which is the accuracy reported by Langmuir (1971) for field pH measurements in ground waters from noncarbonate rock terrains. Improved agreement between results obtained by these two methods over that observed for samples from the Judith Basin is probably due to the higher buffer capacity of the Powder River Basin samples. Average buffer capacity of the pertinent Judith Basin samples is 0.63 meq/L per pH unit and of the powder River Basin samples is 1.45 meq/L per pH unt. With a higher buffer capacity, similar amounts of CO_2 could escape (or enter) the solution with less of a change in pH.

Nitrogen partial pressures for most samples are higher than would be expected, assuming atmospheric equilibration with recharge waters (P_{N_2atm}=0.69), suggesting that Lance-Fox Hills ground waters become enriched in N_2 after isolation from the atmosphere. Nitrate

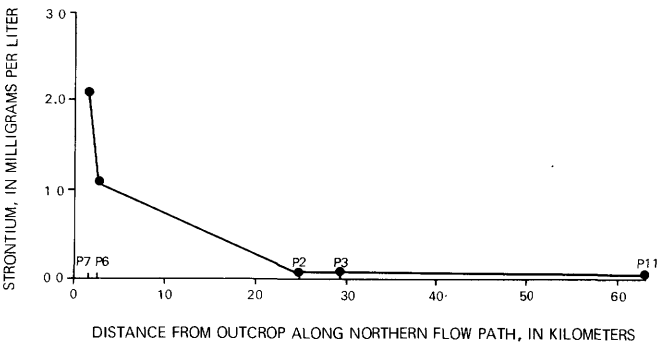

FIGURE 44.—Strontium concentrations in waters from the northern flow path of the Fox Hills Sandstone, Powder River Basin, Wyoming.

TABLE 22.—*Oxidation potentials calculated for waters from the Lance-Fox Hills aquifer, Powder River Basin, Wyoming, using O_2-H_2O or SO_4^{-2}-H_2S redox couples*

[O_2-H_2O, oxygen-water; SO_4^{-2}-H_2S, sulfate-hydrogen sulfide; mV, millivolt]

Sample	Calculated Eh (mV)	Redox couple
P1	-307	SO_4^{-2}-H_2S
P2	-317	SO_4^{-2}-H_2S
P3	-302	SO_4^{-2}-H_2S
P4	809	O_2-H_2O
P5	-203	SO_4^{-2}-H_2S
P6	-219	SO_4^{-2}-H_2S
P7	801	O_2-H_2O
P8	-302	SO_4^{-2}-H_2S
P9	-314	SO_4^{-2}-H_2S
P10	-208	SO_4^{-2}-H_2S
P11	-322	SO_4^{-2}-H_2S
P12	-321	SO_4^{-2}-H_2S
P13	-201	SO_4^{-2}-H_2S
P14	788	O_2-H_2O
P15	769	O_2-H_2O
P16	808	O_2-H_2O
P17	-321	SO_4^{-2}-H_2S
P18	-187	SO_4^{-2}-H_2S

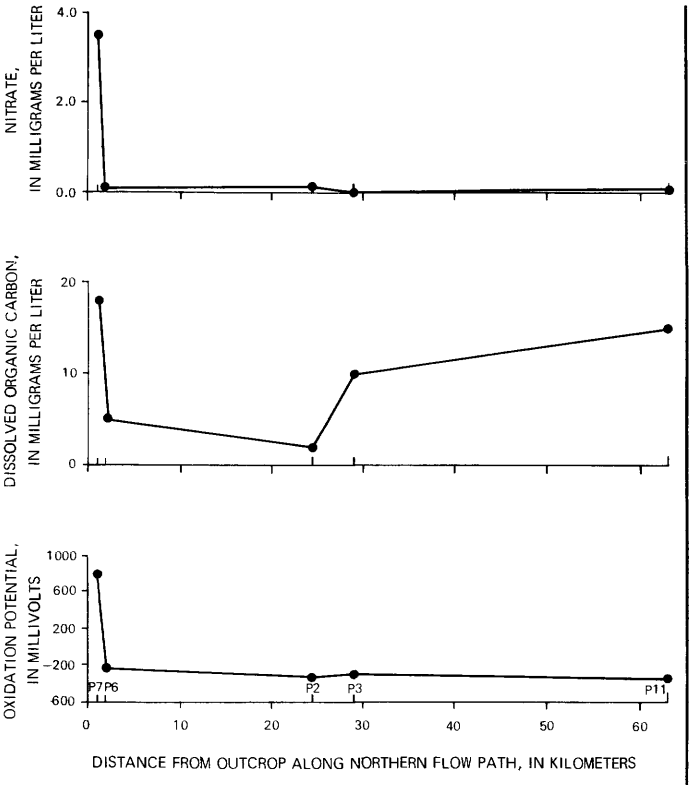

FIGURE 45.—Calculated oxidation potentials and dissolved organic carbon and nitrate concentrations in waters from the northern flow path of the Fox Hills Sandstone, Powder River Basin, Wyoming.

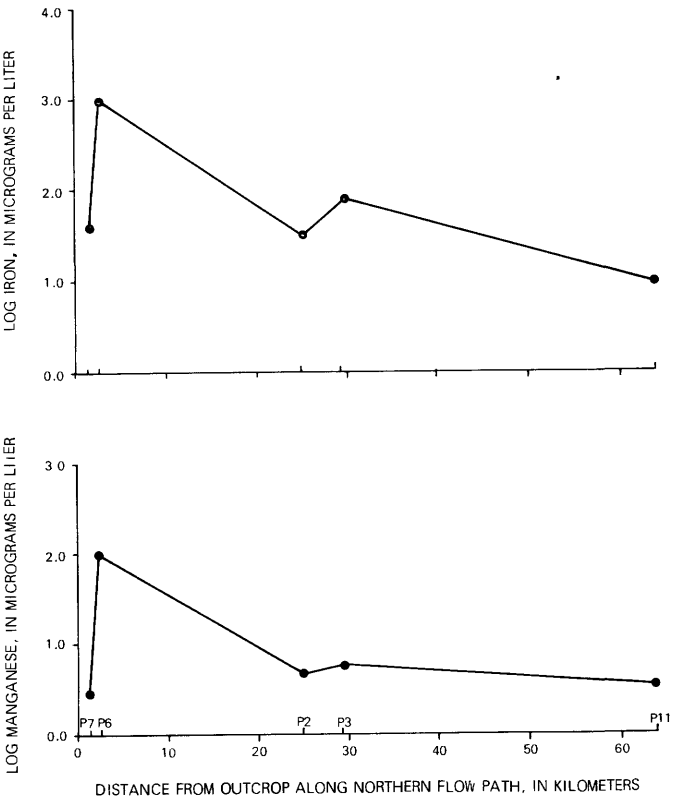

FIGURE 46.—Iron and manganese concentrations in waters from the northern flow path of the Fox Hills Sandstone, Powder River Basin, Wyoming.

may be reduced to N_2 by denitrifying bacteria (reaction 2), thereby increasing N_2 while simultaneously decreasing NO_3^- concentrations, as observed. The data are insufficient to test this hypothesis, however.

The temperature of recharge waters may be calculated from the concentration of argon present in the ground water (Mazor, 1972). Based on an atmospheric abundance of 0.934 percent, an atmospheric pressure of 0.885 atm at 1,220 m elevation, and measured solubility coefficients for argon (Douglas, 1964), the temperature dependence of argon solubility has been calculated and compared to measured argon concentrations. Excluding sample P17, which appears to have lost argon and nitrogen as a result of displacement by methane (D. W. Fisher, U.S. Geological Survey, written commun., 1980), the calculations yield recharge temperatures ranging between 0°C and 6°C, with a mean of 2.75°C. This temperature is significantly less than the annual average of approximately 7°C, and suggests that spring snowmelt provides a higher proportion of recharge to the Fox Hills than warmer spring and early summer storms and that paleo-recharge has been derived from similar events. This interpretation is consistent with the observation that precipitation from spring and summer storms results in runoff and increased streamflow rather than infiltration into bedrock aquifers (Whitcomb, 1965). Another noble gas, helium, is absent in detectable quantities in all but one sample, P17. This is presumably the most mature ground water sampled, so it seems likely that helium has accumulated through the radioactive decay of alpha emitting radionuclides, as in the Judith Basin, and has reached detectable levels in only the oldest ground waters.

Methane is present in trace quantities in samples P13 and P15, where oxidation potentials appear too high to allow methanogenic bacteria to function. The methane in these samples probably originated in more reducing environments and subsequently migrated to these waters. Methane occurs in greater concentrations in the two deep basin samples: P9 (not previously discussed due to bubbles in the gas sampler) and P17. Methanogenic bacteria generate CH_4 by either acetate fermentation (reaction 7) (Carothers and Kharaka, 1980) or CO_2 reduction (reaction 8) (Nissenbaum and others, 1972; Claypool and Kaplan, 1974). Although insufficient data are available to determine which of these processes dominates in the deeper waters of the Fox Hills Sandstone, low oxidation potentials and the absence of sulfate in quantities greater than 1 millimole per liter suggest that the methane was produced in situ, rather than migrating from even deeper strata. Based on

TABLE 23.—*Concentrations and partial pressures of dissolved gases in water samples from the Lance-Fox Hills aquifer, Powder River Basin, Wyoming*

[mg/L, milligrams per liter; atm, atmospheres]

Sample	Oxygen		Carbon dioxide		Nitrogen		Argon		Helium		Methane	
	mg/L	atm	mg/L	atm	mg/L	atm	mg/L	atm	mg/L	atm	mg/L	atm
P4	0.5	0.009	47	0.021	22	0.93	0.76	0.010	0.000	0.000	0.00	0.000
P13	.04	.0008	23	.010	25	1.05	.83	.011	.000	.000	.03	.001
P15	1.3	.024	13	.006	21	.86	.74	.010	.000	.000	.03	.001
P16	3.6	.065	33	.014	21	.85	.67	.009	.000	.000	.00	.000
P17	.3	.010	7.2	.007	10	.70	.38	.008	.001	.001	9.7	.56

TABLE 24.—*Comparison of field-measured pH values and pH calculated from measured P_{CO_2} for water samples from the Lance-Fox Hills aquifer, Powder River Basin, Wyoming*

Sample	pH, field measured	pH, calculated	Difference
P4	7.15	7.23	−0.08
P13	7.59	7.50	.09
P15	8.03	8.05	−.02
P16	7.42	7.47	−.05
P17	8.18	8.22	−.04

TABLE 25.—*Isotopic ratios or activities of isotopes in waters from the Lance-Fox Hills aquifer, Powder River Basin, Wyoming*

[pCi/L, picocuries per liter; <, indicates concentrations below detection limit for that analysis]

Sample	Oxygen ($\delta^{18}O$)	Hydrogen (δD)	Carbon ($\delta^{13}C$)	Tritium (pCi/L)	Carbon-14 (percent modern)
P1	−20.5	−158	−10.60	<5	1.3
P2	−19.4	−149	−11.05	<5	>6.2
P3	−19.1	−147	−10.10	<5	1.1
P4	−18.7	−144	−11.15	<5	40.9
P5	−18.9	−145	−12.35	6	66.3
P6	−18.2	−140	−12.90	<5	81.4
P7	−18.5	−143	−11.40	58	61.6
P8	−18.3	−143	−12.80	<5	16.3
P9	−19.6	−151	−5.95	<5	<2.7
P10	−19.8	−151	−11.85	22	42.4
P11	−19.2	−147	−11.25	<5	<2.1
P12	−20.7	−160	−13.45	<5	3.4
P13	−18.8	−144	−12.85	<5	52.7
P14	−17.5	−136	−10.35	560	97.0
P15	−19.2	−114	−11.45	50	26.4
P16	−18.5	−141	−12.50	25	42.9
P17	−19.0	−145	−3.75	<5	<1.0
P18	−18.7	−143	−13.65	<5	---

observations of natural systems, Nissenbaum and others (1972) suggested that, despite the stability of CH_4 over CO_2 at oxidation potentials less than −250 millivolts, catalytic methanogenic bacteria are inhibited by the presence of more efficient sulfate reducers (*Desulfovibrio* sp.). Once sulfate has been nearly consumed, methanogenic bacteria become more efficient in utilizing the available nutrients than the sulfate reducers, and the methanogenic bacteria become the dominant anaerobes (Claypool and Kaplan, 1974).

ISOTOPIC COMPOSITION

Isotopic compositions of ground waters in the Lance-Fox Hills are presented in table 25. Oxygen and hydrogen isotopic measurements in ground waters of both the Fox Hills Sandstone and the Lance Formation correspond to the compositon of North American continental precipitation as reported by Gat (1980) ($\delta D = 7.95\delta^{18}O + 6.03$), indicating the presence of only meteoric waters in the aquifer (fig. 47). Values for $\delta^{18}O$ range from −20.7 to −17.5, and for δD, from −158 to −136. Comparison with the continental precipitation isotopic data of Yurtsever (1975), as reported by Gat (1980), suggests that recharge is derived from precipitation events occurring at temperatures of roughly 0°C. This temperature is consistent with dissolved argon recharge temperatures and supports the conclusion that the major portion of recharge to the Lance-Fox Hills aquifer is derived from spring snowmelt or similar paleo-events, rather than from warmer late spring and summer storms. Differences between Lance and Fox Hills $\delta^{18}O$ and δD values appear insignificant, indicating similar means of recharge for the two formations.

Carbon isotopic compositions remain relatively constant for all but the two deepest samples from the Fox Hills Sandstone, ranging along the flow path from $\delta^{13}C$ values of −12.9 and −11.4 in the recharge area to values of −11.0, −10.1, and −11.2 downflow. As discussed in the Supplemental Data section, $\delta^{13}C$ values near −15 or higher suggest control of ground-water chemistry by carbonate rather than aluminosilicate solid phases, assuming the system is closed to exchange with a gas phase CO_2 reservoir but receiving CO_2 inputs;

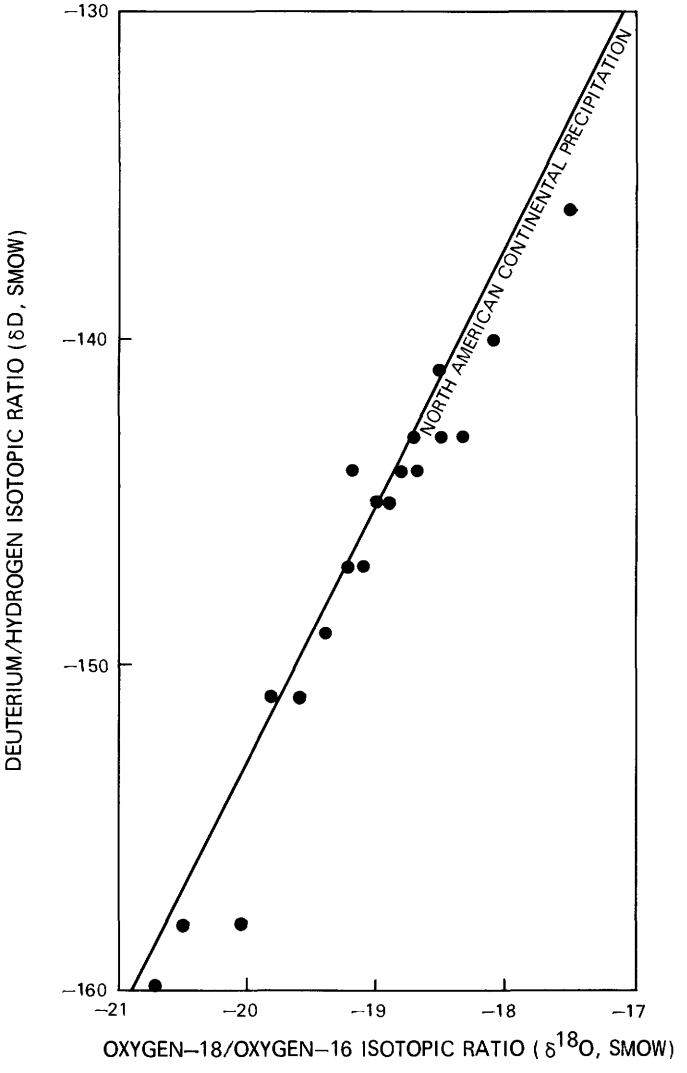

FIGURE 47.—Isotopic composition of North American continental precipitation (Gat, 1981) with isotopic compositions of waters from the Lance-Fox Hills aquifer, Powder River Basin, Wyoming, superposed.

exchange with a CO_2 gas phase would result in $\delta^{13}C$ values of −23 to −15. The observed carbon isotopic compositions therefore imply geochemical control of dissolved carbonate chemistry by carbonate mineral phases.

The deepest, and presumably the most mature, ground waters sampled, P9 and P17, exhibit $\delta^{13}C$ values of −6.0 (P9) and −3.8 (P17), which are much higher values than found in any of the other waters sampled fromthe Lance-Fox Hills aquifer. The presence of significant quantities of methane in these deep basin samples strongly suggests enrichment of ^{13}C in dissolved carbonate species as a result of isotopic fractionation during the bacterial production of methane. Sackett and Chung (1979) have shown that isotopic equilibrium between coexisting CH_4 and CO_2 does not occur at aquifer temperatures; therefore, migration of methane would be unable to produce these isotopic variations. Similarly, oxidation of migrating CH_4 to CO_2, which is not known to occur in the absence of molecular O_2, would tend to lower $\delta^{13}C$ values from the addition of the isotopically light CO_2 produced.

The similarity in geochemical environments and isotopic evolution between known methanogenic waters (Rosenfeld and Silverman, 1959; Oana and Deevey, 1960; Nissenbaum and others, 1972; Carothers and Kharaka, 1980) and the deep basin Fox Hills samples is therefore taken as evidence of active methanogenesis in the deeper portions of the aquifer. Because mass balance information regarding the compositions of these waters before the onset of methanogenesis is lacking, a determination of which process actually produces the methane—CO_2 reduction or acetate fermentation—is impossible.

Tritium concentrations for the majority of Lance-Fox Hills ground waters are below 10 pCi/L, indicating that the confined system is not open to recharge by, or mixing with, recently recharged surface waters. Higher tritium concentrations in the outcrop area, ranging from 22 to 560 pCi/L, indicate the presence of waters less than 25 years in age. These younger waters are also evident in the aquifer outcrop near the Belle Fourche River, proving the existence of recent recharge, and substantiating the hypothesized mixing of mature waters with recent recharge in this area.

GEOCHEMICAL COMPUTER MODELING

SATURATION INDICES

Mineral saturation indices, computed using the WATEQ2 aqueous speciation model (Ball and others, 1980), indicate that solution-mineral equilibria in both the Lance Formation and the Fox Hills Sandstone are sufficiently similar to allow a discussion of the aquifer as a whole. Saturation indices for the Powder River Basin samples are presented in table 26 for silicates and aluminosilicates, and in table 27 for carbonates, sulfates, and phosphates.

Quartz, a major constituent in the Fox Hills Sandstone, is oversaturated; amorphous silica is undersaturated. Chalcedony is undersaturated or near saturation, but petrographic evidence (Dobbin and Reeside, 1930) suggested that this mineral is not an important diagenetic phase. Albite, another important clastic constituent, is undersaturated, but its alteration phase allophane is saturated in most samples, reflecting groundwater equilibration with this feldspar alteration phase rather than with unaltered albite. Muscovite, a

TABLE 26.—*Saturation indices of silicate and aluminosilicate aquifer minerals in waters from the Lance Formation and the Fox Hills Sandstone, Powder River Basin, Wyoming*

Sample	Quartz	Chalcedony	Amorphous silica	Albite	Allophane	Muscovite	Chlorite	Beidellite	Kaolinite
Lance Formation									
P1	0.31 ± 0.08	−0.21 ± 0.08	−0.72 ± 0.08	−1.13 ± 0.72	−0.86 ± 0.66	−1.86 ± 2.12	−0.75 ± 1.82	−0.38 ± 1.66	0.09 ± 1.37
P8	.46 ± .07	−.08 ± .07	−.59 ± .07	−1.04 ± 1.38	−.80 ± 1.32	−1.98 ± 4.02	−2.84 ± 3.40	−.42 ± 3.13	−.06 ± 2.73
P12	.35 ± .08	−.18 ± .08	−.68 ± .08	−1.31 ± 1.38	−1.24 ± 1.37	−3.01 ± 4.02	−.16 ± 3.13	−1.33 ± 3.13	−.82 ± 2.73
P13	.66 ± .06	.12 ± .06	−.39 ± .06	−1.36 ± 1.29	−.35 ± 1.00	−.96 ± 2.74	−7.83 ± 1.85	1.14 ± 2.14	1.37 ± 2.55
P14	.58 ± .06	.04 ± .06	−.48 ± .06	−2.23 ± .52	.01 ± .38	1.15 ± 1.48	−4.35 ± 1.01	1.91 ± 1.16	2.10 ± .97
P18	.64 ± .06	.10 ± .06	−.42 ± .06	−2.28 ± 1.46	−.38 ± 1.07	−1.23 ± 2.74	−7.99 ± 1.84	.99 ± 2.14	1.31 ± 2.90
Mean and standard deviation	0.50 ± 0.15	−0.40 ± 0.14	−0.55 ± 0.14	−1.56 ± 0.55	−0.60 ± 0.45	−1.48 ± 1.07	−3.99 ± 3.39	0.32 ± 1.22	0.66 ± 1.10
Fox Hills Sandstone									
P2	0.28 ± 0.08	−0.22 ± 0.08	−0.73 ± 0.08	−1.22 ± 0.72	−1.24 ± 0.66	−2.37 ± 2.12	−1.18 ± 2.14	−0.77 ± 1.66	−0.26 ± 1.37
P3	.36 ± .07	−.15 ± .07	−.66 ± .07	−.09 ± .27	−.15 ± .15	.85 ± .54	−3.69 ± 5.90	1.87 ± .46	1.98 ± .34
P4	.71 ± .05	−.17 ± .05	−.34 ± .05	−2.75 ± 1.37	−.37 ± .99	−.84 ± 4.01	−8.63 ± 2.68	1.29 ± 3.12	1.52 ± 2.73
P5	.63 ± .06	.09 ± .06	−.42 ± .06	−2.08 ± 1.29	−.37 ± .98	−.74 ± 2.74	−7.26 ± 1.84	1.06 ± 2.14	1.36 ± 2.56
P6	.47 ± .08	−.08 ± .08	−.59 ± .08	−2.15 ± 1.38	−.38 ± 1.09	−1.14 ± 4.02	−6.45 ± 2.69	.23 ± 3.13	.78 ± 2.73
P7	.52 ± .07	−.03 ± .07	−.54 ± .07	−2.93 ± 1.38	−.39 ± 1.05	−1.10 ± 4.02	−5.99 ± 2.69	.48 ± 3.13	.96 ± 2.73
P9	.25 ± .07	−.22 ± .07	−.73 ± .07	−1.18 ± .52	−1.56 ± .45	−2.08 ± 1.48	−4.81 ± 5.97	−.59 ± 1.17	−.08 ± .98
P10	.46 ± .08	−.08 ± .08	−.60 ± .08	−1.65 ± 1.38	−.38 ± 1.09	−1.55 ± 4.02	−5.21 ± 2.69	.31 ± 3.13	.78 ± 2.73
P11	.30 ± .07	−.19 ± .07	−.70 ± .07	−.72 ± .34	−1.14 ± .27	−1.33 ± .87	−2.56 ± 5.91	.08 ± .69	.42 ± .56
P15	.42 ± .08	−.12 ± .08	−.63 ± .08	−.65 ± .41	.20 ± .28	.50 ± .99	−3.74 ± .72	1.85 ± .81	2.09 ± .67
P16	.48 ± .08	−.07 ± .08	−.58 ± .08	−2.24 ± 1.30	−.40 ± .97	−1.58 ± 2.75	−5.39 ± 1.85	.38 ± 2.14	.88 ± .56
P17	.24 ± .06	−.19 ± .06	−.69 ± .06	−1.27 ± .42	−2.05 ± .34	−1.87 ± 1.16	−3.17 ± 1.79	−.43 ± .92	.06 ± .78
Mean and standard deviation	0.43 ± 0.15	−0.09 ± 0.12	−0.60 ± 0.12	−1.58 ± 0.87	−0.68 ± 0.66	−1.10 ± 0.96	−4.84 ± 2.10	−0.48 ± 0.88	0.87 ± 0.76

TABLE 27.—*Saturation indices of carbonate, sulfate, and phosphate minerals in waters from the Lance Formation and the Fox Hills Sandstone, Powder River Basin, Wyoming*

Sample	Calcite	Dolomite	Siderite	Rhodochrosite	Strontianite	Gypsum	Celestite	F-apatite	F-CO_3 apatite	$MnHPO_4$
Lance Formation										
P1	0.13 ± 0.21	−0.03 ± 0.31	0.40 ± 0.56	−0.51 ± 1.40	−0.70 ± 0.28	−2.92 ± 0.21	−2.96 ± 0.28	−1.13 ± 1.11	3.15 ± 2.13	−0.24 ± 0.72
P8	.30 ± .11	−.48 ± .44	−.54 ± 2.08[1]	−.27 ± .45	−.68 ± .19	−2.15 ± .11	−2.35 ± .19	---	---	---
P12	.14 ± .19	−.28 ± .37	−.30 ± 2.08[1]	−.44 ± 1.06	−.74 ± .28	−2.54 ± .19	−2.62 ± .28	−1.09 ± 1.01	2.96 ± 1.01	−.13 ± .55
P13	−.21 ± .06	−.74 ± .08	−.28 ± .11	−.14 ± .06	−1.17 ± .10	−1.44 ± .06	−1.62 ± .10	---	---	---
P14	.13 ± .05	.02 ± .07	−11.76 ± 1.06	−.48 ± .08	−1.13 ± .60	−2.30 ± .20	−2.79 ± .22	−1.70 ± 1.38	2.00 ± 2.48	.72 ± .23
P18	.16 ± .05	.07 ± .07	.20 ± .06	−.33 ± .06	−.80 ± .09	−1.14 ± .05	−1.33 ± .09	---	---	---
Mean and standard deviation	0.11 ± 0.17	−0.24 ± 0.32	−0.10 ± 0.39[2]	−0.34 ± 0.14[2]	−0.87 ± 0.22	−2.08 ± 0.67	−2.28 ± 0.66	−1.31 ± 0.34	2.70 ± 0.62	0.12 ± 0.52
Fox Hills Sandstone										
P2	0.20 ± 0.25	−0.04 ± 0.40	0.35 ± 0.73	−0.53 ± 1.67	−0.65 ± 0.28	−2.85 ± 0.25	−2.88 ± 0.28	−1.40 ± 1.07	2.12 ± 2.05	−0.43 ± 0.85
P3	−.04 ± .25	−1.00 ± 1.13[1]	.66 ± .30	−.58 ± 1.40	−.76 ± .28	−2.97 ± .26	−2.90 ± .28	−2.38 ± 1.33	.42 ± 2.56	−.36 ± .72
P4	.04 ± .05	−.21 ± .07	−9.56 ± .07	−.52 ± .06	−1.06 ± .09	−1.41 ± .06	−1.74 ± .10	−1.47 ± .74	2.31 ± 1.31	.80 ± .12
P5	.00 ± .05	−.30 ± .07	−.46 ± .13	−.81 ± .11	−.98 ± .10	−1.80 ± .08	−2.02 ± .11	−2.53 ± 1.38	.41 ± 2.48	.14 ± .23
P6	.11 ± .06	.02 ± .08	.43 ± .07	−.56 ± .12	−.81 ± .10	−1.88 ± .07	−2.03 ± .11	---	---	---
P7	.09 ± .05	.14 ± .07	−11.44 ± .56	−2.41 ± 2.76	−.82 ± .10	−1.71 ± .07	−1.85 ± .10	---	---	---
P9	.13 ± .22	−.67 ± 1.13[1]	.70 ± .39	−.79 ± 2.76	−.51 ± .21	−3.12 ± .22	−2.90 ± .21	−3.08 ± 1.28	−1.79 ± 2.42	−1.07 ± 1.41
P10	.33 ± .05	.44 ± .07	.43 ± .06	−.81 ± .12	−.69 ± .10	−.57 ± .05	−.83 ± .09	---	---	---
P11	.07 ± .29	−.67 ± 1.14[1]	−.01 ± 2.08	−.55 ± 2.08	−.64 ± .31	−3.11 ± .29	−2.99 ± .31	−1.38 ± 1.50	1.49 ± 2.90	−.22 ± 1.07
P15	.48 ± .06	.58 ± .08	−11.26 ± .39	−1.21 ± .86	−.58 ± .11	−1.19 ± .06	−1.48 ± .11	−1.40 ± .73	.48 ± 1.27	−.81 ± .45
P16	.38 ± .05	.78 ± .06	−10.30 ± .09	−.64 ± .08	−.48 ± .09	−.49 ± .05	−.58 ± .09	---	---	---
P17	.16 ± .16	−.15 ± .36	.12 ± 1.06	−.70 ± 1.40	−.53 ± .16	−4.70 ± 1.56	−4.44 ± 1.56	−3.00 ± 1.02	−3.22 ± 1.89	−.79 ± .73
Mean and standard deviation	0.16 ± 0.16	−0.09 ± 0.53	0.28 ± 0.38[2]	−0.67 ± 0.12[2]	−0.71 ± 0.18	−2.15 ± 1.23	−2.22 ± 1.06	−2.08 ± 0.75	0.65 ± 2.22	−0.34 ± 0.60

[1]Calculated assuming minor element concentration equals analytical detection limit.
[2]Calculated without oxidized samples—P4, P7, P14, P15, and P16

potassium mica, is near saturation, indicating possible ground-water equilibration with this phase. Apparent undersaturation may indicate that muscovite, as well as sericitic alterations of a similar composition, are unstable under current geochemical conditions and might be alterating to more stable phases such as

hydromuscovite, illite, or kaolinite. Chlorite is highly undersaturated in most of the samples analyzed, indicating that this detrital phase does not control solution chemistry. Beidellite, a sodium smectite, is saturated in waters of the Lance–Fox Hills aquifer, as is kaolinite, suggesting that equilibrium between kaolinite and beidellite may control silica and aluminum concentrations in solution. This conclusion is in agreement with petrographic descriptions that describe kaolinite and beidellite as authigenic, and quartz, albite, muscovite, and chlorite as detrital phases (Dobbin and Reeside, 1930).

Saturation indices for carbonate minerals (table 27) are remarkably similar to their counterparts in the Kootenai Formation. Calcite is saturated or slightly oversaturated in waters of the Lance–Fox Hills aquifer, suggesting equilibrium with, or possible precipitation of, this phase. Apparent oversaturation may be the result of cationic substitutions in the calcite lattice or may reflect small errors in the field pH measurements. Dolomite is saturated in most samples, although those from the discharge area are clearly oversaturated with respect to dolomite. These oversaturations may indicate limited dolomitization of calcite in the outcrop area due to mixing of high C_T, high pH waters with recharged waters containing high concentrations of magnesium. Siderite saturation indices indicate saturation with respect to this phase in all but oxygenated waters.

Fox Hills rhodochrosite saturation indices cluster near a value of −0.67, with significant deviations occurring only in oxygenated waters, where manganese oxyhydroxides are thought to control aqueous manganese concentrations. Using the distribution coefficient measured by Bodine and others (1965) for partitioning manganese between the aqueous phase and a coexisting calcite phase, and the mean concentrations of calcium (0.28 mmol/L) and manganese (0.00049 mmol/L) in anoxic ground waters of the Lance–Fox Hills aquifer, it has been calculated that a calcite in equilibrium with these ground waters should contain an average of 3-mole percent rhodochrosite. Saturation indices computed for a percent Mn calcite ideal solid solution (Berner, 1975) with a calculated stability of −1,121 kilojoules per mole, presented in table 28, indicate saturation with respect to this phase in most samples and suggest possi- ble control of manganese concentrations by such a solid solution in all but oxygenated waters.

Saturation indices for strontianite clearly indicate undersaturation, but, unlike Judith Basin samples, cluster near a value of −0.76, again suggesting possible mineralogic control by a carbonate solid solution. The distribution coefficient of 0.14 measured by Holland others (1964) for the partitioning of strontium between an aqueous phase and calcite, and the mean concentrations of strontium (0.013 mmol/L) and calcium

TABLE 28.—*Saturation indices of a 3.0-mole percent manganese calcite solid solution in waters from the Lance–Fox Hills aquifer, Powder River Basin, Wyoming*

[Free energy for the phase $Mn_{0.03}Ca_{0.97}CO_3$ was calculated by assuming an ideal solid solution (Berner, 1975)]

Sample	Saturation indices	
	Calcite	Manganese calcite
Lance Formation		
P1	0.13	0.07
P8	.30	.23
P12	.14	.08
P13	−.21	−.26
P14	.13	.06
P18	.16	.09
Mean and standard deviation	0.11 ± 0.17	0.04 ± 0.16
Fox Hills Sandstone		
P2	0.20	0.15
P3	−.04	−.09
P4	.04	−.03
P5	.00	−.07
P6	.11	.02
P7	.09	−.05
P9	.13	.07
P10	.33	.24
P11	.07	.02
P15	.48	.37
P16	.38	.29
P17	.16	.09
Mean and standard deviation	0.16 ± 0.16	0.08 ± 0.15

(0.94 mmol/L), indicate that a calcite in equilibrium with ground waters of the Lance–Fox Hills Sandstone should contain 0.2-mole percent strontianite. The free energy of a $Sr_{0.002}Ca_{0.998}CO_3$ ideal solid solution (Berner, 1975) is −1,130 kilojoules per mole, and saturation indices calculated from this value demonstrate saturation with respect to this solid solution in most samples (table 29). Strontium, derived from the dissolution of impure carbonates and sulfates, may be controlled in the aqueous phase, then, by sorption effects and equilibrium with a Sr-calcite solid solution.

Sulfate mineral phases also demonstrate relationships similar to those observed in the Kootenai Formation. Both gypsum and celestite show widely fluctuating, but invariably negative, saturation indices. Control of strontium, calcium, or sulfate concentrations by these phases is therefore unlikely, as is the presence of substantial quantities of these phases.

Apatite saturation indices (table 27), computed for both a pure fluorapatite [$Ca_5(PO_4)_3F$] and a cryptocrystalline carbonate fluorapatite [$Ca_{9.74}Na_{0.21}Mg_{0.05}(PO_4)_{3.19}(CO_3)_{0.81}F_{2.32}OH_{0.28}$, $pK_{sp}=-120.7$] (Chien and Black, 1975), suggest saturation with respect to an apatite

TABLE 29.—*Saturation indices of a 0.2-mole percent strontium calcite solid solution in waters from the Lance–Fox Hills aquifer, Powder River Basin, Wyoming*

[Free energy for the phase $Sr_{0.002}Ca_{0.998}CO_3$ was calculated by assuming an ideal solid solution (Berner, 1975)]

Sample	Saturation indices	
	Calcite	Strontium calcite
Lance Formation		
P1	0.13	0.06
P8	.30	.21
P12	.14	.06
P13	−.21	−.30
P14	.13	.04
P18	.16	.07
Mean and standard deviation	0.11 ± 0.17	0.02 ± 0.17
Fox Hills Sandstone		
P2	0.20	0.13
P3	−.04	−.11
P4	.04	−.06
P5	.00	−.09
P6	.11	01
P7	.09	−.01
P9	.13	.06
P10	.33	.23
P11	.07	.00
P15	.48	.38
P16	.38	.28
P17	.16	.08
Mean and standard deviation	0.16 ± 0.16	0.08 ± 0.15

having a composition and stability intermediate between these two phases. The two deep basin samples, P9 and P17, are undersaturated with respect to both of these apatites, indicating that these samples may be in equilibrium with a more crystallized apatite or one of slightly different composition. The occurrence of apatite in the Fox Hills Sandstone implies that phases similar to these are present in the aquifer, and are probably in equilibrium with the waters sampled. The phase manganese biphosphate ($MnHPO_4$) is also saturated in most samples from the Lance–Fox Hills aquifer, indicating that aqueous manganese and phosphorous concentrations may also be influenced by such a phase.

Although ferric oxyhydroxides have been identified in neither X-ray nor petrographic analyses, their presence in the Lance–Fox Hills outcrop is implied by numerous references to ferruginous concretions in the stratigraphic descriptions of Robinson and others (1964). Control of aqueous iron concentrations by amorphous ferric hydroxide, rather than by goethite or hematite, in oxidizing waters is apparent from the saturation indices presented in table 30. Oversaturation with respect to $Fe(OH)_{3(am)}$(pK=38.5) is indicative of active precipitation of this phase (IAP=−37.1 to −38.1) (Whittemore and Langmuir, 1975), possibly due to the oxidation of pyrite by O_2 (reaction 9), followed by the hydrolysis and precipitation of ferric iron. Oxidation of pyrite would also account for increases in sulfate concentration in the outcrop area, as well as the localization of ferric hydroxides in concretions, similar to the occurrence of pyrite in the reduced environment.

Although manganese oxides were not detected by X-ray diffraction in samples from the Fox Hills outcrop, it is possible that these common phases have escaped detection by their poorly crystallized nature. In the five oxidizing ground-water samples of the Lance–Fox Hills aquifer, both manganite and birnessite are highly oversaturated, with mean saturation indices and standard deviations of 4.24±0.76 and 7.61±0.74, respectively, indicating that these phases probably do not control aqueous manganese concentrations in the oxidizing environment.

In sulfidic waters, amorphous ferrous sulfide, rather than crystallized ferrous sulfides such as pyrite, controls dissolved iron cncentrations (table 30). Slight oversaturations with respect to $FeS_{(am)}$ are most likely due to interferences from other reduced species during the determination of dissolved sulfide. Although goethite saturation indices in sulfidic waters approach zero in many cases, the absence of hematite (a well crystllized oxyhydroxide) in core samples, as well as the occurrence of pyrite in the aquifer, suggests control of iron concentrations by amorphous ferrous sulfide in reduced waters, rather than by a ferric oxyhydroxide phase.

REACTION SIMULATION

The discussion of ground-water chemistry, mineralogy, and petrography of the Lance–Fox Hills aquifer has led to the proposal of several mineral phases and chemical reactions that may control ground-water chemistry in this aquifer. Saturation with respect to the aluminosilicates beidellite, muscovite, kaolinite, and allophane, in addition to the carbonates calcite and dolomite, suggests that one or more of these phases may control the ground-water chemistry of the Lance–Fox Hills aquifer. Carbon isotopic ratios indicate possible control of dissolved carbonate concentrations by carbonate minerals.

Oxidation potentials decrease within the aquifer outcrop area from highly oxidizing to strongly reducing values. Consumption of O_2 and NO_3^- in combination with the production of additional N_2 and C_T is indicative of biologically mediated O_2 and NO_3^- reduction reactions. Saturation indices for $Fe(OH)_{3(am)}$ in oxidized ground waters imply active precipitation of this phase, possibly as a result of the oxidation of pyrite. An abun-

TABLE 30.—*Saturation indices of iron oxyhydroxides and sulfides in waters from the Lance-Fox Hills aquifer, Powder River Basin, Wyoming*

[$Fe(OH)_{3(am)}$, amorphous ferric hydroxide; $FeS_{(am)}$, amorphous ferrous sulfide; K_{sp}, solubility product]

Sample	Hematite	Goethite	$Fe(OH)_{3(am)}$ [a]	Pyrite	$FeS_{(am)}$ [b]
			Sulfide absent		
P4	18.89 ± 0.32	6.98 ± 0.16	3.06 ± 0.16	---	---
P7	16.41 ± 1.15	5.74 ± .57	1.73 ± .57	---	---
P14	16.01 ± 2.15	5.54 ± 1.07	1.57 ± 1.07	---	---
P15	17.05 ± .82	6.06 ± .41	2.06 ± .41	---	---
P16	18.36 ± .34	6.71 ± .17	2.70 ± .17	---	---
Mean and standard deviation	17.34 ± 1.24	6.21 ± 0.62	2.22 ± 0.64	---	---
			Sulfide present		
P1	6.79 ± 1.15	0.91 ± 0.57	−2.68 ± 0.57	8.60 ± 1.02	1.00 ± 0.70
P2	6.70 ± 1.48	.86 ± .74	−2.48 ± .74	8.87 ± .81	1.22 ± .75
P3	6.99 ± .67	1.01 ± .33	−2.43 ± .33	8.81 ± .91	1.15 ± .52
P5	2.57 ± .39	−1.18 ± .20	−5.10 ± .20	9.18 ± .87	−.11 ± .45
P6	4.36 ± .32	−.28 ± .16	−4.34 ± .16	11.03 ± .58	1.39 ± .30
P8	5.34 ± 4.17	.20 ± 2.09	−3.68 ± 2.09	8.85 ± 2.13	.74 ± 2.09
P9	7.02 ± .82	1.00 ± .41	−1.87 ± .41	8.06 ± .94	.89 ± .58
P10	4.88 ± .31	−.02 ± .16	−4.06 ± .16	10.32 ± .86	.86 ± .43
P11	6.21 ± 4.17	.61 ± 2.09	−2.51 ± 2.09	7.42 ± 2.25	.33 ± 2.12
P12	6.46 ± 4.17	.75 ± 2.09	−2.95 ± 2.09	8.46 ± 2.13	.86 ± 2.09
P13	3.45 ± .36	−.75 ± .18	−4.69 ± .18	8.20 ± .59	−.62 ± .31
P17	4.94 ± 2.15	−.07 ± 1.07	−2.22 ± 1.07	6.64 ± 1.37	.02 ± 1.15
P18	3.31 ± .31	−.81 ± .16	−4.77 ± .16	10.20 ± 1.71	.49 ± .86
Mean and standard deviation	5.31 ± 1.53	0.17 ± 0.76	−3.37 ± 1.11	8.82 ± 1.19	0.63 ± 0.58

[a] $K_{sp} = 10^{-37.0}$

[b] $K_{sp} = 10^{-3.92}$

dance of organic carbon both in the aquifer and in the ground water, the presence of sulfate reducing bacteria in the Powder River Basin, and the appearance of dissolved sulfide following the reduction of O_2 and NO_3^- are suggestive of sulfate reduction. However, isotopic and mass transfer data are insufficient to prove this point. In the deeper portions of the basin, the disappearance of sulfate, with a concurrent increase in methane concentrations and $\delta^{13}C$ values, indicates the activity of methanogenic bacteria. In the reducing ground waters, saturation with respect to both siderite and $Fe(OH)_{3(am)}$ suggests control of dissolved iron concentrations by these phases.

Increasing sulfate concentrations along the flow path are most likely due to the dissoluton of gypsum present in the upper part of the Lance Formation. Increasing chloride concentrations are probably the result of minor upward leakage from the underlying Pierre Shale, or from the leaching of interbedded shales. Finally, uniformly decreasing log molar $([Ca]+[Mg])/[Na]^2$ ratios are indicative of cation exchange.

Simulation of the above reactions and concurrent equilibration with appropriate minerals has allowed for a determination of possible controlling phases along the northern flow path of the Fox Hills Sandstone. As in the Second Cat Creek sandstone models, ion exchange was simulated by fixing $(a_{Ca^{+2}})/(a_{Na^+})^2$ and $(a_{Mg^{+2}})/(a_{Na^+})^2$ ratios to their observed values for each sample. Minor additions of chloride from shale confining beds were simulated by dissolution of appropriate amounts of halite. Increases in sulfate concentration, originating from either gypsum dissolution or pyrite oxidation, were modeled by dissolving appropriate amounts of gypsum in the outcrop area or natrona (Na_2SO_4) downdip. The choice of these two phases to represent sulfate dissolution is based on the predominant cation in solution, calcium in the outcrop area and sodium downdip, and does not directly imply the presence of these minerals in the aquifer. Dissolved iron concentrations were controlled through equilibration with $FeS_{(am)}$ and siderite in reducing waters, and with $Fe(OH)_{3(am)}$ ($pK_{sp}=37.0$) in oxidizing waters.

A water similar in major element composition to Wyoming rainwater (Junge and Werby, 1958) was equilibrated with atmospheric partial pressures of CO_2 and O_2 using PHREEQE and was used as the initial solution for the following reaction simulations. In order to attain C_T values identical to those calculated for outcrop

area waters, the unsaturated zone P_{CO_2} before equilibration with mineral phases were required to be on the order of $10^{-1.2}$ atm for the carbonate simulations and $10^{-0.9}$ atm for the aluminosilicate simulations. Thorstenson and others (1979) measured a P_{CO_2} of $10^{-0.7}$ atm in the unsaturated zone at Gascoyne, North Dakota, indicating that although these modeled CO_2 concentrations appear somewhat high, they are realistic for lignitic sediments of the type found in the study area. The O_2 and NO_3^- present in the simulated recharge water were reduced by the addition of an appropriate amount of organic carbon. For the reaction simulations, the stability of beidellite was assumed to be similar to that of another smectite, the fixed-composition Na-montmorillonite phase calculated by Helgeson (1969). As shown in figure 48, subsequent equilibration with neither calcite, dolomite, calcite and dolomite, kaolinite and Na-montmorillonite, kaolinite and muscovite, kaolinite, Na-montmorillonite and muscovite, nor allophane results in sufficiently high C_T concentrations for the downdip samples, indicating that additional CO_2 sources must be present. As a result, CO_2 was added to the simulated ground waters in order to match the calculated C_T concentration for each sample along the northern flow path. The pH values resulting from equilibration with the phases listed above are shown in figure 49.

The calcite and dolomite model predicts the field-measured pH values more precisely than the remaining models, and mass transfer calculated using this model is indicative of dedolomitization driven by cation exchange and dissolution of CO_2. A problem arises at this point, however, regarding the choice of CO_2 sources. If CO_2 is derived from a maturing high-volatile organic carbon, the associated mass transfers for siderite and ferrous sulfide will be relatively low. Alternatively, if CO_2 is produced within the aquifer during oxidation of organic matter by sulfate reducing bacteria, H_2S will be generated in quantities of roughly half the amount of CO_2 produced. In order to maintain equilibrium, siderite will be required to dissolve, releasing enough ferrous iron to precipitate the sulfide produced. The dissolution of siderite will consume a portion of the CO_2 acidity, thereby decreasing the solubility of dolomite and altering carbonate mass transfer. This effect is demonstrated in figures 50 and 51, which present calculated mass transfers for lignite coalification (fig. 50) and sulfate reduction (fig. 51) CO_2 sources. The differences between these two models appear minimal, but should be considered in the adjustment of carbon-14 ages and the calculation of flow rates.

Calculated mass transfers indicate controls on ground-water chemistry similar to those proposed for the Second Cat Creek sandstone, namely dedolomitization driven by lignite coalification or sulfate reduction:

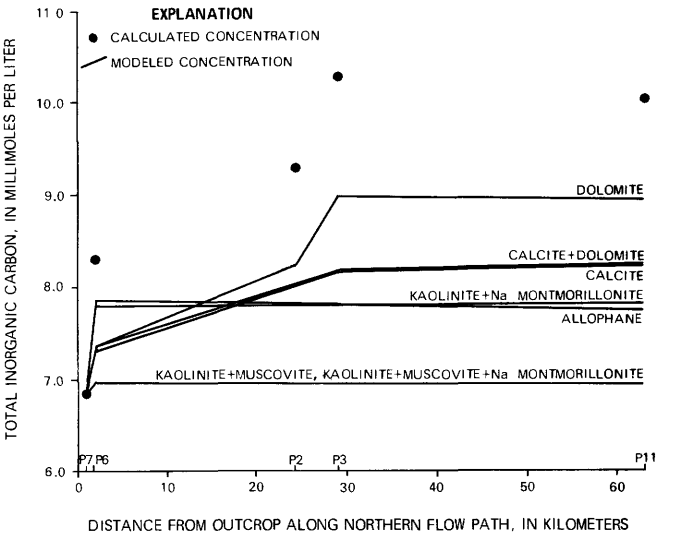

FIGURE 48.—Comparison of calculated total inorganic carbon concentrations with modeled concentrations for mineral equilibration with no CO_2 dissolution following the reduction of O_2 and NO_3^-, northern flow path of the Fox Hills Sandstone, Powder River Basin, Wyoming. All simulations include equilibration with calcium-sodium exchange and magnesium-sodium exchange. Simulations P6, P2, P3, and P11 also include equilibration with amorhous ferrous sulfide and siderite; simulation P7 includes equilibration with amorphous ferric hydroxide.

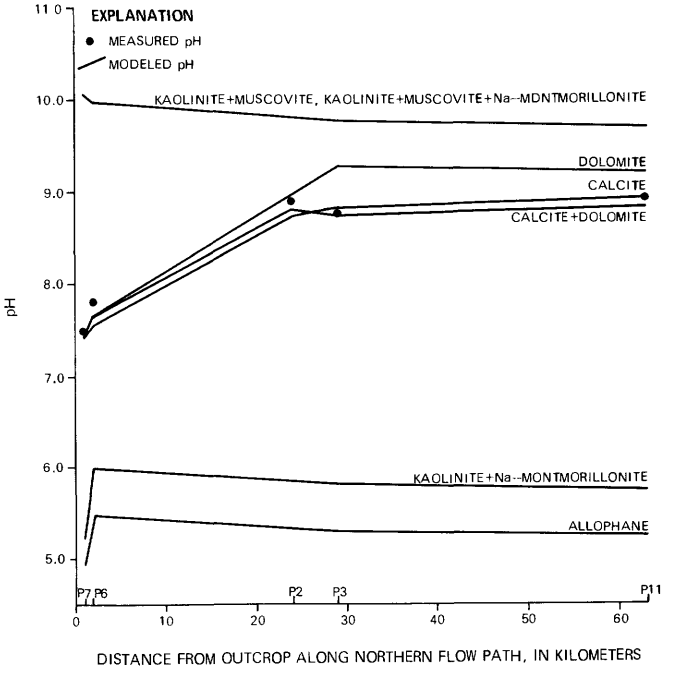

FIGURE 49.—Comparison of field-measured pH values with modeled pH values for mineral dissolution with CO_2 dissolution, northern flow path of the Fox Hills Sandstone, Powder River Basin, Wyoming. All simulations include equilibration with calcium-sodium exchange and magnesium-sodium exchange. Simulations P6, P2, P3, and P11 also include equilibration with amorphous ferrous sulfide and siderite; simulation P7 includes equilibration with amorphous ferric hydroxide.

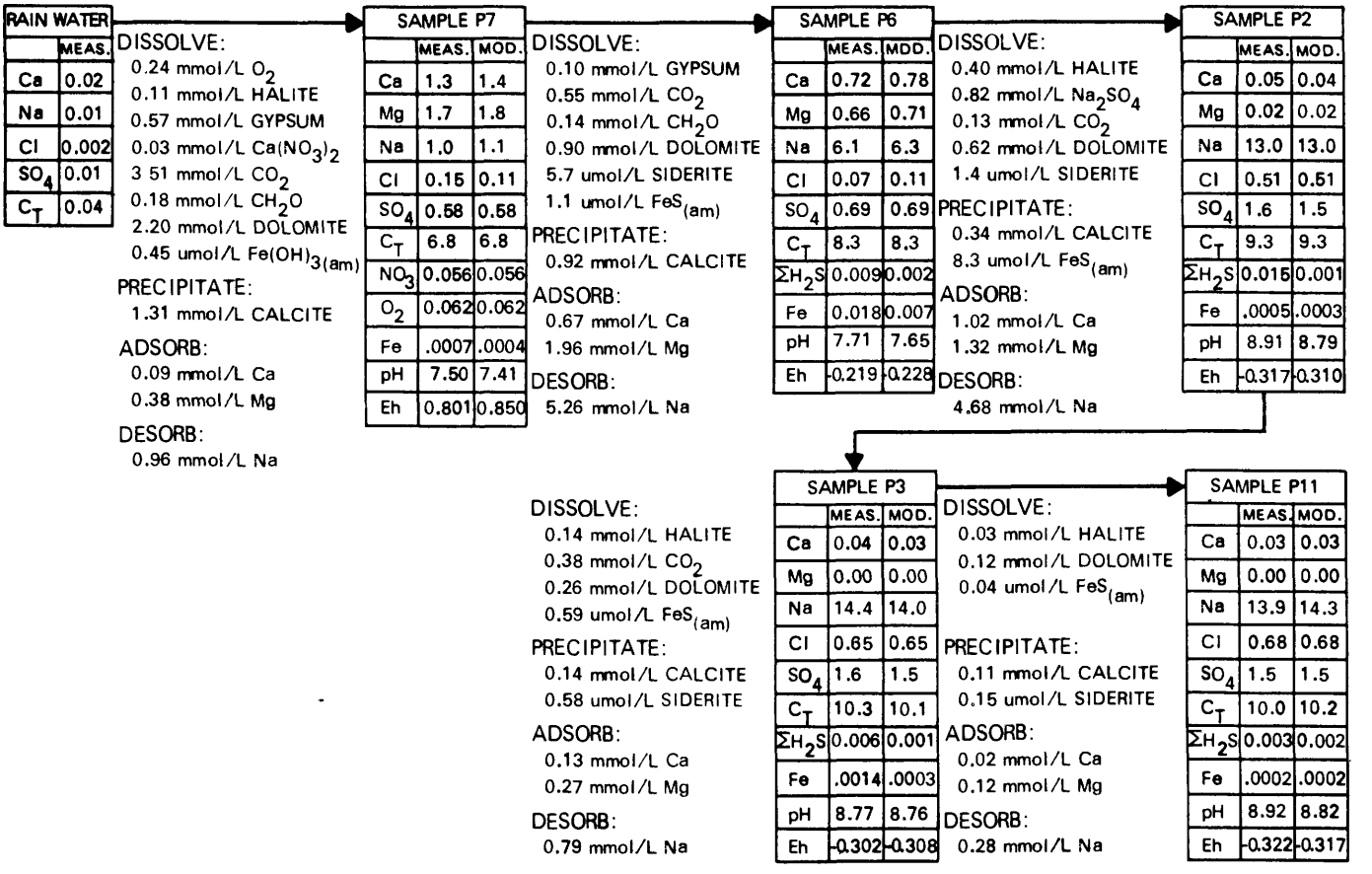

FIGURE 50.—Calculated mass transfer for the calcite-dolomite-cation exchange-CO_2 dissolution model of ground-water evolution along the northern flow path of the Fox Hills Sandstone, Powder River Basin, Wyoming. Concentrations in millimoles per liter (mmol/L) and micromoles per liter (μmol/L); Eh in volts.

$$2CaMg(CO_3)_2+FeCO_3+2CH_2O+SO_4^{-2}+2Na_2EX+Ca^{+2}$$

$$=3CaCO_3+FeS+4HCO_3^-+2MgEX+4Na^+$$

in combination with additional cation exchange (reaction 28 and 29). The addition of kaolinite and Na-montmorillonite to these models results in only minor mass transfer changes, indicating that these aluminosilicates influence major element geochemistry primarily as cation exchange substrates. As illustrated previously in the discussion of CO_2 sources, these proposed mass transfer models are not mathematically unique solutions, but instead represent plausible hypotheses to explain the geochemical evolution of ground-water composition in the Fox Hills Sandstone.

Comparison of measured or calculated concentrations to simulated concentrations, plotted in figure 52, shows good agreement in most cases. Iron presents the largest deviations, with analytical concentrations being much higher than modeled concentrations in several cases. As discussed previously, such deviations may indicate sample contamination by windblown dust.

CARBON ISOTOPIC EVOLUTION

Simulation of carbon isotopic compositions was accomplished using a FORTRAN computer code that incorporates the isotopic evolution equations of Wigley and others (1978). The freshwater carbonate $\delta^{13}C$ value of Keith and Weber (1964) (-4.8 ± 5.1), and the organic $\delta^{13}C$ value of Craig (1954) (-28 ± 4) were chosen to represent the isotopic composition of carbon sources in the aquifer. These estimated $\delta^{13}C$ source values were applied to the mass transfers calculated in figures 50 and 51 to yield downgradient $\delta^{13}C$ values to be expected assuming that these reaction schemes actually control ground-water carbon composition. The coalification of lignite and sulfate reduction models yield nearly identical $\delta^{13}C$ values. Therefore, carbon isotopes do not allow for differentiation between these two carbon sources. Modeled and observed $\delta^{13}C$ values are plotted in figure 53, and show relatively good agreement, although two of the analytical values fall slightly above or below their corresponding modeled values. The scatter in observed $\delta^{13}C$ values may be caused by several influencing factors, the most significant of which is the

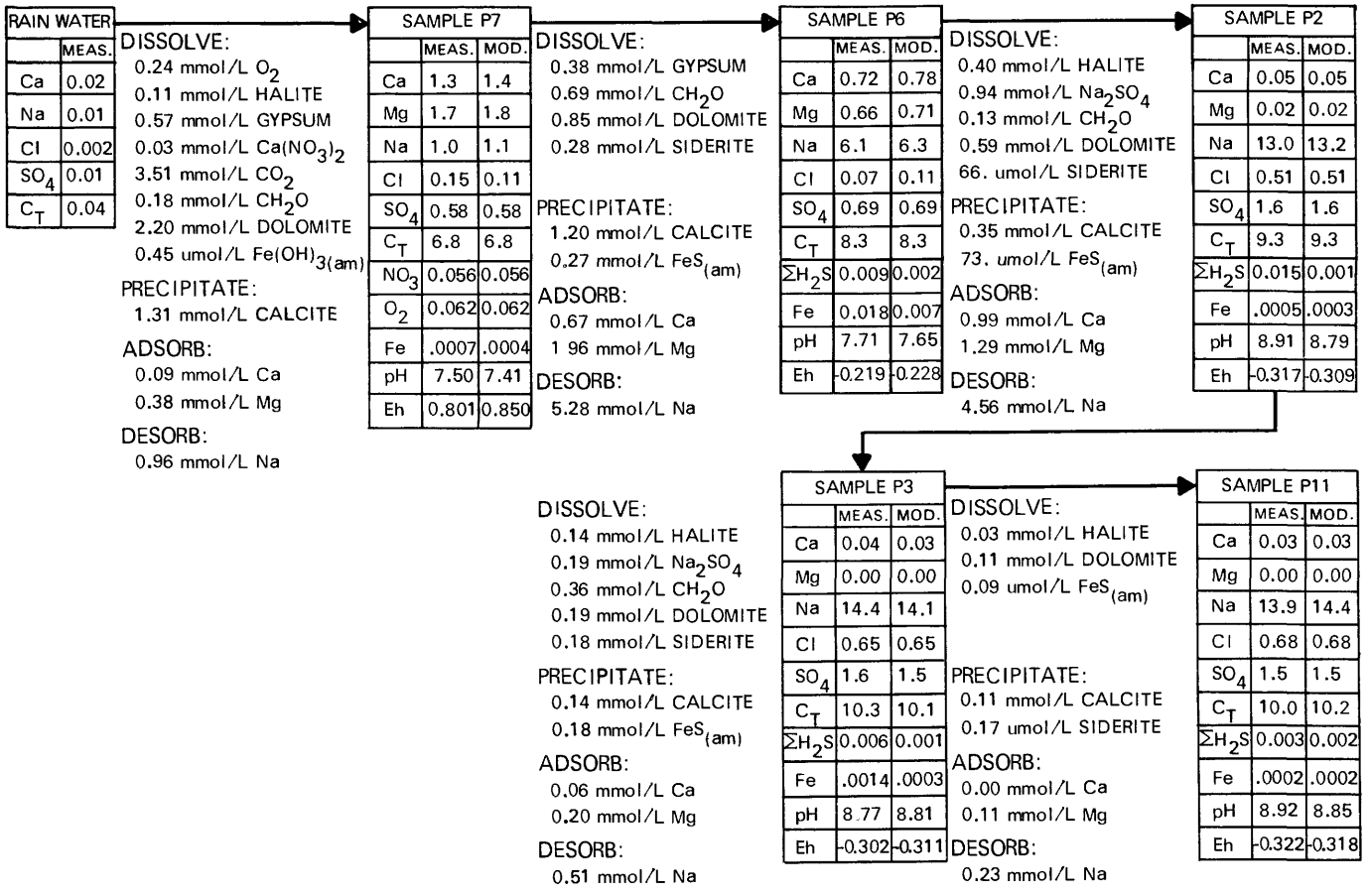

FIGURE 51.—Calculated mass transfer for the calcite-dolomite-cation exchange-sulfate reduction model of ground-water evolution along the northern flow path of the Fox Hills Sandstone, Powder River Basin, Wyoming. Concentrations in millimoles per liter (mmol/L) and micromoles per liter (μmol/L); Eh in volts.

uncertainty of siderite $\delta^{13}C$ values and the lenticular nature of the flow system. Siderite has been shown to vary in $\delta^{13}C$ from highly negative (Hodgson, 1966) ($\delta^{13}C=-33.3$) to moderately positive (Fritz and others, 1971) ($\delta^{13}C=12.8$) values, with large variations possible in samples collected within a meter of each other. The sulfate reduction model requires dissolution of significant amounts of siderite, and isotopic modeling considered siderite $\delta^{13}C$ values to be equivalent to freshwater carbonate $\delta^{13}C$ values (Weber and others, 1964). Variations in siderite $\delta^{13}C$ values might cause significant variations in $\delta^{13}C$ values of dissolved carbonate. The lenticular nature of the aquifer impedes vertical mixing within the formation, thus samples obtained from different areas may have slightly different evolutionary histories and, therefore, different $\delta^{13}C$ values due to contact with carbonates of differing isotopic composition.

Calculation of adjusted carbon-14 ages yields virtually identical values for both models and suggests that the mechanism of CO_2 production may not be an important factor in determining ground-water ages. Adjusted ages of 19,800 to 33,400 years were computed for P2, P3, and P11 using the model of Wigley and others (1978) and measured initial carbon-14 activities as discussed in the section on Radioactive Isotopes. The isotopic compositions and mass transfers used in the model are listed in table 25 and figures 50 and 51, respectively. Flow rates calculated from these ages, presented in table 31, compare favorably with hydrologically derived values of 0.16–1.08 m/yr. Scatter in the ages may be the result of variable flow rates within the aquifer due to the lenticular nature of sand lenses and the presence of many interbedded shale beds, as well as failure to consider possible extreme $\delta^{13}C$ values for siderite.

CONCLUSIONS

Although the controlling reactions cannot be unequivocally determined, the major element geochemistry of confined ground waters in the Second Cat Creek sandstone and Lance–Fox Hills aquifers of the Northern

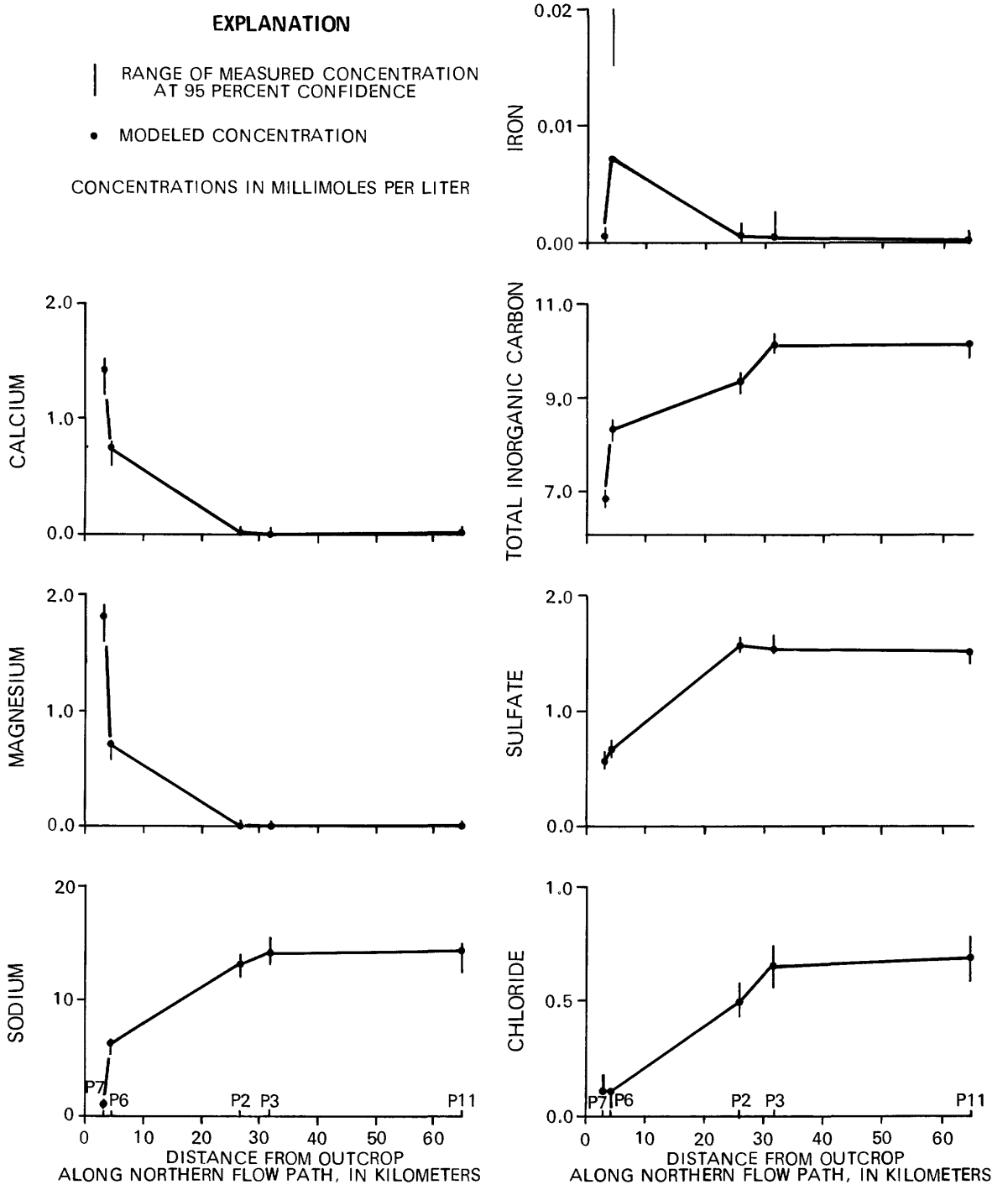

FIGURE 52.—Comparison of measured and modeled concentrations of selected constituents in waters from the northern flow path of the Fox Hills Sandstone, Powder River Basin, Wyoming.

Great Plains appears to be controlled by the incongruent dissolution of dolomite driven by CO_2 dissolution and cation exchange. As a result, the waters evolve from a near neutral pH, low dissolved solids, calcium, and magnesium bicarbonate types to high pH, high dissolved solids, sodium bicarbonate types. The source of CO_2 cannot be unequivocally determined, but is assumed to be either the coalification of lignite or the oxidation of organic carbon by sulfate-reducing bacteria. Mass transfer and carbon isotopic evolution computations indicate that these reactions will affect dissolved carbonate $\delta^{13}C$ values similarly, with modeled isotopic compositions corresponding favorably to measured $\delta^{13}C$ values for both processes.

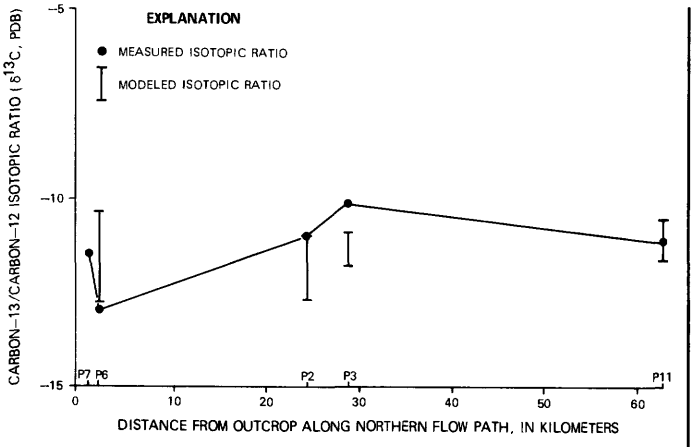

FIGURE 53.—Comparison of measured $\delta^{13}C$ values and the range of modeled $\delta^{13}C$ values for waters from the northern flow path of the Fox Hills Sandstone, Powder River Basin, Wyoming. The range of modeled $\delta^{13}C$ values reflects the uncertainty in the actual $\delta^{13}C$ compositions of aquifer carbon sources.

TABLE 31.—*Comparison of radiometric and hydrologic flow rates for the Lance-Fox Hills aquifer of the Powder River Basin, Wyoming*

Sample	Hydrologic flow rate (meters per year)	Radiometric flow rate (meters per year)
P2 ----------	0.16-1.08	1.07
P3 ----------	.16-1.08	.77
P11 ----------	.16-1.08	<2.14

Despite the profusion of aluminosilicate minerals in the aquifers studied, ground-water pH and dissolved-carbonate chemistry appear to be controlled by equilibration with the often less abundant carbonate minerals. Clay minerals indirectly influence ground-water chemistry by providing substrates for cation exchange, thereby allowing for the high-pH, high- bicarbonate conditions attained in many aquifer systems. Similar conclusions were reached by Thorsten- son and others (1979) in their modeling study of the Fox Hills-Hell Creek aquifer in the Williston Basin, and by Foster (1950) in her laboratory study of carbonate- cation exchange equilibria.

The paucity of organic carbon poises oxidation potentials at values near the redox interface and effectively prevent the onset of sulfate reduction in the Second Cat Creek sandstone, suggesting that CO_2 may be migrating into the aquifer from adjacent carbonaceous strata. In the Lance-Fox Hills aquifer, the presence of H_2S and large quantities of carbonaceous material, as well as the ubiquitous nature of sulfate reducing bacteria, supports the hypothesis that CO_2 is generated primarily within the aquifer, probably through the reduction of sulfate.

Significant quantities of methane were observed in dissolved gases extracted from the two deepest, and presumably oldest, samples from the Fox Hills Sandstone. Anomalously high $\delta^{13}C$ values indicate that methanogenic bacteria are active in these waters, becoming the dominant microbial population following the depletion of sulfate by more energetically efficient bacteria.

Dissolved gas samples also verify that measured P_{CO_2} values may be significantly different than those calculated from field-measured pH due to exchange with atmospheric CO_2 between the time of sample collection and measurement. Calculation of pH from measured P_{CO_2} indicates that the in situ aquifer pH may differ from the field-measured value by up to 0.2 units for poorly buffered, low alkalinity waters, whereas the effects of CO_2 exchange appear minimal for well buffered, high alkalinity samples.

Sulfate is presumed to be derived from the dissolution of gypsum or the oxidation of pyrite, either within the aquifer or in adjacent strata, whereas chloride enters the aquifer as minor amounts of leakage or diffusion through shale confining layers. As demonstrated in the Judith Basin study area, large increases in the concentrations of either of these constituents may be indicative of leakage into the aquifer through faults, fractures, or other highly permeable zones. In the Powder River Basin, recharge of oxidized waters and subsequent mixing with older, reduced waters results in high sulfate concentrations from migration of the redox interface and concurrent pyrite oxidation.

Aqueous iron concentrations are effectively controlled by amorphous ferric hydroxide, siderite, or amorphous ferrous sulfide, depending on Eh conditions. Manganese concentrations appear to be regulated by a solid solution between calcite and rhodochrosite, although saturation with respect to $MnHPO_4$ in waters of the Lance-Fox Hills aquifer may indicate control of dissolved manganese by a phosphate phase. Apatite is also saturated in the Lance-Fox Hills aquifer, and probably controls dissolved phosphate concentrations. A solid solution between calcite and strontianite may influence strontium concentrations in the Lance-Fox Hills aquifer, although such solid solution behavior is unlikely in the Second Cat Creek sandstone.

The use of ground-water geochemistry can provide invaluable information regarding the hydrology of confined sandstone aquifers, especially when used in conjunction with available hydrologic data. Areas of significant recharge to the artesian systems are identified by the presence of relatively low dissolved solids concentration, calcium, and magnesium as the predominant cations, and high tritium and carbon-14 activities. Several samples of the waters from the outcrop did not exhibit all of these properties, serving as an indication

of minimal recharge to the confined system in these areas. Flow directions, determined by regional potentiometric surface maps, were geochemically characterized by increasing dissolved solids concentrations and log molar $([Ca]+[Mg])/[Na]^2$ ratios. It was determined, however, that variations in these operational parameters may become ambiguous in zones where waters of dissimilar chemistry converge and mix. Recharge temperatures for both the Second Cat Creek sandstone and Lance–Fox Hills aquifer, calculated from $\delta^{18}O$ and δD measurements and dissolved argon concentrations, are significantly lower than mean annual surface temperatures, suggesting that recharge to these systems is derived primarily from spring snowmelt, rather than warmer late spring and summer storms.

Areas of leakage or mixing between aquifers are geochemically characterized by abrupt changes in major element and isotopic chemistry, which are not characteristic of normally observed ground-water evolution. Such changes in a fractured, structurally deformed area of the Judith Basin were interpreted as evidence of upward leakage from deeper aquifers. Areal variations in major element chemistry similarly indicate the presence of a discharge zone along the Belle Fourche structural arch in the Powder River Basin.

Perhaps the most significant contribution of ground-water chemistry to the characterization of the hydrology of a confined aquifer system lies in the determination of ground-water ages and flow rates. The adjustment of carbon-14 ages using computed mass transfer and stable carbon isotopic data allows for the calculation of flow rates that are directly comparable to those derived from measured aquifer constants and potentiometric data. The recent success in the adjustment of carbon-14 ages utilizing mass transfer data obtained from detailed geochemical models, both in this study and in others using this approach, is indicative of the usefulness of this technique in determining flow rates in geochemically well-defined systems.

REFERENCES CITED

Anna, L. O., and Croft, M. G., 1977, Confining beds in aquifer systems overlying the Pierre Shale, Fort Union Coal Region [abs.]: Geological Society of America, Rocky Mountain Section, Missoula, Mont., 1977, Abstracts, v. 9, no. 6, p. 707.

Ball, J. W., Jenne, E. A., and Nordstrom, D. K., 1979, WATEQ2—A computerized chemical model for trace and major element speciation and mineral equilibria of natural waters, *in* Jenne, E. A., ed., Chemical modeling in aqueous systems: American Chemical Society Symposium, Miami Beach, Fla., 1978, Series 93, p. 815–835.

Ball, J. W., Nordstrom, D. K., and Jenne, E. A., 1980, Additional and revised thermochemical data and computer code for WATEQ2—A computerized chemical model for trace and major element speciation and mineral equilibria of natural waters: U.S. Geological Survey Water-Resources Investigations 78–116, 114 p.

Ballard, W. W., 1966, Petrography of Jurassic and Cretaceous sandstones, north flank Little Belt Mountains, Montana, *in* Jurassic and Cretaceous stratigraphic traps, Sweetgrass arch: Billings Geological Society Annual Field Conference, 17th, 1966, Guidebook p. 56–70.

Barnes, Ivan, and Clarke, F. E., 1969, Chemical properties of ground water and their corrosion and encrustation effects on wells: U.S. Geological Survey Professional Paper 498-D, p. D1–D37.

Bassett, R. L., Kharaka, Y. K., and Langmuir, Donald, 1979, Critical review of the equilibrium constants for kaolinite and sepiolite, *in* Jenne, E. A., ed., Chemical modeling in aqueous systems: American Chemical Society Symposium, Miami Beach, Fla., 1978, Series 93, p. 389–400.

Berner, R. A., 1963, Electrode studies of hydrogen sulfide in marine sediments: Geochimica et Cosmochimica Acta, v. 27, p. 563–575.

_____1964a, Iron sulfides formed from aqueous solution at low temperatures and atmospheric pressure: Journal of Geology, v. 72, p. 293–306.

_____1964b, Distribution and diagenesis of sulfur in some sediments from the Gulf of California: Marine Geology, v. 6, p. 117–140.

_____1970, Sedimentary pyrite formation: American Journal of Science, v. 268, p. 1–23.

_____1975, The role of magnesium in the crystal growth of calcite and aragonite from sea water: Geochimica et Cosmochimica Acta, v. 39, p. 489–504.

Billings, G. K., and Williams, H. H., 1967, Distribution of chlorine in terrestrial rocks (a discussion): Geochimica et Cosmochimica Acta, v. 31, p. 2247.

Blixt, J. E., 1933, Geology and gold deposits of the North Moccasin Mountains, Fergus County, Montana: Montana Bureau of Mines and Geology Memoir 8, 25 p.

Bodine, M. W., Jr., Holland, H. D., and Borcsik, Maria, 1965, Coprecipitation of manganese and strontium with calcite: Symposium on problems of postmagmatic ore deposition, Prague, 1965, v. 21, p. 401–406.

Bottinga, Y., 1969, Calculated fractionation factors for carbon and hydrogen isotope exchange in the system calcite-carbon dioxide-graphite-methane-hydrogen-water vapor: Geochimica et Cosmochimica Acta, v. 33, p. 49–64.

Boulegue, Jacques, and Michard, Gil, 1979, Sulfur speciations and redox processes in reducing environments, *in* Jenne, E. A., ed., Chemical modeling in aqueous systems: American Chemical Society Symposium, Miami Beach, Fla., 1978, Series 93, p. 25–50.

Breckenridge, R. M., Glass, G. B., Root, F. K., and Wendell, W. G., 1974, Campbell County, Wyoming—Geologic map atlas and summary of land, water, and mineral resources: Geological Survey of Wyoming County Resource Series, no. 3, 9 sheets.

Brown, Eugene, Skougstad, M. W., and Fishman, M. J., 1970, Methods for collection and analysis of water samples for dissolved minerals and gases, chap. C1 *of* bk. 5, Laboratory analysis: U.S. Geological Survey Techniques of Water-Resources Investigations, 160 p.

Busenberg, Eurybiades, and Clemency, C. V., 1976, Dissolution kinetics of feldspar at 25°C and 1 atm. CO_2 partial pressure: Geochemica et Cosmochimica Acta, v. 40, p. 41–49.

Calvert, W. R., 1909, Geology of the Lewistown coal field, Montana: U.S. Geological Survey Bulletin 390, 83 p.

Carothers, W. W., and Kharaka, Y. K., 1980, Stable carbon isotopes of HCO_3^- in oil-field waters—Implications for the origin of CO_2: Geochimica et Cosmochimica Acta, v. 44, p. 323–332.

Champ, D. R., Gulens, J., and Jackson, R. E., 1979, Oxidation-reduction sequences in ground water flow systems: Canadian Journal of Earth Sciences, v. 16, no. 1, p. 12–23.

Chatham, J. R., Wanty, R. B., and Langmuir, Donald, 1981, Groundwater prospecting for sandstone-type uranium deposits—The

merits of mineral-solution equilibria versus single element tracer methods: U.S. Department of Energy National Uranium Resource Evaluation Report GJO-79-360-E, 197 p.

Chien, S. H., and Black, C. A., 1975, The activity concept of phosphate rock solubility: Soil Science Society of American Proceedings, v. 39, p. 856-858.

Claypool, G. E., and Kaplan, I. R., 1974, The origin and distribution of methane in marine sediments, *in* Kaplan, I. R., ed., Natural gases in marine sediments: New York, Plenum, p. 99-139.

Craig, Harmon, 1954, Carbon-13 in plants and the relationship between carbon-13 and carbon-14 variations in nature: Journal of Geology, v. 62, p. 115-141.

_____1957, Isotopic standards for carbon and oxygen and correction factors for mass-spectrometric analysis of carbon dioxide: Geochimica et Cosmochimica Acta, v. 12, p. 133-149.

_____1961a, Isotopic variations in meteoric waters; Science, v. 133, p. 1072-1073.

_____1961b, Standard for reporting concentrations of deuterium, and oxygen-18 in natural waters: Science, v. 133, p. 1833-1834.

Crerar, D. A., and Barnes, H. L., 1974, Deposition of deep-sea manganese nodules: Geochimica et Cosmochimica Acta, v. 38, p. 279-300.

Croft, M. G., and Anna, L. O., 1977, Sulfate reduction in aquifers overlying the Pierre Shale, Fort Union Coal Region [abs.]: Geological Society of America, Rocky Mountain Section, Missoula, Mont., 1977, Abstracts, v. 9, no. 6, p. 718.

Deines, Peter, Langmuir, Donald, and Harmon, R. S., 1974, Stable carbon isotope ratios and the existence of a gas phase in the evolution of carbonate ground waters: Geochimica et Cosmochimica Acta, v. 38, p. 1147-1164.

Dobbin, C. E., and Reeside, J. B., Jr., 1930, The contact of the Fox Hills and Lance Formations: U.S. Geological Survey Professional Paper 158-B, p. 9-25.

Dockins, W. S., Olson, G. J., McFeters, G. A., and Turbak, S. C., 1980, Dissimilatory bacterial sulfate reduction in Montana groundwaters: Geomicrobiology Journal, v. 2, no. 1, p. 83-98.

Dodge, H. W., and Spencer, C. W., 1977, Thinning of the Fox Hills Sandstone, Crook County, Wyoming—A possible guide to uranium mineralization: U.S. Geological Survey Circular 753, p. 50-51.

Douglas, Everett, 1964, Solubilities of oxygen, argon and nitrogen in distilled water: Journal of Physical Chemistry, v. 68, p. 169-174.

Doyle, R. W., 1968a, The origin of the ferrous iron-ferric oxide Nernst potential in environments containing dissolved ferrous iron: American Journal of Science, v. 266, p. 840-859.

_____1968b, Identification and solubility of iron sulfide in anaerobic lake sediments: American Journal of Science, v. 266, p. 980-1004.

Eisenman, George, 1962, Cation selective glass electrodes and their mode of operation: Biophysical Journal, v. 2, p. 259-323.

Farrah, H., Hatton, D., and Pickering, W. F., 1980, The affinity of metal ions for clay surfaces: Chemical Geology, v. 28, p. 55-68.

Feltis, R. D., 1973, Geology and water resources of eastern part of Judith Basin, Montana: Montana Bureau of Mines and Geology Bulletin 87, 51 p.

_____1977, Geology and water resources of the northern part of the Judith Basin, Montana: Montana Bureau of Mines and Geology Bulletin 101, 65 p.

Folk, R. L., and Land, L. S., 1975, Mg/Ca ration and salinity—Two controls over crystallization of dolomite: Bulletin of the American Association of Petroleum Geologists, v. 59, no. 1, p. 60-68.

Fontes, J. C., and Garnier, J. M., 1979, Determination of the initial ^{14}C activity of the total dissolved carbon—A review of the existing models and a new approach: Water Resources Research, v. 15, no. 2, p. 399-413.

Foster, M. D., 1950, The origin of high sodium bicarbonate waters in the Atlantic and gulf coastal plains: Geochimica et Cosmochimica Acta, v. 1, p. 33-48.

Freeze, R. A., and Cherry, J. A., 1979, Groundwater: Englewood Cliffs, N.J., Prentice-Hall, Inc., 604 p.

Fritz, Peter, Binda, P. L., Folinsbee, F. E., and Krouse, H. R., 1971, Isotopic composition of diagenetic siderites from Cretaceous sediments in western Canada: Journal of Sedimentary Petrology, v. 41, no. 1, p. 282-288.

Gardner, L. S., 1959, Geologic map of the Lewistown area, Fergus County, Montana: U.S. Geological Survey Oil and Gas Investigations Map OM-199, scale 1:63,360.

Garrels, R. M., and Christ, C. L., 1965, Solutions, minerals and equilibria: San Francisco, Freeman Cooper, 450 p.

Garrels, R. M., and Mackenzie, F. T., 1971, Evolution of sedimentary rocks: New York, W. W. Norton, 397 p.

Gat, J. R., 1980, The isotopes of hydrogen and oxygen in precipitation, *in* Fritz, Peter, and Fontes, J. C., eds., Handbook of environmental isotope geochemistry, part A—The terrestrial environment: New York, American Elseview Publishing Company, kp. 21-47.

Goldhaber, M. B., and Kaplan, I. R., 1974, The sulfur cycle, *in* Goldberg, E. D., ed., The sea: New York, Wiley Interscience, v. 5, p. 569-655.

Grim, R. E., 1968, Clay mineralogy (2d ed.): New York, McGraw-Hill, 596 p.

Hanshaw, B. B., Back, William, and Deike, R. G., 1971, A geochemical hypothesis for dolomitization by ground water: Economic Geology, v. 66, p. 710-724.

Helgeson, H. C., 1969, Thermodynamics of hydrothermal systems at elevated temperatures and pressures: American Journal of Science, v. 267, p. 729-804.

Hobba, W. A., Jr., Chemerys, J. C., Fisher, D. W., and Pearson, F. J., Jr., 1977, Geochemical and hydrologic data for wells and springs in thermal-spring areas of the Appalachians: U.S. Geological Survey Water-Resources Investigations 77-25, 41 p.

Hodgson, W. A., 1966, Carbon and oxygen isotope ratios in diagenetic carbonates from marine sediments: Geochimica et Cosmochimica Acta, v. 30, p. 1223-1233.

Hodson, W. G., 1971, Chemical analyses of ground water in the Powder River Basin and adjacent areas, northeastern Wyoming: Wyoming Department of Economic Planning and Development, 20 p.

Hodson, W. G., Pearl, R. H., and Druse, S. A., 1973, Water resources of the Powder River Basin and adjacent areas, northeastern Wyoming: U.S. Geological Survey Hydrologic Investigations Atlas HA-465.

Holland, H. D., Holland, H. J., and Munoz, J. L., 1964, The coprecipitation of cations with $CaCO_3$, II—The coprecipitation of Sr^{+2} with calcite between 90° and 100°C: Geochimica et Cosmochimica Acta, v. 28, p. 1287-1301.

Holser, W. T., and Kaplan, I. R., 1966, Isotope geochemistry of sedimentary sulfates: Chemical Geology, v. 1, p. 93-135.

Jacobson, R. L., and Langmuir, Donald, 1972, An accurate method for calculating saturation levels of ground waters with respect to calcite and dolomite: Transactions of the Cave Research Group of Great Britain, v. 14, no. 2, p. 104-108.

Jensen, M. L., and Nakai, N., 1963, Sulfur isotope meteorite standards—Results and recommendations, *in* Biogeochemistry of sulfur isotopes: National Science Foundation Symposium, New Haven, Conn., 1962, Proceedings, p. 30-35.

Johns, W. D., and Huang, W. H., 1967, Distribution of chlorine in terrestrial rocks: Geochimica et Cosmochimica Acta, v. 31, p. 35-49.

Joint Committee on Powder Diffraction Standards, 1981, Powder diffraction file: Swarthmore, Penn.

Jones, B. F., Kennedy, V. C., and Zellweger, G. W., 1974, Comparison of observed and calculated concentrations of dissolved Al and Fe in stream water: Water Resources Research, v. 10, no. 4, p. 791-793.

Junge, C. E., and Werby, R. T., 1958, the Concentration of chloride, sodium, potassium, calcium and sulfate in rain water over the United States: Journal of Meteorology, v. 15, no. 5, p. 417-425.

Keith, M. L., and Weber, J. N., 1964, Carbon and oxygen isotopic composition of selected limestones and fossils: Geochimica et Cosmochimica Acta, v. 28, p. 1787-1816.

Kennedy, V. C., Zellweger, G. W., and Jones, B. F., 1974, Filter pore-size effects on the analysis of Al, Fe, Mn, and Ti in water: Water Resources Research, v. 10, no. 4, p. 785-790.

Kielland, Jacob, 1937, Individual activity coefficients of ions in aqueous solutions: Journal of the American Chemical Society, v. 59, p. 1675-1678.

Kinsman, D. J. J., and Holland, H. D., 1969, The coprecipitation of cations with $CaCO_3$, IV—The coprecipitation of Sr^{+2} with aragonite between 16° and 96°C: Geochimica et Cosmochimica Acta, v. 33, p. 1-17.

Langmuir, Donald, 1969, Geochemistry of iron in a coastal plain ground water of the Camden, New Jersey, area: U.S. Geological Survey Professional Paper 650-C, p. C224-C235.

_____1971, Eh-pH determination, *in* Carver, R. E., ed., Procedures in sedimentary petrology: New York, Wiley Interscience, p. 597-634.

Langmuir, Donald, and Whittemore, D. O., 1971, Variations in the stability of precipitated ferric oxyhydroxides, *in* Hem, J. D., ed., Non-equilibrium systems in natural water chemistry: Houston, Tex., American Chemical Society Advances in Chemistry Series 106, p. 209-234.

Mazor, Emanuel, 1972, Paleotempertures and other hydrological parameters deduced from noble gasses dissolved in groundwaters; Jordan Rift Valley, Israel: Geochimica et Cosmochimica Acta, v. 36, p. 1321-1336.

Miller, R. N., 1959, Geology of the South Moccasin Mountains, Fergus County, Montana: Montana Bureau of Mines and Geology Memoir 37, 44 p.

Mook, W. G., 1976, The dissolution-exchange model for dating groundwater with ^{14}C, *in* Interpretation of environmental isotope and hydrochemnical data in groundwater hydrology: Vienna, International Atomic Energy Agency, p. 179-189.

Morgan, J. J., 1967, Chemical equilibria and kinetic properties of manganese in natural waters, *in* Faust, S. D., and Hunter, J. V., eds., Principles and applications of water chemistry: New York, Wiley Interscience, p. 561-624.

Nissenbaum, Arie, Presley, B. J., and Kaplan, I. R., 1972, Early diagenesis in a reducing fjord, Saanich Inlet, British Columbia, I—Chemical and isotopic changes in major components of interstitial water: Geochimica et Cosmochimica Acta, v. 36, p. 1007-1027.

Nordstrom, D. K., Jenne, E. A., and Ball, J. W., 1979, Redox equilibria of iron in acid mine waters, *in* Jenne, E. A., ed., Chemical modeling in aqueous systems: American Chemical Society Symposium, Miami Beach, Fla., 1978, Series 93, p. 51-79.

Oana, Shinya, and Deevey, E. S., 1960, Carbon-13 in lake waters and its possible bearing on paleolimnology: American Journal of Science, v. 258-A, p. 253-272.

Oeschger, H., Gugelmann, A., Loosli, H., Schotterer, V., Siegenthaler, V., and Wiest, W., 1974, ^{39}Ar dating of groundwater, *in* Isotope techniques in groundwater hydrology: Vienna, International Atomic Energy Agency, v. 2, p. 179-189.

Parkhurst, D. L., Thorstenson, D. C., and Plummer, L. N., 1980, PHREEQE—A computer program for geochemical calculations: U.S. Geological Survey Water-Resources Investigations 80-96, 210 p.

Pearson, F. J., Fisher, D. W., and Plummer, L. N., 1978, Correction of ground-water chemistry and carbon isotopic composition for effects of CO_2 outgassing: Geochimica et Cosmochimica Acta, v. 42, p. 1799-1807.

Plummer, L. N., 1977, Defining reactions and mass transfer in part of the Floridan aquifer: Water Resources Research, v. 13, no. 5, p. 801-812.

Plummer, L. N., Thorstenson, D. C., and Parkhurst, D. L., 1983, Development of reaction models for ground water systems: Geochimica et Cosmochimica Acta, v. 47, p. 665-686.

Potter, R. M., and Rossman, G. R., 1979, Mineralogy of manganese dendrites and coatings: American Mineralogist, v. 64, p. 1219-1226.

Raines, G. L., Offield, I. W., and Santos, E. S., 1978, Remote-sensing and subsurface definition of facies and structure related to uranium deposits, Powder River Basin, Wyoming: Economic Geology, v. 73, p. 1706-1723.

Reeves, Frank, 1931, Geology of the Big Snowy Mountains, Montana: U.S. Geological Survey Professional Paper 165-D, p. 135-149.

Rightmire, C. T., and Hanshaw, B. B., 1973, Relationship between the carbon isotope composition of soil CO_2 and dissolved carbonate species in groundwater: Water Resources Research, v. 9, no. 4, p. 958-967.

Robinson, C. S., Mapel, W. J., and Bergendahl, M. H., 1964, Stratigraphy and structure of the northern and western flanks of the Black Hills Uplift, Wyoming, Montana, and South Dakota: U.S. Geological Survey Professional Paper 404, 134 p.

Rosenfeld, W. D., and Silverman, S. R., 1959, Carbon isotope fractionation in bacterial production of methane: Science, v. 130, p. 1658-1659.

Sackett, W. M., and Chung, H. M., 1979, Experimental confirmation of the lack of carbon isotope exchange between methane and carbon oxides at high temperatures: Geochimica et Cosmochimica Acta, v. 43, p. 273-276.

Sato, Motoaki, 1960, Oxidation of sulfide ore bodies, I—Geochemical environments in terms of Eh and pH: Economic Geology, v. 55, p. 928-961.

Skougstad, M. W., Fishman, M. J., Friedman, L. C., Erdmann, D. E., and Duncan, S. S., eds., 1978, Methods for analysis of inorganic substances in water and fluvial sediments: U.S. Geological Survey Open-File Report 78-679, 1,159 p.

Slack, P. B., 1981, Paleotectonics and hydrocarbon accumulation, Powder River Basin, Wyoming: Bulletin of the American Association of Petroleum Geologists, v. 65, no. 4, p. 730-743.

Stiff, H. A., 1951, The interpretation of chemical water analyses by means of patterns: Journal of Petroleum Technology, v. 3, no. 10, p. 15-17.

Stumm, Werner, and Morgan, J. J., 1981, Aquatic chemistry (2d. ed.): New York, Wiley-Interscience, 780 p.

Suttner, L. J., 1968, Clay minerals in the Upper Jurassic-Lower Cretaceous Morrison and Kootenai Formations, southwest Montana: Wyoming Geological Association Earth Science Bulletin, v. 1, no. 4, p. 5-14.

_____1969, Stratigraphic and petrographic analysis of Upper Jurassic-Lower Cretaceous Morrison and Kootenai Formations, southwest Montana: Bulletin of the American Association of Petroleum Geologists, v. 53, no. 7, p. 1391-1410.

Tamers, M. A., 1975, Validity of radiocarbon dates on ground water: Geophysical Surveys, v. 2, p. 217-239.

Teichmuller, Marlies, and Teichmuller, Rolf, 1979, Diagenesis of coal (coalification), *in* Larsen, Gunnar, and Chilingar, G. V., eds., Developments in sedimentology 25A—Diagenesis in sediments and sedimentary rocks: New York, American Elsevier Publishing Company, p. 207-246.

Thorstenson, D. C., Fisher, D. W., and Croft, M. G., 1979, The geochemistry of the Fox Hills-Basal Hell Creek aquifr in southwestern North Dakota and northwestern South Dakota: Water Resources Research, v. 15, no. 7, p. 1479-1498.

Truesdell, A. H., and Jones, B. F., 1974, WATEQ—A computer program for calculating chemical equilibria of natural waters: U.S. Geological Survey Journal of Research, v. 2, no. 2, p. 233-274.

Usdowski, Eberhard, 1973, Das geochemische verhalten des striums bei der genese und diagenese von Cakarbonat -und Casulfat-mineralen: Contributions to Mineralogy and Petrology, v. 38, p. 177-195.

van Olphen, Hendrick, 1963, An introduction to colloid chemistry: New York, Wiley Interscience, 301 p.

Vine, J. D., 1956, Geology of the Stanford-Hobson area, central Montana: U.S. Geological Survey Bulletin 1027-J, p. 405-470.

Vine, J. D., and Hail, W. J., Jr., 1950, Geology of the Hobson area, central Montana: U.S. Geological Survey Oil and Gas Investigations Preliminary Map 108, scale 1:63,360.

Vogel, J. C., 1970, Carbon-14 dating of groundwater, *in* Isotope hydrology: Vienna, International Atomic Energy Agency, p. 235-237.

Wahlberg, J. S., Baker, J. H., Vernon, R. W., and Dewar, R. S., 1965, Exchange adsorption of strontium on clay minerals: U.S. Geological Survey Bulletin 1140-C, 26 p.

Wahlberg, J. S., and Dewar, R. S., 1965, Comparison of distribution coefficients for strontium exchange from solutions containing one and two competing cations: U.S. Geological Survey Bulletin 1140-D, 10 p.

Wallace, S. R., 1953, The petrology of the Judith Mountains, Fergus County, Montana: U.S. Geological Survey open file report, 189 p.

Weber, J. N., Williams, E. G., and Keith, M. L., 1964, Paleoenvironmental significance of carbon isotopic composition of siderite nodules in some shales of Pennsylvanian age: Journal of Sedimentary Petrology, v. 34, no. 4, p. 814-818.

Whitcomb, H. A., 1965, Ground-water resources and geology of Niobrara County, Wyoming: U.S. Geological Survey Water-Supply Paper 1788, 101 p.

Whitcomb, H. A., and Morris, D. A., 1964, Ground-water resources and geology of northern and western Crook County, Wyoming: U.S. Geological Survey Water-Supply Paper 1698, 92 p.

Whittemore, D. O., and Langmuir, Donald, 1975, The solubility of ferric oxyhydroxides in natural waters: Groundwater, v. 13, no. 4, p. 360-365.

Wigley, T. M. L., Plummer, L. N., and Pearson, F. J., Jr., 1978, Mass transfer and carbon-isotope evolution in natural water systems: Geochimica et Cosmochimica Acta, v. 42, p. 1117-1139.

Wiklander, Lambert, 1964, Cation and anion exchange phenomena, *in* Bear, F. E., ed., Chemistry of the soil (2d ed.): New York, Reinhold, p. 163-205.

Wood, W. W., 1976, Guidelines for collection and field analysis of ground water samples for selected unstable constituents, Book 1, chap. D2: U.S. Geological Survey Techniques of Water-Resources Investigations, 24 p.

Wyoming Water Planning Program, 1972, Water and related land resources of northeastern Wyoming—Wyoming water planning program report no. 10: Cheyenne, Wyo., Wyoming State Engineer, 209 p.

Yurtsever, Y., 1975, Worldwide survey of stable isotopes in precipitation, *in* Environmental isotope data no. 5—World survey of isotope concentration in precipitation (1970-1971): Vienna, International Atomic Energy Agency, Technical Report Series no. 165, 40 p.

Zimmerman, E. A., 1966, Geology and ground-water resources of western and southern parts of Judith Basin, Montana: Montana Bureau of Mines and Geology Bulletin 50-A, 33 p.

SUPPLEMENTAL DATA

GEOCHEMICAL PRINCIPLES

SOLUTION-MINERAL EQUILIBRIA

LAW OF MASS ACTION

The driving force of a chemical reaction can be related to the effective concentrations, or activities (a_i) of the reactants and products, through the Law of Mass Action. In a system at equilibrium, for a particular set of pressure and temperature conditions, the rate of reaction in a forward direction is equal to the rate of reaction in a reverse direction. For the reaction:

$$bB+cC=dD+eE,$$

equilibrium conditions may be defined at a particular temperature and pressure by the thermodynamic equilibrium constant (K_{eq}):

$$K_{eq}=\frac{(a_D)^d\,(a_E)^e}{(a_B)^b\,(a_C)^c}.$$

EQUILIBRIUM CONSTANTS

The K_{eq} for a reaction of 25° Celsius (°C) and one bar total pressure may be calculated from the difference in the standard free energies of formation (ΔG^0_f) between products and reactants:

$$\Delta G^0_{f\ reaction}=\Sigma\Delta G^0_{f\ products}-\Sigma\Delta G^0_{f\ reactants},$$

$$\Delta G^0_{f\ reaction}=d\Delta G^0_{fD}+e\Delta G^0_{fE}-(b\Delta G^0_{fB}+c\Delta G^0_{fC}),$$

$$G^0_{f\ reaction}=-RT_r\,ln\,K_{eq},$$

where:

R=gas constant (8.3147 $\frac{\text{Joules}}{\text{mole °Kelvin}}$), and

T_r=standard temperature (298.15° Kelvin).

Because an equilibrium constant is dependent on temperature, the value calculated for 25°C (298.15° Kelvin) must be adjusted if it is to be used at another temperature. In a system at constant pressure, the equilibrium constant is related to temperature by the standard enthalpy of reaction (ΔH^0_{RX}) and the heat capacity of reaction at constant pressure (ΔC^0_{pRX}):

$$\log K_{eq\,T_2}=\log K_{eq\,T_r}-\frac{\Delta H^0_{RX\,T_r}}{2.303R}\left(\frac{1}{T_2}-\frac{1}{T_r}\right)$$

$$-\frac{1}{2.303RT_2}\int_{T_r}^{T_2}\Delta C^0_{pRX\,T_2}\,dT$$

$$+\frac{1}{2.303R}\int_{T_r}^{T_2}\Delta C^0_{pRX\,T_2}\,d\ln T,$$

where T_2 represents the temperature of interest and T_r represents the reference temperature (298.15°K). Unfortunately, heat capacity data are unavailable for a majority of aqueous species; in most instances, the above expression cannot be solved. A simplification of the above expression, the Van't Hoff equation, assumes that ΔC^0_{pRX} equals zero:

$$\log K_{eq\,T_2}=\log K_{eq\,T_r}-\frac{\Delta H^0_{RX\,T_r}}{2.303R}\left(\frac{1}{T_2}-\frac{1}{T_r}\right).$$

Except when ΔH^0_{RX} is close to zero at 25°C, the Van't Hoff equation allows the estimation of K_{eq} values from 0 to 50°C, which are sufficiently accurate for most purposes.

Standard enthalpies of reaction are computed in a manner analogous to ΔG^0_{RX}:

$$\Delta H^0_{RX}=\Sigma\Delta H^0_{f\ products}-\Sigma\Delta H^0_{f\ reactants},$$

$$\Delta H^0_{RX}=(d\Delta H^0_{fD}+e\Delta H^0_{fE})-(b\Delta H^0_{fB}+c\Delta H^0_{fC}).$$

ACTIVITIES AND ACTIVITY COEFFICIENTS

It can be shown experimentally that an ionic compound is generally more soluble in an electrolyte solution than in pure water, provided the electrolyte does not consist of the same ions as the compound. This effect is the result of interactions between oppositely charged ions in solution, which cause an apparent shift in the chemical equilibria involved. For dilute solutions, the magnitude of this interaction is dependent on the ionic strength (I) of the solution, which provides a measure of the molal concentrations (m_i) and charges (Z_i) of the respective ions in solution:

$$I=\tfrac{1}{2}\,\Sigma m_i Z_i.$$

To quantitatively describe the effects of ionic strength on equilibria, the concentrations of species in solution are adjusted by activity coefficients (γ_i) to yield the effective concentrations, or activities, of the species:

$$a_i = \gamma_i m_i .$$

Activity coefficients for pure solids and liquids, and for dissolved species in infinitely dilute solutions, are equal to unity. As the ionic strength of the soluton increases, the dissolved ionic species lose some of their effectiveness, and the activity coefficient decreases. Activity coefficients may be calculated for individual ions in dilute solutions ($I \leq 0.05$) (Garrels and Christ, 1965) through the use of the Debye-Hückel equation:

$$\log \gamma_i = \frac{-AZ_i^2 I^{1/2}}{1 + \mathring{a}_i BI^{1/2}};$$

or the Davies equation:

$$\log \gamma_i = -AZ_i^2 \left(\frac{I^{1/2}}{1+I^{1/2}}\right) + 0.2I ;$$

where A and B are constants dependent on the temperature of the solution, and $\mathring{a}_i$ is the experimentally determined ion size parameter (Kielland, 1937).

For gases at 25°C and at pressures of less than 40 atmospheres, the activity is essentially equal to the partial pressure of the gas:

$$a_i = P_i .$$

COMPLEX EQUILIBRIA

For simple ions in solution, activities may be calculated from their respective activity coefficients and molalities. The activities of complex ions and ion pairs are, in turn, related to the activities of simple ions through mass action expressions; molalities of these complex ions and ion pairs may be calculated from their respective activity expressions. Conservation of mass and electro-neutrality constraints provide two additional expressions, allowing the set of simultaneous equations to be solved for the activities and molalities of all species in solution.

For instance, consider the dissolution of gypsum in pure water. The chemical reactions required to describe this system are:

$$H_2O = H^+ + OH^- ,$$
$$CaSO_4 \cdot 2H_2O_{(c)} = Ca^{+2} + SO_4^{-2} + 2H_2O ,$$
$$CaSO_4^0 = Ca^{+2} + SO_4^{-2} ,$$
$$CaOH^+ = Ca^{+2} + OH^- ,$$
$$HSO_4^- = H^+ + SO_4^{-2} .$$

Five mass action equations can be formulated to describe these chemical reactions in terms of activities, and the molalities of the aqueous species can be related to these activities by seven activity coefficients, provided by the ionic strength and Debye-Hückel equations. At this point, there are seven unknown molalities, seven unknown activities, seven unknown activity coefficients, and the unknown ionic strength. However, there are only five mass action equations, seven activity equations, seven Debye-Hückel equations, and the ionic strength equation. To solve the problem, two additional equations are required to equal the number of unknowns. These additonal equations are provided by the mass balance and charge balance constraints. Because the solution is initially devoid of both calcium and sulfate, and because the independent addition of either calcium or sulfate during the dissolution of gypsum would result in the accumulation of a net electrical charge in the solution, the following mass balance:

$$m_{Ca^{+2}} + m_{CaSO_4^0} + m_{CaOH^+} = m_{SO_4^{-2}} + m_{CaSO_4^0} + m_{HSO_4^-}$$

and charge balance:

$$2m_{Ca^{+2}} + m_{CaOH^+} + m_{H^+} = 2m_{SO_4^{-2}} + m_{HSO_4^-} + m_{OH^-}$$

expressions must be valid. Thus, the 22 independent equations may be solved iteratively to yield values for the 22 unknowns.

This example demonstrates that the set of simultaneous equations required to solve for the unknowns in even a simple natural solution rapidly becomes too large to calculate by hand. As a result, computer programs such as WATEQ2 (Ball and others, 1980) and PHREEQE (Parkhurst and others, 1980) have been developed to solve the necessary equations to describe complex equilibria in natural aqueous systems.

SATURATION INDICES

The activities of aqueous chemical species may be used to calculate the saturation state of a mineral in that solution. If a solution is undersaturated with respect to a

mineral, the mineral will tend to dissolve; if a solution is oversaturated with respect to a mineral, the mineral will tend to precipitate. Saturation with respect to a mineral indicates that the solution and the mineral are in equilibrium. It is important to realize, however, that equilibrium calculations indicate the direction in which a particular reaction will tend to proceed, but not the rate at which it will proceed.

The dissolution of calcite may be presented by the reaction:

$$\underset{\text{(calcite)}}{CaCO_{3(c)}} + H^{+} = Ca^{+2} + HCO_3^{-} ;$$

so the corresponding mass action expression would be:

$$K_{sp} = \left[\frac{(a_{Ca^{+2}})\,(a_{HCO_3^-})}{(a_{H^+})} \right]_{\text{equilibrium}} .$$

Substitution of calculated activities into the above mass action expression will yield an ion activity product (IAP):

$$IAP = \left[\frac{(a_{Ca^{+2}})\,(a_{HCO_3^-})}{(a_{H^+})} \right]_{\text{calculated}} .$$

Comparison of the calculated IAP value with the equilibrium K_{sp} value will allow a determination of the saturation state of a mineral. The saturation index (SI) relates measured compositions to the equilibrium state, and is defined as:

$$SI = \log \left(\frac{IAP}{K_{sp}} \right) .$$

An SI equal to zero indicates saturation with respect to that mineral phase because the observed conditions are equivalent to equilibrium conditions. Similarly, examination of the above equations will reveal that if an SI value is greater than zero, the mineral is oversaturated, and that an SI value less than zero indicates undersaturation.

Knowledgeable interpretation of the saturation indices generated from complete and precise chemical analyses will, therefore, yield important information regarding the degree of equilibrium (or disequilibrium) attained between aquifer mineral phases and the aqueous solution, and will suggest which solid phases may control aqueous chemistry. However, caution must be exercised in the evaluation of plausible controlling phases for a particular system. As discussed previously, thermodynamic equilibrium calculations do not indicate the rate at which a system will approach equilibrium. Thus, oversaturation with respect to a particular phase does not directly imply that the phase will precipitate from solution at a measurable rate.

PHASE DIAGRAMS

Phase diagrams were also utilized to determine which aquifer minerals are stable in a given aqueous solution. Aqueous dissolution reactions for pairs of mineral phases may be combined and balanced to yield an expression relating the stabilities of the two phases to the activities of their aqueous dissolution products. Solution of these equations in terms of two of three parameters—ion activities, gas partial pressures, or oxidation potentials—allows the stability boundary for that mineral pair to be plotted as a function of variation in the two parameters chosen. Activities of species not represented by either the ordinate or abscissa are fixed at values approximating solution composition. Superposition of aqueous compositions on such a diagram reveals the stable mineral or minerals in that water. For further discussion of such diagrams, or of solution-mineral equilibria in general, the reader is directed to Garrels and Christ (1965) and Stumm and Morgan (1981).

AQUEOUS SOLUBILITY OF GASES

The equilibrium activity of a particular gas in water (a_{gas}) is related by its Henry's Law solubility constant (K_{gas}) to the partial pressure of that gas (P_{gas}) in an adjacent gas phase by:

$$K_{gas} = \frac{a_{gas}}{P_{gas}} .$$

Thus, knowing the atmospheric fractional abundance (N) of a gas and the total atmospheric pressure (P_{atm}) at the location of interest, one can calculate the equilibrium activity of that gas in solution:

$$K_{gas} = \frac{a_{gas}}{NP_{atm}} .$$

Because Henry's Law solubility constants often vary with temperature, the aqueous concentration of a relatively inert gas, such as argon, krypton, or xenon, can reveal the temperature of ground-water recharge, assuming that the water has neither gained nor lost the gas of interest after contact with the unsaturated zone (Mazor,

1972). Additions of argon due to the radioactive decay of ^{40}K are generally insignificant for time intervals less than several million years.

OXIDATION-REDUCTION

Because the mobility of most elements exhibiting multiple oxidation states in natural systems is highly dependent on the oxidation potential (Eh) of the system, and because the oxidation of organic carbon provides an important driving force for many geochemical reactions, the recognition of redox zones and the estimation of Eh are very important in ground-water modeling studies.

The oxidation potential of a ground water is generally observed to decrease as the water flows from upland recharge areas to lowland discharge areas under confined conditions. Champ and others (1979) discussed such variations in Eh and the corresponding variations in concentrations of elements with variable oxidation states, including oxygen, nitrogen, iron, manganese, sulfur, and carbon. They concluded that a sequence of oxidation-reduction reactions, based on thermodynamic principles and microbial catalysis, can account for the variations in oxidation potential. Their sequence of reactions defines three redox zones in ground-water flow systems that are described as: (1) oxygen-nitrate; (2) iron-manganese; and (3) sulfide. Ground water entering the recharge area of a confined aquifer system is oxidizing, containing both dissolved oxygen and nitrate. organic carbon present in the aquifer serves as the reductant, being catalytically oxidized to CO_2 by micro-organisms that utilize these redox reactions as a source of energy for their metabolic requirements. The reductant, organic carbon with an oxidation sate of zero, is represented simplistically as CH_2O in the following reactions. The pertinent geochemical reactions have been sequentially numbered for ease of reader reference.

Once the oxygen and nitrate have been microbially reduced by organic carbon:

$$O_{2(g)}+CH_2O=CO_{2(g)}+H_2O \quad (1)$$

$$4NO_3^-+5CH_2O+4H^+=2N_{2(g)}+5CO_{2(g)}+7H_2O \quad (2)$$

$$NO_3^-+2CH_2O+2H^+=NH_4^++2CO_{2(g)}+H_2O \quad (3)$$

the more reducing iron-manganese zone is encountered. Fe(III) and Mn(III)-Mn(IV) oxyhydroxides, stable in the oxygen-nitrate zone, are reduced to Fe(II) and Mn(II):

$$4Fe(OH)_{3(am)}+CH_2O+8H^+=4Fe^{+2}+CO_{2(g)}+11H_2O, \quad (4)$$

$$2MnO_2+CH_2O+4H^+=2Mn^{+2}+CO_{2(g)}+3H_2O. \quad (5)$$

After the reduction of iron and manganese, the ground water becomes sufficiently reducing to allow the onset of microbial sulfate reduction:

$$SO_4^{-2}+2CH_2O+H^+=HS^-+2CO_{2(g)}+2H_2O, \quad (6)$$

followed by acetate fermentation or CO_2 reduction to form methane:

$$CH_3COOH=CH_{4(g)}+CO_{2(g)} \quad (7)$$

$$CO_{2(g)}+H_{2(g)}=CH_{4(g)}+2H_2O. \quad (8)$$

The hydrogen required to reduce CO_2 is derived from organic compounds present in the aquifer.

In some cases compounds other than organic carbon may act as reductants in the presence of oxidized species. Sulfide species originating from the dissolution of pyrite [$FeS_{2(c)}$] can act to reduce both oxygen:

$$FeS_{2(c)}+(7/2)O_{2(g)}+H_2O=Fe^{+2}+2SO_4^{-2}+2H^+ \quad (9)$$

and ferric iron:

$$\underset{\text{(pyrite)}}{FeS_{2(c)}}+14Fe^{+3}+8H_2O=15Fe^{+2}+2SO_4^{-2}+16H^+. \quad (10)$$

Reduced gases such as methane may also serve as reductants on exposure to more oxidized species:

$$CH_{4(g)}+2O_{2(g)}=H_2CO_3^0+H_2O. \quad (11)$$

In this study, Eh was calculated using the appropriate oxidation-reduction reactions in conjunction with the Nernst-Peters equation:

$$Eh=E^0+\frac{0.0592}{n}\log\frac{(\text{oxidized})}{(\text{reduced})},$$

where:

E^0=standard electrode potential, for the combined half reactions, in volts,

n=number of moles of electrons transferred,

$\frac{(\text{oxidized})}{(\text{reduced})}$=the mass action expression for the combined half reactions.

For the oxygen-nitrate zone, the appropriate reaction involves the O_2-H_2O redox couple:

$$O_{2(g)}+4H^{+}+4e^{-}=2H_2O\,;\ E^0=1.229\ \text{volts}, \quad (12)$$

$$Eh=1.229-0.0592pH-0.0148\log(a_{H_2O})^2/(P_{O_2})\,.$$

The Fe(II)-Fe(III) couple (Doyle, 1968a; Whittemore and Langmuir, 1975) was used to calculate Eh when neither O_2 nor H_2S were present, as in many of the Judith Basin samples. Amorphous ferric hydroxide [$Fe(OH)_{3(am)}$] and siderite [$FeCO_{3(c)}$] are known to coexist in the Kootenai aquifers, and preliminary WATEQ2 computations indicated that both of these phases were in equilibrium with sampled waters. Assuming that both $Fe(OH)_{3(am)}$ and siderite are in equilibrium with the solution, deciding on a pK_{sp} range of 37 to 39 for the $Fe(OH)_{3(am)}$ dissolution reaction (Langmuir and Whittemore, 1971), and assuming the presence of a highly soluble amorphous siderite, the following reactions may be used to calculate Eh:

$$Fe(OH)_{3(am)}=Fe^{+3}+3OH^{-};\quad pK_{Fe(OH)_{3(am)}}=37\text{-}39\,, \quad (13)$$

$$FeCO_{3(c)}=Fe^{+2}+CO_3^{-2};\quad pK_{FeCO_3}=10.22\,, \quad (14)$$

$$Fe^{+3}+e^{-}=Fe^{+2};\quad E^0=0.771\ \text{volts}\,. \quad (15)$$

Adding reactions and substituting into the Nernst equation, the Eh expression becomes:

$$Eh=0.771+0.0592(pK_{FeCO_3}-pK_{Fe(OH)_{3(am)}}-3\log(a_{OH^-})$$
$$+3\log(a_{CO_3^{-2}}))\,. \quad (16)$$

WATEQ2 was used to calculate a_{OH^-} and $a_{CO_3^{-2}}$, which were in turn substituted into the above expression to evaluate the Eh of these waters. Saturation indices for siderite and $Fe(OH)_{3(am)}$, derived using the calculated Eh values and the WATEQ2 crystalline siderite stability constant, indicate equilibrium between these phases and all solutions for which this calculation was performed. The precision of the estimates, based on the variable stability of $Fe(OH)_{3(am)}$, was calculated to be ±60 millivolts of the intermediate ($pK_{Fe(OH)_{3(am)}}=38$) value.

Finally, when measurable sulfide was present in the sampled waters, the SO_4^{-2}-H_2S couple was used to calculate Eh:

$$SO_4^{-2}+10H^{+}+8e^{-}=H_2S^0+4H_2O;\ E^0=0.301\ \text{volts}\,, \quad (16)$$

$$Eh=0.301-0.0740pH-0.00740\log(a_{H_2S})(a_{H_2O})^4/(a_{SO_4^{-2}})\,.$$

Although recent evidence suggests that electroactive polysulfide (S_n^{-2}) and thiosulfate ($S_2O_3^{-2}$) ions in equilibrium with dissolved sulfide control Eh in waters where these species are present (Boulegue and Michard, 1979), the use of the more readily determined SO_4^{-2}-H_2S couple will result in minimal errors of approximately 50 millivolts.

MINERAL DISSOLUTION AND WEATHERING

The CO_2 produced during the microbial oxidation of organic matter provides an important driving mechanism for many important mineral dissolution and weathering reactions. Carbon dioxide dissolves, increases total inorganic carbon (C_T) concentrations in the aquifer, and decreases pH through dissociation of the carbonic acid ($H_2CO_3^0$) formed:

$$CO_{2(g)}+H_2O=H_2CO_3^0\,, \quad (17)$$

$$H_2CO_3^0=HCO_3^{-}+H^{+}\,, \quad (18)$$

$$HCO_3^{-}=CO_3^{-2}+H^{+}\,. \quad (19)$$

Although some mineral dissolution reactions can proceed without the consumption of acidity:

$$\underset{\text{(gypsum)}}{CaSO_4\cdot 2H_2O_{(c)}}=Ca^{+2}+SO_4^{-2}+2H_2O\,, \quad (20)$$

the acidity produced by the dissociation of carbonic acid provides a driving force for the weathering and dissolution of many other groups of minerals, including carbonates:

$$\underset{\text{(calcite)}}{CaCO_{3(c)}}+H^{+}=Ca^{+2}+HCO_3^{-}\,, \quad (21)$$

$$\underset{\text{(dolomite)}}{CaMg(CO_3)_{2(c)}}+2H^{+}=Ca^{+2}+Mg^{+2}+2HCO_3^{-}\,, \quad (22)$$

$$\underset{\text{(dolomite)}}{CaMg(CO_3)_{2(c)}}+2H^{+}=\underset{\text{(calcite)}}{CaCO_{3(c)}}+Mg^{+2}+HCO_3^{-}\,, \quad (23)$$

and aluminosilicates:

$$\underset{\text{(illite)}}{K_{0.6}Mg_{0.25}Al_{2.5}Si_{3.5}O_{10}(OH)_{2(c)}}+3.15H_2O+1.1H^{+}=$$
$$\underset{\text{(kaolinite)}}{1.15Al_2Si_2O_5(OH)_{4(c)}}+0.6K^{+}+0.25Mg^{+2}+1.2H_4SiO_4^0, \quad (24)$$

$$\underset{\text{(Na-montmorillonite)}}{3Na_{0.33}Al_{2.33}Si_{3.67}O_{10}(OH)_{2(c)}}+H^{+}+11.5H_2O=$$
$$\underset{\text{(kaolinite)}}{3.5Al_2Si_2O_5(OH)_{4(c)}}+Na^{+}+4H_4SiO_4^0\,, \quad (25)$$

$$\underset{\text{(muscovite)}}{3KAl_2Si_3O_{10}(OH)_{2(c)}}+3H_2O+2H^{+}=$$

$$3\underset{\text{(kaolinite)}}{Al_2Si_2O_5(OH)_{4(c)}} + 3K^+ , \quad (26)$$

$$NaAlSi_3O_{8(c)} + 6.1H_2O + 1.1H^+ =$$
(albite)

$$1.4\underset{\text{(allophane)}}{[Al(OH)_3]_{0.7}}[SiO_2]_{0.3(am)} + Na^+ + 2.6H_4SiO_4^0 . \quad (27)$$

The coalification of lignite and other carbonaceous materials also results in the generation of CO_2, as well as in the release of considerable quantities of CH_4 (Teichmüller and Teichmüller, 1979). Experimental work by Foster (1950) has demonstrated the importance of CO_2 derived from lignite, in combination with calcite dissolution and cation exchange, in producing the high-bicarbonate waters of the Atlantic Coastal Plain.

ION EXCHANGE

Fine-grained sediments exhibit the capability of exchanging ions adsorbed on electrically charged particle surfaces. The net positive or negative charge on the particle is the result of ionic substitutions, imperfections, and broken bonds within the crystal lattice, or association-dissociation reactions that occur on the particle surfaces. To maintain electrical neutrality, ions of opposite charge, known as counter ions, are attracted to the particle and form adsorbed layers immediately surrounding the particle. These ion-exchange processes are most important for colloidal-sized particles, because of their relatively high charge-to-size ratio.

In natural systems, clay minerals form an important class of ion exchangers. The ion-exchange capacity of these layered aluminosilicates, which include the kaolinite, smectite, illite, chlorite, and vermiculite groups, results from imperfections and isomorphous substitutions in the crystal lattice, which generally create a net negative charge. In the kaolinite group, broken bonds at crystal plate corners and edges are the chief cause of the negative charge on the particles.

The oxide minerals, including silica and iron and manganese oxides, form a second important class of exchangers. The surfaces of these minerals contain incompletely coordinated metal and silicon cations at low pH, and an excess of hydroxyl or oxygen groups at high pH. The dissociation of water at these charged sites results in a charged surface layer surrounding the particle, the nature of which is dependent on solution pH. Positive surfaces prevail in low pH solutions; negative surfaces are formed in high pH solutions. Neutrality is attained at some intermediate pH, known as the zero point of charge (pH_{zpc}), so the oxide has a tendency to adsorb major anions below the pH_{zpc}, and major cations above.

As defined by van Olphen (1963), the cation exchange capacity (CEC) of a material is the excess of counter ions that can be reversibly exchanged for other cations in solution. Cation exchange capacity is usually expressed as the number of equivalents of cations that can be exchanged by 100 g dry weight of a material. The CEC's of several natural exchangers, as reported by Grim (1968) and Donald Langmuir, (Colorado School of Mines, oral commun., 1980), are presented in table 32. Clay exchangers generally have a greater affinity for divalent than monovalent cations due to the greater charge density of the former (Wiklander, 1964). Similarly, within groups IA and IIA of the periodic table, the affinity for adsorption by clays generally decreases with increasing hydrated ionic radii (Eisenman, 1962), as given by the Hoffmeister series:

$$Cs^+ > K^+ > Na^+ > Li^+$$

$$Ba^{+2} > Sr^{+2} > Ca^{+2} > Mg^{+2} .$$

The thermodynamics of exchange reactions can be described in terms of mass action expressions that relate the activities of cations in solution and on the exchanger to a thermodynamic exchange constant, K_{ex}. Thus, for the following absorption-desorption reactions:

$$Ca^{+2} + Na_2EX = 2Na^+ + CaEX, \quad (28)$$

$$Mg^{+2} + Na_2EX = 2Na^{+2} + MgEX , \quad (29)$$

where EX represents the negatively charged exchange site, the corresponding mass action expressions are given by:

$$K_{ex}^{NaCa} = \frac{(a_{Na^+})^2 (a_{CaEX})}{(a_{Ca^{+2}}) (a_{Na_2EX})}$$

and:

$$K_{ex}^{NaMg} = \frac{(a_{Na^+})^2 (a_{MgEX})}{(a_{Mg^{+2}}) (a_{Na_2EX})} ,$$

where a_{Na_2EX}, a_{CaEX}, and a_{MgEX} represent the activities of these cations on the surface of the exchanger.

Because exchange reactions occur at a relatively fast rate, cation concentrations in ground water can be expected to be in equilibrium with the exchange surface. However, according to Freeze and Cherry (1979), many millions of pore volumes of water may have to pass through an aquifer before the ratios of absorbed cations completely adjust to the cationic composition of the input waters. This process may require time periods on the order of millions of years to complete, because of the relatively low concentration of cations in the input water

TABLE 32.—*Cation exchange capacities (CEC) of several clay mineral groups and iron and manganese oxyhydroxides*

[Grim (1968), Donald Langmuir, Colorado School of Mines, oral commun., 1980]

Material	CEC (milliequivalents per 100 grams at pH 7)
Kaolinite	3–15
Glauconite	11–20
Illite, Chlorite	10–40
Smectites (montmorillonite)	80–150
Vermiculite	100–150
Mn(IV) and Fe(III) oxyhydroxides	100–740

compared to the large surface area of the clay particles. Clays in strata deposited in marine or transitional environments are initially saturated with exchangeable sodium ions, the prevalent cation in seawater. These ions can be systematically desorbed by calcium and magnesium ions derived from mineral dissolution and present in infiltrating ground waters. The result is that, until exchanger compositions completely adjust to the cationic composition of infiltrating ground waters, a progressive decrease in aqueous calcium and magnesium concentrations, accompanied by a concurrent increase in sodium concentration, will occur as water flows through the aquifer.

ENVIRONMENTAL ISOTOPES

STABLE ISOTOPES

Many elements exhibit natural variations in their isotopic compositions because of the fractionation of isotopes during phase transitions and chemical and biological reactions. These isotopic fractionations are due to slight differences in the physical and chemical properties of different isotopes of an element, and are directly proportional to relative differences in their masses. As a result, isotopic fractionation of this type is most pronounced among elements with atomic masses less than or equal to that of calcium. The hydrologically significant elements considered in this report are hydrogen, carbon, oxygen, and sulfur.

The magnitude of isotopic fractionation associated with a particular process is indicated by the fractionation factor (α):

$$\alpha = R_A / R_B ,$$

where R_A and R_B are the appropriate equilibrium isotopic ratios in phases A and B. Fractionation factors may be calculated by means of statistical mechanics or measured experimentally; they generally approach unity with increasing temperature.

Isotopic composition is expressed in δ(Del) notation as per mil differences in the measured isotopic ratios of sample and standard. For example, the relationship for carbon isotopes is:

$$\delta^{13}C = \left[\frac{(^{13}C/^{12}C)_{sample}}{(^{13}C/^{12}C)_{standard}} - 1 \right] \times 1000$$

The carbon isotope ratios may be replaced by $^{2}H/^{1}H$ (D/H), $^{18}O/^{16}O$, or $^{34}S/^{32}S$ ratios to obtain the corresponding δ values for these other elements. Typical standards used in evaluating isotopic composition include the SMOW (standard mean ocean water, for $\delta^{18}O$ and δD) (Craig, 1961a), PDB-1 (CO_2 gas produced from a belemnite of the Cretaceous Peedee Formation for $\delta^{13}C$) (Craig, 1957) and Cañon Diablo troilite standards (troilite from the Cañon Diablo meteorite, for $\delta^{34}S$) (Jenson and Nakai, 1963).

OXYGEN AND HYDROGEN

Natural variations in the $\delta^{18}O$ and δD values of water occur from differences in the vapor pressures of waters containing different isotopes of oxygen and hydrogen. Water containing lighter isotopes will exhibit a significantly greater vapor pressure than water containing heavier isotopes. As a result, vapor formed from liquid water will be depleted (decreased δ) in ^{18}O and D, and the remaining liquid will be enriched (increased δ) in these heavier isotopes. Because of this fractionation, $\delta^{18}O$ and δD vary characteristically as a function of latitude, elevation, condensation temperature, and distance inland, and can, therefore, be used as indicators of ground-water source and temperature of the recharge waters. Deviations from expected meteoric water compositions (Craig, 1961b; Gat, 1980) in natural systems are indicative of evaporation and transpiration, mixing with nonmeteoric waters, or of isotopic exchange with the hydroxyl groups of silicate minerals at elevated temperatures.

CARBON

Stable carbon isotopes provide an extremely useful tool in the study of ground-water chemistry, aiding in the determination of controlling chemical reactions and mass transfer. Carbon isotopic data places an additional constraint on proposed mass transfer models, in that a geochemical model must correctly predict both the chemical and isotopic composition of a system.

In some instances, the relative importance of chemical control of ground-water chemistry by carbonates or aluminosilicates may be evaluated using $\delta^{13}C$ data. In temperate climates, plants use the Calvin photosynthetic cycle, which produces organic carbon with $\delta^{13}C$ values of -25 ± 5 (Rightmire and Hanshaw, 1973). CO_2 produced in the unsaturated zone by the oxidation of this type of plant material should also have $\delta^{13}C$ values of approximately -25. Ground water in the unsaturated zone will exhibit $\delta^{13}C$ values representative of equilibration between dissolved bicarbonate, the predominant carbonate species between pH 6.4 and 10.3, and an essentially infinite gaseous reservoir of CO_2. Equilibrium fractionation of ^{13}C between HCO_3^- and $CO_{2(g)}$, $\alpha_{HCO_3^- - CO_2}$, was reported by Deines and others (1974) to be 1.0092 at 10°C, leading to a 9.2 per mil ^{13}C enrichment in $\delta^{13}C_{HCO_3^-}$ over $\delta^{13}C_{CO_{2(g)}}$, or a value of -16 for bicarbonate in unsaturated zone waters. On reaching the water table, ground water is effectively isolated from the CO_2 gas reservoir, and isotopic evolution proceeds under conditions that are closed with respect to exchange with that reservoir. Freshwater diagenetic carbonates, which are common in transitional sandstones, have $\delta^{13}C$ values of -4.8 ± 5.1 (Keith and Weber, 1964), whereas CO_2 derived from the oxidation of sedimentary organic carbon would have $\delta^{13}C$ values in the range of -28 ± 4 (Craig, 1954). Congruent dissolution of calcite (reaction 21) or dolomite (reaction 22) driven by the oxidation of organic carbon (reactions 1-6) would liberate bicarbonate with a $\delta^{13}C$ value of 16, allowing $\delta^{13}C$ solution to remain approximately constant, as seen from mass balance considerations:

$$\delta^{13}C_{final} = \frac{m^{C_T}_{initial}\delta^{13}C_{initial} + (m^{C_T}_{final} - m^{C_T}_{initial})\left(\frac{\delta^{13}C_{carbonate} + \delta^{13}C_{CO_2}}{2}\right)}{m^{C_T}_{final}}$$

where m^{C_T} is the molality of total inorganic carbon in solution.

Dissolution of aluminosilicates (reactions 24-27) also driven by the oxidation of organic carbon (reactions 1-6) would generate bicarbonate of the same isotopic composition as the organic carbon from which it was derived, causing the $\delta^{13}C$ of the evolving ground water to asymptotically approach a value of -28:

$$\delta^{13}C_{final} = \frac{m^{C_T}_{initial}\delta^{13}C_{initial} + (m^{C_T}_{final} - m^{C_T}_{initial})\delta^{13}C_{CO_2}}{m^{C_T}_{final}}$$

Using similar arguments, Wigley and others (1978) examined the isotopic evolution of a system controlled by dedolomitization, the incongruent dissolution of dolomite to form calcite (reaction 23). Again assuming an organic carbon CO_2 source and a $\delta^{13}C_{carbonate}$ value representative of either freshwater or marine ($\delta^{13}C=-0.2\pm2.0$) (Craig, 1954) carbonates, the authors calculated that solution $\delta^{13}C$ will asymptotically increase during closed (to a CO_2 gas reservoir) system conditions, reaching a final value representative of equilibrium between input and output $\delta^{13}C$ values. Consideration of carbon mass balance and isotopic evolution should, therefore, allow for a distinction between the above types of reactions in a system where CO_2 is being produced, but does not exist as a discrete gas phase.

Carbon isotopes may also be used to substantiate active methanogenesis (reactions 7 and 8) in aqueous sytems. Methane generated during these microbially mediated reactions is strongly depleted in ^{13}C with respect to CO_2 (Claypool and Kaplan, 1974), with $\alpha_{CO_2-CH_4}=1.071$ at 25°C (Bottinga, 1969). The activity of methanogenic bacteria would therefore be evident form the presence of methane and also from the ^{13}C enrichment of dissolved carbonate. Migration of methane into an aquifer could not produce a similar increase in the $\delta^{13}C$ of dissolved carbonate species, as Sackett and Chung (1979) have demonstrated that CO_2 and CH_4 do not attain isotopic equilibrium at low temperatures.

SULFUR

Sulfur isotopes can be used in geochemical studies to calculate the amount of sulfate reduction (reaction 6) that has occurred in an aquifer. Anaerobic bacteria, such as *Desulfovibrio* sp., reduce SO_4^{-2} to form H_2S, which is depleted in ^{34}S with respect to SO_4^{-2}. The remaining sulfate is therefore enriched in ^{34}S, and $\delta^{34}S_{sulfate}$ will increase accordingly. If both $\delta^{34}S_{sulfide}$ and $\delta^{34}S_{sulfate}$ values are known, calculated mass transfer in the sulfur system can be used to compute the expected final $\delta^{34}S_{sulfate}$ value, as demonstrated by Plummer and others (1983). Because $\delta^{34}S_{sulfide}$ determinations were unsuccessful in both study areas examined here, a discussion of this method is beyond the scope of this paper.

Sulfur isotopes have another use in hydrologic studies. Holser and Kaplan (1966) measured the $\delta^{34}S$ values in numerous samples of marine evaporate rocks of Phanerozoic age, and concluded that the $\delta^{34}S$ value of marine sulfate varied significantly during this period. Sulfate derived from marine sediments of one age will therefore differ from that derived from sediments of another age, so that differences in sulfur isotopic composition can be used to identify sulfate associated

with leakage between strata of different ages. However, considerable overlap exists between marine sulfates of different ages, so the age of the strata from which the sulfate was derived may not be unequivocally determined in many cases.

RADIOACTIVE ISOTOPES

TRITIUM

Tritium (^3H) is a naturally occurring, radioactive isotope of hydrogen, which is produced in the upper atmosphere by the interaction of nitrogen with cosmic ray-generated neutrons (n):

$$^{13}N+n=^{12}C+^3H \quad (30)$$

The newly created tritium then combines with oxygen to form water, which is subsequently dispersed throughout the hydrosphere. As a result of the atmospheric testing of hydrogen bombs, naturally produced tritium has been far overshadowed during the past 25 years by much higher levels of artificially produced tritium. These artificial tritium levels, which are between one and three orders of magnitude greater than pre-bomb levels, serve as a hydrologic tracer with which relatively young waters may be identified. Tritium concentrations on the order of 10 picocuries per liter (pCi/L) or less (2–4 tritium units or less; 1 TU=1 tritium atom per 10^{18} hydrogen atoms) are indicative of waters with ages of greater than 25 years, whereas greater concentrations indicate the presence of waters younger than 25 years in age.

CARBON-14

The measurement and adjustment of carbon-14 ages of waters from confined aquifers remains the most suitable and widely used method of ground-water dating. Past attempts to use other radioactive isotopes, such as ^{39}Ar and ^{32}Si (Oeschger and others, 1974) have met with limited success, although refined analytical techniques may allow the routine use of such dating schemes in future studies.

Carbon-14 is produced in the upper atmosphere by the interaction of cosmic ray-produced neutrons with stable isotopes of carbon, oxygen, and nitrogen. The most significant of these is the reaction between slow cosmic ray-produced neutrons and nitrogen:

$$^{14}N+n=^{14}C+^1H\,. \quad (31)$$

The ^{14}C atoms are incorporated into molecules of carbon dioxide and then rapidly mixed throughout the atmosphere, attaining constant concentrations representative of steady-state equilibrium.

Carbon-14 dating is based on the principle that, upon isolation from the atmospheric ^{14}C reservoir, the concentration of this unstable isotope begins to decrease from radioactive decay by beta emission to ^{14}N:

$$^{14}C=^{14}N+\beta^-\,. \quad (32)$$

In ground-water systems, ^{14}C concentrations may also be altered by mixing or interaction with other carbon sources, so that the accuracy of a date is dependent on one's ability to successfully isolate the effects of radioactive decay from those of other processes that change ^{14}C content. In the absence of such processes, the equation for determining time (t, in years) since isolation from the atmosphere based on the ^{14}C activity is:

$$t=\frac{t_{1/2}}{0.301}\log\left(\frac{A_{ND}}{A}\right),$$

where:

$t_{1/2}$ = ^{14}C half life, 5,730 years
A = measured ^{14}C activity, in percent modern carbon
A_{ND} = ^{14}C activity to be expected in the absence of radioactive decay, in percent modern carbon.

Estimation of A_{ND} is dependent on quantitatively determining the magnitude of carbonate sources and sinks in the aquifer system. Under favorable conditions, this can be accomplished through the use of geochemical mass transfer models.

Wigley and others (1978) divided carbon mass transfer into three stages for the purpose of ^{14}C dating:

1. Evolution in the unsaturated zone, where infiltrating ground water is open to isotopic exchange with an effectively infinite, gaseous CO_2 reservoir.
2. Congruent dissolution of carbonates (reactions 21 and 22) in the saturated zone, where ground water is assumed to be closed to exchange with a CO_2 gas reservoir.
3. Incongruent dissolution of carbonates (reaction 23) in the saturated zone, with closed system conditions continuing.

The effects of these three stages are dependent on isotopic fractionation between gas and aqueous phases, carbon mass transfer, and isotopic fractionation between

aqueous and solid phases. Substitution of expressions representing the effects of each of the three evolutionary stages into the above decay equation yields:

$$t=19035\left[\log\left(\frac{100}{A}\right)+\log\left(\frac{\delta^{13}C_2-\delta^{13}C_*}{\delta^{13}C_1-\delta^{13}C_*}\right)+\log\left(\frac{\beta\delta^{13}C_{final}-\delta^{13}C_*+\frac{\epsilon ps}{\Gamma}}{\beta\delta^{13}C_2-\delta^{13}C_*+\frac{\epsilon ps}{\Gamma}}\right)\right],$$

where:

$\delta^{13}C_1$ = solution $\delta^{13}C$ at the end of stage 1,
$\delta^{13}C_2$ = solution $\delta^{13}C$ at the end of stage 2,
$\delta^{13}C_*$ = dissolving carbonate $\delta^{13}C$,
β = composite parameter representing reaction progress,
ϵps = additive fraction factor between solution and precipitate,
Γ = ratio of carbon input to output rate.

For a detailed derivation of this expression and examples of its use, the reader is directed to Wigley and others (1978). Application of the above expression to analytical data and computed mass transfer allows an estimation of ground-water age, which in turn can be used to derive flow rates and aquifer constants.

GEOCHEMICAL COMPUTER MODELS

WATEQ2

The computer program WATEQ2 (Ball and others, 1979; 1980) was used to compute the equilibrium distribution of aqueous species and then calculate mineral saturation indices for the sampled ground waters. This PL/1 code is a revised and expanded version of WATEQ, the computerized aqueous chemical model of Truesdell and Jones (1974). The method of calculation involves solution of mass action and mass-balance equations through an iterative back-substitution on cation and anion mass-balance equations. Options are provided for calculation of activity coefficients using either the Debye-Hückel or Davies equations.

WATEQ2 allows for consideration of ion association and solubility equilibria for several trace metals (Ag, As, Cd, Cu, Mn, Ni, Pb, and Zn), solubility equilibria for various metastable solids, and polysulfide speciation. Calculations of redox potential from various couples and from propagated standard deviations for many ion activity products are also provided. The program utilizes an extensive, low-temperature thermodynamic data base, which has been updated by using recent compilations of critically evaluated data (Ball, 1979; 1980).

Input data consist of laboratory determinations of total concentrations of major, minor, and trace elements, and field-measured temperature, alkalinity, and pH values. Eh may be determined in the field using a platinum electrode (Langmuir, 1971), or may be calculated from any of several appropriate redox couples (reactions 12-16). The significance of the calculated saturation indices is determined by the propagation of analytical errors, with saturation being considered any value of SI within the 95 percent confidence interval of zero. For many minerals, 95 percent confidence lies within several tenths of zero; for others, saturation may be implied at greater than one unit deviation from zero because of the poor precision of analytical results near the detection limit.

PHREEQE

Reaction simulation and mass transfer modeling of aquifer geochemistry was accomplished using PHREEQE (Parkhurst and others, 1980), a FORTRAN computer program designed to simulate chemical reactions. PHREEQE utilizes an ion-pairing aqueous-speciation model similar to that in WATEQ2 to simulate aqueous-solution chemistry. It can equilibrate an initial solution with one or more mineral or gas phases, calculating the final equilibrium solution composition, Eh and pH, as well as the associated mass transfer between solid, aqueous, and gaseous phases. The code also allows the user to add net stoichiometric reac- tions to a solution, to mix solutions of different composi- tion (constant volume), or to titrate one solution with another (additive volume).

PHREEQE was used to simulate changes in groundwater chemistry associated with equilibration of an initial rainwater solution with ion exchangers and various mineral phases. A computational problem arises in the attempt to mathematically equilibrate a given solution with Na/Ca and Na/Mg exchange, and with the mineral phases calcite and dolomite, simultaneously. Both ion-exchange and mineral-equilibrium equations specify a $a_{Ca^{+2}}/a_{Mg^{+2}}$ ratio, indicating that the four equations simulating these reactions are not independent, and a

unique algebraic solution is not available. In natural systems, an additional variable is provided by the surface composition of the exchanger, resulting in an additional equation. PHREEQE is currently unable to consider the variable surface composition of an exchanger; therefore, simultaneous equilibration with Na/Ca and Na/Mg exchange in combination with calcite and dolomite equilibration was accomplished in a stepwise manner. Solutions were first equilibrated with calcite and dolomite, followed by equilibration with ion exchange. This two-step procedure was repeated until the resulting solution composition had stabilized, and the saturation indices of calcite and dolomite were within analytical uncertainty of zero. Comparisons of this stepwise method and simultaneous mineral-ion exchange equilibration for calcite-ion exchange and dolomite-ion exchange simulations result in similar mass transfers and final solution compositions via the two methods.

ISOTOPIC EVOLUTION EQUATIONS

A. U.S. Geological Survey FORTRAN computer program was used to calculate carbon isotopic evolution associated with simulated mass transfers. This code utilizes a finite difference method to solve the isotopic evolution equations of Wigley and others (1978), yielding final $\delta^{13}C$ and A_{ND} values from initial $\delta^{13}C$ and ^{13}C measurements, simulated carbonate mass transfer and solution composition. Fractionation factors have been calculated from the temperature-dependent functions of Deines and others (1974).

☆ U.S. GOVERNMENT PRINTING OFFICE:1985—576-049 / 26001